ARSENIC AND FLUORIDE REMOVAL FROM DRINKING WATER BY A NOVEL ADSORBENT

By

P.DHANASEKARAN

(ENGG 02200904010)

INDIRA GANDHI CENTRE FOR ATOMIC RESEARCH,

KALPAKKAM

A thesis submitted to the

Board of Studies in Engineering Sciences

In partial fulfillment of requirements

For the Degree of

DOCTOR OF PHILOSOPHY

Of

HOMI BHABHA NATIONAL INSTITUTE

August, 2015

Homi Bhabha National Institute

Recommendations of the Viva Voce Committee

As members of the Viva Voce Committee, we certify that we have read the dissertation prepared by **P. Dhanasekaran** entitled "**Arsenic and Fluoride Removal from Drinking Water by a Novel Adsorbent**" and recommend that it may be accepted as fulfilling the thesis requirement for the award of Degree of Doctor of Philosophy.

Chairman – Dr. M. Saibaba	**Date:** 21-3-16
Guide / Convener – Dr. P.M. Satya Sai	**Date:** 21/3/16
Examiner – Prof. Indra Deo Mall	**Date:** 21/3/16
Member 1 – Dr. S. Rangarajan	**Date:** 21.03.2016
Member 2- Dr. N. Sivaraman	**Date:** 21/3/16

Final approval and acceptance of this thesis is contingent upon the candidate's submission of the final copies of the thesis to HBNI.

I hereby certify that I have read this thesis prepared under my direction and recommend that it may be accepted as fulfilling the thesis requirement.

Date: 21/03/16

Place: Kalpakkam

Guide

STATEMENT BY AUTHOR

This dissertation has been submitted in partial fulfillment of requirements for an advanced degree at Homi Bhabha National Institute (HBNI) and is deposited in the Library to be made available to borrowers under rules of the HBNI.

Brief quotations from this dissertation are allowable without special permission, provided that accurate acknowledgement of source is made. Requests for permission for extended quotation from or reproduction of this manuscript in whole or in part may be granted by the Competent Authority of HBNI when in his or her judgment the proposed use of the material is in the interests of scholarship. In all other instances, however, permission must be obtained from the author.

P.Dhanasekaran

DECLARATION

I, hereby declare that the investigation presented in the thesis has been carried out by me. The work is original and has not been submitted earlier as a whole or in part for a degree at this or any other Institution /University.

P.Dhanasekaran

LIST OF PUBLICATIONS

Journal papers

1. Arsenic removal from groundwater by *Anjili tree* sawdust impregnated with ferric hydroxide and activated alumina, Water Science and Technology: Water supply 16(1) (2016) 115-127
2. Defluoridation of water by chemical impregnated *Artocarpus hirsutus* sawdust, Water Science and Technology: Water supply , DOI: 10.2166/ws.2016.032
3. Fixed bed adsorption of arsenic from water by chemical impregnated *Artocarpus hirsutus* sawdust, Journal of Environmental Sciences (Under Review)
4. Fixed bed adsorption of fluoride by *Artocarpus hirsutus* based adsorbent, Journal of Fluorine Chemistry (Communicated)
5. Arsenic and fluoride adsorption from water by Aanjili tree sawdust impregnated with ferric hydroxide and activated alumina, Separation Science and Technology (Under Review)

Conference Proceedings

1. Removal of fluoride from ground water by sawdust impregnated with ferric hydroxide and activated alumina, The Second International Conference on Emerging Technologies for Clean Water (SICETCW-2014), IIT- Madras, Chennai, India, 23-24 October 2014.

2. Defluoridation of ground water by a novel adsorbent, SESTEC-2014 Mumbai, Bhabha Atomic Research Centre, Mumbai, India, 25-28 February, 2014.

3. Arsenic removal from drinking water by a novel adsorbent, International Conference on Innovative Technologies and Management for Water Security, INDACON-2014, NIOT, Chennai, India, 12-14 February 2014.

4. Arsenic(V) removal from drinking water by modified adsorbent, SESTEC-2012, Bhabha Atomic Research Centre, Mumbai, India. February 27 – March 1, 2012.

P.Dhanasekaran

Dedicated to

My Parents

ACKNOWLEDGEMENT

I am delighted to express my thanks and gratitude to those who rendered their support during the project. I am indebted to my guide, Prof. P.M.Satya Sai, DGM, NRB, BARCF for his conscientious guidance and constant encouragement which enhanced me to approach this research with enthusiasm and confidence. I am particularly thankful for spending his precious time in productive discussions and suggestions in improving the quality of research work.

I would like to express my sincere gratitude to Dr. C.Anand Babu, former guide, for the great opportunity to take up this research in water treatment direction and for arranging experimental and analysis facilities. My special thanks to Dr. M. Sai Baba, AD, RMG for his benevolent support in administrative processes and helpful suggestions in doctoral committee meetings. I sincerely thank other members Dr. S. Rangarajan, Head, SCMTSS, BARCF, Dr. N. Sivaraman, Head, SCSS, FChD for their precious thoughts and proposals during review meetings.

I am thankful to Mr. K. K. Rajan, Director, FRTG and Mr. G. Padmakumar, Head, CTD, FRTG for their administrative support and providing experimental facilities.

I express my deepest gratitude to Dr. K. I. Gnanasekar, MCD, Chemistry Group for the prolific discussions, fruitful suggestions and helping in strenuous characterization studies. I delightfully thank Dr. B. K. Sharma, FBTR and Dr. E. Isaac Samuel, MMD, MMG for their fervent support and constant encouragement in various times.

I thankfully acknowledge the support of Dr. R.Krishna Prabhu MCD, arsenic analysis and adsorbent characterization studies. I am indebted to Dr. V. Jayaraman, Mr. A. Sree Rama Murthy, MCD, Chemistry Group, Dr. P. Chandra Mohan, Dr. Pushpalatha, Mr. T. V. Krishna Mohan, Head, ESS, BARCF for their assistance in BET studies. I am grateful to Mrs. Clinsha, UGC-DAE for XPS analysis and Mr. Dasarath Maji, FChD, Chemistry group for porosity analysis. I appreciate the technical support rendered by the beloved senior Dr. P. Illayaraja and my batch mate Dr. Ravikirana in FTIR and SEM analysis.

I dedicate my special thanks to all the members of CTD for providing tender and friendly ambience. I gratefully remember their extended supported in administrative and experimental aspects during the project.

I relish the cheerful friendship with Mr. Mahendra Chinthala, Mr. Masilamani Chelladurai, Mr. Saswath Kumar Swain, Mr. Srihari, Mr. Rahul Trikha, Mr. Suranjan Bera, Mr. Balaji, Mr. Solomon, Mr. Arun, Mr. Sadu Venkatesu and other research scholars.

My heart is filled with the joy of thanks to beloved mother Mrs. P. Kamala for her enduring love and prayers which encouraged me a lot in accomplishing this project. I appreciate the loving fellowship and persistence of my brothers, sister and their family members throughout my academic life.

CONTENTS

SYNOPSIS

Water contains natural contaminants, particularly inorganic contaminants that arise from the natural sources and due to anthropogenic pollution. Dissolved and suspended solids are present in most surface waters. Arsenic is 20th in natural abundance, 14th in the sea water [1]. Arsenic finds its way into surface and groundwater by erosion of arsenic containing rocks, industrial and mine discharges. Arsenic contaminated drinking water has been found in Argentina, Chile, Mexico, USA, China, Hungary, India (West Bengal), Bangladesh, Romania and Vietnam, Southeast Asian deltas being most severely arsenic affected region [2, 3]. Arsenic concentration in sea water varies between 0.09 µg/L and 24 µg/L, and in freshwater between 0.15 µg/L and 0.45 µg/L [1].

As per the Bureau of Indian Standards, a maximum acceptable limit for arsenic is 0.01 mg/L and fluoride 1 mg/L for drinking water [4]. Arsenic is classified as a Group I carcinogen (human carcinogen) [5]. Arsenic exposure (> 50 µg/L) via drinking water is related to lung, kidney, bladder, liver cancer, cardiovascular disease, diabetes. Skin cancer is caused by exposure to low arsenic level (< 50 µg/L) [6-8].

In water, arsenic is present predominantly in the As(V) (arsenate) form. As(III) (arsenite), when present, is readily oxidized to As(V) (arsenate) in aerobic waters at pH values above 7.0 [9]. Arsenic removal technologies can be classified into Chemical and Physical methods. Chemical methods involve oxidation-reduction, lime softening and coagulation. Physical methods are adsorption, ion exchange, electrodialysis, reverse osmosis and nanofiltration [10, 11].

Fluorine is the most reactive element of halogen family. Fluoride is essential for human being as it helps in normal mineralization of bones and formation of dental enamel [12]. It has been estimated that fluoride is the 17th most abundant element constituting about 0.065% of the earth's crust, in a number of minerals, of which fluorspar (CaF_2), cryolite (Na_3AlF_6), and fluorapatite [$3Ca_3(PO_4)_2Ca(F,Cl_2)$] are the most common. Weathering of these minerals along

with volcanic and fumarolic processes lead to higher fluoride levels in groundwater [13].

Fluorosis is a common symptom of high fluoride ingestion manifested by mottling of teeth in mild cases and embrittlement of bones and neurological damage in severe cases. High fluoride intake is reported to result in a range of adverse health problems in addition to fluorosis, including cancer, impaired kidney function, digestive and nervous disorders, reduced immunity, Alzheimer's disease, nausea, adverse pregnancy outcomes, respiratory problems, lesions of the endocrine glands, thyroid, liver and other organs [14, 15].

For defluoridation of water, chemical additive, contact precipitation, adsorption, ion exchange methods are used. Among these, adsorption is integral to a broad spectrum of physical, biological, and chemical processes and operations in the environmental field. Adsorption of dissolved impurities from solution has been widely employed for water purification [16].

Objective of the thesis

In view of the adverse health impact of arsenic and fluoride, both must be removed from water by suitable methods to make it potable. In the present work a sawdust based novel adsorbent is synthesized and used for adsorption of both arsenic and fluoride from water. The work constitutes of:

- Synthesis of a novel adsorbent containing different functional groups for efficient removal of arsenic and fluoride from groundwater.
- Characterization of adsorbent to study the surface morphology and identify the presenting functional groups.
- Studies on the effects of various parameters on arsenic and fluoride adsorption in batch studies.
- Column studies to obtain breakthrough and its variation by the influence of parameters like flow rate, initial concentration, adsorbent particle size and bed height.

- Evaluation of the efficiency of the synthesized adsorbent for the removal of arsenic and fluoride from groundwater.

Adsorbent preparation and characterization

Sawdust from different trees was assessed for use as a base material for the adsorbent. The sawdust samples were chemically treated to remove lignin, dried and tested for their capacity for adsorption of arsenic and fluoride. Sawdust of *Artocarpus hirsutus*, called "Anjili" locally, showed the highest adsorption capacity for arsenic and fluoride from water and hence it was selected for preparation of the adsorbent. A novel adsorbent was synthesized by impregnating the Sawdust with Ferric hydroxide and Activated Alumina (SFAA). To optimize composition of the adsorbent, various mass ratios of the constituents were studied and the mass ratio of 1.5:1:1 was chosen based on the adsorption capacity. Detailed characterization of the adsorbent was carried out before and after the adsorption of arsenic or fluoride, by studying the pore size distribution and surface morphology. Surface area and pore volume were evaluated by Sorptomatic 1990 Brunauer Emmet Teller (BET) analyzer (France) using liquid nitrogen at 77 K as a coolant. Micropore volume and surface area in mesopores and external surface are determined from t-plots, which is a method of comparing an isotherm of a micro porous material with a standard type II isotherm [17]. Mercury porosimetry is used to determine the macropore volume and macropore surface area by employing Thermo scientific Pascal 140 mercury porosimeter with a maximum test pressure of 400 kPa at 298 K.

The morphology was investigated using Philips XL-30 Scanning Electron Microscopy (SEM). EDX analysis was performed to find the elemental constituents of pure SFAA. The atomic% of Al and Fe on the basis of chemicals presented in SFAA was found to be 35.9 and 37.1%. Fourier Transform Infra-Red spectroscopy (FTIR) spectra were recorded between 500 cm^{-1} and 4000 $cm^{-1}$with 16 cm^{-1} resolution using ABB-MB3000 FTIR spectrometer. X-ray photoelectron spectroscopy (XPS) was performed with XPS spectrometer (M/s. Specs, Germany) provided with a monochromatic AlK_{α} radiation and a hemispherical analyzer. The base vacuum was

observed to be better than 5.0 × 10^{-10} mbar during the analysis. The selected area scans were collected with 20 eV pass energy.

Adsorption of arsenic (Batch studies)

Arsenic concentration in the raw and treated water was analyzed by Inductively Coupled Plasma Mass Spectrometer (ICP-MS) (Model-ELAN 250). BET surface area, pore volume and pore size distribution of sawdust, SFAA, As(V) and As(III) adsorbed SFAA were identified. EDX studies showed the presence of Al, Fe, As(V), As(III) in SFAA after adsorption. FTIR study confirms that SFAA contains several functional groups on its surface. The XPS survey of SFAA, arsenic loaded, specimens shows the signatures of As 3d, As 3p, C 1s, O1s, Al 2s and Fe 2p along with the auger lines of arsenic, oxygen and Fe. Point of Zero Charge of SFAA was obtained by mass titration method was 5.85 [18]. The pH study of arsenic adsorption by SFAA gave optimum pH range of 6.5-7.0 for both As(V) and As(III). As(V) adsorption, both electrostatic attraction and chemical bonding take place. But in case of As(III), only chemisorption takes place, and hence the As(III) adsorption is less compare to As(V) [19]. The optimum adsorbent dose was taken as 10 g/L for complete removal of As(V) from an initial solution concentration of 2 mg/L. The removal of As(V) increased from 27.33 to 98.64 percent with increase in the adsorbent dose from 1 to 10 g/L and with further increase in dose, %removal remained constant.

The Distribution coefficient (K_{DC}), which reflects the binding ability of the surface for an element and is dependent on pH and type of surface [20, 21] is evaluated. K_{DC} value is 7271.43 L/kg at the dose rate of 10 g/L which increased to 9263.96 L/kg at the dose rate of 30 g/L. Both removal percentage and adsorption capacities of the adsorbent decreased with increase in the particle size of the adsorbent. Interference of other ions on As(V) adsorption by SFAA adsorbent was observed to be in the order of $PO_4^{3-} > SO_4^- > HCO_3^- > NO_3^-$.

Equilibrium isotherms for As(V) and As(III) adsorption on SFAA were studied. The maximum equilibrium uptake capacities were found to be 77.60 mg/g and 54.32 mg/g for As(V) and

As(III), respectively for an initial concentration of 3000 mg/L. The studies confirm that the As(V) and As(III) adsorption by SFAA follows Freundlich isotherm. Kinetic studies showed that the uptake of As(V) was rapid in the first 10 min and was constant subsequently. Pseudo second order kinetics explained the experimental data well. The intra particle diffusion model was applied to describe the competitive adsorption.

When the temperature was increased from 303 K to 313 K, the adsorption was almost constant. However, when temperature was increased from 313 to 318 K, there was a slight increase in the uptake of As(V). Thermodynamic studies gave three basic thermodynamic parameters, standard enthalpy (ΔH^o = 13.57 kJ/mol), standard entropy (ΔS^o = 0.138 kJ/mol.K) and standard free energy (ΔG^o). The value of ΔH^o indicates that the process is chemisorption, negative value of ΔG^o indicates the process is spontaneous.

A fixed bed study on arsenic adsorption by different adsorbents was carried out. Adsorption by SFAA was higher than that of activated alumina, as can be seen. Fixed bed adsorption of As(V) using SFAA by varying the flow rate, particle size, initial concentration and bed height were studied and optimum operating parameters were established. Column experiments showed that removal of As(V) from water was better for low flow rates, small particle sizes, low initial concentrations and large adsorbent bed heights. Thomas, Yoon-Nelson, Bohart-Adam and Clark models were tested with the experimental data and model parameters were estimated. Clark model explained arsenic adsorption by SFAA well.

Fluoride concentration in the water before and after defluoridation was analyzed by ion selective electrode. Pore size distribution of SFAA before and after adsorption of fluoride, along with that of sawdust and activated alumina were studied. Pore volumes and surface area are calculated. It can be seen that the sawdust has substantial macropore volume and micropore surface area. In case of activated alumina the surface area is mostly in the mesopore region and the macropore volume is moderate. As a result, the combination adsorbent, SFAA has a well-balanced pore size

distribution with the pore volumes and surface areas distributed in macro, meso and micropore regions. The distribution of surface areas and pore volumes for SFAA before and after fluoride adsorption shows that the micropore surface area reduced to 7.7% of the original, as against 95% for activated alumina. This indicates that the micropores have been filled very effectively in case of SFAA. Similarly, the S_{meso} reduced to 49% of the original for SFAA as against 86% for activated alumina. Thus, even in the mesopore region, adsorption has been more effective by SFAA.

There is no difference in Macropore volumes before and after adsorption in case of both activated alumina and SFAA, as the adsorption takes place only in meso and micropores. Thus, though the BET surface area of activated alumina is more than that of SFAA, the utilization of the micro/meso pores for adsorption is better in case of SFAA because of the well-developed approach paths to the micropores in case of SFAA. This is also reinforced by the column studies.

Surface morphology of SFAA was studied by SEM before and after fluoride adsorption. The SEM images show that the granules remain intact after grafting. FTIR study indicated exchange of hydroxide and fluoride during defluoridation of water by SFAA. The XPS survey scans of fluoride loaded SFAA showed the signatures of F 1s, C 1s, O 1s and Fe 2p.

From the pH study it was seen that until pH 9 the fluoride adsorption was constant and beyond 9 it decreased. In the range of pH 1 to 5.85, the surface is protonated and being positively charged, attracts fluoride ions. From pH 5.85 to pH of 9.0 the adsorption continues to be nearly constant due to the replacement of hydroxyl ion by fluoride ion as the hydroxyl ion concentration was relatively low in this pH range.

Kinetic studies conclude that 40 min contact time is required for fluoride adsorption. Pseudo second order Ho model [22] explained fluoride adsorption by SFAA. The equilibrium capacity (q_e) was calculated to be 0.680 mg/g which is closed to the experimental data. Intra particle, external mass transfer and Boyd models were also tested with the experimental data. Fluoride

removal increased with increase in adsorbent dose and reached asymptotically a value of 99%. It is seen that the rate of removal is high for low doses of 10 g/L and this was the dose used for studying the effect of many other parameters, in the present study.

Distribution Coefficient (K_{DC}) for dose of 10 g/L was found to be 97.6 L/kg and this increased to 1226 L/kg at the dose rate of 100 g/L. For an initial concentration of 1000 mg/L, fluoride adsorption capacity by SFAA was found to be 40.28 mg/g, which is higher than that of activated alumina, 8.60 mg/g. Comparison of adsorption capacity with many other adsorbents reported earlier, establishes the efficiency of SFAA for fluoride removal for wide range of initial concentrations. Adsorption of fluoride by SFAA and activated alumina for various initial concentrations were studied. There was a marked decrease in the adsorption capacity with increasing particle size of the adsorbent, SFAA. The order of ions reducing fluoride removal efficiency by SFAA was observed to be $OH^- > CO_3^{2-} > HCO_3^- > NO_3^- > SO_4^{2-} > Cl^-$. Increasing sodium or potassium reduced fluoride adsorption, possibly due to the high solubility of sodium or potassium fluoride. Calcium enhanced (77% to 87%) the fluoride adsorption by forming calcium fluoride, which is insoluble in water.

When the temperature was increased from 303 K to 308 K, 313 K, 323 K and subsequently to 333 K, the adsorption increased, indicating that the mechanism is chemisorption. Defluoridation follows Freundlich adsorption isotherm. From thermodynamic studies ΔH^o and ΔS^o were calculated to be 17.86 kJ/mol and 0.1 kJ/mol.K. The value of ΔH^o indicates that the process is chemisorption. The negative value of ΔG^o confirms the feasibility of adsorption at all the temperatures and indicates that it is a spontaneous process. The positive value of ΔS^o indicates that both enthalpy and entropy are responsible for making ΔG^o negative, which showed the increasing randomness at the solid – solution interface during adsorption. The adsorption mechanism of defluoridation is mainly by F^- and OH^- exchange [23].

Column studies were carried out with different adsorbents; viz., sawdust (S.D), activated alumina (A.A) and SFAA to assess their fluoride adsorption. From the result it was observed that

SFAA gives an effective removal of fluoride from groundwater than other adsorbent. From the column studies it was found that with increasing the particle size of SFAA from 0.089 mm to 0.182 mm, the breakthrough was obtained earlier for the adsorbent of larger particle size (0.182 mm). As expected, higher flow rates resulted in earlier breakthrough due to low bed contact time of the feed. Higher influent concentration showed sharper breakthrough curves due to quick adsorbent saturation, which causes a decrease in adsorption zone length and exhaustion time. Clark model explained the results for different parameters viz., initial concentration, particle size and flow rate.

Arsenic and fluoride present together above World Health Organization levels in Pakistan, Tanzania, and India [24, 25]. The SEM studies of SFAA before and after arsenic and fluoride adsorption were carried out. EDX studies showed the presence of Al, Fe, As, F in the adsorbed SFAA. The XPS survey of SFAA, arsenic with fluoride loaded specimens shows the signatures of As 3d, As 3p, F 1s, C 1s, O 1s and Fe 2p along with the auger lines of arsenic, Al and Fe.

Effect of initial concentrations of arsenic and fluoride was studied. Isotherm studies showed that combined arsenic and fluoride adsorption by SFAA followed Freundlich isotherm. Column studies with combined arsenic and fluoride showed that arsenic was preferred to fluoride.

Outline of thesis

The thesis contains six chapters. Chapter 1 gives an outline of the water quality standards for the purpose of drinking. Sources for contamination of water by arsenic and fluoride are also discussed. Health effects of consumption of arsenic and fluoride are explained in detail. Literature review of arsenic and fluoride removal from groundwater was presented, particularly with reference to adsorption. Chapter 2 discusses the materials and methods used for in the current study for investigating the adsorption of arsenic and fluoride from water. Method adopted for synthesis of the adsorbent and the characterization methods have been given in this chapter. Chapter 3 explains the results and discussion of arsenic adsorption by batch and column study in detail. The results of characterization of SFAA and their significance for arsenic

adsorption are presented. Effects of different operating parameters, such as pH, adsorbent dose, initial concentration, contact time, temperature and interference of other ions are discussed. Column studies include arsenic adsorption by different adsorbents, effects of flow rate, initial concentration, bed height and particle size. The experimental data is tested with four different models, Thomas, Yoon-Nelson, Bohart-Adam and Clark model and the best model to explain the data was identified. Chapter 4 presents the results and discussion of fluoride adsorption by batch and column experiments in detail. The batch studies include surface characterization and effect of operating parameters such as contact time, pH, adsorbent dose, initial fluoride concentration, temperature, particle size and the presence of competing anions and cations. Column studies include fluoride adsorption by different adsorbents, effects of flow rate, initial concentration, bed height and particle. The experimental data is tested with four different models, Thomas, Yoon-Nelson, Bohart-Adam and Clark model and the best model that explains the data is identified. Experimental studies to adsorb both arsenic and fluoride simultaneously are discussed in chapter 5. Chapter 6 summarizes the results of the current study.

A novel adsorbent SFAA is developed for adsorption of arsenic and fluoride from water and the parameters for effective removal were identified. This adsorbent is economic, ecofriendly and minimizes generation of secondary wastes. The treated water conforms to WHO limits for potable water, with respect to arsenic, fluoride, iron and aluminium. Suggestions for future study include use of fine sawdust for adsorbent development for arsenic and fluoride removal. Use of SFAA for removal of heavy metals and other pollutants for water can be carried out.

References

1. B.K. Mandal, K.T. Suzuki, Arsenic round the world: a review. Talanta, 58 (2008) 201-235.
2. C. Wang, H. Luo, Z. Zhang, Y. Wu, J. Zhang, S. Chen, Removal of As(III) and As(V) from aqueous solutions using nanoscale zero valent iron-reduced graphite oxide modified composites. Journal of Hazardous Materials, 268 (2014) 124-131.

3. K. Qureshi, S. Almani, Z. Solangi, Z. Bhatti, I. Bhatti, Modified hematite iron for removing arsenic(V) from water. Sindh University Research Journal, 46 (2014) 83-86.
4. Indian Standard Drinking Water – Specification (Second Revision), Bureau of Indian Standards (2012) 1-18.
5. IARC, Arsenic and arsenic compounds. IARC Working Group (2004) 41-93.
6. C.M. George, L. Sima, M.H.J. Arias, J. Mihalic, L.Z. Cabrera, D. Danz, W. Checkley, R.H. Gilman, Arsenic exposure in drinking water: an unrecognized health threat in Peru. Bulletin of the World Health Organization, 92 (2014) 565-572.
7. Environmental health criteria 224 arsenic and arsenic compound. (2001) WHO. http://www.inchem.org/documents/ehc/ehc/ehc224.htm
8. Desarrollo, Relationship between arsenic, heart disease and diabetes discovered. Medical X press (2014). http://www.sciencedaily.com/releases/2014/10/141014083547.htm
9. S. Goldberg, Competitive adsorption of arsenate and arsenite on oxides and clay minerals. Soil Science Society of America Journal, 66 (2002) 413-421.
10. B. Pan, Z. Li, Y. Zhang, J. Xu, L. Chen, H. Dong, W. Zhang, Acid and organic resistant nano-hydrated zirconium oxide (HZO)/polystyrene hybrid adsorbent for arsenic removal from water. Chemical Engineering Journal, 248 (2014) 290-296.
11. Y. Salameh, A.B. Albadarin, S. Allen, G. Walker, M.N.M. Ahmad, Arsenic(III,V) adsorption onto charred dolomite: Charring optimization and batch studies. Chemical Engineering Journal, 259 (2015) 663-671.
12. D. Dayananda, V.R. Sarva, S.V. Prasad, J. Arunachalam, N.N. Ghosh, Preparation of CaO loaded mesoporous Al_2O_3: Efficient adsorbent for fluoride removal from water. Chemical Engineering Journal, 248 (2014) 430-439.
13. WHO, Inadequate or excess fluoride: A major public health concern, in Preventing Disease through healthy environments. WHO: Geneva, Switzerland, (2010) 1-5.
14. J.K. Fawell, Fluoride in Drinking-water, in Background document for development of WHO Guidelines for Drinking-water Quality. World Health Organization (2004).
15. A. Tewari, A. Dubey, and others, Defluoridation of drinking water: efficacy and need. Journal of Chemical and Pharmaceutical Research, 1 (2009) 31-37.
16. Q. Zhou, X. Lin, B. Li, X. Luo, Fluoride adsorption from aqueous solution by aluminum alginate particles prepared via electrostatic spinning device. Chemical Engineering Journal, 256 **(**2014) 306-315.

17. B.C. Lippens, J.H. De Boer, Studies on pore systems in catalysts: V. The t method. Journal of Catalysis, 4 (1965): p. 319-323.
18. J.S. Noh, J.A. Schwarz, Estimation of the Point of Zero Charge of simple oxides by mass titration. Journal of Colloid and Interface Science, 130 (1989) 157-164.
19. T.S. Anirudhan, P. Senan, Adsorptive potential of sulfonated poly(glycidylmethacrylate)-grafted cellulose for separation of lysozyme from aqueous phase: Mass transfer analysis, kinetic and equilibrium profiles. Colloids and Surfaces A: Physicochemical and Engineering Aspects, 377 (2011) 156-166.
20. X. Yu, S. Tong, Maofa Ge, L. Wu, J. Zuo, C. Cao, W. Song, Synthesis and characterization of multi-amino-functionalized cellulose for arsenic adsorption. Carbohydrate Polymers, 92 (2013) 380-387.
21. G. Alagumuthu, M. Rajan, Equilibrium and kinetics of adsorption of fluoride onto zirconium impregnated cashew nut shell carbon. Chemical Engineering Journal, 158 (2010) 451-457.
22. Y.S. Ho, G. McKay, Pseudo-second order model for sorption processes. Process biochemistry, 34 (1999) 451-465.
23. H. Wu, Treatment effect on the adsorption capacity of alumina for removal fluoride Abstract. Nano Biomedicine and Engineering, 2 (2010) 239-245.
24. A. Farooqi, H. Masuda, M. Kusakabe, M. Naseem, N. Firdous, Distribution of highly arsenic and fluoride contaminated groundwater from east Punjab, Pakistan, and the controlling role of anthropogenic pollutants in the natural hydrological cycle. Geochemical Journal, 41 (2007) 213-234.
25. K.D. Brahman, T.G. Kazi, H. I. Afridi, S. Naseem, S.S. Arian, N. Ullah, Evaluation of high levels of fluoride, arsenic species and other physicochemical parameters in underground water of two sub districts of Tharparkar, Pakistan: A multivariate study. Water Research, 47 (2013) 1005-1020.

LIST OF FIGURES

LIST OF TABLES

LIST OF ABBREVATIONS

AA	Activated Alumina
As(III)	Arsenite
As(V)	Arsenate
BET	Brunauer-Emmet-Teller
BIS	Bureau of Indian Standard
EDX	Energy Dispersive X-ray spectroscopy
FTIR	Fourier Transform Infra Red Spectrophotometer
ICP-MS	Inductively Coupled Plasma Mass Spectrometer
MTZ	Mass Transfer Zone
PSD	Pore Size Distribution
SEM	Scanning Electron Microscopy
SFAA	Sawdust impregnated with ferric hydroxide and activated alumina
UNICEF	United Nations Children's Fund
WHO	World Health Organization
XPS	X-ray Photoelectron Spectroscopy

LIST OF SYMBOLS

ϕ	Particle size (mm),
τ	Time required for 50% adsorbate breakthrough (min)
ΔG^o	Standard free energy (kJ/mol)
ΔH^o	Standard enthalpy (kJ/mol)
ΔS^o	Standard entropy change (kJ/mol.K)
C_{As}	Concentration of arsenic (mg/L)
C_e	Equilibrium concentration (mg/L)
C_F	Concentration of fluoride (mg/L)
C_0	Initial concentration of solute (mg/L)
C	Final concentration of solute (mg/L)
D_i	Diffusion coefficient (cm^2/s)
F	Fractional capacity
H	Bed height (cm)
H_{MTZ}	Height of the mass transfer zone (cm)
K_1	Pseudo first order rate constants for adsorption (1/min)
K_2	Pseudo second order rate constants for adsorption (g/mg.min)
K_{BA}	Bohart-Adam model constant (L/mg.min),
K_C	Clark model constant (L/mg.min)
K_D	Distribution coefficient (L/Kg)
K_F	Freundlich constant [(mg/g) (L/mg) $^{1/n}$]
K_{id}	Intra particle diffusion rate constant (mg/g .$min^{0.5}$)
K_L	Langmuir constant (mg/g)
k_s	External mass transfer rate constant (1/min).
k_{Th}	Thomas model constant (L/mg.min)

K_{YN}	Yoon-Nelson model constant (1/min)
m	Mass of adsorbent (g)
n	constant
N_0	Saturation concentration (mg/L)
q_e	Equilibrium uptake (mg/g)
q_{exp}	Experimental equilibrium uptake (mg/g)
q_t	Adsorption capacity at time 't' (mg/g)
q_∞	Equilibrium uptake at infinite time (mg/g)
Q	Volumetric flow rate (mL/min)
R	Universal gas constant (J/mol.K)
R^2	Coefficient of determination
S_{BET}	BET Surface area (m^2/g)
S_m	Amount of solute removed by the adsorption zone at complete exhaustion (g)
S_Z	Solute that removed by the adsorption zone from breakthrough to exhaustion (g)
t_E	Exhaustion time (min)
t_B	Breakthrough time (min)
ν	Linear velocity (cm/min).
$V_{meso+micro}$	Meso and micro pore volume (cm^3/g)
V_{micro}	Micropore Volume (cm^3/g)
V_{meso}	Mesopore Volume (cm^3/g)
S_{meso}	Mesopore surface area (m^2/g)
S_{micro}	Micropore surface area (m^2/g)
V_{macro}	Macropore Volume (cm^3/g)
S_{macro}	Macropore surface area (m^2/g).
U_Z	Rate of movement of mass transfer zone (cm/min)
% Sat	Percentage saturation.

1 INTRODUCTION

Water is essential for survival of life. About 60 percent of the weight of the human body is water. In many parts of the world, water is a limited resource. About 71 percent of the earth's surface is water, but unfortunately 97 percent of it is sea water. Of the remaining, 2 percent is locked in icecaps and glaciers and only 1 percent is available for drinking [1]. With the onset of industrialization, pollution of groundwater became a threatening menace to the health of mankind.

1.1 WATER QUALITY AND ITS LIMITS

Both groundwater and surface water become polluted as a result of the improper management of wastes and natural dissolution of minerals. Access to safe drinking water is essential to health, a basic human right and hence is an important component of any effective policy for health protection. Safe drinking water, as defined by the guidelines, is that, which does not represent any significant risk to health over a lifetime of consumption. Around the world, millions of people still lack access to safe drinking water. During recent years there has been an increasing awareness of, and concern about, water pollution and new approaches for achieving sustainable exploitation of water resources have been developed internationally. In a number of industrialized countries, as well as some countries in transition, it has become a common practice to base limits for discharges of hazardous substances taking into account the best available technology. Such hazardous water pollutants include substances that are toxic at low concentrations, carcinogenic, mutagenic, teratogenic and/or can be bio-accumulated, especially when they are persistent. In order to reduce inputs of phosphorus, nitrogen and pesticides from non-point sources (particularly agricultural sources) to water bodies, environmental and agricultural authorities are advocating the use of best environmental practices [2].

Surface waters (rivers and reservoirs) and groundwater are the two basic sources of drinking water. All waters contain natural contaminants, particularly inorganic contaminants that arise

from the geological strata (erosion of soils and rocks, natural weathering reactions and volcanic emissions) and, to a varying extent, anthropogenic pollution by both microorganisms and chemicals. In general, groundwater is less vulnerable to pollution than surface waters [3]. As per the Bureau of Indian Standards, the maximum acceptable limits for drinking water are: iron : 0.3 mg/L, aluminium : 0.03 mg/L, arsenic : 0.01 mg/L and fluoride : 1 mg/L [4]. Environmental Protection Agency prescribes iron : 0.3 mg/L, aluminium : 0.05-0.2 mg/L, arsenic : 0.01 mg/L and fluoride : 2 mg/L as drinking water standards [5]. World Health Organization (WHO) 2011 guidelines for drinking water are: iron : 0.3 mg/L, aluminium : 0.2 mg/L, arsenic : 0.01 mg/L, and fluoride : 1.5 mg/L [6]. European Union regulations for drinking water are: iron : 0.2 mg/L, aluminium : 0.2 mg/L, arsenic : 0.01 mg/L and fluoride : 0.8-1.5 mg/L.

1.2 ARSENIC AND FLUORIDE-OCCURRENCE AND HEALTH EFFECTS

Arsenic ranks 20th in natural abundance and 14th in case of sea water abundance [7]. Total amount of arsenic in the upper earth crust is estimated to be 4.01 $\times 10^6$ kg with an average of 6 mg/kg. Oxide and sulfide minerals of arsenic are: arsanolamprite, arsanlite (As_2O_3), realgar (AsS), uzonite (As_4S_5), dimorphite (As_4S_3), duranusite (As_4S) [8]. Arsenic finds its way into surface and groundwater by erosion of arsenic containing rocks or industrial and mine discharges. One important mechanism through which the groundwater is polluted with arsenic is the reduction of iron oxyhydroxide (FeOOH) by bacteria and subsequent desorption of arsenic from the iron surfaces. In the Bengal Basin (part of Bangladesh and West Bengal), it is the main mechanism by which groundwater becomes contaminated with arsenic [9]. However, inorganic arsenic is predominant in natural water and is the most likely form of arsenic to exist at concentrations that cause regulatory concern [10, 11]. Arsenic contaminated drinking water has been found in Argentina, Chile, Mexico, USA, China, Hungary, India (West Bengal), Bangladesh, Romania and Vietnam [12], Southeast Asian delta being the most severely arsenic affected region. Of these, West Bengal and Bangladesh are seriously affected in terms of the size of the population at risk and the magnitude of the health problems [13].

Table 1.1 Arsenic concentration of groundwater across the globe

Country/ Region	**Population (lakhs)**	**As conc. (µg/L)**	**Environmental conditions**
Argentina	2.0	<1 to 9900	Natural; loess and volcanic rocks, thermal springs; high alkalinity
Bangladesh	30	<1 to 2500	Natural; alluvial/deltaic sediments with high phosphate, organics
Bolivia	0.50	–	Natural; similar to Chile and parts of Argentina
Brazil	–	0.4 to 350	Gold mining
Canada (Moira Lake, Ontario)	–	50 to 3000	Mine tailings
Chile	4.0	100 to 1000	Natural and anthropogenic; volcanogenic sediments; closed basin lakes, thermal springs, mining
Germany	–	<10 to 150	Natural: mineralized sandstone
Ghana	<1.0	<1 to 175	Anthropogenic and natural; gold mining
Greece	1.50	–	Natural and anthropogenic; thermal springs & mining
India (W. Bengal)	60	<10 to 3200	Similar to Bangladesh
Inner Mongolia	1.0 to 6.0	<1 to 2400	Natural; alluvial and lake sediments; high alkalinity
Mexico	4.0	8 to 620	Natural and anthropogenic; volcanic Sediments, mining
Southern Carson Desert Nevada	–	up to 2600	Holocene mixed Aeolian, alluvial, lacustrine sediments, some thin volcanic ash bands
Spain	>0.5	<1 to 100	Natural; alluvial sediments
Taiwan	1.0 to 2.0	10 to 1820	Natural; coastal zones, black shales
Thailand	0.15	1 to 5000	Dredged Quaternary alluvium (some problems in limestone), mine tailings
Tulare Basin, San Joaquin Valley, California	–	<1 to 2600	Holocene and older basin fill sediments
United Kingdom, southwest England	–	<1 to 80	Mining
USA and Canada	–	<1 to >100000	Natural and anthropogenic; mining, pesticides, As_2O_3 stockpiles, thermal springs, alluvial, closed basin lakes, various rocks
USA (Fairbanks, Alaska)	–	up to 10000	Schist, alluvium, mine tailings
Vietnam	>10	1 to 3050	Natural; alluvial sediments
Xinjiang, Shanxi	>0.005	40 to 750	Natural; alluvial sediments

According to a UNICEF report [14], a total of 4.7 million tube wells in Bangladesh have been tested and 1.4 million of these were found to contain arsenic above the government drinking water limit of 50 parts per billion. Two main rivers of Northern Chile, the Loa River and the Lluta River, have As concentrations of around 1400 and 240 µg/L respectively [15]. In sea water, the concentration of arsenic varies between 0.09 µg/L and 24 µg/L, and in freshwater not polluted by arsenic, it varies between 0.15 µg/L and 0.45 µg/L. In mineral and thermal waters, the average concentration of arsenic increases by a factor of up to 300 as compared to groundwater [16, 17]. Arsenic concentration of groundwater globally is given in Table 1.1.

Fluorine is the most highly reactive element of the halogen family. It has been estimated that fluorine is the 17th most abundant element constituting about 0.065% of the earth's crust. In India, fluoride commonly occurs in earth's crust as fluorspar (CaF_2), appetite and rock phosphate and phosphorites. These fluoride minerals are nearly insoluble in water. Weathering of these minerals, along with volcanic and fumarolic processes, leads to higher fluoride levels in groundwater. The most well known and documented area associated with volcanic activity follows the East African Rift system from the Jordan valley down through Sudan, Ethiopia, Uganda, Kenya and the United Republic of Tanzania. Many of the lakes of the Rift Valley system, especially the soda lakes, have extremely high fluoride concentrations; 1640 mg/L and 2800 mg/L respectively in the Kenyan Lakes Elmentaita and Nakuru [18], and up to 690 mg/L in the Tanzanian Momella soda lakes [19]. Fluorides of monovalent cations such as NaF and KF are water soluble, while those of divalent cations such as CaF_2 and PbF_2 are generally insoluble. Small amounts of fluorides are found in seawater, bones and teeth. Fluoride is widely distributed in the geological environment [20] and generally released into the groundwater by slow dissolution of fluorine-containing rocks [21]. Various minerals, e.g., fluorite, biotites, topaz, and their corresponding host rocks such as granite, basalt, syenite, and shale, contain fluoride that can be released into the groundwater [22-25].

Table 1.2 Fluoride concentration of groundwater across the globe

Country/ Region	Fluoride conc. (mg/L)	Environmental conditions
Argentina	0.03-29	Quaternary loess, La Pampa
Canada	0.02-28	Carboniferous clastic rocks, Gaspe
China	1.0-7.8	Quaternary sands, Hunchun basin, northeast China
Ethiopia	6.1-20	Volcanic bedrock (Wonji/Shoa area), Pleistocene sediment above volcanic bedrock (Wonji/Shoa)
France	3.8-8.0, 1.9-7.0	Vichy water; Plombieres springs
Germany	0.01-8.9	Cretaceous Chalk Marls
Ghana	1.07	Crystalline basement. Including granite and meta sediment
India	<20	Crystalline basement, Andhrapradesh; Quaternary alluvium Agra, Uttarpradesh
Kenya	141-166	Hot spring, Lake Elmentaita & Lake Nakuru:1640, 2800 mg/L
Libya	0.63-3.6	Miocene, Upper Sirte Basin
New Zealand	0.3-8.4	Geothermal springs
Norway	1.89	Caledonian basic and ultra basic rocks
Portugal	0.04-20.5	Rio Vouga hot springs
Senegal	0.1-12.5	Granitoids, pelites, schists, amphibolites, Palaeocene sediments
South Africa	0.1-10	Western Bushveld Complex
Sri Lanka	0.02-10	Crystalline basement, including granite and charnockite
Sudan	0.29-6.2	Cretaceous, Nubian Sandstone (Butana area)
Taiwan	7.3	Spring, Tatun
Tanzania	40-140; 330, 690	Ngorongoro Crater and Lemagrut volcanic cone , Kimberlites, Shinyanga, Lake Natron thermal springs, Lake Momella
Tunisia	0.1-2.3	Cretaceous to Quaternary sediments
United Kingdom	0.1-5.8	Cretaceous Chalk, London Basin
USA	0.05-5.9 0.8-30.8	Carboniferous sediments, Ohio; Western state geothermal springs

Thus, groundwater is a major source of human intake of fluoride. In seawater, a fluoride concentration of 1.3 mg/L has been reported. In groundwater, fluoride concentrations vary with the type of rock the water flows through but do not usually exceed 10 mg/L [26]. Fluoride concentrations in the groundwater of some villages in China were greater than 8 mg/L. In the Rhine in the Netherlands, levels are below 0.2 mg/L [19]. More than 25 countries across the world have high fluoride concentration in drinking water sources [27]. Fluoride concentrations of groundwater globally are given in Table 1.2.

Arsenic is classified as a Group I carcinogen [28] and severe health effects have been observed in populations all over the world drinking arsenic rich water for long periods [29]. Arsenic exposure (> 50 µg/L) via drinking water is related to cancer of lung, kidney, bladder and liver. Skin cancer is caused by exposure to low arsenic concentrations (< 50 µg/L) [30]. Effects on vascular system have also been observed, including peripheral vascular disease, which in its most severe form, results in gangrene or Blackfoot Disease. Other potential effects include neurologic impairment [31]. Therefore, the presence of arsenic in water supply poses a serious risk to human health. The higher the exposure to arsenic, the higher the blood levels of asymmetric dimethylarginine (ADMA) amino acid, which is associated with problems in the arteries and leads to a cardiovascular risk [32]. Those who consume arsenic contaminated water for a long time since childhood, have a greater chance of cardiovascular problems at a young age and development of diabetes [33]. Lifetime exposure to low-level (15-20 µg/L) inorganic arsenic in drinking water was associated with increased risk for Coronary Heart and Cardio Vascular diseases [34, 35].

Excessive intake of fluoride, mainly through drinking water, is a serious health hazard affecting humans worldwide. Fluorosis is a common symptom of high fluoride ingestion manifested by mottling of teeth in mild cases and embrittlement of bones and neurological damage in severe cases. The symptoms of skeletal fluorosis are pain in neck, back bone or joints, stiffness in the neck, backbone or joints, severe pain and rigidity in the pelvic girdle. Construction of vertebral

canal and intervertebral forearm exerts pressure on nerves and blood vessels leading to paralysis and pain. Skeletal fluorosis is an irreversible process similar to dental fluorosis [36, 37]. Further, high fluoride intake has been reported to a range of cause health problems including cancer, impaired kidney function, digestive and nervous disorders, reduced immunity, Alzheimer's disease, nausea, adverse pregnancy outcomes, respiratory problems, lesions of the endocrine glands, thyroid, liver and other organs [38, 39].

1.3 ARSENIC CHEMISTRY AND SPECIATION

Arsenic is a metalloid- a natural element that is not actually a metal but which has some of the properties of a metal. Arsenic has atomic number of 33, atomic weight of 74.92, with symbol As and is placed in the group Va of the periodic table of elements together with Nitrogen, Phosphorus, Antimony and Bismuth. Arsenic is a redox-sensitive element; it can change its form through reduction (gain of an electron) or oxidation (loss of an electron). Its occurrence, distribution, mobility, and forms rely on the interplay of several geochemical factors, such as pH conditions, reduction-oxidation reactions, distribution of other ionic species, aquatic chemistry and microbial activity [40]. Arsenic occurs in 5 different valence states: arsine (-3), Elemental arsenic (0), arsonium metals (+1), arsenites (+3), arsenates (+5) [41].

In water, arsenic is predominantly in the arsenate - As(V) form. Arsenite - As(III), when present, is readily oxidized to arsenate in aerobic waters at pH values above 7.0. Conversely, arsenate can be reduced to arsenite at low pH values. Arsenite is considerably more toxic than the pentavalent - As(V) form, although it has been demonstrated that As(V) is better absorbed by the human body because it tends to react less with the membranes in the gastrointestinal tract [42]. Iron, copper, manganese, aluminum, calcium and magnesium metal ions have been used in an attempt to trap and remove arsenic species from drinking water. Metal salts of arsenite and arsenate have widely different solubilities: arsenate salts are less soluble than arsenite. It is reported that in Bangladesh, more than 60% of arsenic in groundwater occurs in As(III) (arsenite) form [16].

Groundwater is in anoxic conditions and arsenic is found in its arsenite or reduced trivalent form As(III). Surface water generally has aerobic conditions and arsenic is found in its oxidized pentavalent form (arsenate). Both arsenite and arsenate exist in four different species. The speciation of these molecules changes by dissociation and is pH dependent. The kinetics of dissociation for each is nearly instantaneous. The pH dependencies of arsenate and arsenite are depicted in Fig.1.1 and Fig.1.2, respectively.

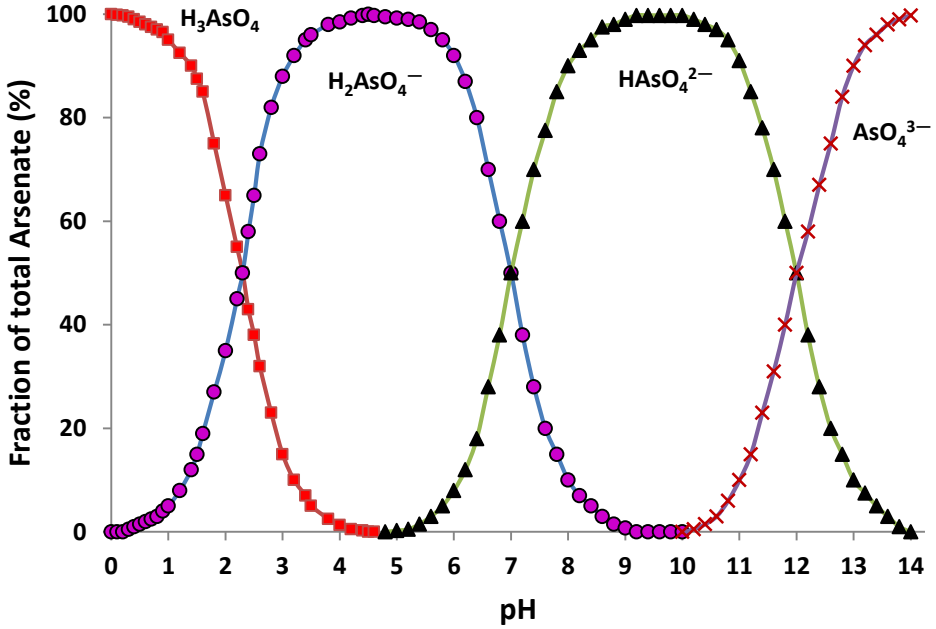

Fig.1.1. Dissociation of Arsenate [As(V)]

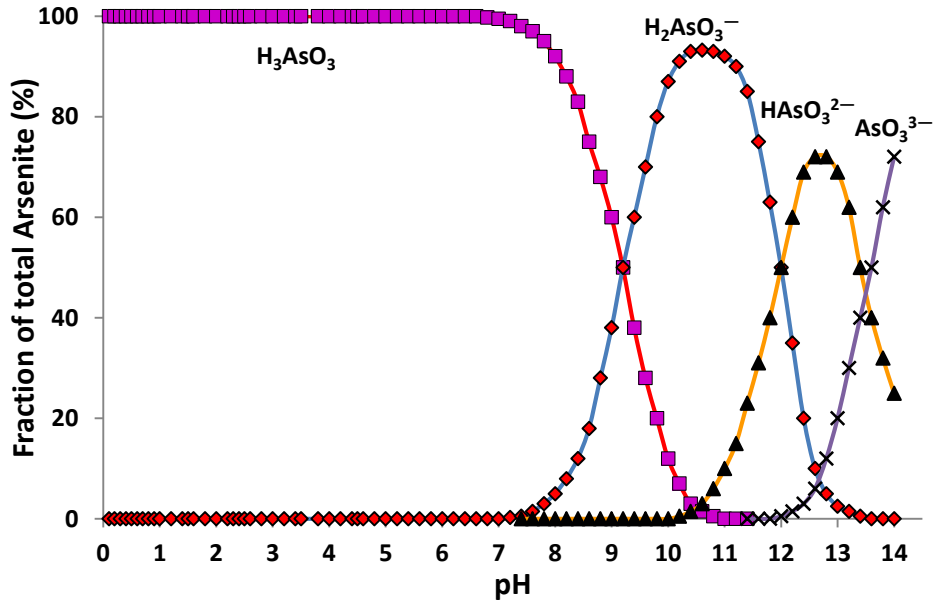

Fig.1.2. Dissociation of Arsenite [As(III)]

Chemical speciation is a critical element of arsenic treatability. Negative surface charges facilitate removal by adsorption, anion exchange, and co-precipitative processes. Since the net charge of As(III) is neutral at natural pH levels (6-9), this form is not easily removed. However, the net molecular charge of As(V) is negative (-1 or -2) at natural pH levels, enabling it to be removed with greater efficiency. High percentage of $H_2AsO_4^-$ and $HAsO_4^{2-}$ species are present in the pH range 2.7–11.5. Conversion to As(V) is a critical element of most arsenic treatment processes. This conversion can be accomplished by adding an oxidizing agent such as chlorine or permanganate [43]. As(V) exists in four forms in aqueous solution based on pH: H_3AsO_4, $H_2AsO_4^-$, $HAsO_4^{2-}$, and AsO_4^{3-}. Similarly, As(III) exists in five forms: $H_4AsO_3^+$, H_3AsO_3, $H_2AsO_3^-$,$HAsO_3^{2-}$, and AsO_3^{3-}. The ionic forms of As(V) dominate at pH >3, and As(III) is neutral at pH <9 and ionic at pH >9.

1.4 PROCESSES FOR REMOVAL OF ARSENIC FROM GROUNDWATER

1.4.1 Oxidation /Reduction

Most treatment methods are effective in removing arsenic in pentavalent form and hence the processes include an oxidation step as pretreatment to convert arsenite (trivalent) to arsenate (pentavalent). Arsenite can be oxidized by oxygen, ozone, free chlorine, hypochlorite, permanganate, hydrogen peroxide and Fulton's reagent, but atmospheric oxygen, hypochloride and permanganate are commonly used for oxidation in developing countries. The oxidation processes convert predominantly noncharged arsenite to charged arsenate, which can be easily removed from water [44].

1.4.2 Lime softening

Arsenic is removed by the addition of quick lime [CaO] or hydrated lime [$Ca(OH)_2$] in the process called lime softening. Lime treatment is a process similar to coagulation with a metal salt. The precipitated calcium hydroxide [$Ca(OH)_2$] acts as a sorbing flocculent for arsenic. Excess of lime will not dissolve, bu77t remains as a coagulant aid, which has to be removed along with precipitates through sedimentation and filtration. It has been observed that arsenic

removal by lime is relatively low, usually between 40-70%. The highest removal is achieved at pH 10.6 to 11.4 [45]. Lime softening may be used as a pretreatment to be followed by alum or iron coagulation. Lime softening operated within the pH range of greater than 10.5 is likely to provide a high percentage of As removal for influent concentrations of 50 µg/L. However, it may be difficult to reduce consistently to 1.0 µg/L by lime softening alone, necessitating secondary treatment. Removal of As(III) and As(V) are low at pH less than 10; however, removal of As(V) approaches 100% and removal of As(III) approaches 75% at pH greater than 10.5 [46].

1.4.3 Coagulation

Using coagulation technology, it is possible to reduce arsenic from 400 µg/L to 10 µg/L at a rate of 500 L/sec, by controlling pH, oxidising and coagulation agents [47]. Coagulation-flocculation processes using alum, ferric chloride, or ferric sulphate are effective at removing arsenic. They are the most well known arsenic treatments and have been extensively tested in both laboratory and field studies [48]. When added into water, the chemicals dissolve under efficient stirring for one to few minutes. During this flocculation process, all kinds of micro-particles and negatively charged ions are attached to the flocs by electrostatic attachment. Arsenic is also adsorbed onto coagulated flocs. It can be removed partially by sedimentation, while filtration may be required to ensure complete removal of flocs. Removal of arsenic by coagulation is mainly controlled by pH and coagulant dose. Coagulation with ferric chloride works best at pH below 8 and Alum has a narrower effective range from pH 6 to 8 [49].

1.4.4 Ion Exchange

Ion exchange was investigated for arsenic removal by several researchers. Issa et al. [50] investigated three types of resins: a strong base anion exchange (SBAE) and two hybrid (HY) resins: HY-Fe and HY-AgCl for the removal of arsenic in natural and wastewater. Donia et al. [51] investigated the glycidyl methacrylate/methelene bisacrylamide resin with immobilized tetra ethylene pentamine ligand was used to adsorb As(V). The regeneration efficiency of the loaded resins was found to be 99 and 98% for RI and RII. He et al. [52]

prepared a new cerium-loaded cation exchange resin by impregnating cerium into the cation exchange resin.

1.4.5 Electro coagulation/dialysis

Electrodialysis Reversal (EDR) was reported to achieve removal efficiencies of 80%. One study demonstrated removal of arsenic to 3 µg/L from an influent concentration of 21 µg/L [53]. The Fe-Al-Al-Fe electrode pairs gave the highest arsenic removal efficiency (96%; 6.30 µg/L) at the lowest operating time (1 min) in a batch Electro Coagulation process, thus reducing arsenic levels to lower than the permissible level -10 µg/L [54].

1.4.6 Reverse Osmosis and Nanofiltration

Reverse Osmosis (RO) provided removal efficiencies of greater than 95% when operated at ideal pressures. Discharge of reject water or brine may be a concern. Increased water recovery, defined as the volume of water produced by the process divided by the volume of influent stream, can lead to increased costs for removal of arsenic [55, 56]. Nanofiltration (NF) was capable of removal of arsenic over 90%. The recoveries ranged between 15 and 2%. A recent study showed that the removal efficiency dropped significantly during pilot-scale tests, where the process was operated at more realistic recoveries. Nanofiltration (NF) is a promising technology for removal of arsenic, since it requires less energy than traditional reverse osmosis membranes. In a recent study, the removal of arsenic from synthetic waters by nanofiltration membranes was investigated [57]. The studies included variation of arsenic feed concentration, pH, and existence of other ionic compounds.

The possible influence of natural organic matter on As(V) rejection by nanofiltration membranes was also explored. The study showed that nanofiltration point-of-use (POU) systems were particularly suitable to treat arsenic-rich groundwater in suburban China. Magnetite nanocrystals were also reported to be useful in arsenic remediation [58]. Microwave-assisted synthesis of the cellulose-carbonated hydroxyl apatite nano composites (CCHA) with CHA nanostructures dispersed in the cellulose matrix was carried out by using cellulose solution, $CaCl_2$, and

NaH_2PO_4. As(V) adsorption onto the synthetic CCHA was an endothermic process indicating As(V) adsorption capacity increased with an increase in reaction temperature [59]. Multiwall boron nitride nanotubes (BNNTs) functionalized with Fe_3O_4 nanoparticles (NPs) were used for removal of arsenic from water solutions possessing high surface area, open tube ends, and well-crystallized Fe_3O_4. NPs coating exhibited high adsorption capacity to inorganic As(V) [60]. Aluminium doped nano manganese copper ferrite (average size of 13 nm) was used as an adsorbent for the removal of arsenic from aqueous solution [61]. Novel nano-composite materials, where iron nanoparticles are embedded into the walls of a macroporous polymer were effective in removing of As(III) from aqueous solution [62].

Oxidized micro/mesoporous activated carbon was used as a support for the deposition of iron oxyhydroxide and was tested for adsorption of arsenate from water phase [63]. Modification of LECA (light expanded clay aggregate) with Fenton reagent removed arsenite and arsenate ions from an aqueous solution [64]. The presence of chromate significantly increased the removal efficiency of arsenate by Fe(II) at pH 6–8 [65]. TiO_2 is one of the most promising materials for removal of arsenic from groundwater by adsorption based processes. The TiO_2 surface is capable of photo-catalytic oxidation (PCO) changing the arsenite [As(III)] to arsenate [As(V)], which is more easily adsorbed by the surface [66]. Ferric-impregnated volcanic ash (FVA), which consisted mainly of different forms of iron and aluminum oxide minerals was developed for arsenate removal from an aqueous medium [67]. Synthesized magnetic wheat straw (MWS) with Fe_3O_4 could be used for adsorption of arsenic from water, and could be easily separated by applied magnetic field [68]. A solid phase preconcentration procedure using hybrid sorbent based on nano zirconium dioxide–boron oxide for the speciation and determination of As(III), As(V) and total in water by atomic absorption spectrometry (HGAAS) was presented [69].

1.4.7 Biosorption

Water hyacinths reduced the arsenic level from a typical Bangladeshi well water concentration (300 ppb) to U.S. EPA's proposed drinking water standard (10 ppb) for one trial, to the

Bangladeshi drinking water standard (50 ppb) for two trials and lost all ability to remove arsenic after five trials [70]. Phytofiltration involves the use of plants to remove toxic compounds from water. A laboratory-constructed hydroponic system was employed to characterize phytofiltration for the uptake of arsenic and macronutrients by two arsenic hyper accumulators, Pteris cretica cv Mayii (Moonlight fern) and Pteris vittata (Chinese brake fern) [71]. The biomass of Calotropis procera roots and aerial parts brought the level of arsenic in arsenic contaminated water to the EPA standard (10 µg/L) within a very short time and more effectively than biomass of roots and aerial parts of Pteris vitata and Eichhornia crassipes [72]. Saccharomyces cerevisiae BU-MBT-CY1 isolated from coconut shell sap was used for both removal of arsenic and microbial decontamination of drinking water in water purification plant [73]. Urick et al. (2009) studied biosorption of arsenic from natural and model waters by native or chemically modified (with urea or ferric oxyhydroxides) plant biomass prepared from sawdust of Picea abies. The maximum biosorption capacity of the sawdust modified with ferric oxyhydroxides, evaluated by Langmuir adsorption model, was 9.26 mg/g [74]. Biogenic schwertmannite by Acidithiobacillus ferro oxidants gives efficient adsorption capacity of 113.9 mg As(III) at pH 7.5 [75].

1.4.8 Adsorption

Adsorption on a solid adsorbent, usually in dispersed form, has been especially prominent. The main adsorbents of choice have been iron oxides, modified iron oxides and hydroxides, aluminium oxide and hydroxide, layered double hydroxides, and also silica, carbon, and organic polymers either as adsorbents in their own right or as supports for other active materials. Approaches for removal of arsenic were reviewed by several researchers [48, 76-85]. Various iron oxy-hydroxides were synthesized in a continuous flow kilogram-scale production reactor through the precipitation of $FeSO_4$ and $FeCl_2$ to serve as arsenic adsorbents [86]. Iron hydroxide has better selectivity towards As(V) in the presence of other anions (especially phosphate) than aluminum hydroxide [87]. Use of granular ferric hydroxide (GFH) was examined for removal of both arsenate [As(V)] and arsenite [As(III)] from drinking water. Kinetic studies were conducted

as a function of pH, and arsenic concentration of less than 5 μg/L was achieved from an initial concentration of 100 μg/L for both As(III) and As(V) with GFH at a pH of 7.6, which is in the pH range typically encountered in drinking water supplies. In the isotherm studies, the observed data fitted well to both the Freundlich and the Langmuir models [88]. Three commercially available adsorbents used for removal of arsenic (E33, GFH and Metsorb) and its adsorption capacity were tested. Results indicated that GFH was more susceptible to water quality changes than Metsorb and E33 under conditions tested. GFH also adsorbed more anions than the other two media [89].

Iron–zirconium (Fe–Zr) binary oxide adsorbent was amorphous with a specific surface area of 339 m^2/g. It was effective for both As(V) and As(III) removal; the maximum adsorption capacities were 46.1 and 120.0 mg/g [90]. As(V) has long been known to be strongly adsorbed by aluminium hydroxides, whereas As(III) is considerably less readily adsorbed [91-94]. Iron hydroxide is usually considered to be a superior arsenic adsorbent when compared to aluminium hydroxide [92, 95, 96], but iron(III) hydroxide can release arsenic if its environment causes it to be reduced to soluble iron(II) hydroxide [97]. Zeng investigated arsenate and arsenite adsorption on an iron(III) oxide/silica adsorbent that had a Fe/Si molar ratio of 3 [98]. It was reported that the adsorption of arsenite was faster than that of arsenate. The equilibrium adsorption capacity for As(III) was larger than that for As(V). The capacity for both As(III) and As(V) increased with temperature. The arsenate adsorption significantly reduced at pH above 7.5, while the arsenite adsorption was almost independent of pH in the range of 3-9.

Masue et al. (2007) studied the adsorption of As(V) and As(III) by combined aluminum-iron(III) oxyhydroxide adsorbents. It appeared from Masue's work [99] that 1:1 iron-aluminum mixtures either behaved the same way as ferrihydrite alone or were less effective adsorbents. Aluminum hydroxide was consistently less effective than iron(III) hydroxide or iron-aluminum mixtures except, for As(V), in acidic solution [99]. Guo et al. (2007) prepared a new adsorbent by loading iron oxyhydroxide (b-FeOOH) on bead cellulose. Both arsenite and arsenate were strongly and

specifically adsorbed by akaganeite adsorptive centers by an inner-sphere mechanism [100]. Jia et al. (2003) found large differences in the adsorption of As(V) on ferrihydrite precipitated from nitrate or sulphate solution. In addition to chloride, sulphate and nitrate, species in natural water which compete with arsenate and arsenite for adsorption on ferrihydrite and other adsorbents include hydroxide, carbonate, phosphate, fluoride, silicate and organic species [101].

An alternative to adsorption is precipitation of arsenic compounds followed by filtration, but this process is slower and less effective in removing arsenic salts than adsorption [102]. Both carbonate and ferrous iron are often present at high concentrations in groundwater and influence the sorption of arsenic [103]. A synthesized Fe-Al binary oxide has better adsorption capacity for As(V) and As(III) than iron(III) oxide or aluminium oxide, accepting four times as much adsorbed arsenic as either single-metal oxide. It has been attributed to the large surface area of the binary oxide [104]. Iron-oxide-coated natural rock (IOCNR) an adsorbent of arsenic from real arsenic-bearing groundwater collected from the Lanyang Plain, North East Taiwan [105].

Zeng et al., (2003) studied the preparation of iron(III)-based binary oxide adsorbents in a granulated form for removal of arsenic. The key step in the method was the simultaneous generation of hydrous ferric oxide (FeOOH) solution and silica solution in situ in one reactor. This eventually led to the formation of Fe-Si complexes. The addition of silica enhanced the granulated adsorbent strength but reduced the arsenic adsorption capacity [106]. Mesoporous Alumina (MA) with a wide surface area (307 m^2/g) and uniform pore size (3.5 nm) was prepared [107] and a sponge like interlinked pore system was developed through a post hydrolysis method. The resulting MA was insoluble and stable within the range of pH 3-7. The maximum uptake of As(V) by MA was found to be 7 times higher [121 mg of As(V)/g and 47 mg of As(III)/g] than that of conventional AA, 0.05 M NaOH was found to be the most suitable desorption agent [107]. Abedin et al. (2009) found that Zero Valent Iron(ZVI) was more practical and promising to mitigate arsenic from the contaminated water resources especially groundwater [108].

Pajany et al. (2009) studied the adsorption of arsenic onto commercially available goethite and haematite [109]. Asta et al. (2009) investigated arsenic adsorption on synthetic goethite and jarosite at acidic pH (1.5-2.5) at two ionic strengths (0.02-0.15 mol/dm^3, NaCl) and at sulphate concentrations in the range of $5x10^{-3}$ to $2.8x10^{-1}$ mol/dm^3 [110]. Iron oxide coated sponge (IOCSp) is used in removal of arsenic. It was found that maximum adsorption capacity of IOCSp for As(III) and As(V) calculated by Sips isotherm was 4.2 and 4.6 mg/g of IOCSp, respectively [111]. Zhu et al [112] found that nano-sized zero-valent iron is an effective adsorbent for removal of arsenic from drinking water. The adsorption capacity of the synthesized sorbent for arsenite and arsenate at pH 6.5 calculated from Langmuir adsorption isotherms in batch experiments was 18.2 and 12.0 mg/g, respectively.

Rahmani et al. [113] was conducted experiments for As(III) removal, which one of the most poisonous groundwater pollutants, by synthetic nano size zero-valent iron (nZVI). Up to 99.9% removal efficiency for As(III) was obtained by nZVI . Fe(III)-modified montmorillonite (Fe-M) is a porous sample with Fe(III) present as a mix of monomeric and polymeric Fe(III) species in the interlayer and on the external surface. These Fe(III) species were responsible for arsenate adsorption [114]. Gang et al. [115] studied a newly developed iron-impregnated chitosan granular adsorbent to evaluate its ability to remove arsenic from water. At pH 8 the maximum adsorption capacity reached 6.48 mg/g, with initial As(III) concentration of 1007 µg/L. Based on batch experiments more than 60% of the arsenic was adsorbed by the iron-chitosan within 30 min of contact time.

A variety of synthetic zeolites were investigated for removal of arsenic from water [116]. Zeolite NH_4^+/Y(NY6) showed significant arsenate removal capacity over a wide initial pH range of 2-12. Although arsenic was poorly adsorbed by freshly precipitated aluminium hydroxide, As(III) was strongly adsorbed on activated alumina at pH 7-8 whereas arsenate [As(V)] was best adsorbed at pH 5-6 [117]. Mohan et al. [80] is a review paper and they have incorporated most of the valuable available literature on arsenic remediation by adsorption (~600 references). Existing

purification methods for drinking water; wastewater; industrial effluents, and technological solutions for arsenic have been listed. Sorption of arsenic by commercially available carbons and other low-cost adsorbents are surveyed and critically reviewed and their sorption efficiencies are compared. Adsorption of arsenic behavior in presence of other impurities has been discussed. Some commercially available adsorbents are also surveyed [80].

Setyono and Valiyaveettil incorporated lanthanum/ zirconium oxide nanoparticles in sawdust and used it for the removal of arsenic anions from water [118]. Nagarnaik et al.[119] used sawdust carbon at room temperature (25 ± 1°C) for the removal of As(III) by adsorption. Silicic acid and organic compounds that form complexes with iron(III), interfere substantially in arsenic adsorption on ferrihydrite and related materials [120]. Auffan et al. (2008) notified that when normalized per unit of surface area, the quantity of arsenic adsorbed at the maghemite surface remains constant for particles between 20 to 300 nm. However, nanoparticles smaller than 20nm exhibit enhanced adsorption capacity [121]. Liu et al. [122] studied the characteristics of adsorption of arsenic with the magnetism ferromanganese oxide compound (MFO). As(III) and As(V) were effectively removed by MFO via adsorption.

Alum-impregnated activated alumina has been reported to be a much better adsorbent for As(V) than untreated activated alumina in the pH range 2.8-11.5, and when employed in batch mode arsenate [As(V)] concentration could be brought down from 10 mg/L (10,000 ppb) to 0.04 mg/L (40 ppb) [123, 124]. Guan et al. (2009) used an iron(II)-$KMnO_4$ solution to provide an iron(III)hydroxide as an adsorbent in order to study the influence of competitors for adsorption of arsenic introduced as As(III) in the pH range 4-9. It was reported that the influence of competing species on the adsorption of arsenic was in the order phosphate > humic acid (HA) > silicate > sulphate, and that the interference, especially by humic acid, increased at more alkaline pH [125]. Yavuz et al. [58] have proved magnetite nanocrystals to be useful in arsenic remediation and could feasibly be synthesized by a thermal decomposition method that employs refluxing of FeOOH and oleic acid in 1-octadecene in a laboratory setup.

Calcined LDHs can adsorb anions by a more powerful mechanism than simple ion exchange because of a "memory effect" in which the pyrolysed residue, when brought into contact with an aqueous medium, is able to reconstitute the original LDH along with anions present in the supernatant solution. Adsorption of arsenic on layered double hydroxides has been reported by various researchers [126-130]. A novel $KMnO_4$-modified form of iron oxide, MnBT-4, using a fluidized bed reactor (FBR) was reported for the adsorptive removal of As(III) and As(V) [131]. Novel composite adsorbents for As(V) removal from aqueous solution were synthesized by successfully incorporating α-MnO_2 nano rods and γ-Fe_2O_3 nanoparticles onto ball-milled expanded perlite carrier material. The materials prepared in this work are suitable adsorbents for the removal of As(V) from drinking water due to their high adsorption capacity, natural availability and relatively low cost of the carrier material [132].

Magnetic binary oxide particles (MBOP) synthesized using chitosan template have been used for the removal of arsenic from aqueous system [133]. Studies on the adsorption kinetics of As(V) onto nano sized iron oxide-coated perlite reported that a 100% As(V) adsorption was achieved at pH value of 4–8 from the initial concentration containing 1.0 mg-As(V)/L [134]. The mechanism of arsenate (As(V)) adsorption on an Fe–Ce bimetal (hydrous) oxide (Fe–Ce) was investigated using complementary analysis techniques including extended X-ray absorption fine structure (EXAFS) and surface complexation modeling [135]. Manganese (Mn) and iron (Fe) oxides are ubiquitous solids in terrestrial systems that have high sorptive capacities for arsenic (As). Manganese oxides in soils act as a temporary sorbent of As, but operate primarily as strong oxidants responsible for transformation of As(III) to As(V), which can then strongly adsorb on the surrounding Fe oxide matrix [136].

Copper ferrite have limited binding sites on the adsorbent surface which used as adsorbent for the removal of As(V) from aqueous system [137]. Adsorption of the two oxy-anions, arsenate [As(V)] and arsenite [As(III)], on a common goethite based granular porous adsorbent is studied. The extended triple layer model (ETLM) was found to be capable of predicting As(III,V)

adsorption in the presence of oxy-anions: phosphate, silicic acid, sulfate and carbonate [138]. Iron-bearing minerals have been used as adsorbents for arsenic anions for many decades, but both the small surface area and the poorly defined pore structure limit their performance in removal of arsenic from aqueous systems. The iron-loaded mesoporous silicas retained their ordered pore structure as well as the large surface area, which enable them a good kinetic performance in uptake of As(V) anions. The Fe/As molar ratio implies they belong to the iron-containing adsorbents with the highest adsorption performance for As(V), and therefore could be used as alternative adsorbents for As(V) adsorption [139].

The individual and combined effects of changes in water quality and empty bed contact time (EBCT) on As(V) removal performance of a fixed-bed adsorber (FBA) packed with a nanostructured goethite-based granular porous adsorbent were systematically studied [140]. The binary mixed oxide (MO) of iron and silicon in the ratio of 3:1 adsorb arsenic from aqueous solution. Arsenate adsorption was found to increase with increase in ionic strength of background solution indicating the formation of inner-sphere complexes [141]. Hematite, magnetite, goethite and iron rich laterite soil used as arsenic adsorbents. Adsorption tests showed that iron rich laterite was most effective for removal of arsenic, followed by goethite, magnetite and hematite [142]. Activated alumina (AA) used for arsenic removal, is regenerated by 2% NaOH solution [143].

An efficient porous adsorbent for arsenic is developed from abundantly available laterite has higher arsenic adsorption capacity [144]. Mining by-products have been tested as adsorbents for arsenic in order to reduce arsenic bioavailability. This study evaluated a red mud (RM) treated with or without phosphogypsum (G) in order to improve it's As retention [145]. Soils, stream sediments and peat cores are tested their adsorption ability of As(V) and As(III). As(III) achieved higher adsorption due to dissolved Fe ions present in groundwater [146]. Byproduct of the iron casting process such as waste cast iron, in foundries used in the removal of As(III) and As(V) from aqueous solution. The adsorption capacity of grind precipitate dust (GPD) was greater than

cast iron shot (CIS), mainly due to the fact that GPD had higher surface area and weight percent of Fe than CIS [147].

Compared with aluminum oxide particles, acid activated palygorskite and natural palygorskite clay, aluminum oxide modified palygorskite shows better arsenate adsorption capacity [148]. Mesoporous alumina was employed as an effective adsorbent for removing As(V) in the pH region of 2.5–7.0. Arsenic adsorption data of MA(400) are well fitted by the Langmuir isotherm model and the maximum adsorption capacity is 36.6 mg/g at near neutral [149]. A method for removal of iron and As(III) from contaminated water using iron oxide-coated sand and limestone has been developed for drinking water. Limestone helps more effectively towards removal of iron than arsenic. The maximum dose of coated sand required for best removal of iron was 5 and 0.2 g/100 mL of limestone. As(III) removal efficiency increased with increasing dose of coated sand. 97.5% removal of arsenic was obtained at a coated sand dosage of 5 g/100 mL with or without limestone [150].

A magnetic composite adsorbent was successfully prepared with activated carbon and iron oxide as raw materials for the removal of As(V) from solution. Moreover, the magnetic composite adsorbent could be easily recovered from the medium by an external magnetic field [151]. Filters that are packed with adsorbent media with a high affinity for arsenic have been used to de-contaminate water, generally iron or aluminium oxides are favored materials, such a material in the form of nano-chains synthesized via a one step flame synthesis. The ultra-long γ-Fe_2O_3 nano-chains possess high surface area (151.12 m^2/g), large saturation magnetization (77.1 emu/g) that aids in their gas phase self-assembly into long chains in an external magnetic field, along with an extraordinary arsenic removal capacity (162 mg/g). A filter made with this material exhibited a relatively low-pressure drop and very little break-through of the iron oxide across the filter than simple aggregated nanoparticles [152]. Nitric acid added with natural iron ores used as adsorbent for removing arsenic from water. Hematite, a cheap indigenous iron ore was found very efficient for the adsorption of arsenic. Column studies showed adsorption capacity of 3.5 mg/g of arsenic

adsorbed [153]. Nanoscale (20 nm) magnetite particles, previously shown to effectively adsorb arsenic in batch systems, were packed in sand columns to create a continuous treatment process for a water of Guanajuato, Mexico, and surrounding areas contains arsenic in some wells above the Mexican drinking water standard of 25 μg/L [154].

Nanoscale zero valent iron (NZVI) has high adsorption capacity of As(III) and As(V) (Langmuir adsorption capacity 35.83 mg/g and 29.04 mg/g) but it is limited in practical use due to its small particle size and aggregation effect. Reduce graphite oxide (RGO) has been used as a support because of its high surface area [155]. Synthetic nanoscale zero valent iron (NZVI) stabilized with two polymers, Starch and Carboxymethyl cellulose (CMC) were examined and compared for their ability in removing As(III) and As(V) from aqueous solutions as the most promising iron nanoparticles form for removal of arsenic. Starch stabilized particle (S-nZVI) obeyed the Langmuir equation with a maximum adsorption capacity of 14 mg/g for As(V), and 12.2 mg/g for As(III). In this work, starch was proven to be an effective stabilizer for Fe^0 nanoparticles[156].

Table 1.3 Adsorption of arsenic by different adsorbents

Adsorbent	**Capacity**		**Experimental conditions**			**Reference**
	As(III) (mg/g)	**As(V) (mg/g)**	**Temp (°C)**	**pH**	**Conc. (mg/L)**	
Activated alumina (grains)	3.48	15.9	25	7, 5.2	4.9,11.5	[157]
Alumina Al_{10} SBA15	–	20.98	25	6.5	10-100	[158]
Alumina Fe_{10} SBA15	–	12.74	25	6.5	10-100	[158]
Al-Loaded Shirasu zeolite	–	10.49	24	3-10	97.4	[159]
Al_2O_3, $FeOH_3$	–	0.09		8-9	0.05	[160]
Bead cellulose loaded FeOOH	99.6	33.20	25	7	75-7500	[161]
Char carbon	89.0	34.50	25	2-3	992,737	[162]
Chitosan coated ceramic alumina	56.5	96.46				[163]
$FeCl_3$ treated tea fungal biomass	5.4	10.26	30	7.2	1.3,0.9	[164]
Ferrihydrite	–	68.75		7	0-150	[165]

Fresh biomass	128.1	–	30	6	50-2500	[166]
Granular ferric hydroxide	–	8.5	25	8-9	5-100	[167]
Granulated Activated Carbon	0.09	4.5	23	7	1	[168]
Iron hydroxide coated alumina	7.64	36.64	25	6.6-6.8	7.5-135	[169]
Iron impregnated Chitosan beads	6.48	22.6		8	1	[163]
La(III), Y(III) impregnated Alumina	–	25	–	6 -8	140	[170]
La(III) impregnated alumina	–	12.88	–	–	–	[170]
Mango Leaves Powder	146.6	–	30	7	1025	[171]
Meso porous alumina	47.2	121.37	30	3 -7		[107]
Methylated biomass	–	3.75	30	6.5	38-187	[172]
Nano Alumina	40.0	–	25	7.5	10	[173]
Oak bark char	0.0074	–	25	3.5	0.01-0.1	[174]
Oak wood char	0.006	–	25	3.5	0.01-0.1	[174]
Penicillium pupurogenum	35.26	–	20	5	10-750	[175]
Pine wood char	0.0012	–	25	3.5	0.01-0.1	[174]
Pine bark char	12.0	–	25		0.01-0.1	[174]
Plants - Calami rizhoma	–	22.04	–	8	1000	[176]
Plants - Withania frutescens	–	16.88	–	8	1000	[176]
Red mud	0.884	0.941	25	7.3,3.5	2.5-30	[177]
Rice husk	0.137	0.149	20	7	–	[178]
Shirasu zeolite	–	65.93	24	3-10	97.4	[159]
Tea fungal biomass	1.11	4.95	30	7.2	1.3,0.9	[164]
TiO_2	32.4	41	25	7	0.4-80	[179]
Zr-Loaded chelating resin	49.15	88.73	25	9,4	–	[180]

1.5 FLUORIDE CHEMISTRY AND SPECIATION

Fluorine (F) is a greenish diatomic gas. Fluorine is so highly reactive that it is never encountered in its elemental gaseous state except in some industrial processes. The fluoride occurs notably as Sellaite (MgF_2), fluorspar (CaF_2), cryolite (Na_3AlF_6), fluorapatite [$3Ca_3(PO_4)_2.Ca(F,Cl_2)$]. It is 17th in the frequency of occurrence and represents about 0.06-0.09% of the earth's crust [181]. Fluoride generally released into groundwater by the slow dissolution of fluorine-containing

rocks [21]. High fluoride concentrations in groundwater, up to more than 30 mg/L, occur widely, notably in the United States of America, Africa and Asia [182, 183]. But its occurrence and distribution are non uniform in different states from one affected district in Jammu and Kashmir to all 32 districts affected in Rajasthan [184].

1.6 PROCESSES FOR REMOVAL OF FLUORIDE FROM GROUNDWATER

1.6.1 Chemical additive method

These methods involve the addition of soluble chemicals to the water. Fluoride is removed either by precipitation, co-precipitation, or adsorption onto the formed precipitate. Precipitation methods are based on the addition of chemicals (coagulants and coagulant aids) and the subsequent precipitation of a sparingly soluble fluoride salt as insoluble fluorapatite [185]. Removal of fluoride was accomplished with separation of solids from liquid. Aluminium salts (eg. Alum), lime, Poly Aluminium Chloride, Poly Aluminium hydroxy sulphate and Brushite are some of the frequently used materials in defluoridation by precipitation technique [185, 186]. The best example for this technique is the famous Nalgonda technique of defluoridation, developed in India.

The Nalgonda technique involves addition of aluminium salts, lime and bleaching powder followed by rapid mixing, flocculation sedimentation, filtration and disinfection in a way similar to what is practiced in conventional water treatment. To be effective the method requires careful control of the alkalinity of the water. Aluminium salt is only responsible for removal of fluoride from water. The dose of Aluminium salt increases with increase in the fluoride and alkalinity levels of the raw water. The selection of either aluminium sulphate or aluminium chloride also depends on sulphate and chloride contents of the raw water to ensure their permissible limits in the treated water. The dose of lime is empirically $1/20^{th}$ that of the dose of aluminium salt. Lime facilitates forming dense floc for rapid setting. Bleaching powder is added to the raw water at the rate of 3.0 mg/L for disinfection. Gong et al., 2012 investigated aluminum salts coagulation with fluoride. High efficiency was achieved at low pH and high fluoride concentration [187].

1.6.2 Contact precipitation method

Contact precipitation is a technique in which fluoride was precipitated as fluorapatite $Ca_{10}(PO_4)_6F_2$, due to chemical reaction with calcium and phosphate compounds. The presence of a saturated bone charcoal medium acts as a catalyst for the precipitation of fluoride either as CaF_2, and/or fluorapatite. The commonly used chemicals in contact precipitation are calcium chloride and sodium di-hydrogen-phosphate [188]. Tests at community level in Tanzania have shown promising results of high efficiency. Reliability, good water quality and low cost are reported advantages of this method [189]. In contact precipitation, there is no sludge and no saturation of the bed, only the accumulation of the precipitate in the bed [190].

1.6.3 Ion exchange

The removal of fluoride from diluted solution with Neosepta AHA anion exchange membrane has been studied by Donnan dialysis. The effects of concentration, pH, and accompanying anion on feed phase and receiving phase composition were investigated. The flux of fluoride with respect to the concentration, pH, and the effect of the counter-ions (HCO_3^-, Cl^-, SO_4^{-2}) were obtained between 34 -136 X 10^{-7} (m.mol/(cm^2.s)). The effect of the fluoride flux increased with increasing of concentration on the feed phase. The flux of fluoride was found to be higher at higher pH in the feed phase. In addition, the accompanying counter-anions also influenced the flux of fluoride and the order of flux was founded as $HCO_3^- > Cl^- > SO_4^{-2}$. The results obtained for AHA membrane were compared with Neosepta AFN and polysulfone SB-6407 membranes. The transport efficiencies of the membranes were found to be in the order AFN>AHA>SB-6407 [191].

1.6.4 Electrodialysis

Studies have been performed on removal of fluoride from Moroccan groundwater by electrodialysis in a continuous operation using a pilot plant. The performances of two anion exchange membranes were compared. An optimisation of electrodialysis operation was carried out for various experimental conditions including, amongst others, the fluoride content in the raw

water. The water quality and other parameters were followed to show the optimum operating conditions. Electro-coagulation was investigated for the effective removal of fluoride from drinking water. Different initial concentrations (2–10 mg/L) of fluoride were considered for the experiment. Two different electrode connections (monopolar and bipolar) were examined for choosing the better alternative in order to intensify the performance of the process. It was observed that the removal of fluoride was better for bipolar connection than for monopolar connection [192].

1.6.5 Adsorption

Activated alumina (AA) was the most widely investigated adsorbent for removal of fluoride from water. The removal performance was investigated as a function of the concentration, flow rate, amount of adsorbent dose and pH. Sorption data have been correlated with Langmuir and Freundlich isotherms [193]. However, major anions reduced adsorption of fluoride on activated alumina in the order of HPO_4^{2-} >HCO_3^- >SO_4^{2-} >Cl^-. Other toxic elements that might coexist with fluoride in groundwater, such as arsenic and selenium, also reduced adsorption of fluoride through competition for the same surface sites [194]. Acid and base treated alumina particles were studied to assess their capacities for the adsorption of fluoride from aqueous solutions. The fluoride adsorption mainly superficially happened on the alumina particle surface. The adsorption capacity of acid treated alumina was about twice compared with that of alumina, while the capacity of base treated alumina was only about half of that of alumina at the solution pH 7 [195]. The maximum sorption capacity of nano-alumina for fluoride removal was found to be 14.0 mg/g at 25°C. Maximum fluoride removal occurred at pH 6.15 [196].

Liu et al. (2011) investigated the adsorptive capability of the freshly prepared aluminum hydroxide, i.e., in-situ $Al_2O_3 \cdot xH_2O$, towards fluoride. The maximum adsorption of above 110 mg F/g Al was observed in pH ranges from 5.0 to 7.2 [197]. Mesoporous alumina (MA450) has been synthesized using biopolymer chitosan as a template and used for defluoridation of water. It was observed that MA450 works effectively over a wide range of pH and showed a maximum

adsorption capacity of 8.26 mg/g at initial fluoride concentration of 5.0 mg/L, which is much better than the conventional alumina. The experimental data fitted well in Langmuir isotherm and followed pseudo-second order kinetics. MA450 showed significantly high removal of fluoride in field water. MA450 was effective in terms of removal of fluoride performance and also appears to be cost effective [198]. Goswami et al. (2012) investigated acidic alumina for the adsorption of fluoride at different process parameters and conclude that the maximum fluoride adsorption capacity by acidic alumina was found to be 8.4 mg/g and optimum pH was found as 4.4. The endothermic behavior of the process indicates that the fluoride adsorption by acidic alumina was physical adsorption [199].

Nie et al. (2012) prepared aluminum modified hydroxyapatite (Al-HAP) for the defluoridation of aqueous solution with fluoride adsorption capacity 16.8 mg/g [200]. They concluded that Al-HAP have abundant hydroxyl groups (adsorption sites) on the surface Lunge et al. (2012) synthesized a new alumina supported carbon composite from eggshell waste for selective fluoride adsorption. This calcium containing eggshell composite effectively removed fluoride from ground and waste water, with an adsorption capacity of 37 mg/g [201]. Mixed nano iron oxides powder containing goethite (FeOOH), hematite (Fe_2O_3) and ferrihydrite ($Fe_5HO_8{\cdot}4H_2O$) was synthesized through surfactant mediation n-precipitation route using cetyltrimethyl ammonium bromide (CTAB). Adsorption of fluoride onto the synthesized sample was investigated using batch adsorption method [202]. Kumar et al. (2009) used granular ferric hydroxide (GFH) as adsorbent for the removal of fluoride from aqueous solution. Maximum fluoride adsorption capacity by granular ferric hydroxide was found to be 7 mg/g. He studied the interference of anions for the adsorption of fluoride on GFH [203].

Raichur et al. (2001) found that rare earth oxide adsorbed fluoride rapidly and effectively from aqueous solution. Fluoride adsorption by rare earth oxide followed Langmuir adsorption model [204]. The fluoride ion was adsorbed into pores in carbonaceous materials produced from wood; the larger the specific surface area, the more fluoride ions were adsorbed. Bone char was the

most effective adsorbent. The composition of bone char includes calcium phosphate, calcium carbonate, and so on [20]. Tembhukar et al. (2006) studied the fluoride adsorption capacity of powdered activated charcoal. It was reported that the removal of fluoride was high at solution pH 2 [205]. Regenerated bone char was found to be a potential medium for the defluoridation of drinking water. The regenerated bone char media at 500°C for a duration of 2 h was found to be the most practical with a potential for fluoride sorption, while the smallest grain size particles of bone char media (0.5–1.0 mm) yielded the best results in terms of fluoride removal [206].

A trimetal oxide was developed as a fluoride adsorbent by coprecipitation of Fe(II), Al(III) and Ce(IV) salt solutions with a molar ratio of 1:4:1 under alkaline condition. The material retained amorphous structure and maintained relatively stable fluoride adsorption performance at calcination temperatures lower than 600°C [207]. A novel bead adsorbent, Fe(III)-loaded ligand exchange cotton cellulose adsorbent [Fe(III)LECCA], was prepared for fluoride removal from drinking water [208]. Coating granulation of the Fe–Al–Ce adsorbent could produce granules that could be used in a packed bed for the removal of fluoride from drinking water [209]. The fluoride adsorption potential of novel nano-hydroxyapatite/chitin (n-HApCh) composite was explored [210]. Zhao et al. (2010) introduced a novel magnetic nano sized adsorbent which was used to remove excessive fluoride from aqueous solution. High affinity of fluoride was based on combination of magnetic separability with magnetic nanoparticle and hydrous aluminium oxide floc formed [211].

Yang et al. (2010) invented a composite metal oxide adsorbent for the removal of fluoride from aqueous solution. These composite metals contain transition metals (Fe, Ti, Mn), Al, Mg, and rare earth metals (Ce, La) in the required mole ratio for the efficient removal of fluoride in the pH range 6.5-7. The saturated adsorption capacity of this composite metal oxide was found to be 229 mg/g [212]. Defluoridation by industrial grade limestone indicated that a combination of precipitation and adsorption of fluoride can be very effective for defluoridation of water. Fluoride containing water acidified using two edible acids, viz. Acetic acid, citric acid was

treated by crushed limestone of diameter 3-4 mm to precipitate fluoride as CaF_2 in addition to adsorption of fluoride on limestone [213].

Adsorption of fluoride on synthetic siderite significantly increased with an increase in contact time. The adsorption rate was high in the first 2 h, and thereafter significantly decreased until adsorption reached equilibrium. Kinetic data were fitted to a pseudo-second order kinetic model, showing that adsorption was controlled by both external mass transfer and intraparticle diffusion [214]. Multi-walled carbon nanotubes (MWCNTs) were investigated as a means of removing fluoride from the drinking water of a number of regions in Iran and from experimental solutions. Sorption capacity of 3.5 mg/g was reported. Sorption follows Freundlich isotherm, indicating that MWCNTs possessed a heterogeneous surface. Experiments using Kohbanan city drinking water, which contained the highest level of fluoride among the drinking water samples studied, showed that MWCNTs could remove over 85% of fluoride content [215]. Wang et al. (2013) studied the fluoride adsorption by Ce(III) incorporated modified aerobic granules (Ce(III)-MAG). The maximum adsorption capacity by Ce(III)-MAG was found to be 45.8 mg/g. Column studies were also carried out [216].

Sivasankar et al. (2013) prepared a hybrid sorbent cerium dispersed carbon (CeDC), for the removal of excess fluoride in drinking water. CeDC was regenerated by alkaline washing followed by acidic neutralization [217]. Zhang et al. (2013) synthesized a novel adsorbent, CeO_2/Mg-Fe layered double hydroxide. The surface of this composite was modified by non thermal plasma to enhance the adsorption of fluoride. Fluoride adsorption capacity on CeO_2/Mg-Fe layered double hydroxide was found to be 38.7-60.4 mg/g [218]. Babaeivelni et al. (2013) synthesized crystalline TiO_2, which was used for adsorption of fluoride. Fluoride adsorption by TiO_2 increased with decrease in pH and maximum removal was obtained in the pH range 7-8. Solution pH was the main factor controlling fluoride adsorption by TiO_2 [219]. Wang et al. (2013) investigated the fluoride adsorption performance by CeO_2–ZrO_2 nanocages and optimum

pH (3.5-4.5) was obtained. The maximum adsorption capacity of 112.7 mg/g by CeO_2–ZrO_2 was achieved at pH 4 [220].

Table 1.4 Adsorption of fluoride by different adsorbents

Adsorbent	Capacity (mg/g)	Experimental conditions			Reference
		Temp (°C)	pH	Conc. (mg/L)	
Activated alumina (OA-25)	2.00	-	7.0	2.5-14	[193]
Acidic alumina	8.40	-	3.6-11.6	5-15	[199]
Acidic and alkaline alumina	3.0 - 20.4	30	3.0-12.0	10	[221]
Aluminium hydroxide (THA & UHA)	23.7&7.0	24	6.0-7.0	5-30	[222]
Alum impregnated activated alumina	40.68	Room temp	6.5	1-35	[223]
$Al(OH)_3$ coated rice husk	9.0	27	5.0	5-25	[224]
Bermuda grass carbon	4.67	Room temp	7.0	3	[225]
CaO modified activated alumina	101.01	25	5.5	1-1000	[226]
Cellulose @hydroxaptite	10.0	25	4.0-5.0	10	[227]
Chitosan	8.0	20-35	7.0	10-15	[228]
CuO coated alumina	7.77	30.5	-	10	[229]
Fe-Al mixed hydroxide	91.7	30		10-90	[230]
Fungal biomass	1.27	30	7.0	5	[231]
Granular ferric hydroxide	7.0	26	4.0	1-100	[203]
Hydrous MnO_2 coated alumina	7.09	25	5.20	10-70	[232]
La(III) impregnated alumina	6.65	Room temp	5.7-8.0	1-35	[233]
Leaves	0.8-1.0	29	2.0-10.0	2-15	[234]
MnO_2 coated alumina	2.85	31	7.10	2.5-30	[235]
Nano alumina	14.0	25	6.15	1-100	[196]
Plant and fungal biomass	0.10	Room temp	5.5	5.0	[236]
Wheat straw, Sawdust, Bagasse carbon	1.93 1.73 1.15	-	6.0	5.0	[237]

Sujana et al. (2013) synthesized new biopolymer beads of hydrous ferric oxide (HFO) and alginate. Point of zero charge of biopolymer bead was found to be 5.15. Tests were conducted on HFO doped alginate beads with groundwater sample containing 5.0 mg/L fluoride. The treated water contained 0.6 mg/L fluoride [238]. Shan et al. (2013) used optimum modified natural siderite (OMNS) for fluoride adsorption, which followed pseudo second order kinetics. Adsorption of fluoride by OMNS was endothermic and spontaneous [239]. Paudyal et al. (2013) studied the sorption of fluoride by Zr(IV), Ce(IV) and Al(III) loaded dried orange juice residue. Adsorption capacity of 1.43 mmol/g was obtained by Zr(IV) loaded dried orange juice residue [240]. Koilraj et al. (2013) prepared Zn, Cr layered double hydroxide for fluoride removal. Maximum fluoride uptake capacity of 31 mg/g was achieved by this adsorbent, which was effective in a wide pH range of 3-10 [241]. Yanhui et al. (2013) investigated fluoride adsorption by MnO_2 coated graphene oxide (MOGO). Optimum removal of fluoride occurred at pH 5.5-6.7. Adsorption of fluoride by MOGO was a spontaneous and endothermic process [242]. Yadav et al. (2013) studied cost effective fluoride adsorption materials like activated bagasse carbon (ABC), sawdust raw (SDR) and wheat straw raw (WSR). Equilibrium uptake of fluoride on ABC, SDR and WSR were 1.15, 1.73 and 1.93 mg/g [237].

1.7 PROCESSES FOR REMOVAL OF ARSENIC AND FLUORIDE TOGETHER

Co-contamination of groundwater with arsenic and fluoride is reported at several regions across the world. To address this problem studies were conducted to remove both these pollutants simultaneously. Groundwater from the state of Assam in India, contains 2.0 mg/L fluoride and 0.68 mg/L arsenic respectively. Groundwater from Manipur, India, contains arsenic 0.986 mg/L and fluoride 1.0 mg/L. Miramontes et al. (2003) studied the combined use of cake alum and a polymeric anionic flocculent (PAF) for removal of arsenic (As) and fluoride (F) from drinking water has been evaluated in water from well at Meoqui City, Chihuahua, Mexico. The water contained 5.9 mg/L of fluoride and 0.134 mg/L of arsenic respectively. Field data revealed that As and F concentrations may, by this method, could be reduced up to 99% and 77%,

respectively. The addition of small amounts of PAF greatly facilitated sedimentation of the precipitate [243]. Farooqi et al. (2007) analysed As and F contaminated groundwater from a small village, Kalalanwala, in East Punjab, Pakistan, and reported As of maximum 2400 μg/L and F^- of maximum 22.8 mg/L in groundwaters from shallow depths down to 30 m from the surface. The contaminated groundwaters were characterized by high pH (max. 8.8), alkalinity (HCO_3^- up to 1281 mg/L), SO_4^{2-} (max. 960 mg/L), Na^+ (max. 1058 mg/L) and maximum electric conductivity >4.6 mS/cm [244].

Devi et al. (2008) investigated the removal of F, As and coliform bacteria from drinking water using modified homemade filter media. The maximum reduction of fluoride, arsenic and coliform bacteria from 5 mg/L, 0.13 mg/L and $2X10^9$ residual values were 0.72 mg/L, 0.009 mg/L and 0 coliform cells/100 mL, respectively after a treatment time of 10 h [245]. Padilla et al. (2010) studied the coexistence of arsenic and fluorine in high concentrations in groundwater from Argentina. The behavior of a spiral membrane of nanofiltration (NF) at pilot-scale was investigated for the simultaneous removal of arsenate, fluoride and bicarbonate from a synthetic solution containing 180 μg As(V)/L, 5 mg F/L and 84 mg HCO_3/L. At pH 8 and 7 bar, the rejections of arsenate, fluoride and bicarbonate were 93%, 89% and 85%, respectively. The separation behavior of the studied membrane corresponds to a typical negatively charged membrane, where the main mechanism driving salt rejection is Donnan exclusion. The results pointed out a high electric repulsion between these ions and the membrane [246]. Tang et al. (2010) identified goethite is an effective material for removing fluoride and As(V) from drinking water. The affinity of As(V) on goethite was much stronger than fluoride. Adsorption of fluoride and As(V) onto goethite obeyed a pseudo second-order kinetic model [247].

Bone char, goethite coated sand (G-IOCS) and hematite coated sand (H-IOCS) were evaluated for treating water with elevated levels of arsenic and fluoride present individually or together. Results obtained were compared to conventional media used in developed countries; viz., activated alumina and granular ferric oxide. Fluoride adsorption capacity was higher in bone char

than in G-IOCS and H-IOCS. Removal of fluoride was not affected by the presence of environmentally significant As(III) and As(V) concentrations. On a mass basis, bone char's fluoride adsorption capacity was comparable to that of activated alumina both in the presence and absence of 0.25 mg/L of As(III) and As(V) in solution. Bone char also showed higher capacity to remove As(III) and As(V) from solution than both G-IOCS and H-IOCS, probably due to its much higher surface area. The 10 mg/L of fluoride did compete with As(V) for adsorption onto the bone char. Both G-IOCS and H-IOCS removed As(III) from solution even in the presence of fluoride; however, G-IOCS had higher As(III) adsorption capacity than H-IOCS, possibly as a result of higher surface area of goethite coated onto the sand. On a mass basis, the bone char and iron oxide coated sands were two to three orders of magnitude less efficient in removing As(III) and As(V) than a commercially produced granular ferric oxide [248].

Tian et al. (2011) prepared an anion adsorbent by surface modification of native cellulose fibers by poly(N,N-dimethyl aminoethyl methacrylate) (PDMAEMA), which was characterized by scanning electron microscopy, Fourier transform infrared spectroscopy and elemental analysis. This adsorbent had high efficiency in removal of F^{-}, AsO_2^{-} and AsO_4^{3-} from aqueous solutions, even at low initial concentrations [249]. Li et al. (2011) synthesized mesoporous aluminas and calcium doped aluminas for removal of fluoride and arsenic from water. Arsenic was reduced from 100 ppb to 1 ppb and defluoridation capacity of 450 mg/g for calcium doped alumina and 300 mg/g for mesoporous alumina were respectively reported [250]. Guo et al. (2012) selected twenty-nine wells for groundwater sampling in the town of Shahai, in the Hetao basin, Inner Mongolia. Four multilevel samplers were installed for monitoring groundwater chemistry at depths of 2.5–20 m. Results showed that groundwater As exhibited a large spatial variation, ranging between 0.96 and 720 μg/L, with 71% of samples exceeding the WHO drinking water guideline value (10 μg/L). Fluoride concentrations ranged between 0.30 and 2.57 mg/L [251].

Kim et al. (2012) studied the co-contamination of arsenic and fluoride in groundwaters by unconsolidated aquifers. Fe-(hydr)oxides plays major role for arsenic reduction. Geochemical

signatures of the groundwater in the study area showed that the As concentrations were enriched by the reductive dissolution of Fe-(hydr)oxides, and the correlations between As and F^- concentrations were poor compared to those observed in the oxidizing aquifers [252]. Brahman et al. (2013) analysed both fluoride and arsenic present in Pakistan groundwater and reported: Fluoride 24.4 mg/L, total arsenic 3.36 mg/L (As(III)-1.26 mg/L, As(V)- 1.97 mg/L, inorganic arsenic-3.26 mg/L) [253]. Alarcon et al. (2013) studied the removal of As and F by membrane technology and coagulation/filtration in Latin America. Despite its simplicity, this method has not been implemented in Latin American countries yet, even though it was thoroughly tested and proven to be successful at the laboratory- and pilot-scale in Mexico, Canada, and the USA [254]. Al-Fe (hydr)oxides with different Al/Fe molar ratios (4:1, 1:1, 1:4, 0:1) were prepared using a co-precipitation method and were then employed for simultaneous removal of arsenate and fluoride. The 4Al: Fe was superior to other adsorbents for removal of arsenate and fluoride in the pH range of 5.0–9.0. The highest adsorption capacity for arsenate and fluoride by 4Al : Fe was mainly ascribed to its highest surface hydroxyl group density, besides its largest pH_{pzc} [255].

1.8 MASS TRANSFER ZONE

Operation of a fixed bed adsorption column can be explained by the so called Mass Transfer Zone concept. In a fixed bed column, adsorption occurs in a certain length of the bed, called mass transfer zone (MTZ) that develops during the dynamic contact of solid and liquid. The MTZ is generally a band, between the spent adsorbent and the fresh adsorbent, where adsorbate is removed. The MTZ starts moving along the bed from the inlet to the outlet. Adsorption in fixed bed column strongly relates to the length and shape of the MTZ. Within the MTZ, the degree of saturation with adsorbate varies from 100% to zero and the fluid concentration varies from the inlet concentration to zero [256]. As the MTZ moves across the sorbent bed it leaves behind a section of adsorbent bed, which is completely exhausted, and in front of the leading edge of the MTZ lays fresh adsorbent. The zone below the MTZ is clean zone, which is free

from adsorbed material on it. The MTZ will continue to travel through the bed until the bed reaches its breakthrough point. The breakthrough point is the point on the breakthrough curve, where the effluent adsorbate concentration reaches its maximum allowable concentration. A steeper mass transfer zone means more of the bed is used for adsorption.

For the adsorbent to be efficient, a sharp breakthrough (narrow MTZ) with a long breakthrough time (t_B) is required. At the time t_B, the adsorbent begins to be saturated with the adsorbate, so the relative concentration (C/C_0) starts to increase from 0.05 to 0.95 [256] which is close to the initial concentration at exhaust time (t_E), because the bed is almost completely saturated, so the adsorbate passes through the column without being adsorbed to any larger extent. In Fig.1.3 and Fig.1.4 the area between t_B and t_E is called the mass transfer zone (MTZ). In this region most of the mass transfer takes place. Eventually, the output concentration reaches the initial concentration and no adsorption occurs. At lower diffusion resistance and faster kinetics, the height of mass transfer zone is small. An important design consideration is the length of the mass transfer zone (L_{MTZ}). The influent flow rate and rate of adsorption influence the length of MTZ. This means that any parameter that changes the rate of adsorption will also change the length of the mass transfer zone to some extent [257]. The column is operational till the MTZ reaches the end of the column. Until this time the outlet of the column is free from adsorbate. Once the MTZ reaches the column end, the adsorbate starts gradually increasing in the effluent. Due to the sorption mechanism and mass transport conditions the real mass transfer zone (MTZ) appears S-shape in the plot [256]. To determine the length of the mass transfer zone (L_{MTZ}) the shape of the curve is very important. The movement of the MTZ through a sorbent bed can be graphically represented by the column effluent concentration versus either the volume treated or the time in operation called a breakthrough curve. The sorbent bed adsorption capacity can be increased by minimizing the length of mass transfer zone. The extent, to which the adsorption capacity of fixed bed can be used, can be obtained by the slope of the breakthrough curve. If the length of the mass transfer zone is zero ($L_{MTZ} = 0$) the breakthrough curve will be vertical.

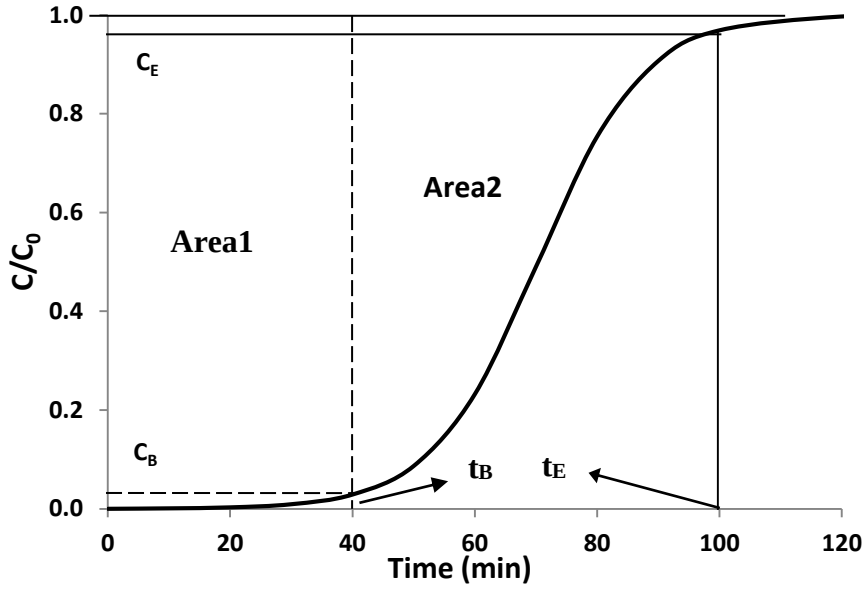

Fig.1.3. Typical adsorption column breakthrough curve

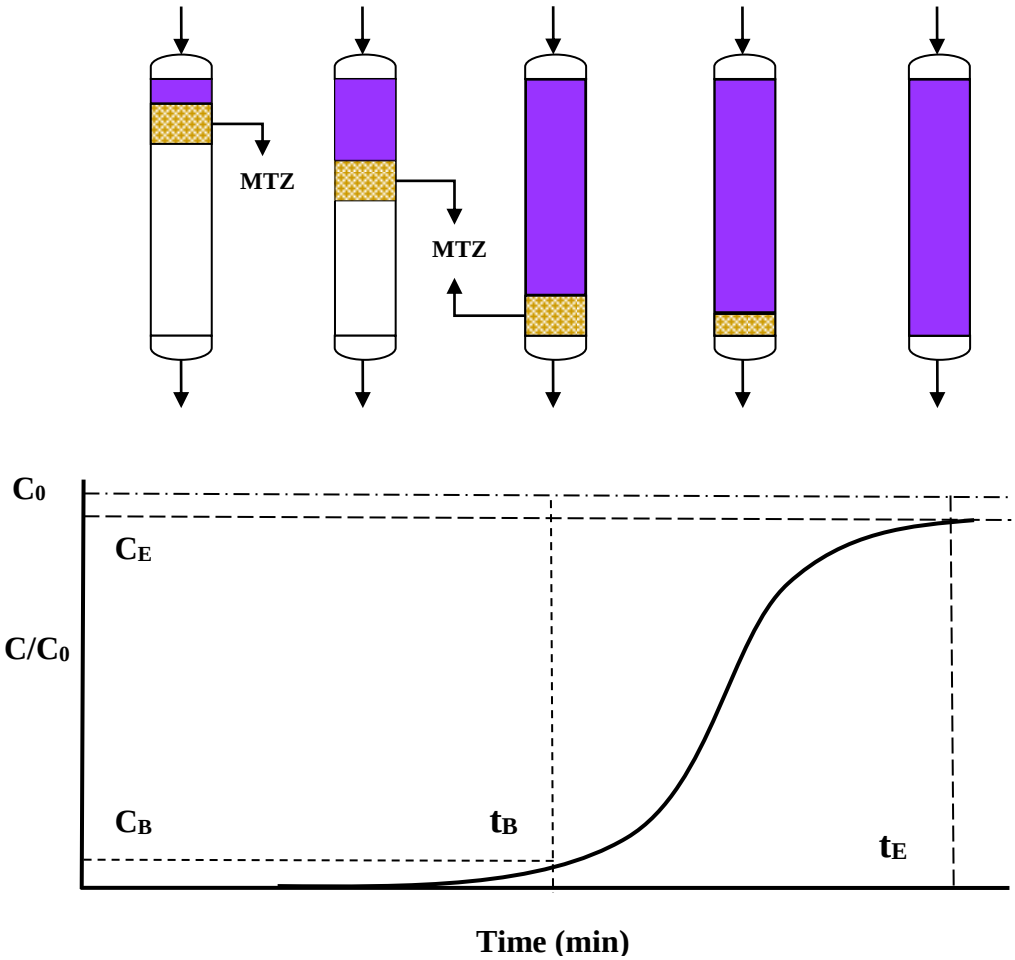

Fig.1.4. Movement of mass transfer zone in fixed bed column

The length of the MTZ, also called the height of the mass transfer zone, can be expressed as

$$H_{MTZ} = \frac{h\,(t_B - t_E)}{t_B + F(t_E - t_B)} \quad \text{..... 1.1}$$

where, H_{MTZ} is the height of the mass transfer zone (cm), h is the height of the adsorbent bed (cm), t_E is the exhaustion time (min), t_B is the breakthrough time (min) and F is the fractional capacity [258]. The smaller the height of mass transfer zone, the faster the rate of adsorption and the more rapid the saturation of adsorption bed.

Fraction of the adsorbent present in the adsorption zone still possessing ability to remove fluoride (adsorbate) at breakthrough is given by

$$F = \frac{S_Z}{S_m} = \frac{\int_{t_B}^{t_E}(C-C_0)dt}{C(t_E-t_B)} \quad \text{..... 1.2}$$

where, F is fractional capacity, S_Z is the amount of solute that has been removed by the adsorption zone from breakthrough to exhaustion (g), S_m is the amount of solute that has been removed by the adsorption zone when completely exhausted (g), C_0, C are initial and final concentration of solute (mg/L), t_E , t_B are exhaust and breakthrough time (min).

The adsorption capacity limiting the rate of movement of the MTZ is linearly proportional to the height of the MTZ.

The rate of movement of MTZ is expressed as

$$U_Z = \frac{H_{MTZ}}{t_Z} = \frac{H_{MTZ}}{t_E-t_B} \text{.....1.3}$$

where, U_Z is rate of movement of MTZ (cm/min), t_Z is the time required for MTZ to travel the length of the column (min).

The column % saturation can be given by

$$\%\ Saturation = \frac{h+(F-1)H_{MTZ}}{h} X\ 100 \text{ .... 1.4}$$

1.9 MODELLING OF COLUMN PERFORMANCE

The ultimate goal of developing and assessing an adsorbent is to use it effectively for a plant scale application, in operator friendly equipment such as a fixed bed column. Several models are available in literature for predicting the performance of fixed bed adsorption columns, four of these, Thomas model, Yoon-Nelson model, Bohart-Adam model and Clark model are used for

the testing the experimental data in the present work. Each one of these models is different from the other in terms of the type of adsorption isotherm, inclusion or exclusion of chemical reaction, significance of mass transfer resistance and the type of rate law used.

1.9.1 Thomas model

Thomas model assumes that the rate adsorption follows second order reversible reaction kinetics and the Langmuir adsorption isotherm [259, 260]. Both axial and radial dispersion are negligible and constant column void fraction is assumed. This model is suitable for the adsorption process where external and internal diffusion resistances are extremely small [261]. Thomas equation can be given as follows:

$$\frac{C}{C_0} = \frac{1}{1+exp\left(k_{Th}\left(q_0 m - C_0 V_{eff}\right)/Q\right)} \quad \ldots\ldots\ldots \mathbf{1.5}$$

The linear form of Thomas equation is given by

$$ln\left[\frac{C_0}{C} - 1\right] = \frac{k_{Th} q_0 m}{v} - k_{Th} C_0 t \quad \ldots\ldots\ldots \mathbf{1.6}$$

where, C_0, C are influent and effluent concentration of adsorbate (mg/L), k_{Th} is Thomas model constant (mL/min.mg), q_0 is equilibrium uptake (mg/g), m is mass of adsorbent (g) and v is linear velocity (cm/min).

1.9.2 Yoon-Nelson model

Yoon and Nelson developed is a less complicated model, which requires no detailed data concerning the characteristics of the adsorbate, properties of the adsorption bed and the type of adsorbent. It is assumed that the rate of decrease in the probability of adsorption is proportional to the probability of adsorption and the probability of adsorbate breakthrough on the adsorbent [262]. Yoon-Nelson equation written as

$$\frac{C}{C_0} = \frac{exp[K_{YN}(t-\tau)]}{1+exp[K_{YN}(t-\tau)]} \quad \ldots\ldots\ldots\ldots\ldots\ldots \mathbf{1.7}$$

where, C_0, C are influent and effluent concentration of adsorbate (mg/L), K_{YN} is the Yoon Nelson rate constant (min^{-1}) and τ is the time required for 50% adsorbate breakthrough (min), t is the breakthrough (sampling) time (min).

A linear form of Yoon Nelson model can be expressed as

$$ln\left(\frac{C}{C_0-C}\right) = K_{YN}t - \tau K_{YN} \text{ ..... 1.8}$$

1.9.3 Bohart-Adam model

Based on Bohart-Adam model [263] assumes that the rate of adsorption is proportional to the adsorption capacity. The relationship between C/C_o and t in the column adsorption was studied by the Bohart Adam model. It describes the initial part of the breakthrough curve and is used to estimate the maximum adsorption capacity (N_0) and Bohart Adam kinetic constant (k_{BA}). The linear form of Bohart Adam equation can be written has:

$$ln\left[\frac{C}{C_0}\right] = k_{BA}C_i t - \frac{k_{BA}N_0 H}{v} \text{ ..... 1.9}$$

where, C_0, C are concentration of adsorbate at initial and at time 't' (mg/L), K_{BA} is Bohart Adam model constant (L/mg.min), v is linear velocity (cm/min), Z is bed depth (cm), N_o is saturation concentration (mg/L) and t is time (min). The value of k_{BA} and N_o can be obtained from the intercept and slope of the plot ln(C/C_0) Vs t.

1.9.4 Clark model

Clark model assumes Freundlich isotherm and that the shape of the mass transfer zone is constant and all the adsorbates are removed at the end of the column [264]. Clark model is expressed by

$$\frac{C_0}{C}^{n-1} - 1 = Ae^{-rt} \text{ ..... 1.10}$$

Where, C_0, C are influent and effluent concentration (mg/L), n is the Freundlich parameter, A and r are Clark constants:

$$A = exp\left(\frac{K_C N_0 Z}{v}\right) \text{ ..... 1.11}$$

$$r = K_C C_0 \text{ ..... 1.12}$$

Where, K_C is Clark constant (L/mg.min), N_o is capacity of removal (mg/L) and v is linear velocity (cm/min). The above equation can be linearized and expressed as

$$ln\left[\left(\frac{C_0}{C}\right)^{n-1} - 1\right] = -rt + lnA \text{ ..... 1.13}$$

A plot of $\ln[(C_0/C)^{n-1}-1]$ versus t gives slope = -r, intercept = lnA.

1.9.5 Application of models for various operating parameters

Applicability of the above models for various ranges of operating parameters, such as particle size, flow rate, initial concentration and different adsorbents is assessed by fitting the model equations to the experimental data. This gives an insight into the mechanism of adsorption. The goodness of fit of a model is assessed by the regression coefficient, R^2 and the % Error defined by

$$\%\ \boldsymbol{Error} = \frac{(q_{calc} - q_{exp})100}{q_{calc}} \quad \text{..... 1.14}$$

Closeness of R^2 to one and minimum % Error, indicate the best fit of a model to the experimental data.

1.10 SCOPE AND AIM OF THE PRESENT WORK

In view of the importance of keeping the levels of arsenic and fluoride to the limits prescribed by the statutory bodies, it is essential that efficient and cost effective treatment techniques are developed, particularly in Indian context, catering to the large population.

The aim of the present is develop a simple to use and economic adsorbent for drinking water treatment. The scope includes

- Synthesis of a novel adsorbent for efficient removal of arsenic and fluoride from groundwater.
- Characterization of adsorbent to study the surface morphology and identify the functional groups present.
- Study the mechanism of adsorption of arsenic and fluoride from water.
- Investigate the effects of various operating parameters in batch and column studies.
- Assess the models available in literature to predict the performance of column operation.

2 MATERIALS AND METHODS

A novel adsorbent has been prepared for removal of arsenic and fluoride from drinking water. Selection of sawdust for the preparation of the adsorbent and optimization of the composition of the adsorbent are presented in this chapter. Procedure adopted for synthesis of the adsorbent and methods for surface characterization are detailed. Experimental techniques followed for studies on batch and column investigation of the adsorbent for its efficacy for removal of arsenic and fluoride are explained.

2.1 SELECTION AND PRETREATMENT OF SAWDUST

Samples of sawdust from different trees of local origin were collected for assessing their suitability as a base material for the adsorbent. The saw dust sample was washed thoroughly with DM water to remove muddy material and was soaked in 0.1N NaOH for 24 h to remove lignin based color material. Subsequently, it was filtered and excess NaOH was neutralized by washing with 0.1N H_2SO_4 followed by DM water. The saw dust was dried to constant weight in an oven at 80±5 $^{\circ}$C for 12 h and cooled to room temperature. These sawdust samples are tested for their capacity for adsorption of arsenic and fluoride from solutions of 1 mg/L and 25 mg/L concentrations of As, F respectively.

Table 2.1 As(V) adsorption by sawdust of various trees

S.No.	Name of the tree	Binomial name	As(V) adsorbed (mg/g)	As(V) adsorption (%)
1	Coconut	Cocos nucifera	0.003	6.0
2	Teak	Tectona grandis	0.004	8.0
3	Karuvelam	Acacia Arabica	0.006	12.0
4	Eucalyptus	Eucalyptus obliqua	0.007	14.0
5	Patauk	Pterocarpus	0.007	14.0
6	Poovarasam	Thespesia populnea	0.013	26.0
7	Aanjili	Artocarpus hirsutus	0.019	38.0

Table 2.2 Fluoride adsorption by sawdust of various trees

S.No.	Name of the tree	Binomial name	F^- adsorbed (mg/g)	F^-adsorption (%)
1	Coconut	Cocos nucifera	0.000	0.08
2	Eucalyptus	Eucalyptus obliqua	0.007	1.33
3	Karuvelam	Acacia Arabica	0.011	2.15
4	Poovarasam	Thespesia populnea	0.028	5.39
5	Teak	Tectona grandis	0.037	7.30
6	Patauk	Pterocarpus	0.036	7.34
7	Anjili	Artocarpus hirsutus	0.069	13.43

It can be seen that *Artocarpus hirsutus*, called "Anjili" locally, has the highest capacity for adsorption of arsenic as well as fluoride. Hence this sawdust selected for preparation of the adsorbent. It can be seen that the adsorption capacity for the saw dust is 38.0% for As(V) and 13.43% for fluoride, which is quite appreciable for a base material.

2.2 OPTIMIZATION OF THE COMPOSITION OF THE ADSORBENT

For optimization of the composition of the adsorbent, mass ratio of the constituents was varied and adsorption capacities of arsenic and fluoride were determined. Mass ratios studied were 2:1:1, 1.5:1:1 and 1:1:1 of sawdust: ferric hydroxide: activated alumina.

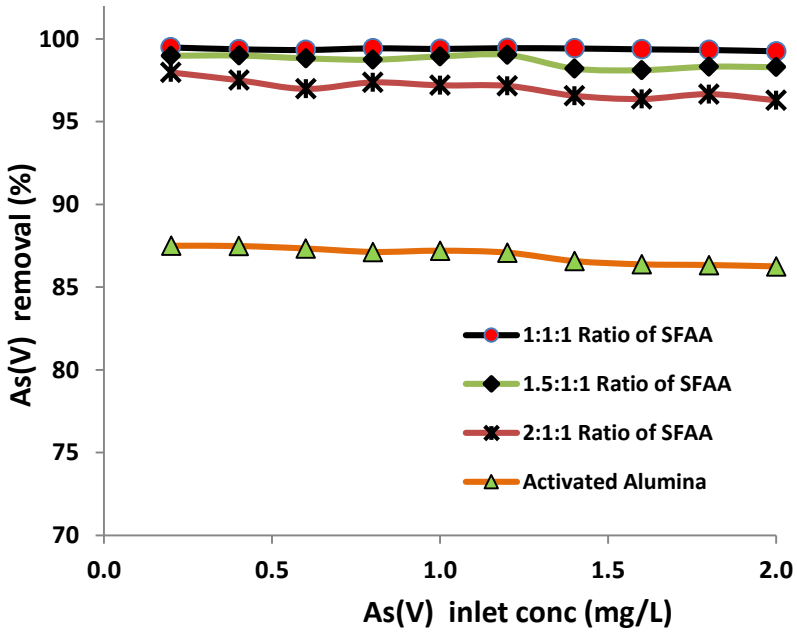

Fig.2.1. Optimization of SFAA mass ratio for As(V) adsorption
(C_o =0.2-2 mg/L, time = 4h, Temp = 303K)

The adsorption capacities for various combinations are given in Fig.2.1 and Fig.2.2 for arsenic and fluoride. It is evident that a mass ratio of 1.5:1:1 of sawdust: ferric hydroxide: activated alumina has the best adsorption capacity for both arsenic and fluoride.

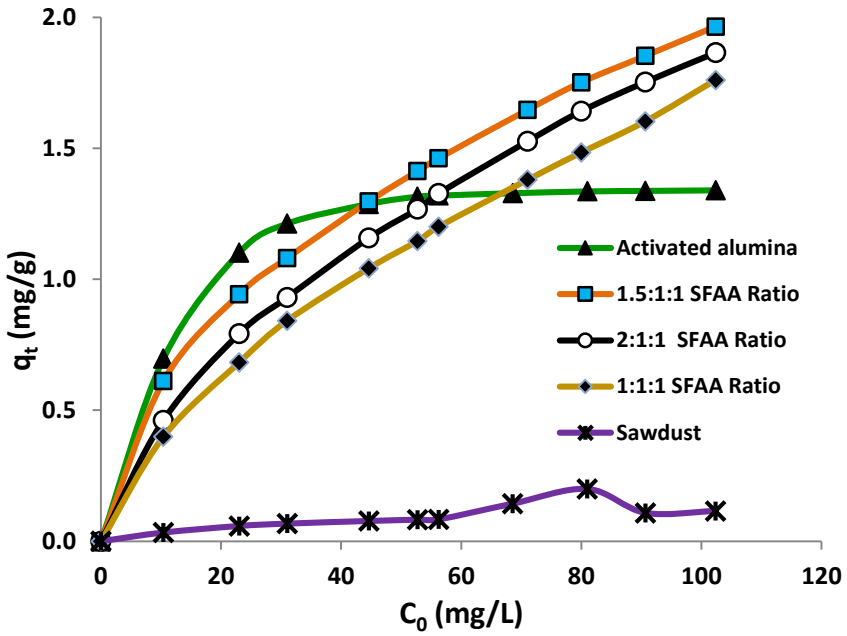

Fig.2.2. Optimization of SFAA mass ratio for fluoride adsorption
(C_o =10-100 mg/L, time = 4hr, Temp = 303K)

2.3 SYNTHESIS OF THE ADSORBENT SFAA

Sawdust (Artocarpus hirsutus), which was pretreated as explained in section 2.1 was mixed with ferric hydroxide and activated alumina in 1.5:1:1 mass ratio (sawdust: ferric hydroxide: activated alumina) and made into a paste with sufficient quantity of water. The paste was dried in an oven to constant weight and the dried mass was sieved to obtain different particle sizes. Adequate quantity was prepared and samples from the same lot were used for all the experiments, thus avoiding the uncertainties in the results due to variation in the method of preparation of adsorbent.

2.4 CHARACTERIZATION OF SFAA

2.4.1 Determination of surface area and pore size distribution

I. By liquid Nitrogen adsorption

The surface area and pore volume of sawdust, SFAA, SFAA after fluoride adsorption, SFAA after As(V) adsorption and SFAA after As(III) adsorption were evaluated by Sorptomatic 1990

Brunauer-Emmet-Teller (BET) analyzer (France) using liquid nitrogen as a coolant.

II. By Mercury Porosimetry

The surface area and pore volume of sawdust, SFAA, SFAA after fluoride adsorption, SFAA after As(V) adsorption and SFAA after As(III) adsorption were evaluated by thermo PASCAL-140 Mercury Intrusion Porosimeter using non-wetting liquid (mercury).

2.4.2 Scanning Electron Microscopy

For surface characterization of SFAA, scanning electron microscopy (SEM) was carried out using Philips XL-30 electron microscope at 15 kV. The SEM images of SFAA, As(V) adsorbed SFAA, As(III) adsorbed SFAA and fluoride adsorbed SFAA were analyzed and the images are recorded under the magnification of 2000x. Energy Dispersive X-ray spectroscopy (EDX) makes use of the X-ray spectrum emitted by a solid sample bombarded with a focused beam of electrons to obtain a localized chemical analysis.

2.4.3 Fourier Transform Infra Red Spectrophotometer

To study the surface of SFAA, Fourier Transform Infra Red Spectrophotometer (FTIR) spectra were recorded between 500 cm^{-1} and 4000 $cm^{-1}$with 16 cm^{-1} resolution using ABB-MB3000 FTIR spectrometer.

2.4.4 X-ray Photoelectron Spectroscopy

X-ray Photoelectron Spectroscopy (XPS), a highly surface sensitive tool is employed to investigate the trace level presence of As and F ions in addition to iron and their oxidations states in the sawdust matrix. The X-ray Photoelectron Spectroscopy (XPS) was performed with XPS spectrometer (M/s. Specs, Germany) provided with a monochromatic AlK_{α} radiation and a hemispherical analyzer. The base vacuum was observed to be better than 5.0×10^{-10} mbar during the analysis. The selected area scans were collected with 20 eV pass energy. Prior to analysis, the XPS pattern of silver was recorded and the spectrometer was calibrated. The full width at half maximum (FWHM) of the Ag $3d_{5/2}$ was around 1 eV. As the samples were insulating, electron flood gun was used to compensate for the charging effect during data acquisition and the electron

energy for the flood gun was appropriately adjusted. The C1s peak position of 285.0 eV for the adventitious carbon was used to calibrate the recorded spectra [265]. The XPS patterns of As 3p, O 1s, F 1s and Fe 2p levels were recorded at room temperature.

2.5 BATCH SORPTION EXPERIMENTS

Experiments were carried out to study the effect of contact time, initial fluoride concentration, pH, temperature, particle size, adsorbent dose and concentration of various co-existing ions on fluoride sorption by SFAA. Dry sorbent of 0.1 g was added to 10 mL of synthetic fluoride solution in sample vials of 15 mL and the pH was adjusted to 6.5. This dose of adsorbent was used in all experiments, except for studying the effect of adsorbent dose, where this was varied over a range. These samples were kept in a thermostatic shaker (Technico Laboratory Products Pvt Ltd., India) for mixing at 30°C and 40 rpm. Samples were removed at predetermined time intervals, centrifuged, filtered using 90 mmϕ Whatman filter paper and analyzed for residual arsenic, fluoride concentration. Experiments were repeated to check for reproducibility. The amount of arsenic, fluoride adsorbed at equilibrium, q_e (mg/g), was computed by

$$q_e = \frac{(C_o - C_e)V}{m} \quad \text{..... 2.1}$$

where, C_o is initial concentration (mg/L), C_e is equilibrium concentration (mg/L), V is volume of solution (L) and m is the mass of adsorbent (g).

2.6 FIXED BED EXPERIMENTS

A glass column of 0.5 or 1.0 cm inner diameter (d_i) and 50 cm height was used for evaluating the column performance of SFAA for the arsenic and fluoride adsorption from water. A schematic of the experimental setup is shown in Fig.2.3. About 1 or 2 g of SFAA was filled in the column. The bottom of the column was filled with glass wool to provide support to SFAA. Synthetic water with known arsenic and fluoride concentration was passed through the column with a constant flow rate using a peristaltic pump. The treated water drawn from the bottom of the column was collected in a storage vessel and samples were analysed at regular intervals.

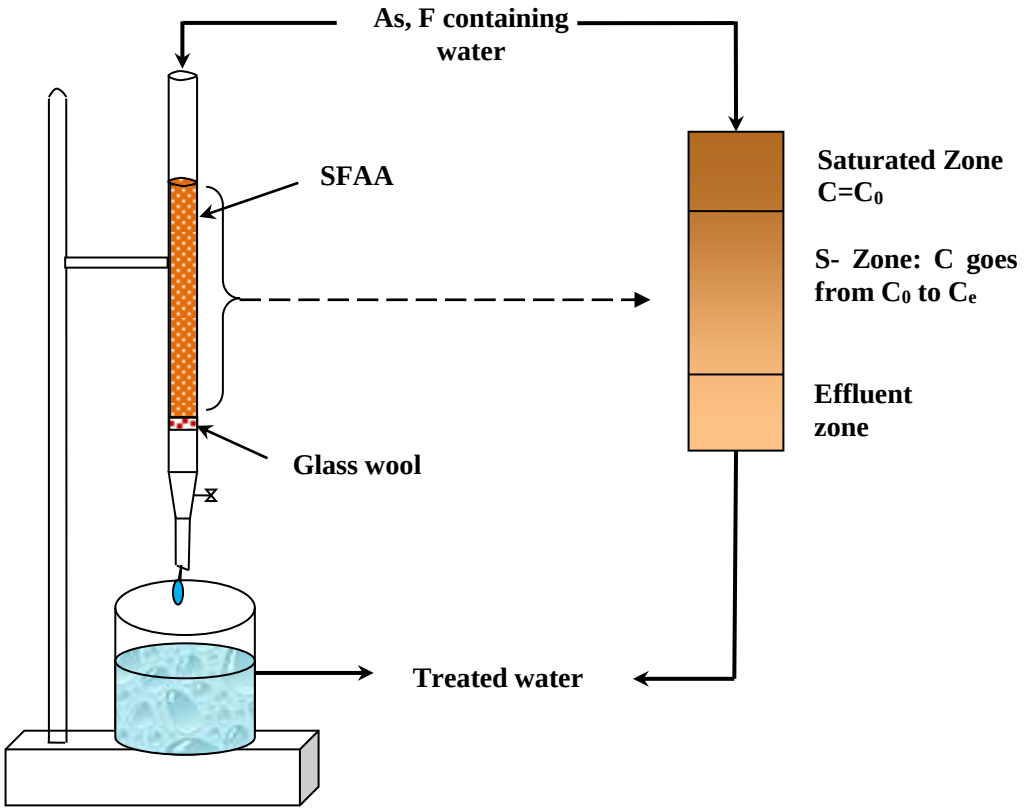

Fig.2.3. Fixed bed adsorption experimental setup

2.7 ANALYSIS OF ARSENIC AND FLUORIDE IN WATER

Arsenic (As) analysed by Inductively Coupled Plasma Mass Spectrometer (ICP-MS) for various concentration samples. A pH/ISE meter (MeterLab Model, PHM240, Expandable Ion Analyzer, U.S.A.) equipped with combination fluoride-selective electrode (pHoenix electrode Co., Model pF-1, U.S.A) was employed for the determination of F^-. A pH meter (ELICO, Model LI 120, India) equipped with ELICO pH electrode was used to measure the pH of solutions at particular experiment condition.

3 ADSORPTION OF ARSENIC FROM WATER BY SFAA

Arsenic adsorption from water by SFAA in batch and fixed bed were studied and presented in detail in this chapter. Characterization studies of SFAA, before and after arsenic adsorption are also presented. Isotherm and kinetic modeling for arsenic adsorption are discussed. Effects of various parameters in batch and fixed bed were studied and different models for column operation are compared with experimental results to identify the model that explains the column performance adequately.

3.1 CHARARCTERIZATION OF THE ADSORBENT AND ITS CONSTITUENTS

3.1.1 Surface area and pore size distribution

Bruner, Emmet and Teller (BET) isotherm provides precise specific surface area evaluation of adsorbents by liquid nitrogen multilayer adsorption measured as a function of relative pressure using a fully automated analyzer. This technique evaluates the total specific surface area contributed by the pores and the external surface. In microporous solids, the contribution of external surface to the surface area is much smaller compared to the contribution of pores. BET surface area of saw dust, as well as SFAA before and after arsenic adsorption is determined to characterize the adsorbent and understand the role of micropores in the adsorbent in arsenic adsorption by SFAA. These are shown in Figs. 3.1 to 3.5. The saw dust has a BET surface area of 22.50 m^2/g, which is reasonably good for a base material. Activated Alumina has a BET surface area of 118.43 m^2/g, where as SFAA has a surface area of 61.10 m^2/g.

To understand the contributions of individual components of SFAA to the properties of the adsorbent, pore size distribution studies of SFAA as well as saw dust and AA were carried out. The pores size distribution (PSD) in the meso pore range determined by nitrogen adsorption is analyzed using t-plots. From this analysis, micropore volume, V_{micro} and mesopore surface area, S_{meso} are estimated. As BET surface area is a combination of meso and micropore surface areas,

the micropore surface area, S_{micro} could be calculated. PSD in the macropore range is determined by mercury porosimetry. From this, the macropore surface area, S_{macro} and macropore volume, V_{macro} are estimated. The PSD is presented for saw sawdust, AA, SFAA and SFAA after adsorption of As (III) & As (V).

It can be seen that the sawdust has substantial macropore volume and micropore surface area. In case of activated alumina the surface area is mostly in the mesopore region and the macropore volume is moderate. As a result, the combination adsorbent, SFAA has a well-balanced pore size distribution with the pore volumes and surface areas distributed in macro, meso and micropore regions. Table 3.1 shows surface areas and pore volumes in all the three ranges for saw dust, activated alumina and SFAA before and after adsorption of arsenic. The distribution of surface areas and pore volumes for SFAA before and after adsorption of As shows that the micropore surface area reduced from 33.50% to 30.26 % in case of As (III) and to 6.33 % in case of As (V). In terms of actual areas, this indicates that the micropores have been filled very effectively in case of As(V) adsorption by SFAA. Similarly, the S_{meso} reduced to 43.90% of the original for SFAA as against 86% for activated alumina. Thus, even in the mesopore region, adsorption has been more effective by SFAA. There is no difference in Macropore volumes before and after adsorption in case of both activated alumina and SFAA, as the adsorption takes place only in meso and micropores. The effectiveness of SFAA is reflected in the maximum adsorption capacities of activated alumina [44.77 mg/g for As(III), 59.06 mg/g for As(V)] and SFAA [54.32 mg/g for As(III), 77.60 mg/g for As(V)] for initial concentration of 3000 mg/L arsenic as shown in Table 3.2. A good adsorbent should have a well-developed pore size distribution, as macropores essentially serve as transport pathways and micro and mesopores contribute to the adsorption sites. Thus, though the BET surface area of activated alumina is more than that of SFAA, the utilization of the micro/meso pores for adsorption is better in case of SFAA because of the well-developed approach paths to the micropores in case of SFAA. This is also reinforced by the column studies presented in section 3.3.

Besides a higher efficiency, this adsorbent is economic as the sawdust constitutes 40% by weight of the total adsorbent, minimizing the concentration of other metallic hydroxides. Thus Artocarpus hirsutus sawdust plays an important role by in preparation of this efficient and cost effective adsorbent.

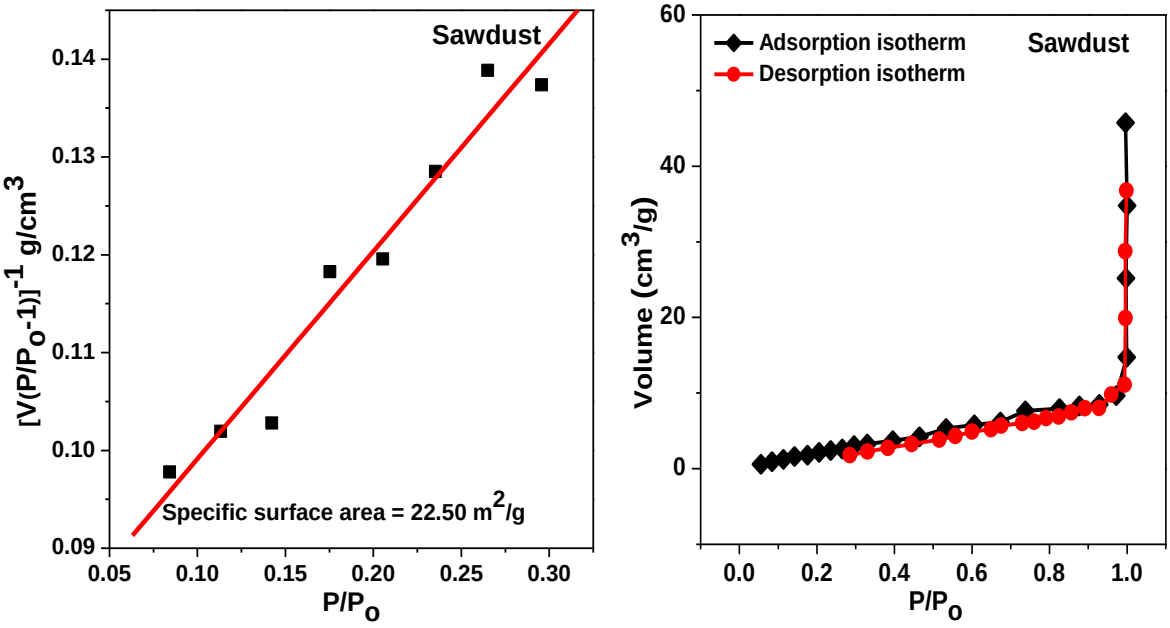

Fig.3.1. BET surface area of Aanjili tree sawdust

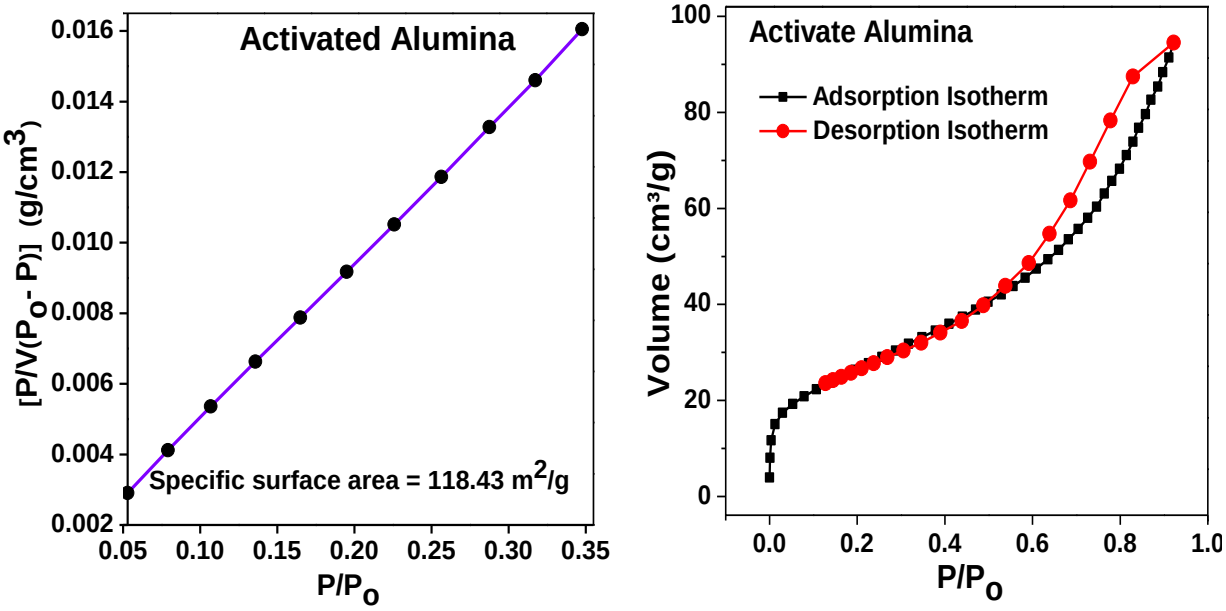

Fig.3.2. BET surface area of Activated Alumina

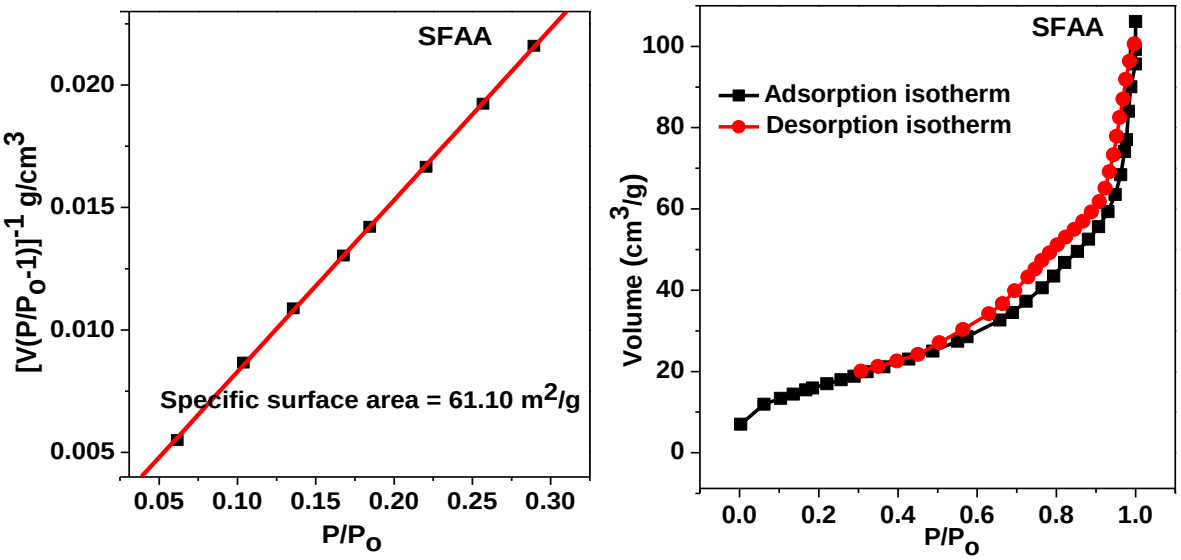

Fig.3.3. BET surface area of SFAA

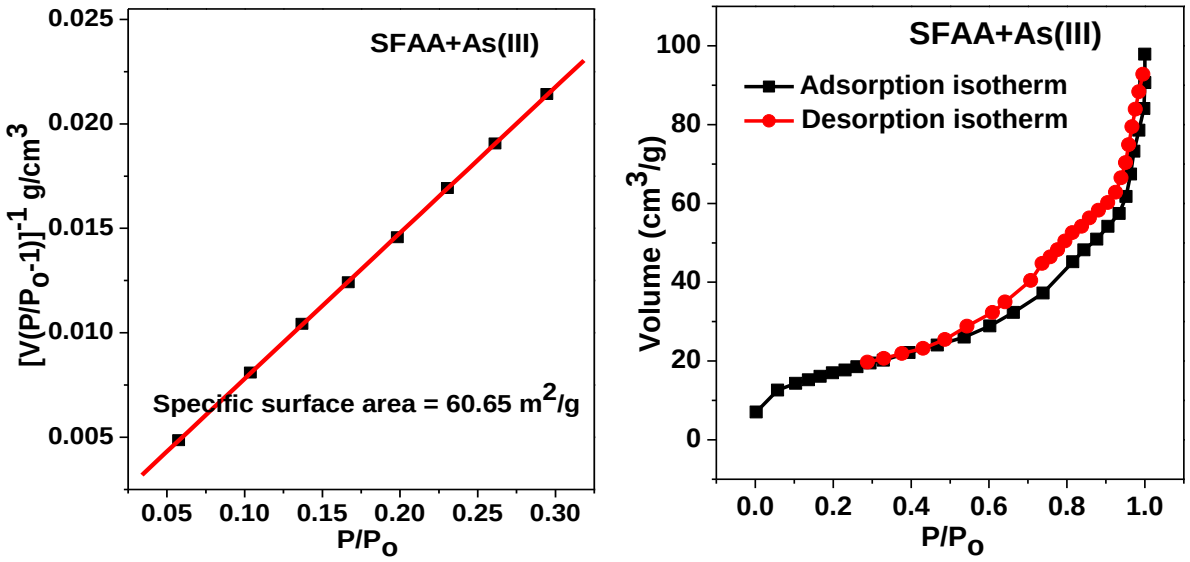

Fig.3.4. BET surface area of SFAA after As(III) adsorption

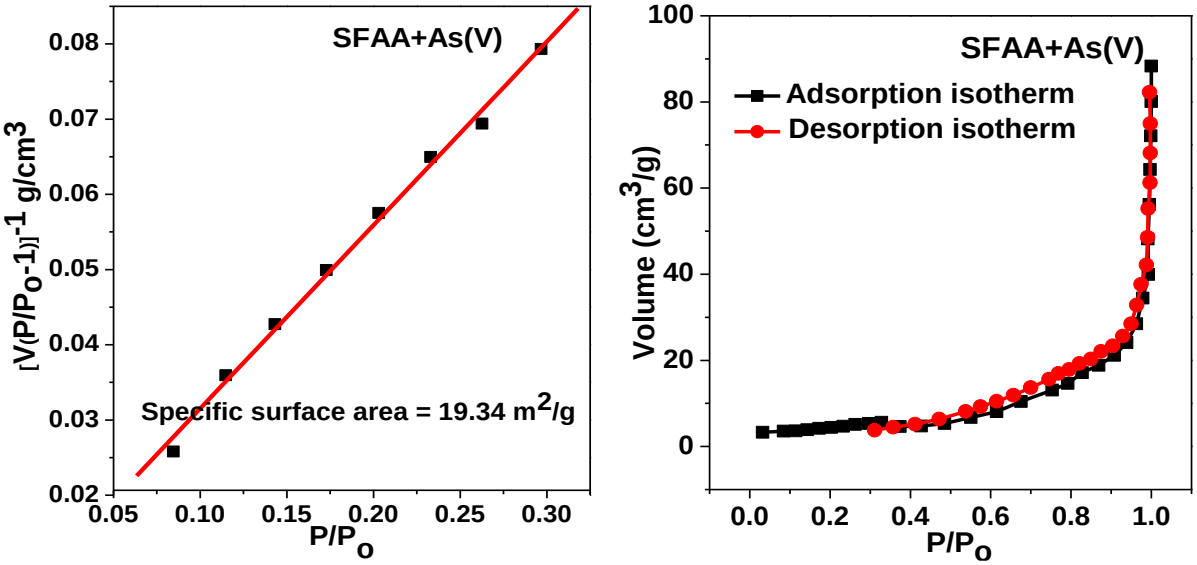

Fig.3.5. BET surface area of SFAA after As(V) adsorption

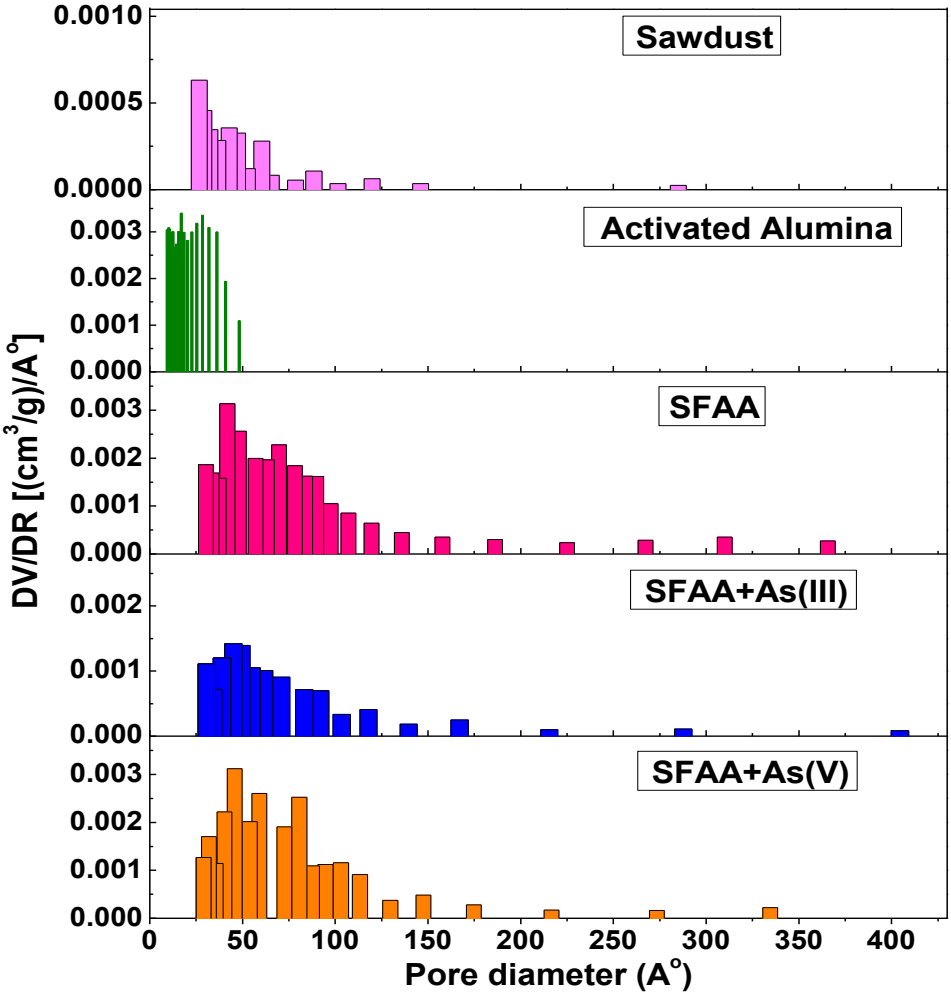

Fig.3.6 (a) Pore size distribution by liquid nitrogen adsorption

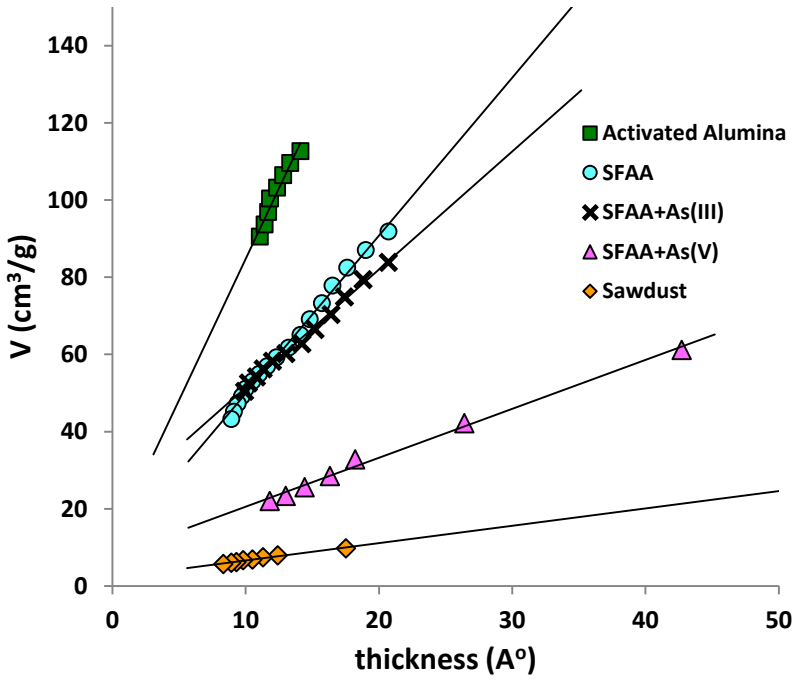

Fig.3.6 (b) t-plot based on N_2 adsorption

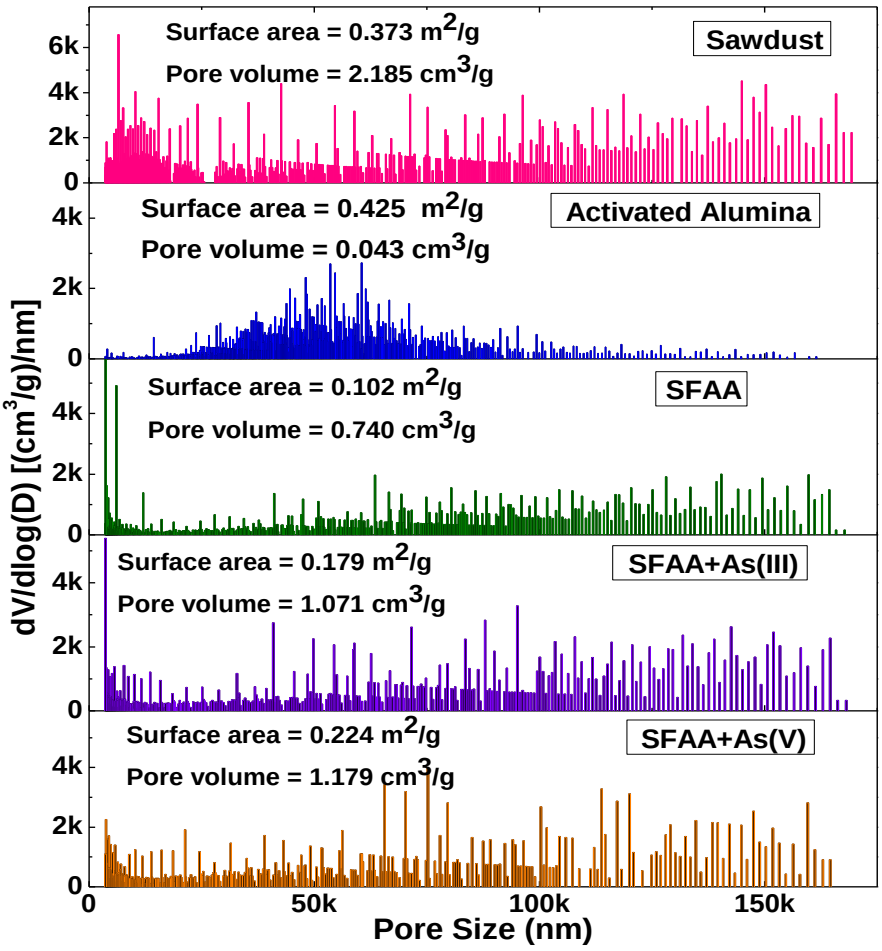

Fig. 3.6 (c) Pore size distribution by mercury porosimetry

$$V_{TOTAL} = V_{micro} + V_{meso} + V_{macro} \text{ ..... 3.1}$$

$$S_{TOTAL} = S_{micro} + S_{meso} + S_{macro} \text{ ..... 3.2}$$

Table 3.1 Surface areas and pore volumes of the adsorbents

Adsorbent	By Liquid N_2 Adsorption		From t-Plots				Mercury Porosimetry	
	S_{BET} (m^2/g)	$V_{meso+micro}$ (cm^3/g)	V_{micro} (cm^3/g)	V_{meso} (cm^3/g)	S_{meso} (m^2/g)	S_{micro} (m^2/g)	V_{macro} (cm^3/g)	S_{macro} (m^2/g)
Sawdust	22.50	0.0133	0.0034	0.00986	7.42	15.08	2.185	0.373
AA	118.43	0.172	0.0179	0.1540	113.22	5.21	0.043	0.425
SFAA	61.10	0.0965	0.0313	0.0652	41.20	19.85	0.740	0.102
SFAA + As(III)	60.65	0.0873	0.0276	0.0597	42.24	18.41	1.071	0.179
SFAA +As(V)	19.34	0.0363	0.0089	0.0274	18.10	1.24	1.179	0.224

Table 3.1 Continued

Adsorbent	V_{TOTAL} (cm^3/g)	% V_{micro}	% V_{meso}	% V_{macro}	S_{TOTAL} (m^2/g)	% S_{micro}	% S_{meso}	% S_{macro}
Sawdust	2.20	0.16	0.45	99.40	22.87	65.93	32.44	1.63
AA	0.60	2.99	25.78	71.23	118.44	4.37	95.59	0.04
SFAA	0.84	3.74	7.80	88.46	62.11	33.50	66.33	0.16
SFAA + As(III)	1.16	2.37	5.15	92.33	60.83	30.26	69.39	0.29
SFAA + As(V)	1.22	0.73	2.25	96.64	19.56	6.33	92.54	1.15

S_{BET} – BET Surface area (m^2/g), $V_{meso+micro}$ – Meso and micro pore volume (cm^3/g), V_{micro} – Micropore Volume (cm^3/g), V_{meso} – Mesopore Volume (cm^3/g), S_{meso} – Mesopore surface area (m^2/g), S_{micro} – Micropore surface area (m^2/g) , V_{macro} – Macropore Volume(cm^3/g), S_{macro} – Macropore surface area (m^2/g).

3.1.2 Scanning Electron Microscopy

The SEM images and EDX spectra of the SFAA before and after adsorption of As(III) and As(V) are shown in Figs. 3.7, 3.8 and 3.9, respectively. From these SEM images, it can be seen that the granules remained intact after grafting, except for the appearance of some pores on the surface of SFAA. EDX analysis was performed to find the elemental constituents of pure SFAA, SFAA+As(III) and SFAA+As(V) (Fig.3.7, 3.8 & 3.9). The atomic % of Al and Fe on the basis of chemicals presented in pure SFAA was found to be 35.9 and 37.1%. As(III) and As(V) adsorption conformed by the presence of corresponding peaks in the EDX spectra of SFAA after adsorption (Fig.3.8 & 3.9).

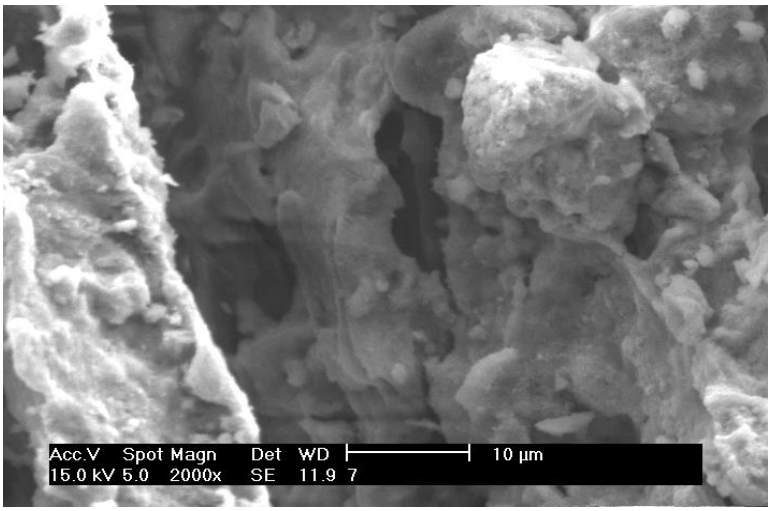

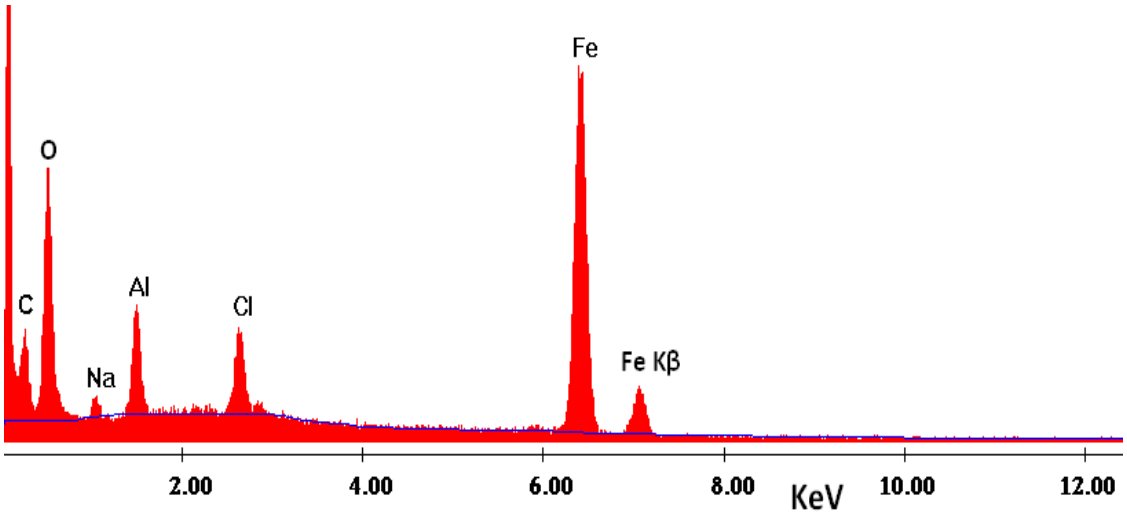

Fig.3.7. SEM image and EDX spectra of SFAA

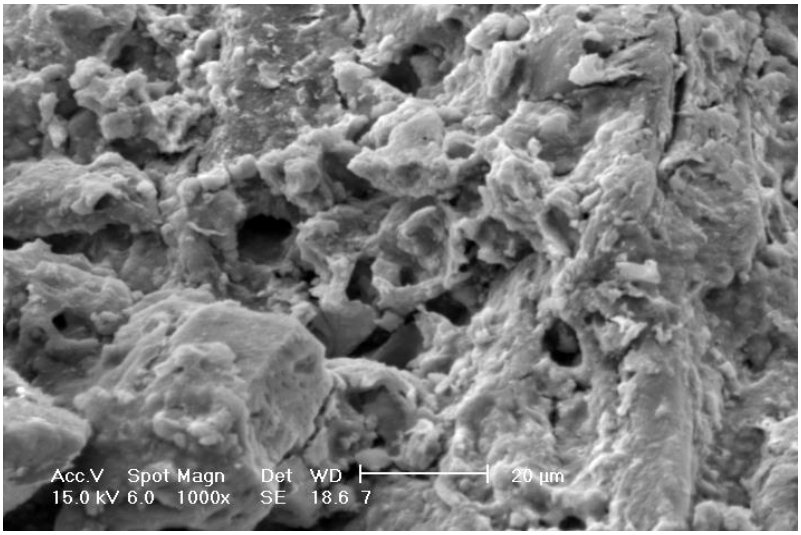

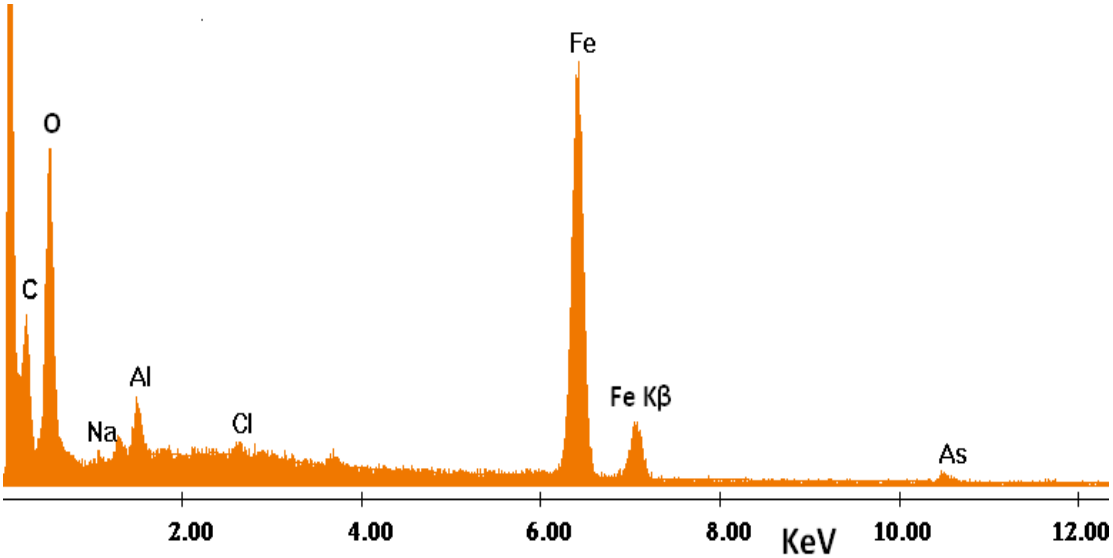

Fig.3.8. SEM image and EDX spectra of SFAA after As(III) adsorption

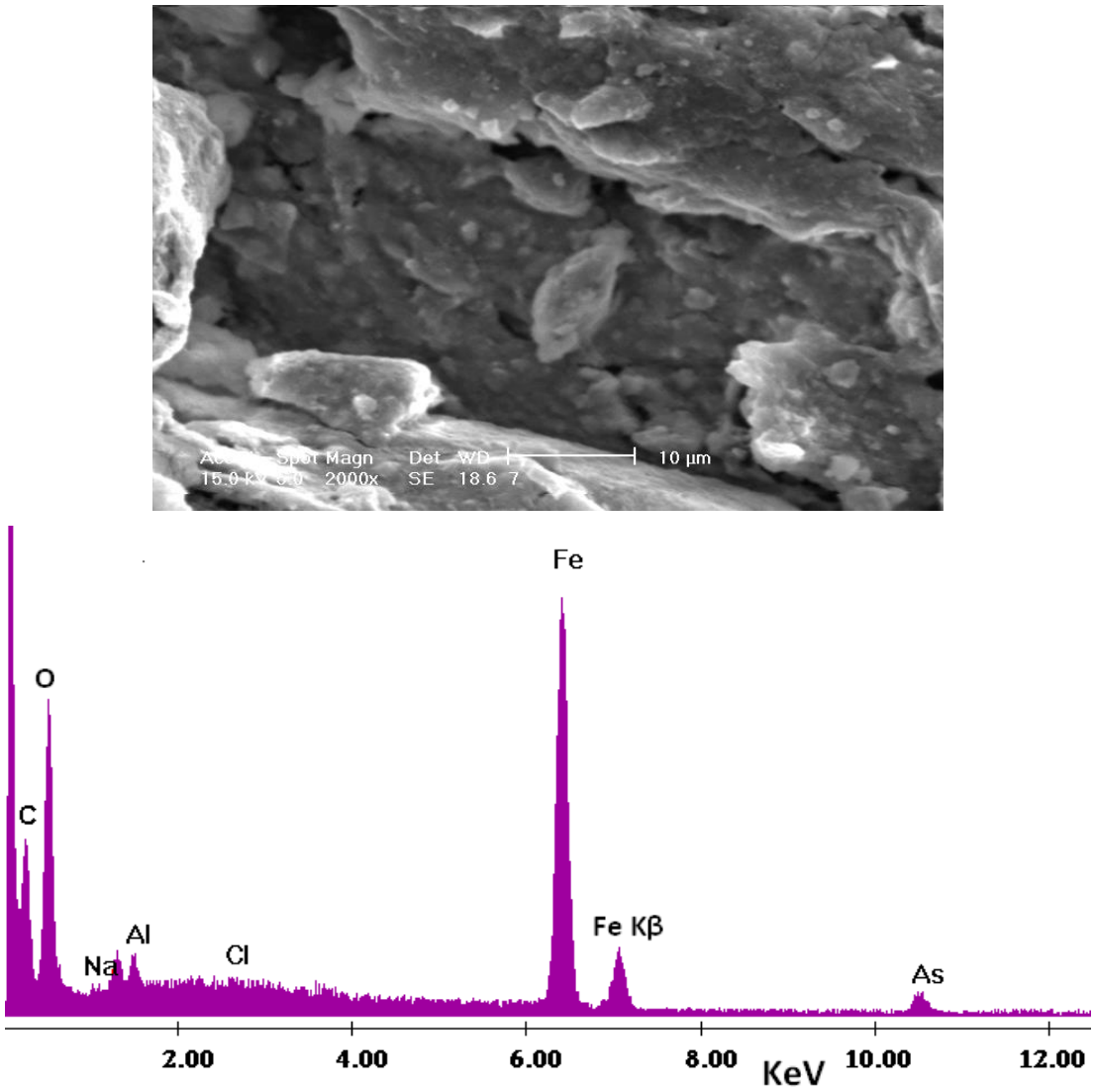

Fig.3.9. SEM image and EDX spectra of SFAA after As(V) adsorption

3.1.3 Fourier Transform Infra Red spectrophotometer

To study the surface of SFAA, FTIR spectra were recorded in a range between 500 cm^{-1} and 4000 cm^{-1} with 16 cm^{-1} resolution using ABB-MB3000 FTIR instrument. Fig. 3.10 shows the FTIR spectra of SFAA before and after arsenic adsorption. The broad and intense peak at 3060-3600 cm^{-1} was assigned to hydroxyl stretching vibration of water and that at 1640 cm^{-1} represents HOH bending vibration of water. The FTIR spectrum shows the prominence of the peaks in the adsorbent and decrease in the peak height after arsenic adsorption. The small peaks at 1504 cm^{-1} and 1427 cm^{-1} were assigned to C=C aromatic stretching. FTIR results also indicated that mainly hydroxide in the carboxylic groups were involved in arsenic sorption. Surface characterization of biosorbents were studied by various researchers and the results of FTIR studies on SFAA showed

similar trends, as sawdust is its major component. Biomass based sorbents contain a high amount of polysaccharides and some of them are associated with proteins and other components [266]. These bio macromolecules on the sorbent surfaces have several functional groups such as amino, carboxyl, thiol, sulfydryl, alcohol, phenol and phosphate groups [267].

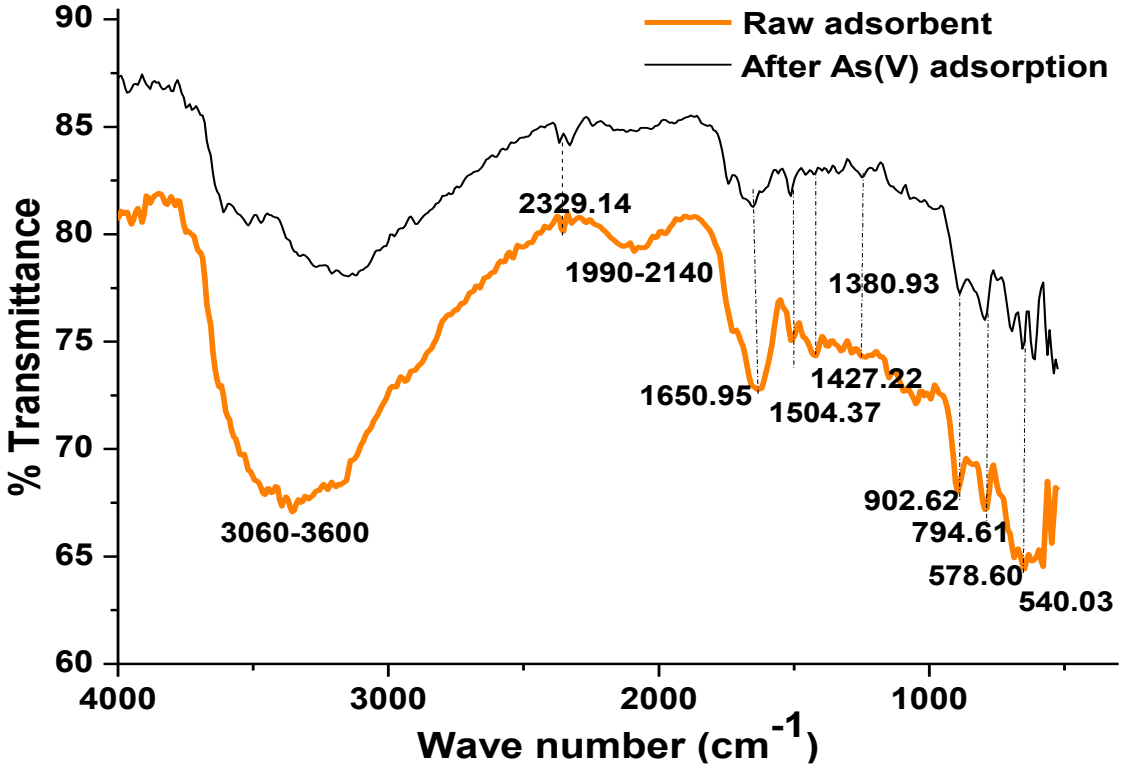

Fig.3.10. FTIR spectra of SFAA before and after As(V) adsorption

3.1.4 X-ray Photoelectron Spectroscopy

The XPS survey scans of SFAA, arsenic loaded specimens were shown in Fig. 3.11. The plot shows the signatures of As 3d, As 3p, C 1s, O 1s and Fe 2p along with the auger lines of arsenic, oxygen and Fe as marked in Fig.3.10. Selected area scans were performed for As 3p, C 1s, O 1s and Fe 2p levels. Figure 3.12(a) shows C 1s pattern for the arsenic loaded specimen. The origin of the peak at 285 eV is characteristic of free carbon whereas the peak at 287 eV may possibly be due to adsorbed CO_2. On the other hand only arsenic loaded specimen exhibited a single C 1s peak at 285 eV indicating the presence of free carbon in these specimens. In addition, there is broad peak starting from 265 eV with a peak centre at 269 eV is characteristic of the auger line of As. This is confirmed by the reduction in intensity of the auger peak of As in simultaneously

loaded arsenic specimen as observed in Fig.3.11. This confirms the presence of As in the specimens as it is absent for only SFAA specimen as seen in Fig. 3.11.

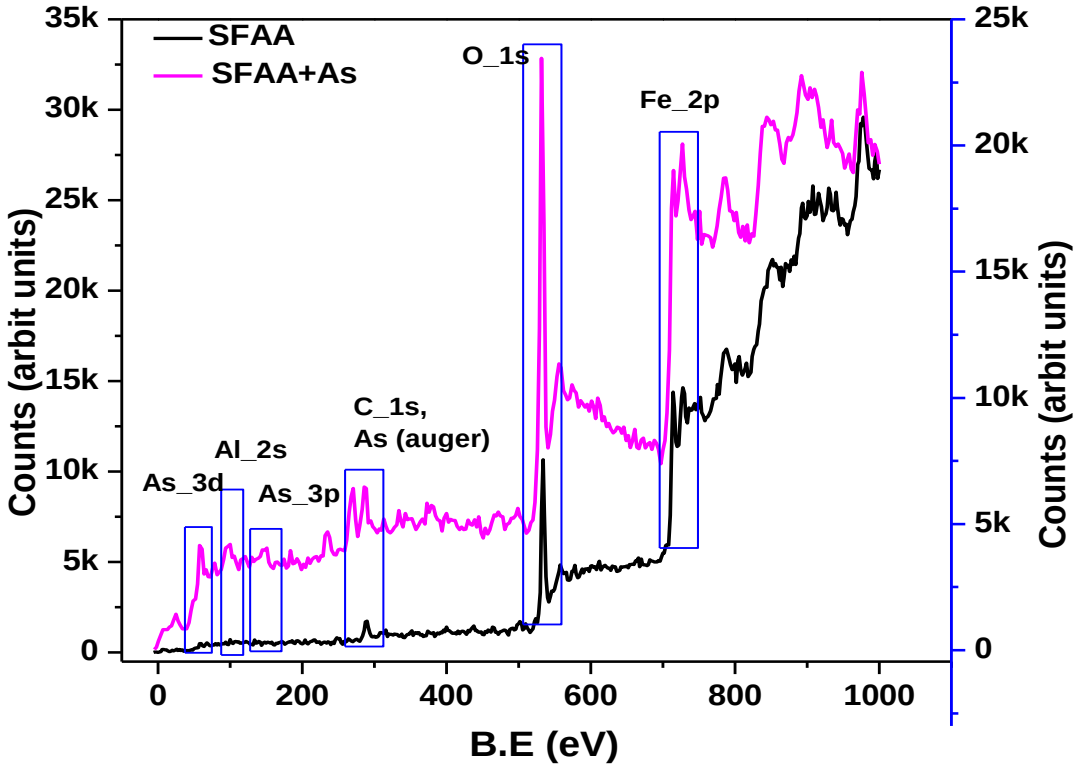

Fig.3.11. XPS survey of SFAA before and after As(V) adsorption

To confirm the presence of arsenic, the region for As 3p is scanned and patterns were recorded for the arsenic loaded specimens and shown in Fig. 3.12(c). The graph can be fitted with Gaussian functions marking $3p_{3/2}$ and $3p_{1/2}$ components of As and the analysis of peak position shows that As in +5 valence state. This again confirms that As is trapped in the matrix and that the oxidation state of As is +5. Finally, Fe 2p patterns were recorded to investigate the oxidation state of Fe under the influence of arsenic ion. Fig. 3.12(b) shows the Fe 2p patterns of arsenic loaded specimen. Fe $2p_{3/2}$, Fe $2p_{1/2}$ and their respective satellites are seen from the graph for both the specimens. In addition, an additional satellite at 736 eV appears for both the specimens. The positions of the peaks and the satellite at 736 eV confirm that Fe is present in 3+ valence state and does not undergo any change. It is clear that Fe in a single valence state. The patterns are similar for both the specimens indicating neither fluoride nor arsenic change the valence state of Fe.

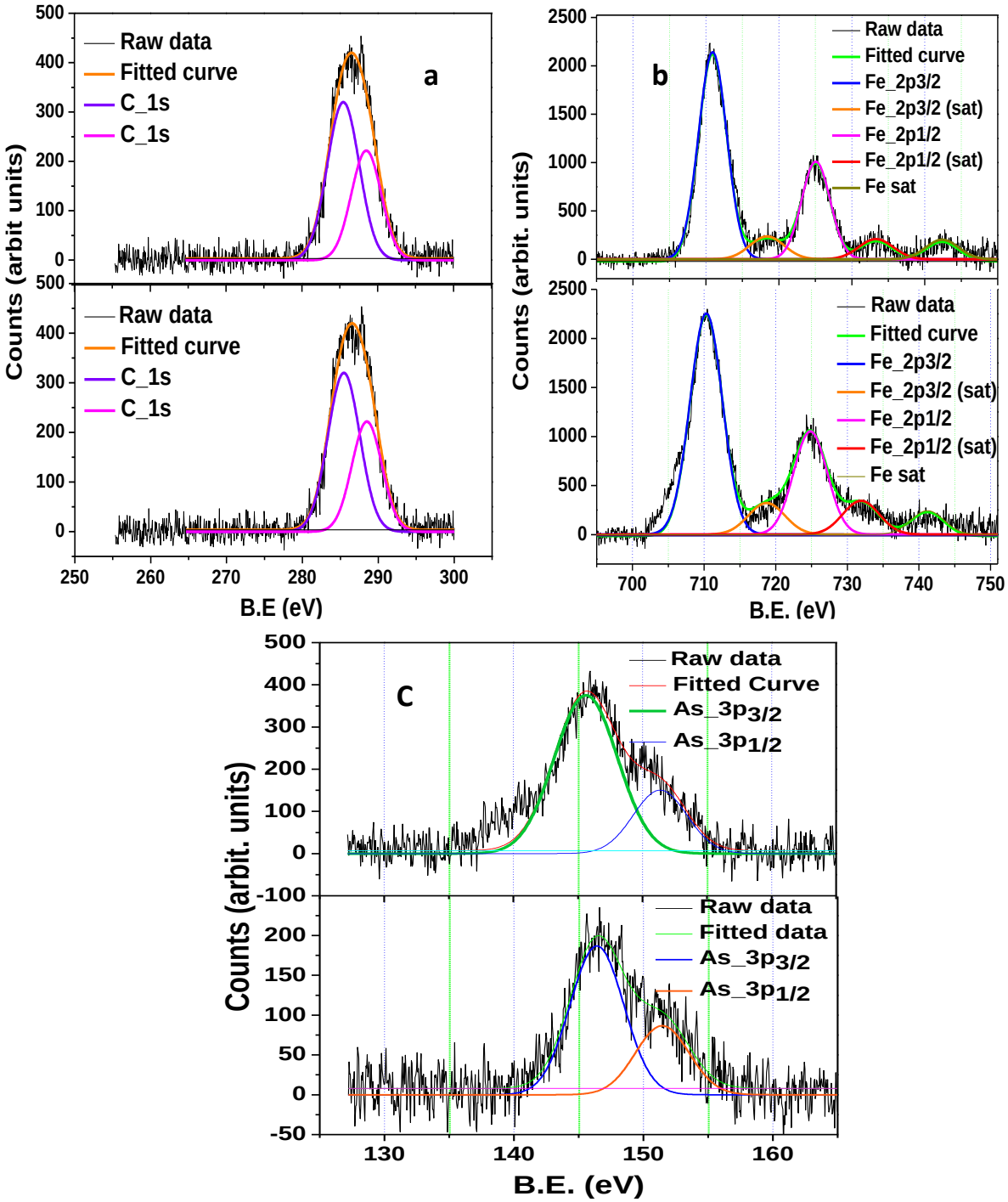

Fig.3.12. XPS spectra of (a) C 1s, (b) Fe 2p, (c) As 3p

3.2 BATCH STUDIES

3.2.1 pH study

The effect of pH on removal of arsenic by SFAA was studied using 0.10 g of adsorbent in 10 mL of 20 mg/L arsenate and arsenite solutions. The pH of the solution was adjusted by adding dilute NaOH or HNO_3 drop wise to obtain pH of 2.0 through 10.0. The equilibrium uptake (q_e) of arsenic from solutions of different pH is shown in Fig. 3.13.

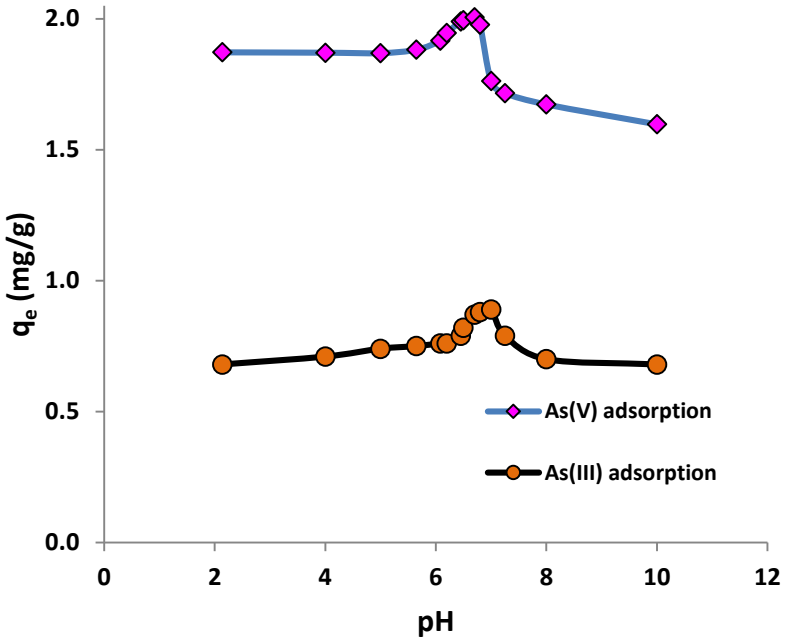

Fig.3.13. Effect of pH on As(V) & As(III) adsorption (C_o = 20 mg/L, time = 4hr, Temp = 303K)

Uptake of As (V) was almost constant in the pH range of 2 to 6, whereas for As (III) the uptake increased in the range of 2 to 7. Maximum uptake was observed in pH range of 6.5-7 for both As(V) and As (III). Maximum As(V) removal was found to be more than 95%, whereas for As (III), it was only 45%. The results can be explained using As chemical forms in different pH ranges. In the pH range of 3-8.5 arsenate [As(V)] exists mostly in its anionic form ($H_2AsO_4^-$, $HAsO_4^{2-}$). The adsorbent has positive charge on the surface up to the point of zero charge (5.85 for SFAA) which attracts negatively charged $H_2AsO_4^-$, $HAsO_4^{2-}$ (electrostatic attraction) thereby favoring adsorption. In the As(V) adsorption as pH increases amount of negative arsenic species increases, while the number of positively charged adsorbent surface sites decreases (up to pH_{PZC}) [268]. At neutral pH, both $H_2AsO_4^-$, $HAsO_4^{2-}$ are present equally hence the adsorption is maximum at this pH. Up to pH≤ 9, arsenite (As(III)) exists as stable and neutral H_3AsO_3, and therefore there is no electrostatic interaction between As(III) and adsorbent surface up to pH_{PZC} [269]. In case of As(V) adsorption, both electrostatic attraction and chemical bonding take place. But in case of As(III), only chemisorption takes place, and hence the As(III) adsorption is less compared to As(V).

3.2.2 Effect of adsorbent dose

The effect of adsorbent dose on arsenic removal was studied for an initial arsenic concentration of 2 mg/L for a contact time of 4h. The results obtained are shown in Fig. 3.14 as percentage removal for adsorbent dose ranging from 1 to 30 g/L. The removal of As(V) increased from 27.33 to 98.64 percent with increase in the adsorbent dose from 1 to 10 g/L and with further increase in dose, % removal remained constant. A greater dosage of sorbent implies a greater amount of available binding sites, which result in increased sorption. The optimum adsorbent dose was taken as 10 g/L for complete removal of As(V) from an initial concentration of 2 g/L.

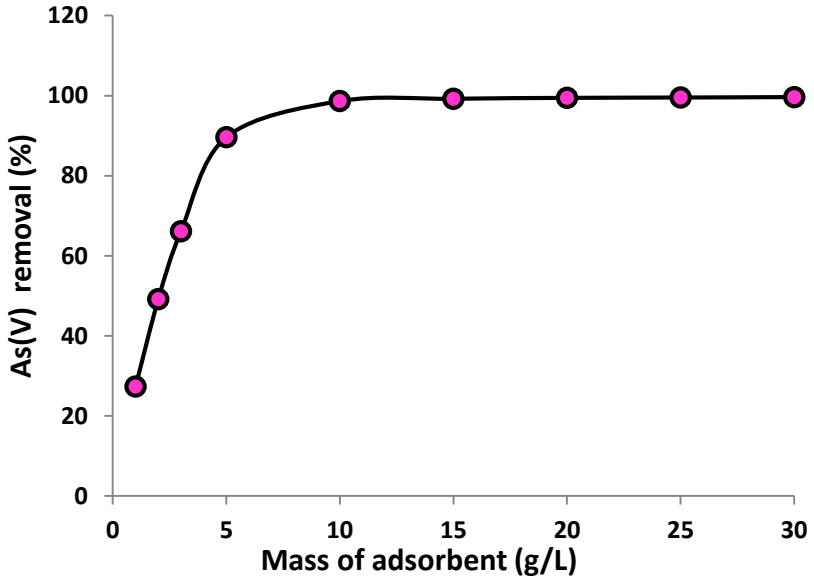

Fig.3.14. Effect of mass of adsorbent on As (V) adsorption

The distribution coefficient (K_{DC}) for As (V) on adsorbent was calculated by

$$K_{DC} = q_e/C_e \quad \ldots\ldots\ldots\ldots\ldots\ldots\ldots\ldots\ldots\ldots \quad 3.3$$

where, q_e is mass of As(V) adsorbed per unit mass of adsorbent and C_e is the concentration of As(V) in the solution at equilibrium. The distribution coefficient reflects the binding ability of the surface for an element and is dependent on pH and type of surface [268, 270]. The K_{DC} values for As(V) on SFAA at initial pH of 6.5 were calculated and presented in Fig. 3.15. It can be seen that K_{DC} values increased with an increase in adsorbent dose, indicating that the adsorbent has a heterogeneous surface [271]. K_{DC} value is 7271.43 L/kg at the dose rate of 10 g/L which increased to 9263.96 L/kg at the dose rate of 30 g/L.

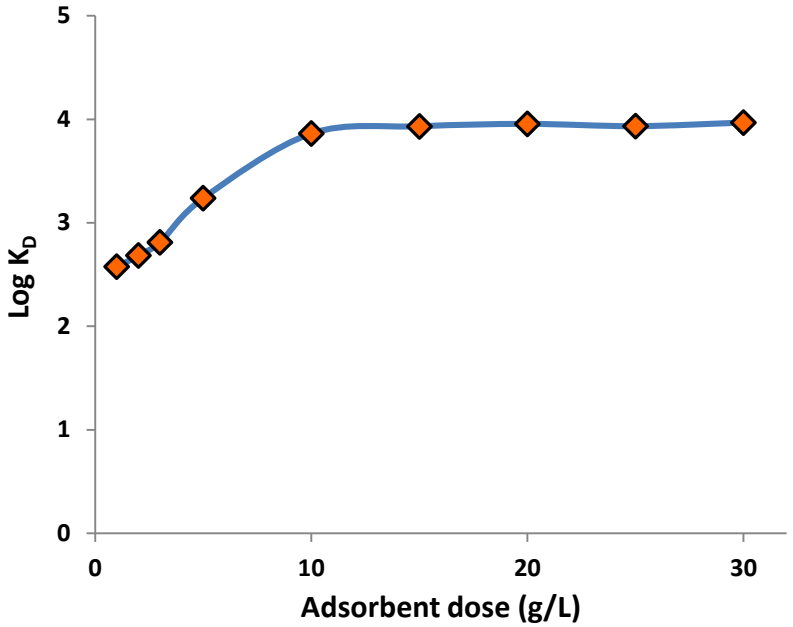

Fig.3.15. Variation of distribution coefficient with adsorbent dose

3.2.3 Equilibrium isotherms

Equilibrium isotherms for As(V) and As(III) adsorption on SFAA are shown in Fig.3.16. The initial concentration of the solutions was varied from 0 to 3000 mg/L at an initial pH of 6.5. The temperature for the equilibrium was maintained at 303K. The maximum equilibrium uptake capacities were found to be 77.60 mg/g and 54.32 mg/g for As (V) and As (III), respectively for an initial concentration of 3000 mg/L. These capacities are better than most adsorbents reported in the literature, as can be seen from Table 3.2.

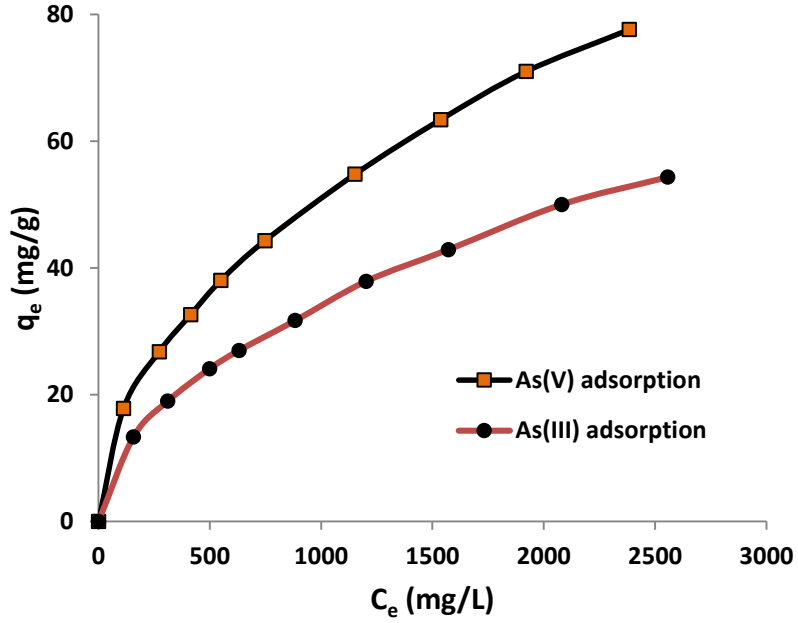

Fig.3.16. Effect of initial concentration (C_o =100-3000 mg/L, Time = 24hr, Temp = 303K)

Table 3.2 Arsenic adsorption capacity of SFAA and Activated Alumina

Adsorbent	Adsorption Capacity		Experimental conditions			Reference
	As(III) (mg/g)	As(V) (mg/g)	Temp (ºC)	pH	Conc. (mg/L)	
SFAA	54.32	77.60	30	6.5	20-3000	Current study
Activated Alumina	44.77	59.06	30	6.5	20-3000	Current study

Freundlich and Langmuir isotherms were used to model the adsorption inorder to have an insight of adsorption mechanism. Freundlich isotherm is an empirical equation based on sorption on a heterogeneous surface and is expressed as

$$q_e = K_F C_e^{1/n} \quad \text{..... 3.4}$$

where, q_e is the equilibrium uptake of arsenic per unit mass of adsorbent (mg/g), K_F is the Freundlich constant ($mg.g^{-1}(Lmg^{-1})^{1/n}$), C_e is the equilibrium concentration (mg/L) and n is a constant.

The Langmuir isotherm, which is valid for a monolayer sorption on to a surface is given below,

$$\frac{C_e}{q_e} = \frac{1}{K_L q_m} + \frac{C_e}{q_m} \quad \text{..... 3.5}$$

where, q_e is the equilibrium uptake of arsenic per unit mass adsorbent (mg/g), q_m is the maximum value of q, K_L is the Langmuir constant (L/mg) and C_e is the equilibrium concentration (mg/L).

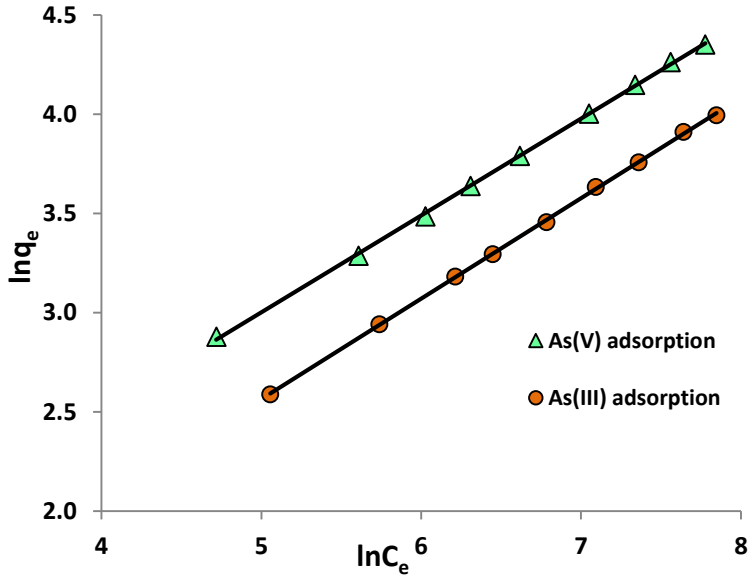

Fig.3.17. Freundlich adsorption isotherm

Table 3.3 Freundlich and Langmuir isotherm model parameters

	Freundlich parameters				Langmuir parameters			q_{exp} (mg/g)
	K_F ($mg.g^{-1}(Lmg^{-1})^{1/n}$)	1/n	q_{max} (mg/g)	R^2	K_L (L/mg)	q_{max} (mg/g)	R^2	
As(V)	1.748	0.488	77.60	0.999	0.0013	98.04	0.971	77.60
As(III)	1.033	0.506	54.90	0.999	0.0011	71.42	0.972	54.32

q_{exp} –experimental equilibrium uptake

The Freundlich and Langmuir models were applied to the experimental results and the model coefficients calculated are given in Table 3.3. The Freundlich constant (K_F) and the Langmuir constant (K_L) are indicators of sorption capacity. From the regression coefficient (R^2), it was observed that Freundlich isotherm fits the adsorption data well, as shown in Fig.3.17.

3.2.4 Adsorption kinetics

The effect of contact time for As(V) adsorption on SFAA was studied with varying feed concentrations (0.2, 0.4, 0.6, 0.8, 1.0, 1.4, 2.0 mg/L) for the adsorbent dose of 0.1g/10mL at pH of 6.5. The sorption capacity of the SFAA adsorbent with time is shown in Fig.3.18. As can be seen, the uptake was rapid in the first 10 min and was constant after 10 min. The adsorption capacity increased from 0.019 to 0.188 mg/g with increasing the initial As (V) concentration from 0.2 to 2 mg/L.

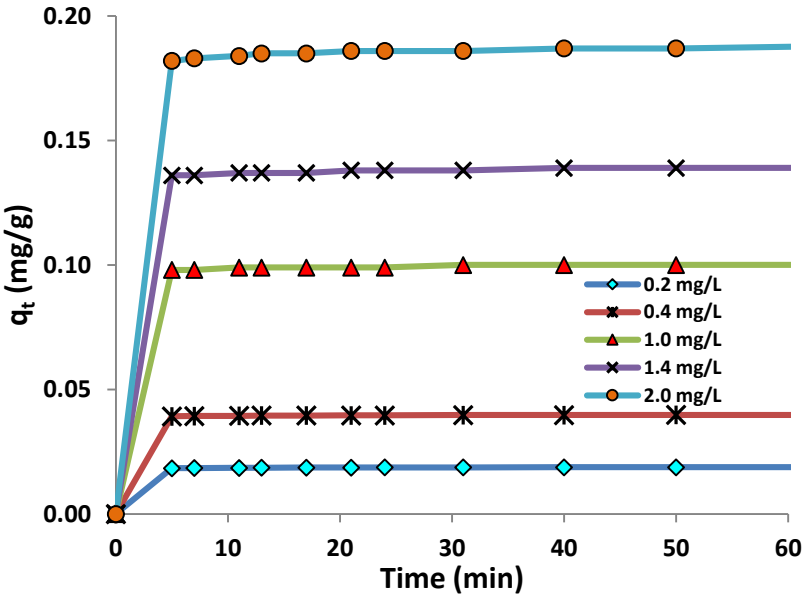

Fig.3.18. Effect of contact time of As(V) on adsorption by SFAA

Different kinetic models like pseudo-first order, pseudo-second order and intra-particle diffusion adsorption kinetic models were tested by various researchers to find the mechanisms of the adsorption and rate controlling steps [272, 273].

I. Chemical reaction based kinetic model

i) Pseudo first order Lagergren model

The Lagergren rate equation [272] is the most widely used rate equation for sorption of a solute from a liquid solution. Proposed in 1898 for adsorption of oxalic acid and malonic acid on to charcoal, this may have been the first rate equation for the sorption in liquid/solid systems based on solid capacity. In recent years, it has been widely used to describe the adsorption of pollutants from wastewater. The pseudo first order equation is presented in terms of adsorption capacity as follows:

$$\frac{dq_t}{dt} = K_1(q_e - q_t) \quad \text{..... 3.6}$$

The linear form of the pseudo-first-order equation is represented as:

$$log(q_e - q_t) = logq_e - \frac{K_1 t}{2.303} \quad \text{..... 3.7}$$

where q_e ,q_t are the adsorption capacity (mg/g) at equilibrium and time t; K_1(min^{-1}) is the rate constant of the pseudo-first-order adsorption.

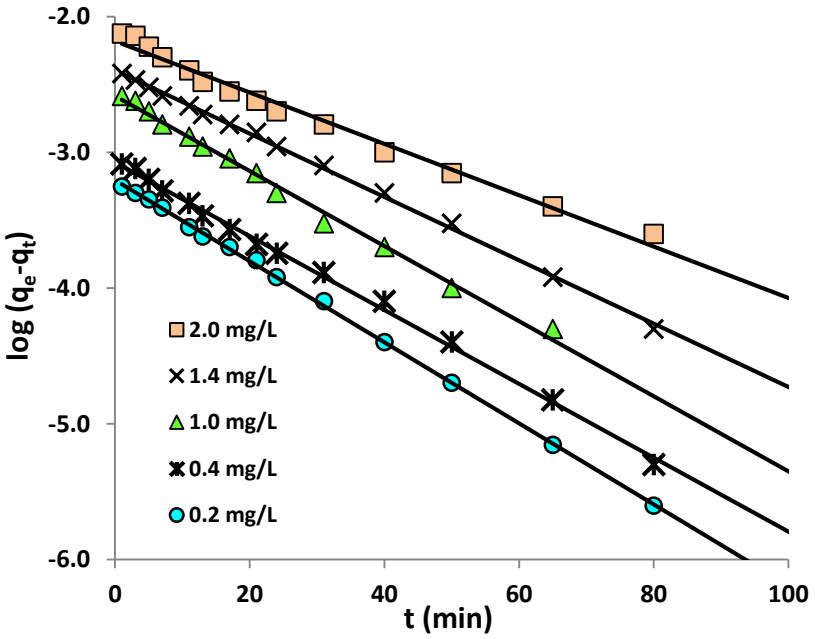

Fig. 3.19. Pseudo first order kinetic model

The plot of $log(q_e - q_t)$ versus t gives a linear relationship (Fig.3.19) from which K_1 and q_e can be determined from the slope and intercept of the plot, respectively.

i) Pseudo second order Ho model

Ho proposed this model in 1995, to describe the adsorption of divalent metal ions onto peat. The main assumptions for this model are that the adsorption is second order with respect to solid concentration, the rate limiting step is chemical adsorption and the adsorption follows Langmuir equation [273]. The typical second-order rate equation in solution systems is as follows;

$$\frac{dq_t}{dt} = K_2(q_e - q_t)^2 \quad \text{..... 3.8}$$

The linear form of pseudo-second order kinetic rate equation may be expressed as:

$$\frac{t}{q_t} = \frac{1}{K_2 q_e^2} + \frac{t}{q_e} \quad \text{..... 3.9}$$

where, q_e and q_t are the adsorption capacity (mg/g) at equilibrium and time t; K_2 is pseudo second order rate constant (g/mg.min^{-1}). From the plot of t/q_t versus t, K_2 and q_e of pseudo second order kinetic model are found (Fig.3.20). The model parameters are given in Table 3.4. It was observed that the adsorption of As (V) on SFAA adsorbent follows second order kinetics and hence it is inferred that the process is chemisorption.

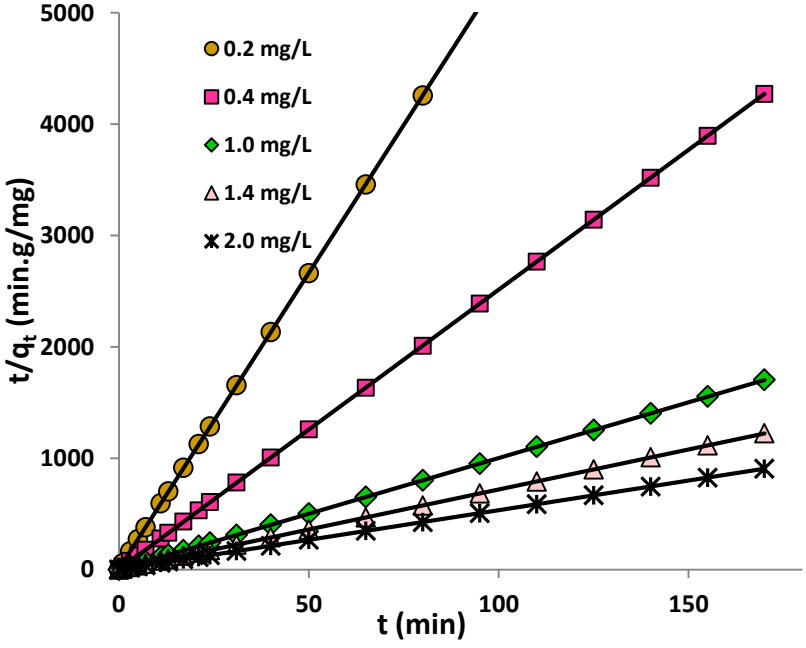

Fig.3.20. Pseudo second order kinetic model

II. Diffusion based kinetic models (Intra particle diffusion model -Pore diffusion)

The intra particle diffusion model was applied to describe the competitive adsorption. In solid-liquid adsorption the solute transfer occurs by particle diffusion. In a solid-liquid system, the fractional uptake of the solute on particle varies according to a fraction of the diffusivity (D) within the particle and r is the particle radius. The sorption rate is shown to be controlled by several factors including the following processes.

Diffusion of the solute; (a) from the solution to the film surrounding the particle (b) from the film to the particle surface (external or film diffusion) (c) from the surface to the internal sites (surface or pore diffusion). As(V) uptake which can involve several mechanisms, such as physico-chemical sorption, ion exchange, precipitation or complexation [266, 274]. The initial rate of intra particle diffusion are obtained by linearization of the curve $q_t = f(t^{0.5})$. The plot of q_t against $t^{0.5}$ may present multi-linearity [275].

$$q_t = K_{id} t^{\frac{1}{2}} + C \quad \ldots\ldots\ldots\ldots\ldots\ldots\ldots\ldots \quad 3.10$$

where, q_t is adsorption capacity (mg/g) at time t, K_{id} intra particle (pore) diffusion rate constant (mg/g $min^{-0.5}$) and C is the intercept that gives an idea about the thickness of the boundary layer. If C value larger means greater boundary layer effect.

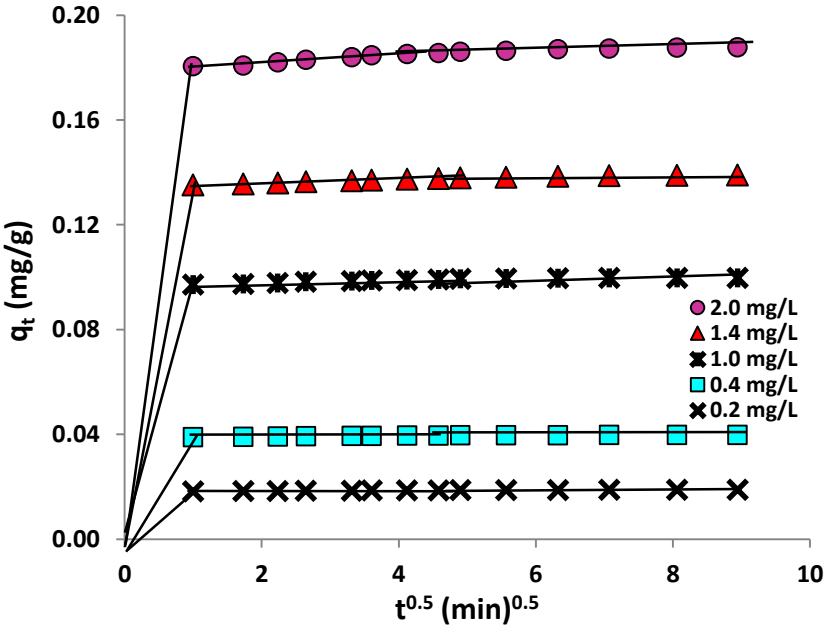

Fig.3.21. Intra particle diffusion model

Figure 3.21 shows the plot of q_t against $t^{0.5}$ for the competitive adsorption occurring in solution. The linear portion of the plot for wide range of contact time between adsorbent and adsorbate does not pass through the origin. This variation from the origin or near saturation may due to the variation of mass transfer in the initial and final stage adsorption [276]. The values are given in Table 3.4.

Table 3.4 Chemical reaction and diffusion based kinetic model parameters

C_o (mg/L)	Pseudo first -order			Pseudo Second order			intra particle diffusion		
	K_1 (min^{-1})	q_1 (mg/g)	R^2	K_2 (g/mg min)	q_2 (mg/g)	R^2	K_{id} (mg/g $min^{0.5}$)	R^2	C
0.2	0.0689	0.041	0.99	413.933	0.0188	1	$8X10^{-5}$	0.89	0.018
0.4	0.0626	0.046	0.99	293.992	0.0398	1	$1X10^{-4}$	0.88	0.039
1.0	0.0557	0.071	0.96	97.124	0.0999	1	$3X10^{-4}$	0.87	0.097
1.4	0.0537	0.091	0.99	54.401	0.1391	1	$5X10^{-4}$	0.93	0.135
2.0	0.0435	0.113	0.98	30.841	0.1879	1	$1X10^{-3}$	0.89	0.180

C_o- initial concentration (mg/L); q- Equilibrium uptake (mg/g); K_{id}- intra particle diffusion model constant (mg/g.$min^{0.5}$); K_s – External mass transfer constant (min^{-1}); D_i– Diffusion coefficient (cm^2/s)

Adsorption contains different resistance for the mass transfer of solute. The first one is bulk diffusion, the second is external mass transfer resistance and the third is intra particle mass transfer resistance. When the intra particle mass transfer resistance is the rate limiting step, then the sorption process is described as being particle diffusion controlled. The contribution of particle diffusion on As adsorption by SFAA was tested using Weber-Morris model. The plot of q_t against $t^{0.5}$ presents linear form of the model [275]. It was observed that the intra-particle diffusion model has a poor coefficient of correlation as shown in Table 3.4.

3.2.5 Effect of temperature and thermodynamic study

To study the effect of temperature on the extent of As sorption on SFAA, temperature was varied from 303 to 318 K for 0.1g of adsorbent (SFAA) in 10 mL of As(V) solution. When the temperature was increased from 303 K to 318 K, the adsorption increased with increase in

temperature (Fig.3.22). When the temperature was increased from 303 K to 308 K, 313 K and subsequently to 318 K, the adsorption increased, indicating that the mechanism is chemisorption. To evaluate the thermodynamic feasibility and to confirm the nature of the adsorption process, three basic thermodynamic parameters, standard enthalpy (ΔH^o), standard entropy (ΔS^o) and standard free energy (ΔG^o) were calculated. Van't Hoff plot of ln(K_d) against reciprocal of temperature (1/T) is shown in Fig.3.23.

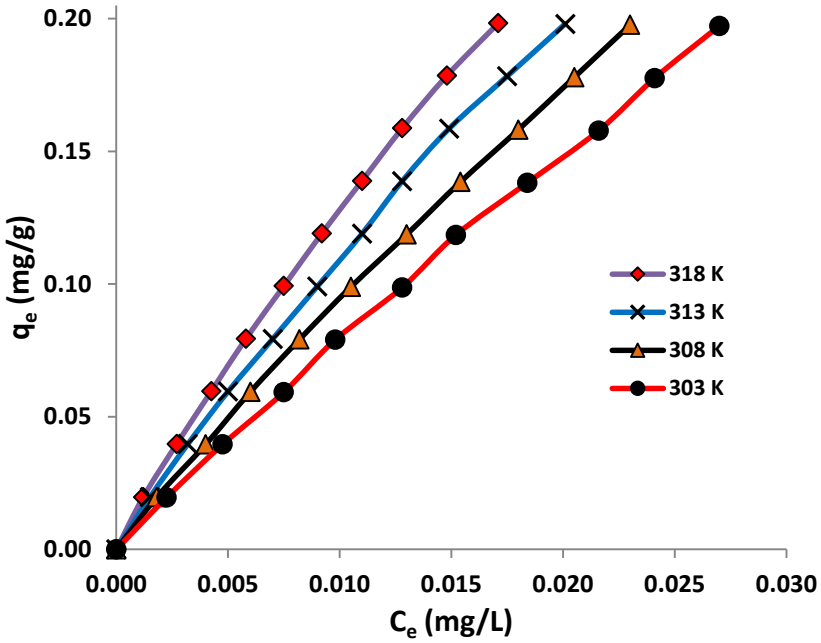

Fig.3.22. Effect of temperature on As(V) adsorption

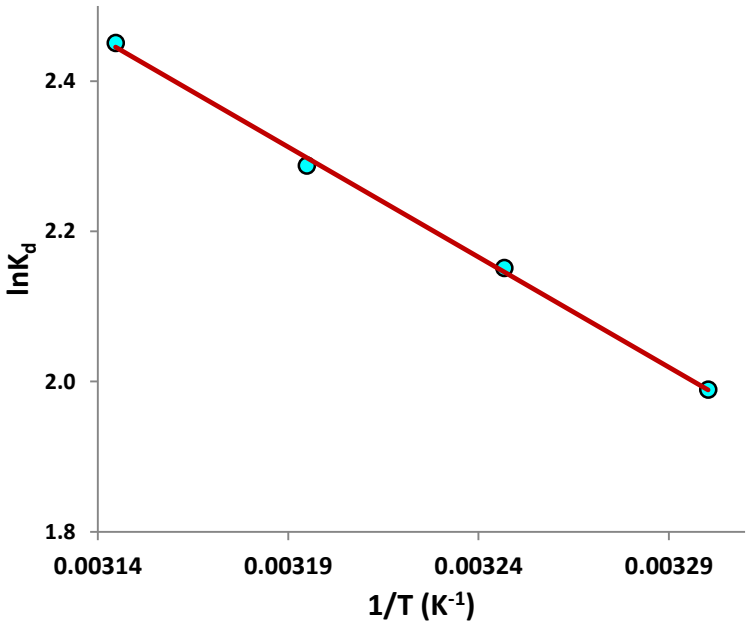

Fig.3.23. Van't Hoff plot for the adsorption of As(V) on SFAA

The thermodynamic equilibrium constant K_d is dimensionless and is obtained by multiplying K_D (in the units of L/g) with water density, 1000 g/L [277]. The value of ΔH^o, and ΔS^o were obtained from the slope and intercept of the plot. The thermodynamic parameters were determined using the following equations [149] and given in Table 3.5.

$$\Delta G^o = -RTlnK_d \quad \text{..... 3.11}$$

$$lnK_d = \frac{\Delta S^0}{R} - \frac{\Delta H^0}{RT} \quad \text{..... 3.12}$$

where ΔG^o is the standard free energy, R is universal gas constant (8.314 J/mol K) and T is the absolute temperature in Kelvin (K).

From Fig.3.23, ΔH^o and ΔS^o were calculated to be 24.37 kJ/mol and 0.097 kJ/mol.K respectively. The endothermic nature of adsorption is indicated by an increase in K_d with the temperature and the positive value of ΔH^o. The value of ΔH^o indicates that the process is chemisorption. The negative value of ΔG^o confirms the feasibility of adsorption at all the temperatures and indicates that it is a spontaneous process. The value of ΔS^o being positive indicates that both enthalpy and entropy are responsible for making ΔG^o negative, which showed the increasing randomness at the solid – solution interface during adsorption. The adsorption mechanism of arsenic is mainly by $H_2AsO_3^-$ and OH^- exchange. Desorption of OH^- attached to active sites on the surface needs some activation energy to leave the surface, which might explain the endothermic nature of the adsorption process.

Table 3.5 Van't Hoff plot parameters

Temp (K)	**1/T (K^{-1})**	**C_e (mg/L)**	**q_e (mg/g)**	**K_d**	**lnK_d**	**ΔG^o (kJ/mol.K)**	**ΔH^o (kJ/mol)**	**ΔS^o (kJ/mol.K)**
303	0.00330	0.0270	1.973	7.31	1.99	-5.01	24.37	0.097
308	0.00325	0.0230	1.977	8.60	2.15	-5.51		
313	0.00319	0.0201	1.979	9.85	2.29	-5.95		
318	0.00314	0.0171	1.983	11.60	2.45	-6.48		

3.2.6 Effect of particle size

The effect of particle size on As (V) adsorption on SFAA was studied with different particle sizes, viz., 89, 152, 210, 354 and 500 μm. The uptake capacities of the adsorbent and the percentage of As (V) removal for different particle sizes are shown in Fig.3.24. Both removal percentage and adsorption capacities of the adsorbent decreased with increase in the particle size of the adsorbent. Decrease in particle size increases the external surface area for adsorption and hence the uptake.

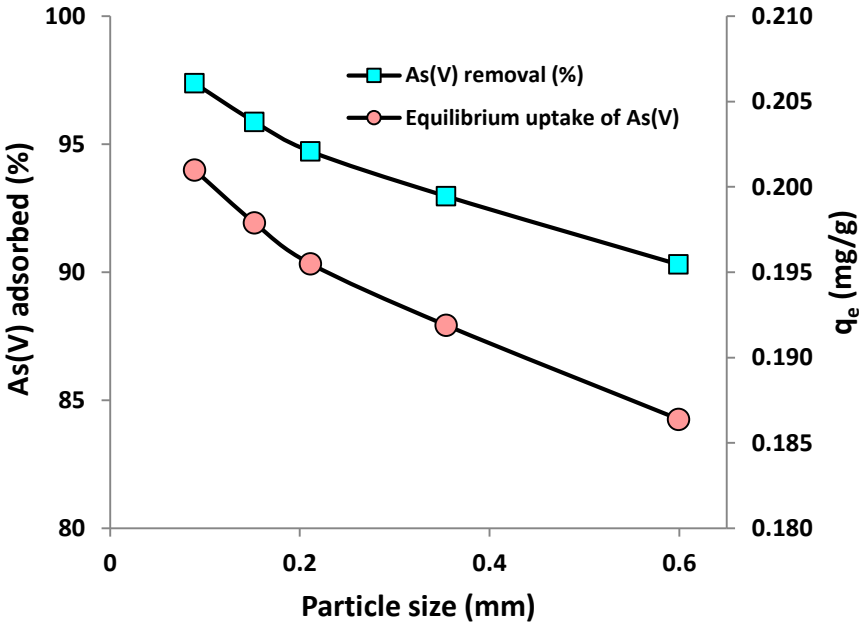

Fig.3.24. Effect of particle size on As (V) adsorption by SFAA

3.2.7 Interference of other ions

Interference of other ions on As adsorption by SFAA was studied for different anions (Nitrate, Sulphate, Bicarbonate, Carbonate, Phosphate). The concentration of other ions was increased from 10 to 500 mg/L, while keeping the As (V) concentration at 2 mg/L. Fig.3.25 shows the percentage removal of As(V) in the presence of different anions. It was seen that presence of nitrate did not effect As adsorption over a wide range of concentration. Bicarbonate and sulphate showed little effect on As adsorption at lower concentrations but with increase in their concentrations the removal of As (V) decreased. The effect of Phosphate is the most significant, as can be seen from Fig.3.25 As(V) adsorption decreased from 99% to 58% with increase in

phosphate concentration from 25 to 500 mg/L. The effect of other ions on As adsorption by SFAA adsorbent was observed to be in the order of $PO_4^{3-} > SO_4^{2-} > HCO_3^- > NO_3^-$.

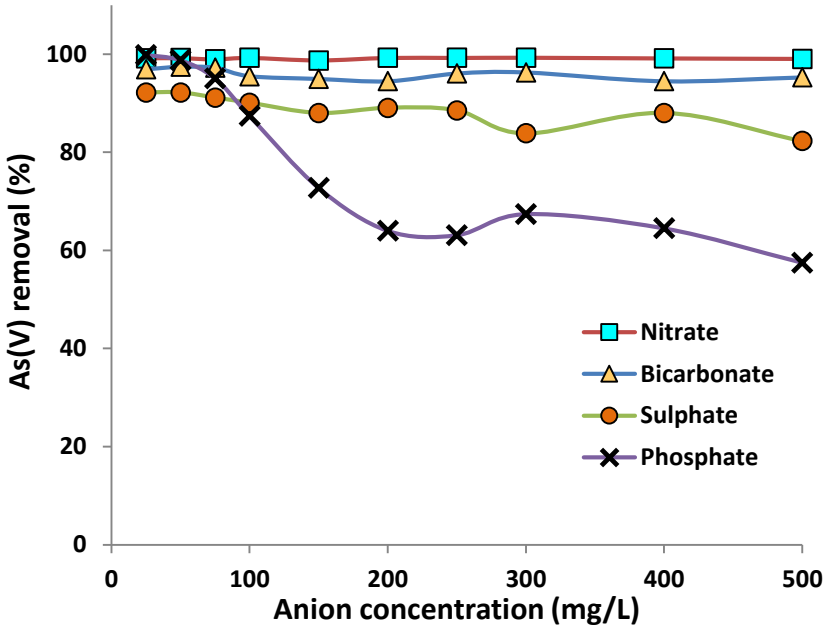

Fig.3.25. Interference of anions on As (V) adsorption by SFAA

3.3 COLUMN STUDIES

Column studies of arsenic adsorption by SFAA were carried out in down flow mode. For all the experiments neutral pH was maintained. A glass column packed with SFAA as mentioned in section 2.4.6. The column consists of several layers of SFAA as shown in Fig.2.3. Water with known As(V) concentration (1, 2, 3 mg/L) was passed through the column at different flow rates (1, 2, 3 mL/min) using a peristaltic pump. Effect of any operating parameter was studied, by changing only that parameter, while keeping all other parameters constant. Water drawn from the bottom of the column has been collected in a sample vials at regular intervals and analyzed for residual arsenic concentration by Inductively Coupled Plasma Mass Spectrometer (ICP-MS). The experimental results were compared with Thomas, Yoon Nelson, Bohart Adam and Clark models.

3.3.1 Performance of different constituents

Removal of arsenic by different adsorbents was studied in the column setup. Sawdust, sawdust with ferric hydroxide and activated alumina (SFAA) and only activated alumina were used for

the column packing and the As(V) solution with 2 mg/L concentration pumped by a peristaltic pump at a constant flow rate (2 mL/min) for the required time. Samples were collected for the frequent time interval and analysed. The results are plotted as shown in Fig.3.26. From Fig.3.26 SFAA shows effective removal of As(V) from water.

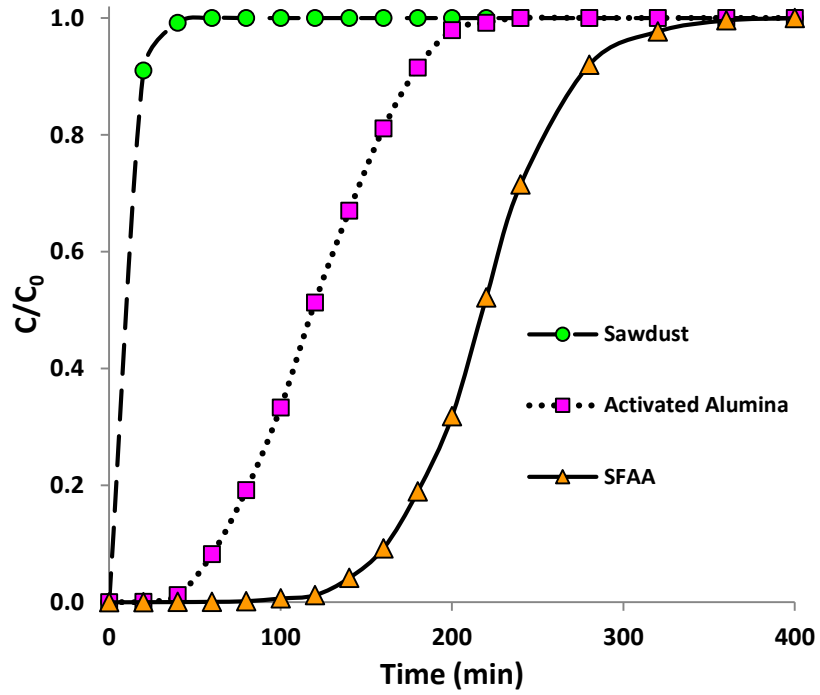

Fig.3.26. Fixed bed adsorption of As(V) by different constituents

3.3.2 Application of models for different constituents

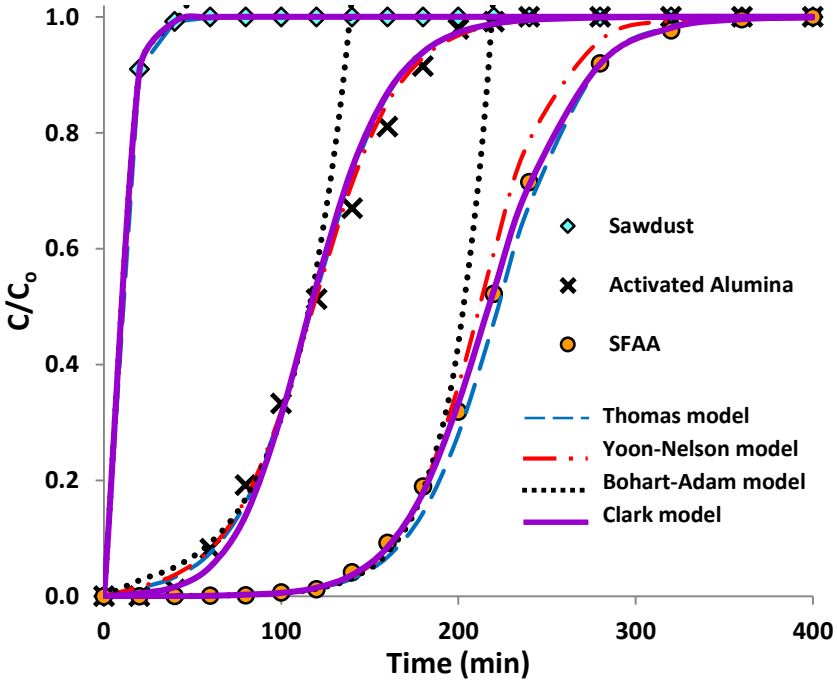

Fig.3.27. Application of models for different constituents

Table 3.6 Model parameters for different constituents

Adsorbent	q_{exp}	Thomas model				Yoon-Nelson model				
		k_{Th}	q	% Error	R^2	K_{YN}	τ	q	% Error	R^2
Sawdust	0.061	0.0050	0.05	21.14	0.959	0.1253	1.54	0.04	21.14	0.954
A.A	3.43	0.0018	3.67	-8.03	0.987	0.0417	118.20	3.68	-7.43	0.987
SFAA	6.37	0.0017	6.93	-8.88	0.997	0.0466	212.00	6.61	-3.84	0.995
		Bohart-Adam model				**Clark model**				
		k_{BA}	N_0	q	% Error	R^2	K_C	N_0	q	% Error	R^2
Sawdust	0.0002	233.6	1.31	-95.33	0.818	0.0050	10.9	0.06	0.16	0.999
A.A	0.0012	3677.3	4.33	26.09	0.976	0.0021	2733.5	3.22	6.26	0.992
SFAA	0.0017	1420.6	6.86	7.63	0.983	0.0018	1358.0	6.55	2.89	0.999

k_{Th}, K_{BA}, K_C – Thomas, Bohart-Adam, Clark rate constants (L/mg.min), K_{YN} –Yoon-Nelson rate constant (min^{-1}), q – Equilibrium uptake (or) adsorption capacity (mg/g), τ – time required for 50% adsorbate breakthrough (min), N_0 – Saturation concentration (mg/L).

The experimental data obtained for different adsorbent fitted with different models discussed in chapter 1 and the corresponding curves plotted as shown in Fig.3.27. The experimental, model rate constants and maximum solid phase concentration of solute or equilibrium uptake (q) are calculated and listed in Table 3.6. Based on adsorption capacity the % error has been calculated and tabulated in Table 3.6. In case of sawdust, activated alumina and SFAA, the experimental data fit well (R^2, % error) with Clark model, indicating that adsorption on these adsorbents follows Freundlich adsorption isotherm. It can be seen that the adsorption capacity of SFAA is significantly higher than its constituents.

3.3.3 Effect of flow rate

2 g of adsorbent was taken in a column and required quantity of 2 mg/L As(V) solution was passed through the column. The flow rate varied (1, 2, 3 mL/min) by varying the speed of pump for each experiment and the samples were collected for every 20 min. From the result the flow rate of 1 mL/min of As(V) solution gives maximum adsorption. High flow rate resulted earlier breakthrough than low flow rate (Fig.3.28). At high flow rate the insufficient contact time causes

low adsorption. But at low flow rate sufficient contact time of solution with sorbent which enhances the As(V) adsorption by SFAA.

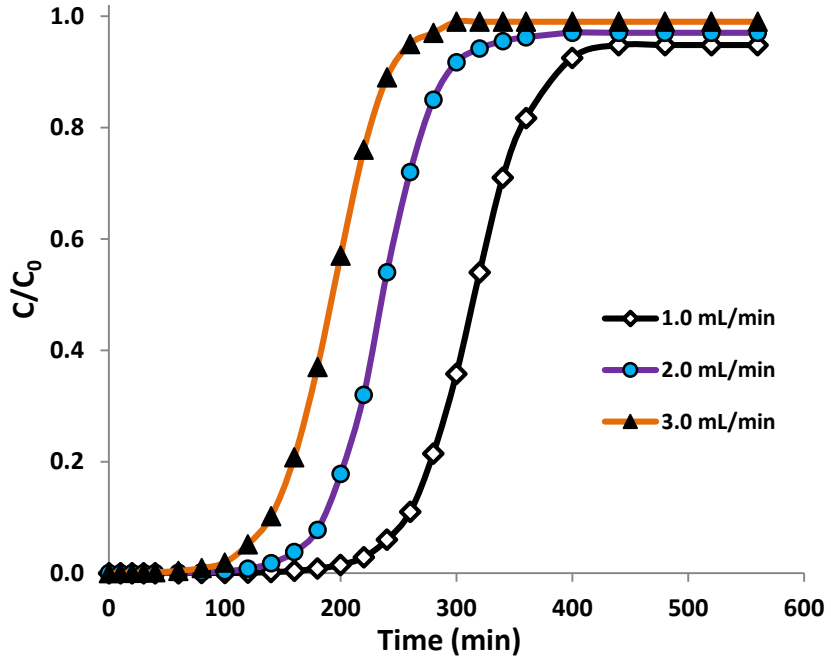

Fig.3.28. Breakthrough curve for different flow rates

3.3.4 Application of models for different flow rates

The experimental data obtained for arsenic adsorption at different flow rate fitted with different models and the corresponding curves plotted as shown in Fig.3.29.

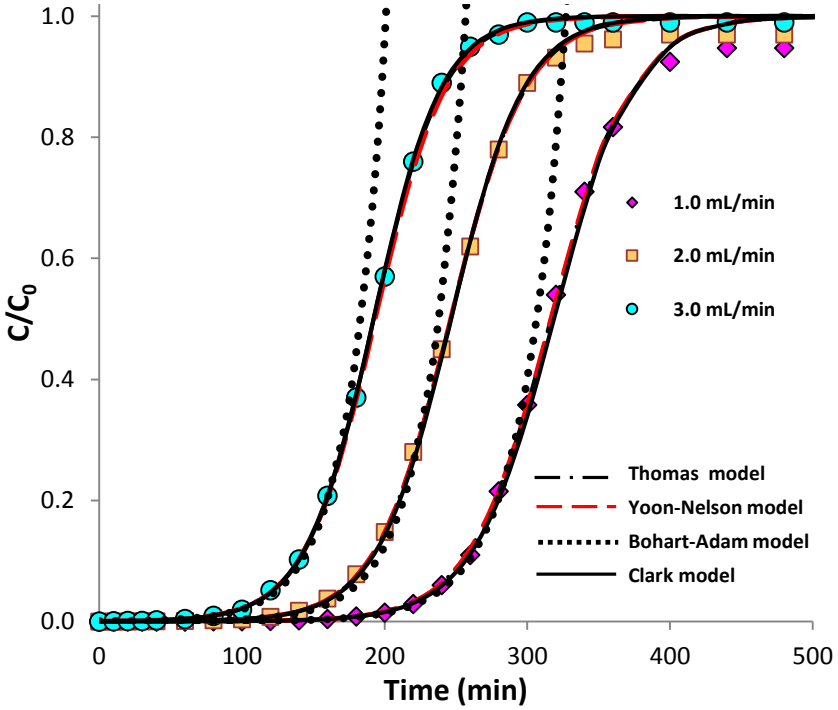

Fig.3.29. Application of models for different flow rates

Table 3.7 Model parameters for different flow rates

Q (mL/min)	q_{exp}	Thomas model				Yoon-Nelson model				
		k_{Th}	q	% Error	R^2	K_{YN}	τ	q	% Error	R^2
1.0	0.317	0.0174	0.316	0.1	0.996	0.0352	316.6	0.319	0.8	0.995
2.0	0.497	0.0185	0.492	1.0	0.997	0.0381	246.1	0.504	1.4	0.989
3.0	0.587	0.0194	0.577	1.7	0.999	0.0407	193.5	0.615	4.7	0.988
		Bohart-Adam model				**Clark model**				
		k_{BA}	N_0	q	% Error	R^2	K_C	N_0	q	% Error	R^2
1.0	0.0168	66.64	0.327	3.1	0.998	0.0181	65.31	0.320	0.9	0.999
2.0	0.0184	103.14	0.506	1.8	0.998	0.0197	101.1	0.496	0.2	0.999
3.0	0.0195	122.83	0.602	2.6	0.998	0.0213	118.5	0.581	1.0	0.999

Q – Flow rate (mL/min), k_{Th} , K_{BA}, K_C –Thomas, Bohart-Adam, Clark rate constants (L/mg.min), K_{YN} –Yoon-Nelson rate constant (min^{-1}), q – Equilibrium uptake (or) adsorption capacity (mg/g), τ – time required for 50% adsorbate breakthrough (min), N_0 – Saturation concentration(mg/L).

The experimental, model rate constants and maximum equilibrium uptake (q) are calculated and listed in Table 3.7. Based on adsorption capacity (q) the % error has been calculated and tabulated in Table-3.7. For all flow rate (1, 2, 3 mL/min) experimental data fitted Thomas, Yoon-Nelson, Clark models. Based on % error, Clark model fit well conforms that SFAA follows Freundlich adsorption isotherm. The adsorption capacity increases with increase in flow rate, which indicates that As(V) adsorption by SFAA is fast and enough active sites are present to attach As(V) ions to the sorbent.

3.3.5 Effect of initial concentration

Arsenic concentrations in natural waters vary over a wide range based on the source and the concentration has a significant effect on the breakthrough due to variation in the driving force. To study the effect of initial concentration, water with As(V) concentration of 1, 2, 3 mg/L was passed through 1 cm inner diameter (d_i) column packed with 2 g of SFAA at a constant flow rate 2 mL/min. The breakthrough curves are shown in Fig.3.30. Higher concentration resulted in earlier breakthrough due to earlier saturation of SFAA.

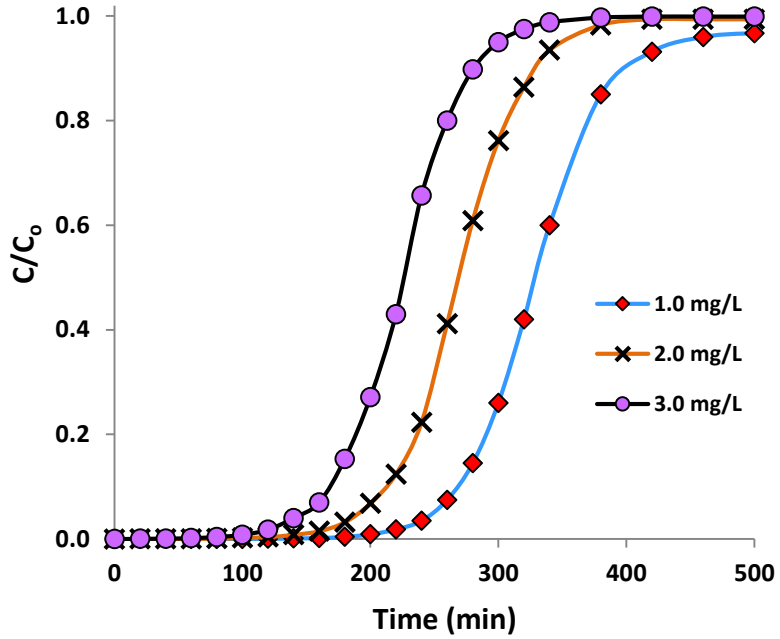

Fig.3.30. Breakthrough curve for different initial concentrations of As(V)

3.3.6 Application of models for different initial concentrations

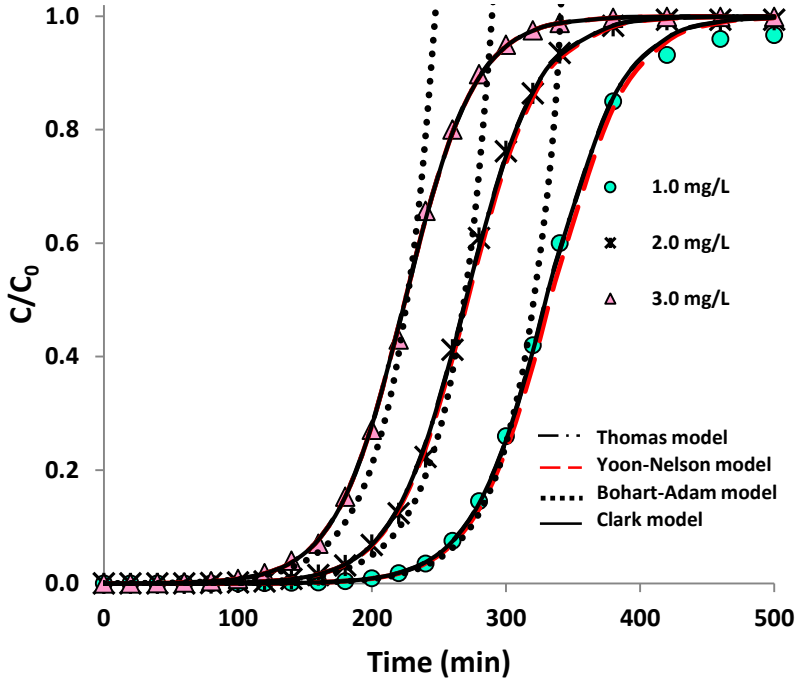

Fig.3.31. Application of models for different initial concentrations of As(V)

Fig.3.31 shows model validation of arsenic adsorption at different initial concentration. The experimental, model rate constants and maximum adsorption capacity (q) are calculated and listed in Table 3.8. Based on adsorption capacity (q) the % error has been calculated and tabulated in Table 3.8. As can be seen from Table 3.8 the adsorption capacity (q_t) increases with

increase in feed concentration, due to increase in driving force for mass transfer, which enhances the adsorption rate and faster consumption of active sites [278]. Higher influent concentration causes sharper breakthrough curves due to quick adsorbent saturation, which causes decrease in adsorption zone length and exhaustion time [279].

Table 3.8 Model parameters for different initial concentrations of As(V)

C_0 (mg/L)	q_{exp}	Thomas model				Yoon-Nelson model				
		k_{Th}	q	% Error	R^2	K_{YN}	τ	q	% Error	R^2
1.0	0.322	0.0359	0.330	2.51	0.999	0.0354	332.9	0.333	3.51	0.999
2.0	0.527	0.0186	0.540	2.58	0.999	0.0368	271.4	0.543	3.11	0.999
3.0	0.648	0.0128	0.674	4.06	0.999	0.0383	224.8	0.674	4.06	0.999
		Bohart-Adam model				Clark model				
		k_{BA}	N_0	q	% Error	R^2	K_C	N_0	q	% Error	R^2
1.0	0.0342	71.21	0.341	5.87	0.998	0.0359	68.96	0.330	2.51	0.999
2.0	0.0168	117.98	0.579	9.95	0.993	0.0186	110.07	0.540	2.58	0.999
3.0	0.0111	154.78	0.741	14.38	0.987	0.0128	140.82	0.674	4.06	0.999

C_0 –Initial concentration (mg/L), k_{Th} , K_{BA}, K_C –Thomas, Bohart-Adam, Clark rate constants (L/mg.min), K_{YN} –Yoon-Nelson rate constant (min^{-1}), q – Equilibrium uptake (or) adsorption capacity (mg/g), τ – time required for 50% adsorbate breakthrough (min), N_0 – Saturation concentration(mg/L).

3.3.7 Effect of particle size

Particle size of the adsorbent (ϕ) is an important parameter in column operation, as smaller particle sizes offer higher pressure drops, in addition to being prone for attrition. Column studies were conducted for different particle sizes by loading 2 g of SFAA in a column of 1 cm inner diameter(d_i) at a constant flow rate of 1 mL/min with C_0 = 2 mg/L. The breakthrough curves obtained for different particle sizes are shown in Fig.3.32. All the breakthrough curves showed the standard S shape, but different breakthrough and exhaustion times. When the particle size was increased from 0.121 mm to 0.281 mm, time for breakthrough decreased considerably from 300 min to 150 min. Decrease in particle size enhances the adsorption capacity (q_t) due to higher available interfacial surface area and shorter intraparticle diffusion paths. Similar observations

were made by El Qada in the study of basic dye removal in a fixed bed micro column by activated carbon [280].

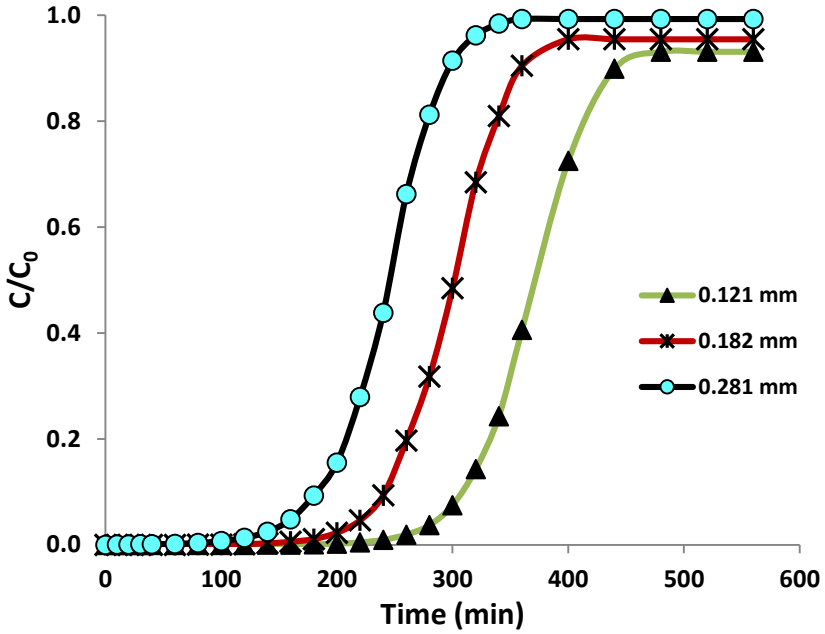

Fig.3.32. Breakthrough curve for different particle sizes

3.3.8 Application of models for different particle sizes

The four models have been tested with data of varying particle size, as shown in Fig.3.33. The model rate constants and maximum solid phase concentration of solute (q) are calculated and listed in Table 3.9.

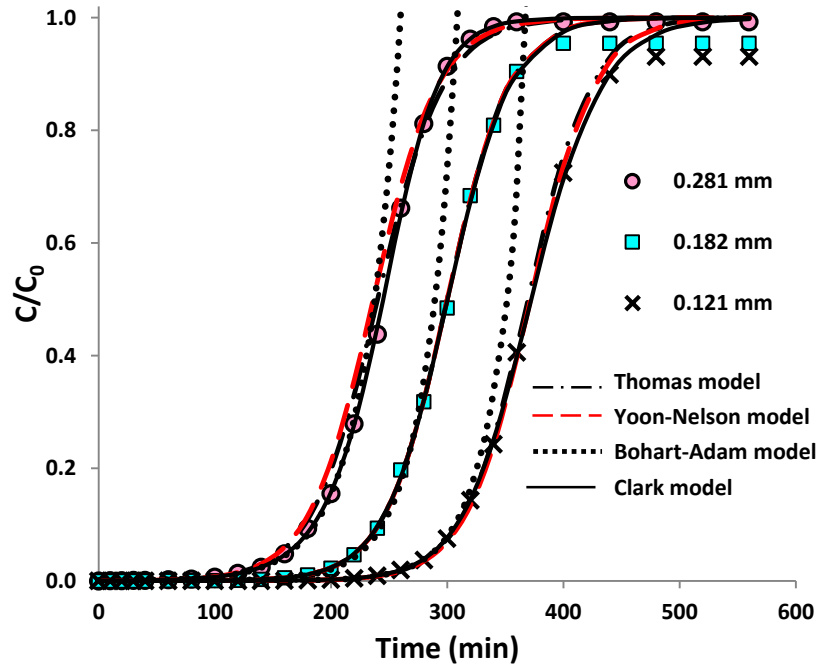

Fig.3.33. Application of models for different particle sizes

It can be seen that of the four models tested, Clark's model gives the best fit of experimental data with R^2 value of 1.0 and % error of 0.23 to 0.47. From experimental data adsorption capacity (q) decreases from 0.385 to 0.241 with increase in particle size from 0.121 to 0.281 mm. Similarly adsorption capacity (q) obtained from models decreases with increase in particle size.

Table 3.9 Model parameters for different particle sizes

ϕ (mm)	q_{exp}	Thomas model				Yoon-Nelson model				
		k_{Th}	q	% Error	R^2	K_{YN}	τ	q	% Error	R^2
0.121	0.384	0.0173	0.389	1.30	0.999	0.0362	371.7	0.391	1.82	0.999
0.182	0.295	0.0188	0.297	0.68	0.999	0.0373	300.1	0.297	0.68	0.999
0.281	0.242	0.0186	0.226	6.61	0.996	0.0360	236.5	0.222	8.26	0.995
		Bohart-Adam model				Clark model				
		k_{BA}	N_0	q	% Error	R^2	K_C	N_0	q	% Error	R^2
0.121		0.0173	79.32	0.389	1.86	0.999	0.0151	78.45	0.385	0.23	1.00
0.182		0.0181	62.30	0.306	3.80	0.998	0.0184	59.94	0.296	0.47	1.00
0.281		0.0167	49.73	0.244	0.79	0.999	0.0242	49.47	0.241	0.24	1.00

ϕ – Particle size (mm), k_{Th} , K_{BA}, K_C –Thomas, Bohart-Adam, Clark rate constants (L/mg.min), K_{YN} –Yoon-Nelson rate constant (min^{-1}), q – Equilibrium uptake (or) adsorption capacity (mg/g), τ – time required for 50% adsorbate breakthrough (min), N_0 – Saturation concentration(mg/L).

3.3.9 Effect of bed height

Adsorbent bed height was varied by varying the mass of adsorbent and column performances for adsorption of As(V) by SFAA were studied. For the same flow rate and particle size the effect of bed height were studied with same inlet concentration of As(V) containing synthetic water. Adsorption performances of various adsorbent bed heights of SFAA are shown in Fig.3.34. Small bed height resulted in earlier breakthrough due to earlier saturation of SFAA. As can be seen from Table 3.10 the adsorption capacity (q_t) increases with increase in bed height, due to increase in contact time and availability of active sites for mass transfer, which enhances the adsorption rate and adsorption capacity.

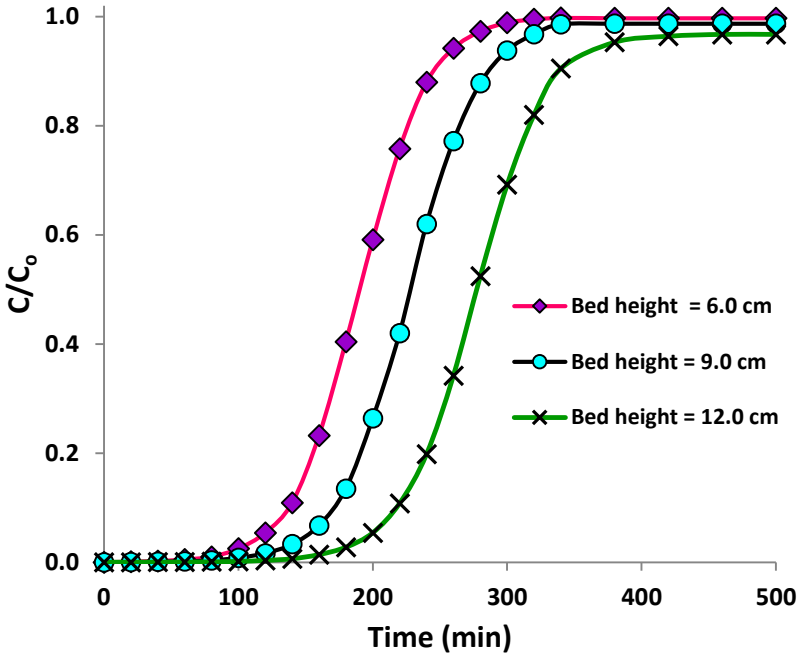

Fig.3.34. Breakthrough curve for different bed heights

3.3.10 Application of models for different bed heights

The experimental data obtained for arsenic adsorption at different bed height fitted with different models and the corresponding curves plotted as shown in Fig.3.35. The experimental, model rate constants and maximum adsorption capacity (q) are calculated and listed in Table 3.10.

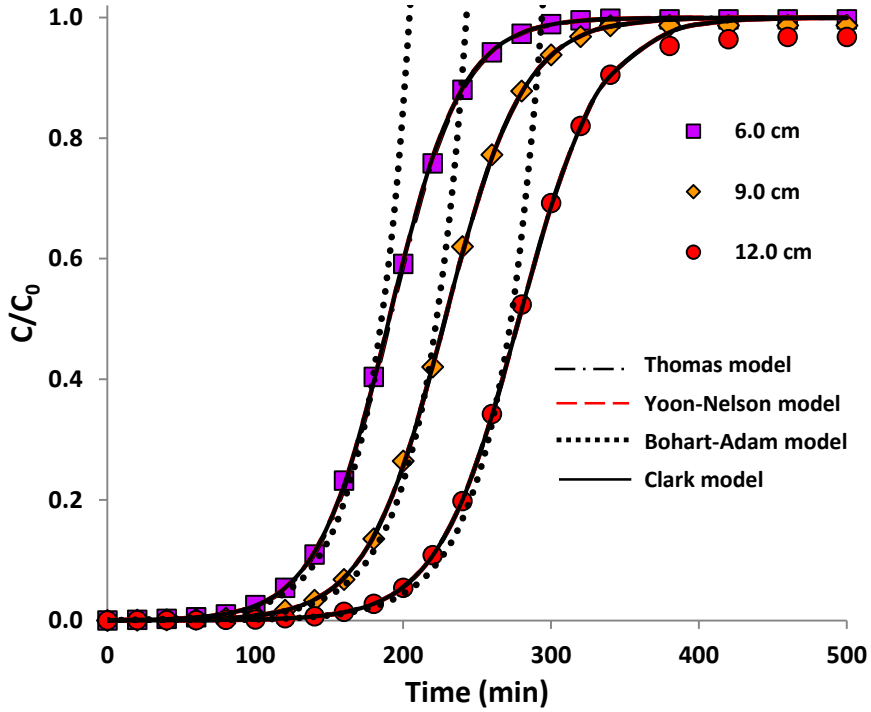

Fig.3.35. Application of models for different bed heights

Table 3.10 Model parameters for different bed heights

H (cm)	q_{exp}	Thomas model				Yoon-Nelson model				
		k_{Th}	q	% Error	R^2	K_{YN}	τ	q	% Error	R^2
6.0	0.724	0.0204	0.762	5.25	0.999	0.0407	190.5	0.762	5.25	0.999
9.0	0.582	0.0189	0.609	4.62	0.999	0.0377	228.4	0.609	4.62	0.999
12.0	0.544	0.0181	0.557	2.37	0.999	0.0362	278.5	0.557	2.37	0.999
		Bohart-Adam model				Clark model				
		k_{BA}	N_0	q	% Error	R^2	K_C	N_0	q	% Error	R^2
6.0	0.0184	173.55	0.817	12.90	0.994	0.0204	161.78	0.762	5.25	0.999
9.0	0.0172	137.48	0.648	11.27	0.995	0.0189	129.29	0.609	4.62	0.999
12.0	0.0167	124.63	0.587	7.90	0.914	0.0181	118.24	0.557	2.37	1.000

H–*Bed height (cm),* k_{Th} *,* K_{BA}*,* K_C *– Thomas, Bohart-Adam, Clark rate constants (L/mg.min),* K_{YN} *–Yoon-Nelson rate constant (*min^{-1}*),* q *– Equilibrium uptake(or) adsorption capacity (mg/g),* τ *– time required for 50% adsorbate breakthrough (min),* N_0 *– Saturation concentration(mg/L).*

Based on adsorption capacity (q) and % error the best fit model was identified. From Table 3.10 based on regression coefficient (R^2) and % error Thomas, Yoon-Nelson and Clark model fits well with experimental data. Based on bed height in a fixed bed column confirms, arsenic adsorption by SFAA follows; Freundlich isotherm, second order reversible reaction and also the external and internal diffusion resistances are extremely small.

3.4 ANALYSIS OF MASS TRANSFER ZONE

The effect of operating parameters such as initial concentration, flow rate and adsorbent particle size on the mass transfer zone were studied. All the mass transfer zone related parameters are calculated and presented in Table 3.11. By increasing the initial concentration, rate of movement of MTZ (U_Z), % saturation and fractional capacity increase, while height of the mass transfer zone (H_{MTZ}) decreases. As initial concentration increases, the bed saturates faster, thus increasing U_Z. As the rate of adsorption is higher, H_{MTZ} decreases. Similarly increasing flow rate increases H_{MTZ} and U_Z. Percentage saturation decreases due to insufficient contact time during

adsorption at higher flow rate. Effect of adsorbent particle size on mass transfer zone was also studied. When particle size is increased, H_{MTZ} and U_Z also increase. Rate of adsorption is better for small particle sizes and hence MTZ is smaller compared to larger particle sizes. For the same reason, % saturation decreases with increase in particle size.

Table 3.11 Mass Transfer Zone (MTZ) related parameters

Conc. (mg/L)	Q (mL/min)	H (cm)	t_B (min)	t_E (min)	t_Z (min)	F	H_{MTZ} (cm)	U_Z (cm/min)	% Sat.
1	2.0	12.2	250	450	200	0.619	6.53	0.033	79.61
2	2.0	12.2	190	370	180	0.840	6.44	0.036	91.56
3	2.0	12.2	150	300	150	0.934	6.31	0.042	96.59
2	1.0	12.2	230	450	220	0.865	6.39	0.029	92.93
2	2.0	12.2	170	340	170	0.840	6.63	0.039	91.30
2	3.0	12.2	120	260	140	0.832	7.22	0.052	90.05
2	1.0	4.0	290	480	190	0.559	1.92	0.010	78.85
2	1.0	6.0	220	400	180	0.454	3.58	0.020	67.43
2	1.0	12.0	170	340	170	0.414	8.49	0.050	58.56

Conc.- concentration (mg/L), Q-Volumetric flow rate (mL/min), H- Bed height (cm), t_B- Breakthrough time (min), t_E- Exhaust time (min), $t_Z = t_E - t_B$, F-Fractional capacity, H_{MTZ} - Height of Mass Transfer Zone (cm), U_Z-Rate of movement of mass transfer zone (cm/min), % Sat.- Percentage saturation.

3.5 REGENERATION OF THE ADSORBENT

To test the reusability of the adsorbent, column studies were conducted for regeneration with a packed bed volume of 9.60 mL. The bed was regenerated for two cycles using 0.002 N NaOH and the breakthrough curves are shown in Fig. 3.36. Data on regeneration and reuse of the adsorbent is presented in Table 3.12. For the fresh adsorbent, breakthrough was achieved after 240 min. After the first regeneration, 95 % of arsenic could be recovered from the bed. In the second cycle breakthrough was achieved after 150 min. For this cycle 0.266 mg/g arsenic was

picked up by the bed. In the second regeneration, 86% of arsenic could be recovered from the bed. In the third cycle breakthrough and exhaustion times being 120 and 320 min respectively. In this cycle 0.238 mg/g arsenic was picked up by the bed.

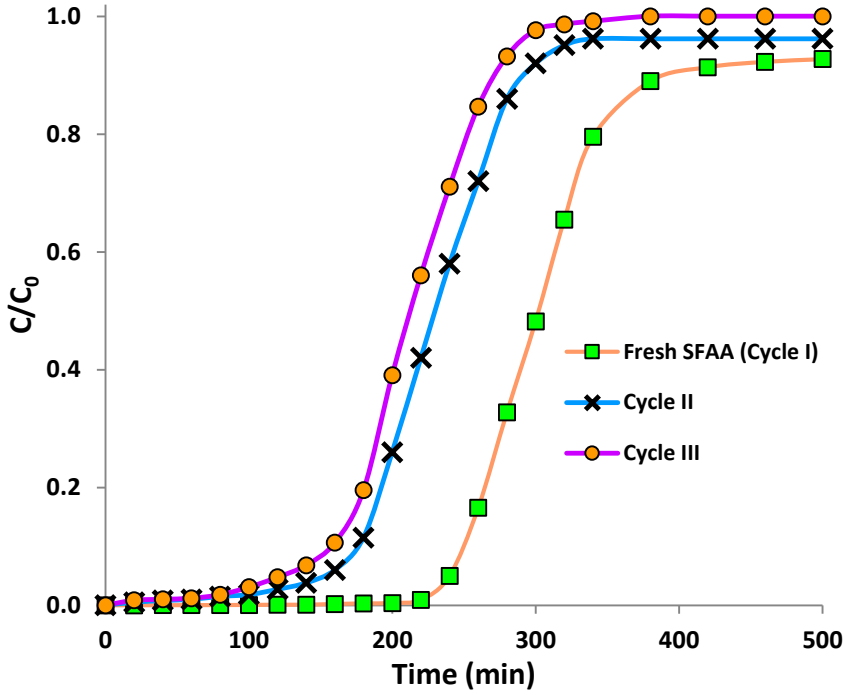

Fig.3.36. Regeneration studies on As(V) loaded SFAA

Table 3.12 Regeneration and reusability of SFAA for arsenic adsorption

Cycle No.	Breakthrough time (min)	Breakthrough uptake (mg/g)	Bed exhaustion time (min)	Regeneration efficiency (%)
1	240	0.327	480	Original
2	150	0.266	380	81
3	120	0.238	320	73

4 ADSORPTION OF FLUORIDE FROM WATER BY SFAA

Studies on fluoride adsorption from water by SFAA in batch and fixed bed are presented in detail in this chapter. Characterization of SFAA and activated alumina, before and after fluoride adsorption was studied to understand the mechanism of adsorption. Isotherm and kinetic modeling for fluoride adsorption were studied and the best fit isotherm and kinetic model were identified. Effects of various parameters in batch and fixed bed operation were studied and different column models were compared with experimental results. Fluoride bearing groundwater sample collected from Avarangattur, Dharmapuri district, Tamilnadu and Chandana village, Godda district, Jharkhand was tested by SFAA.

4.1 CHARACTERIZATION OF THE ADSORBENT AND ITS CONSTITUENTS

4.1.1 Surface area and pore size distribution

As explained in Section 3.1, the adsorbent SFAA and its constituents, saw dust and AA were analyzed for surface areas and pore volumes in micro, meso and macro ranges by use of nitrogen adsorption and mercury porosimetry. As AA is a widely reported adsorbent for fluoride removal, the surface area and pore size distribution studies were carried out on SFAA and AA, after fluoride adsorption and presented in Figs 4.1, 4.2 & 4.3 and Table 4.1.

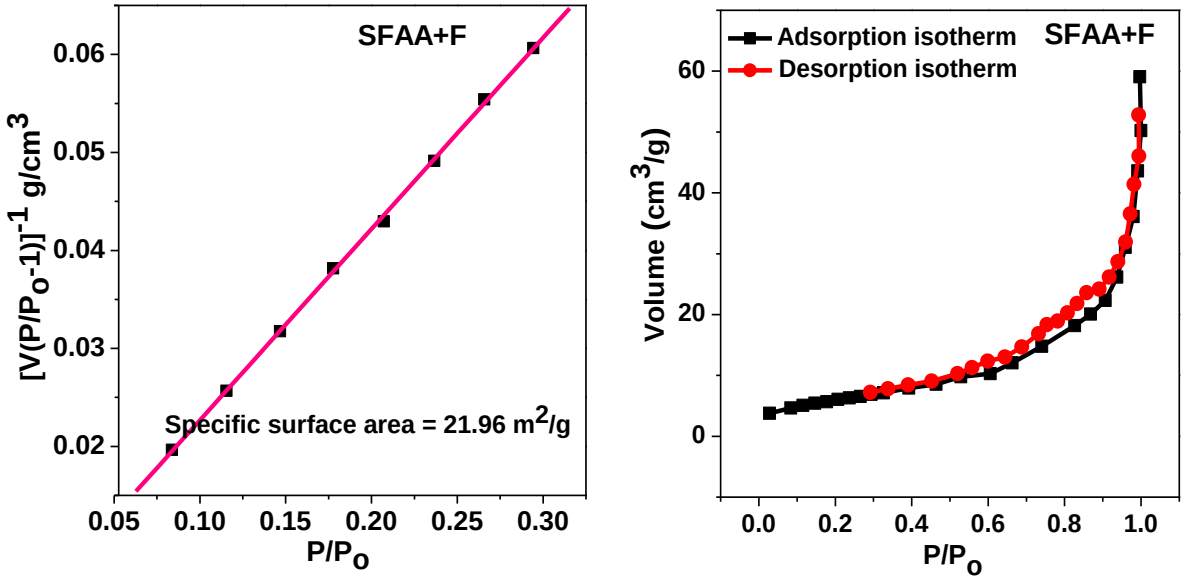

Fig.4.1. BET surface area of SFAA after fluoride adsorption

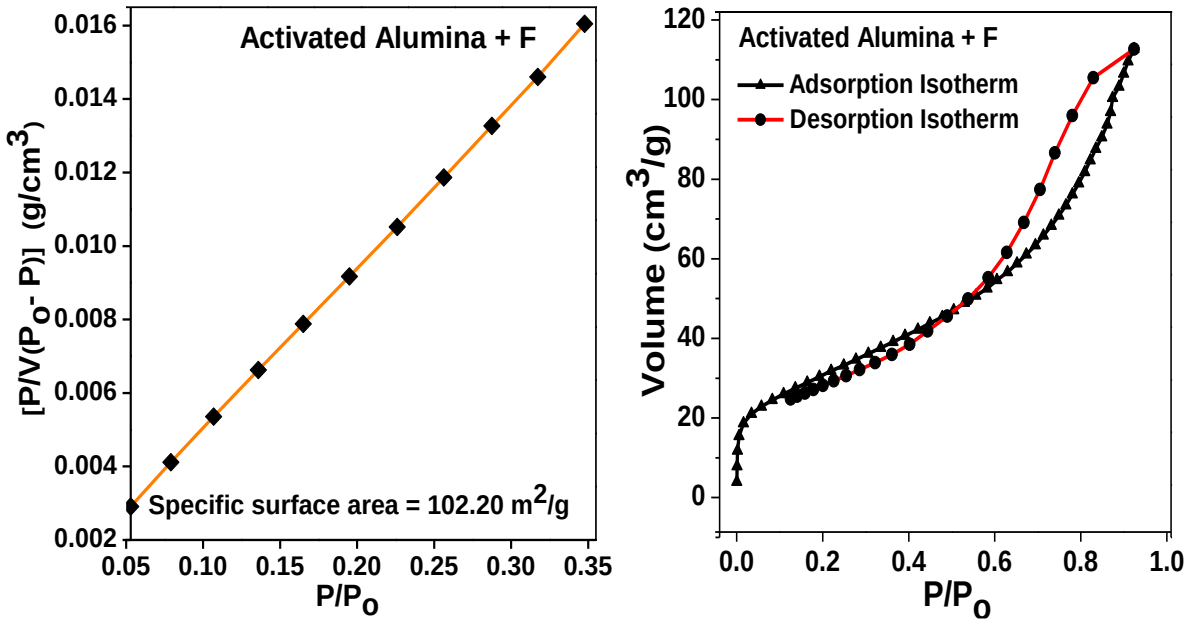

Fig.4.2. BET surface area of Activated alumina after fluoride adsorption

As already discussed, the sawdust has substantial macropore volume and micropore surface area. In case of activated alumina the surface area is mostly in the mesopore region and the macropore volume is moderate. As a result, the combination adsorbent, SFAA has a well-balanced pore size distribution with the pore volumes and surface areas distributed in macro, meso and micropore regions. Table 4.1 shows surface areas and pore volumes in all the three ranges for activated alumina before and after adsorption of fluoride. For activated alumina, reduction in the volumes or the surface areas after fluoride adsorption is not considerable implying that fluoride adsorption is not substantial. The distribution of surface areas and pore volumes for SFAA before and after adsorption of fluoride shows that the micropore surface area reduced to 7.7% of the original, as against 95% for activated alumina. This indicates that the micropores have been filled very effectively in case of SFAA. Similarly, the S_{meso} reduced to 49% of the original for SFAA as against 86% for activated alumina. Thus, even in the mesopore region, adsorption has been more effective by SFAA. There is no difference in Macropore volumes before and after adsorption in case of both activated alumina and SFAA, as the adsorption takes place only in meso and micropores. The effectiveness of SFAA is reflected in the maximum adsorption capacities of activated alumina (8.60 mg/g) and SFAA (40.28 mg/g) for initial concentration of

1000 mg/L fluoride as shown in Table 4.4. A good adsorbent should have a well-developed pore size distribution, as macropores essentially serve as transport pathways and micro and mesopores contribute to the adsorption sites. Thus, though the BET surface area of activated alumina is more than that of SFAA, the utilization of the micro/meso pores for adsorption is better in case of SFAA because of the well-developed approach paths to the micropores in case of SFAA. This is also reinforced by the column studies presented in section 4.3.

Besides a higher efficiency, this adsorbent is economic as the sawdust constitutes 40% by weight of the total adsorbent, minimizing the concentration of other metallic hydroxides. This establishes the pivotal role played by Artocarpus hirsutus sawdust in preparation of this efficient and cost effective adsorbent.

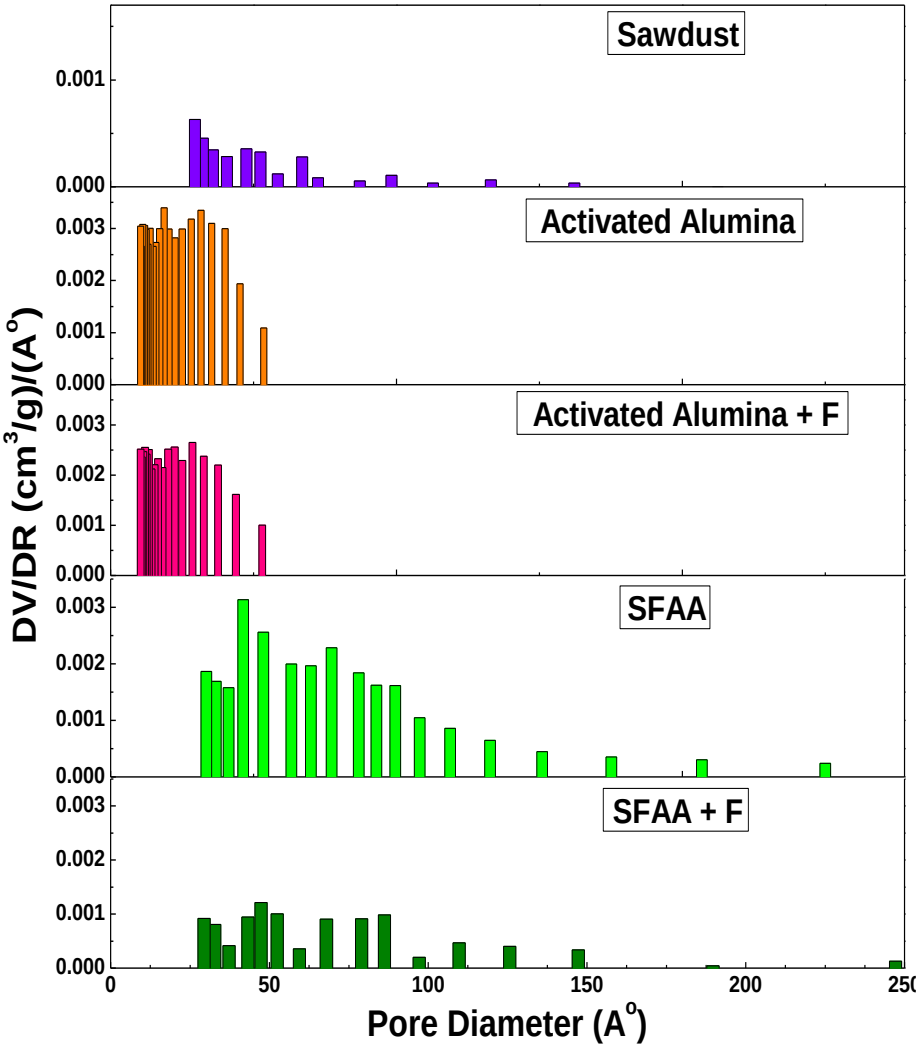

Fig. 4.3 (a) Pore size distribution by N_2 adsorption

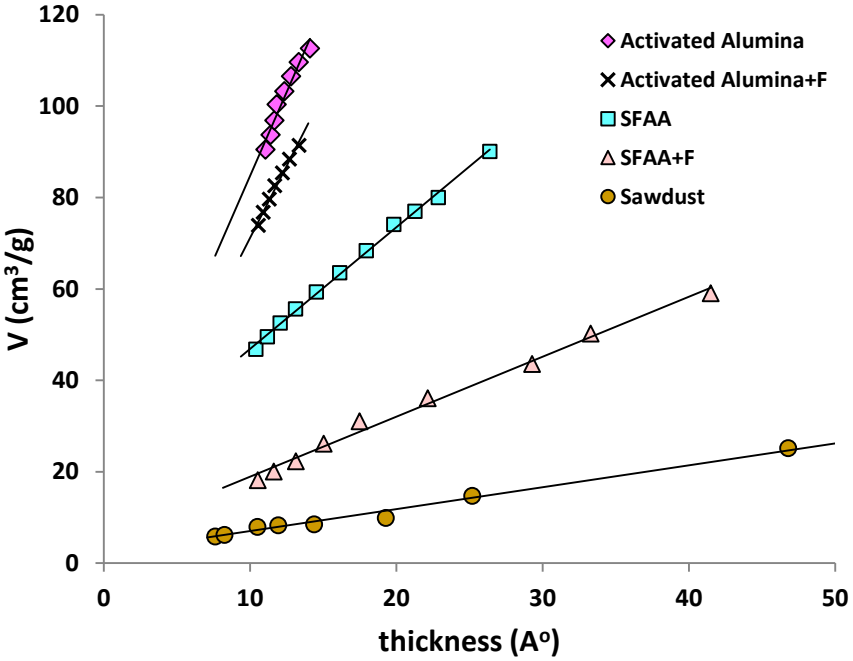

Fig. 4.3 (b) t-plot based on N_2 adsorption

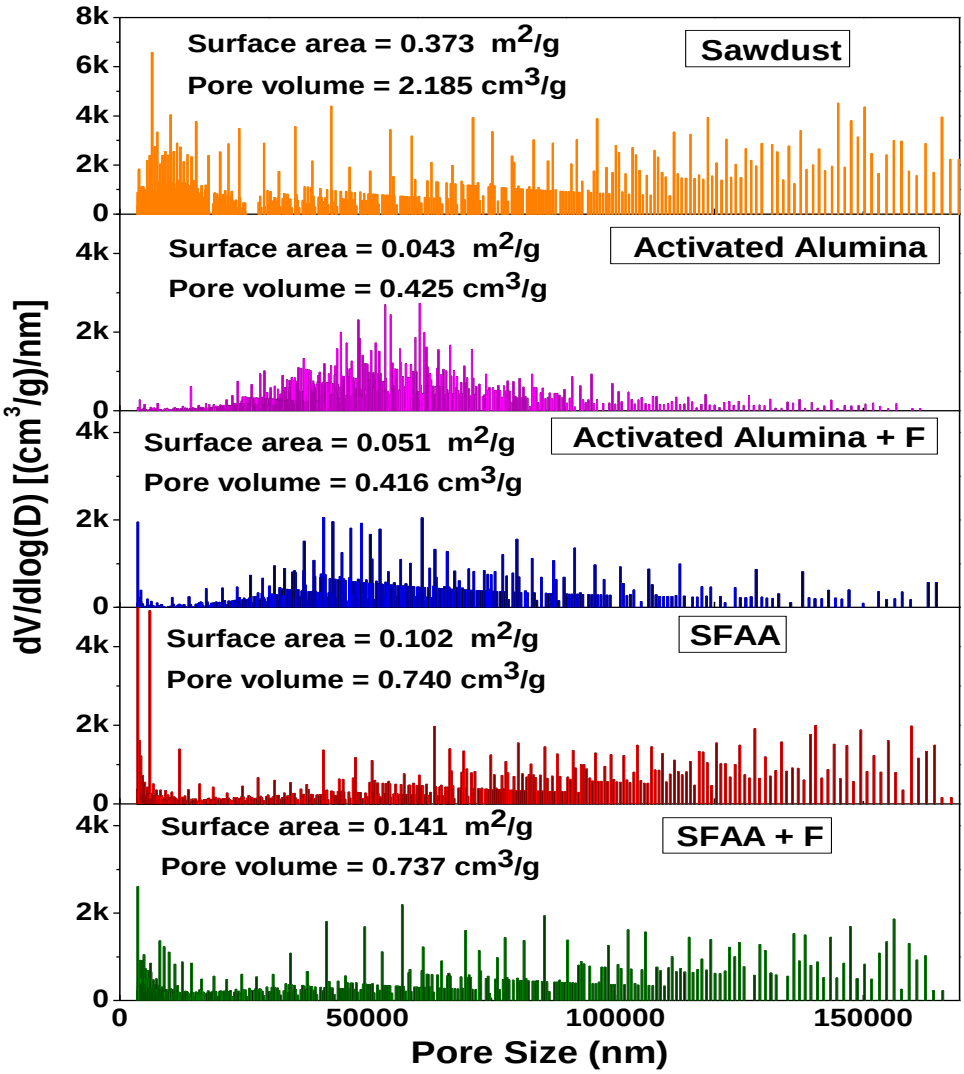

Fig. 4.3 (c) Pore size distribution by mercury porosimetry

Table 4.1 Surface areas and pore volumes of the adsorbents

Adsorbent	By Liquid Nitrogen Adsorption		From t-Plots				Mercury Porosimetry	
	S_{BET} (m^2/g)	$V_{meso+micro}$ (cm^3/g)	V_{micro} (cm^3/g)	V_{meso} (cm^3/g)	S_{meso} (m^2/g)	S_{micro} (m^2/g)	V_{macro} (cm^3/g)	S_{macro} (m^2/g)
Sawdust	22.50	0.0133	0.0034	0.0099	7.42	15.08	2.185	0.373
Activated Alumina	118.43	0.172	0.0179	0.1540	113.22	5.21	0.425	0.043
Activated Alumina + F	102.20	0.143	0.0130	0.1300	97.27	4.93	0.416	0.051
SFAA	61.10	0.0965	0.0313	0.0652	41.20	20.81	0.740	0.102
SFAA + F	21.90	0.0391	0.0090	0.0301	20.29	1.61	0.737	0.141

S_{BET} – BET Surface area (m^2/g), $V_{meso+micro}$ – Meso and micro pore volume (cm^3/g), V_{micro} – Micropore Volume (cm^3/g), V_{meso} - Mesopore Volume (cm^3/g), S_{meso} - Mesopore surface area (m^2/g), S_{micro} – Micropore surface area (m^2/g) , V_{macro} - Macropore Volume(cm^3/g), S_{macro} – Macropore surface area (m^2/g).

Table 4.1 Continued

Adsorbent	V_{TOTAL} (cm^3/g)	% V_{micro}	% V_{meso}	% V_{macro}	S_{TOTAL} (m^2/g)	% S_{micro}	% S_{meso}	% S_{macro}
Sawdust	2.20	0.16	0.45	99.40	22.87	65.93	32.44	1.63
Activated Alumina	0.60	2.99	25.78	71.23	118.47	4.37	95.59	0.04
Activated Alumina + F	0.56	2.32	23.32	74.37	102.25	4.82	95.13	0.05
SFAA	0.84	3.74	7.80	88.46	61.11	33.50	66.33	0.16
SFAA + F	0.78	1.16	3.88	94.96	22.04	7.30	92.06	0.64

4.1.2 Scanning Electron Microscopy

The Scanning Electron Microscopy (SEM) images of SFAA before and after adsorption of fluoride are recorded under the magnification of 2000x and the images are shown in Figs.4.4a & b. The SEM images show that the granules remain intact after grafting. EDX analysis was performed to find the elemental constituents of pure SFAA, SFAA+F (Fig.4.5a & b). The

atomic % of Al and Fe on the basis of chemicals presented in pure SFAA was found to be 35.9 and 37.1%. Fluoride adsorption conformed by the presence of corresponding peak in the EDX spectra of SFAA after fluoride adsorption.

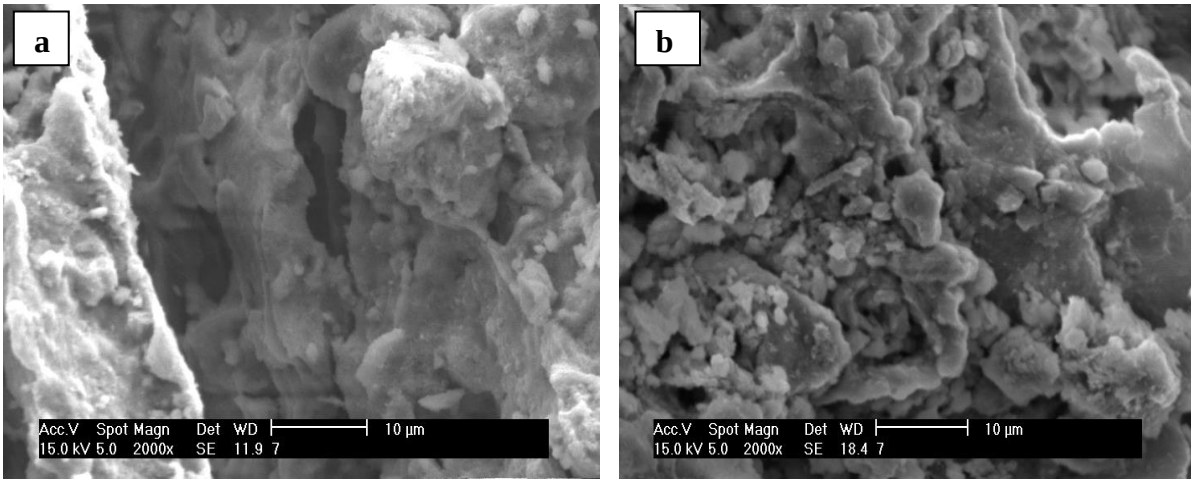

Fig.4.4. SEM image of SFAA (a) before, (b) after fluoride adsorption

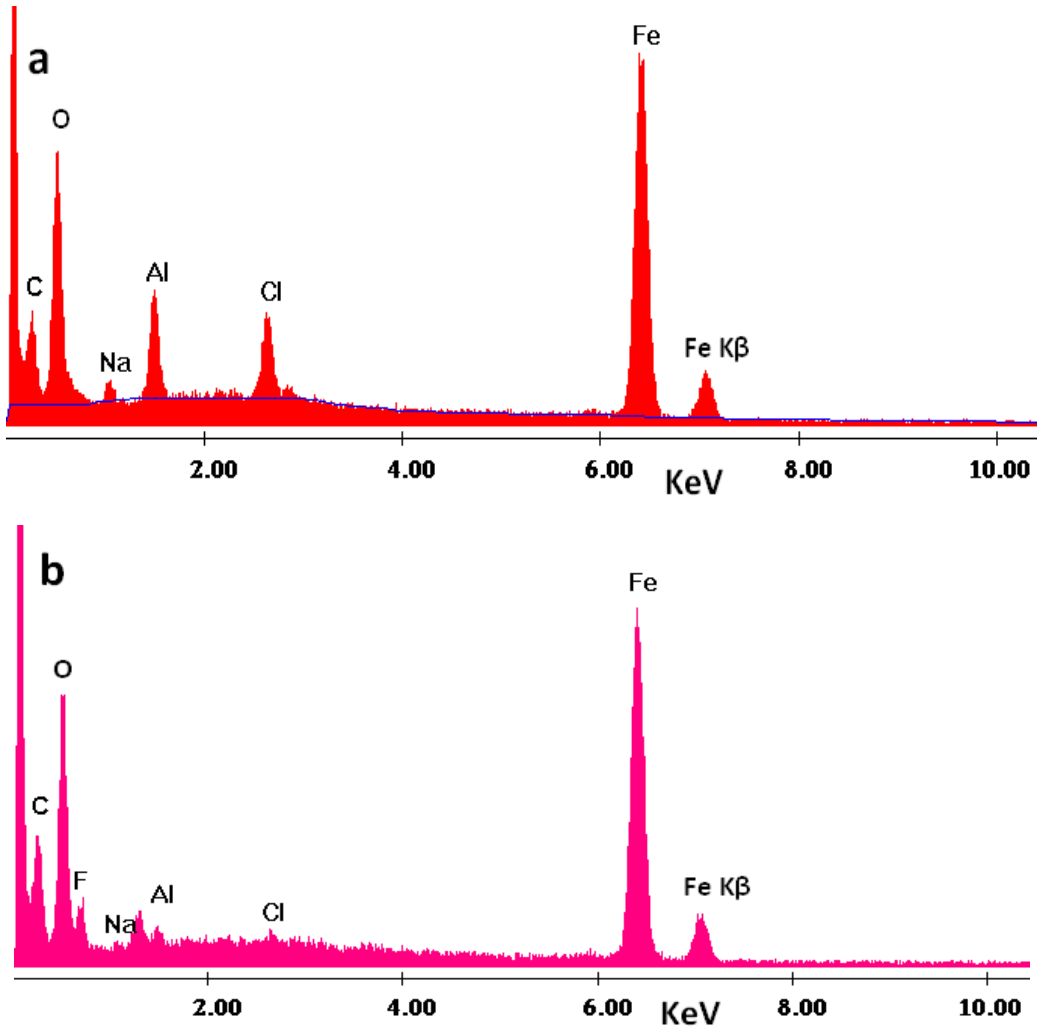

Fig.4.5. EDX spectra of SFAA (a) before, (b) after fluoride adsorption

4.1.3 Fourier Transform Infra Red Spectroscopy

Fig.4.6 shows the FTIR spectra of SFAA before and after fluoride adsorption. The broad and intense peak at 3060-3600 cm^{-1} is characteristic stretching frequency of hydroxyl groups and the peak which is observed at 1640 cm^{-1} is assigned to the bending vibration of adsorbed water. The small peaks at 1504 cm^{-1} and 1427 cm^{-1} are assigned to C=C aromatic stretching. FTIR results indicate that mainly hydroxide ions in different functional groups are involved in fluoride ion sorption. After the fluoride adsorption, increases in intensities of the peaks are observed which might possibly be due to the exchange of OH^- by F^- [25]. These results are in conformity with the earlier studies by various researchers. As sawdust is the major component of SFAA, its functional groups (amino, carboxyl, thiol, sulfydryl, alcohol, phenol, phosphate, polysaccharides and proteins) reflect in the FTIR [26].

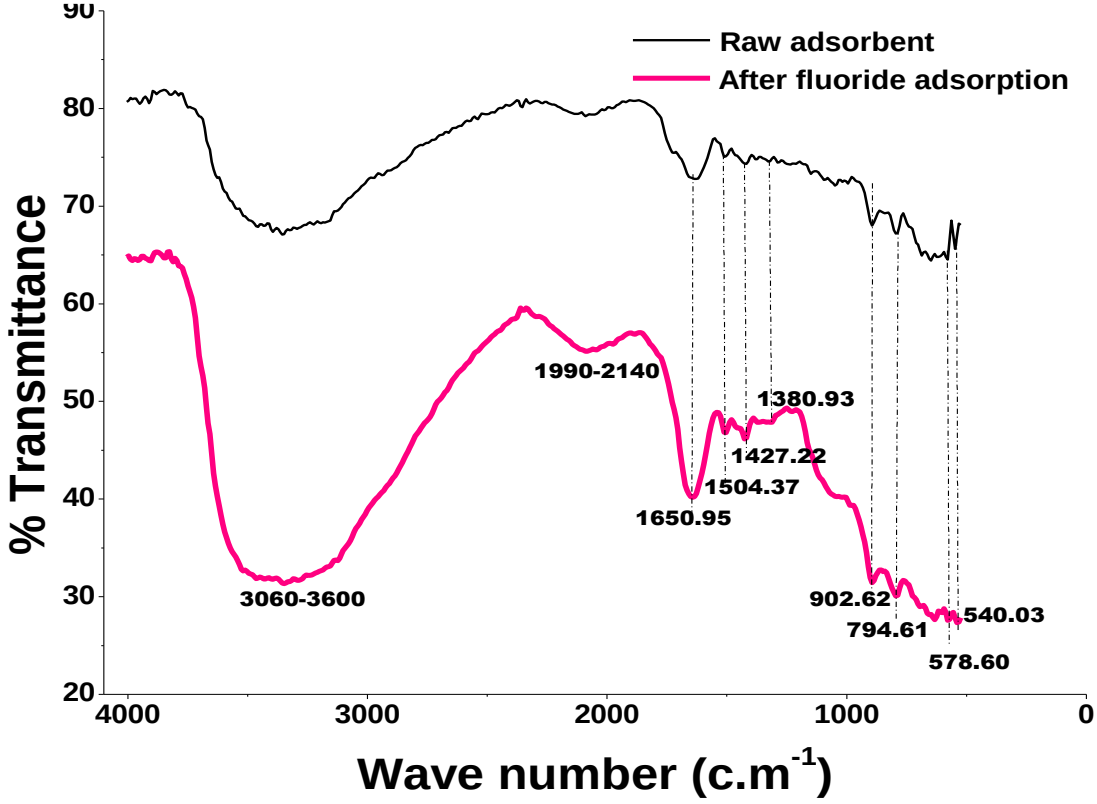

Fig.4.6. FTIR spectra of SFAA before and after fluoride adsorption

4.1.4 X-ray Photoelectron Spectroscopy

The X-ray Photoelectron Spectroscopy (XPS) survey confirmed the distribution of surface elemental composition loaded onto the Artocarpus hirsutus sawdust [27]. Fig.4.7 shows the

survey of wide scan XPS spectrum, which confirms the presence of Al, Fe, C, and O on the surface of SFAA. Selected area scans were performed for C 1s, O 1s, Fe 2p and F 1s levels (Fig.4.8). Iron and Aluminium oxide are present on the SFAA surface which was confirmed by the corresponding peaks. Fe $2p_1$, $2p_3$ peaks have been obtained at 710.8, 724.8 eV, similarly Al 2s peak at 117.9 eV. Samples of SFAA exposed to NaF showed F peak was observed near 685 eV of binding energy (Fig.4.8 c), and indicating SFAA adsorbed fluoride on its surface. To confirm the presence of fluoride, the selected area was scanned for F 1s region and the patterns were recorded for the F^- loaded specimens (Fig.4.8 c). The pattern is fitted with a single Gaussian peak giving rise to a correlation coefficient of 0.98. The position of the peak indicates that fluoride ion is –1 valence state. Thus, XPS studies reveal that fluoride ions are trapped by the matrix.

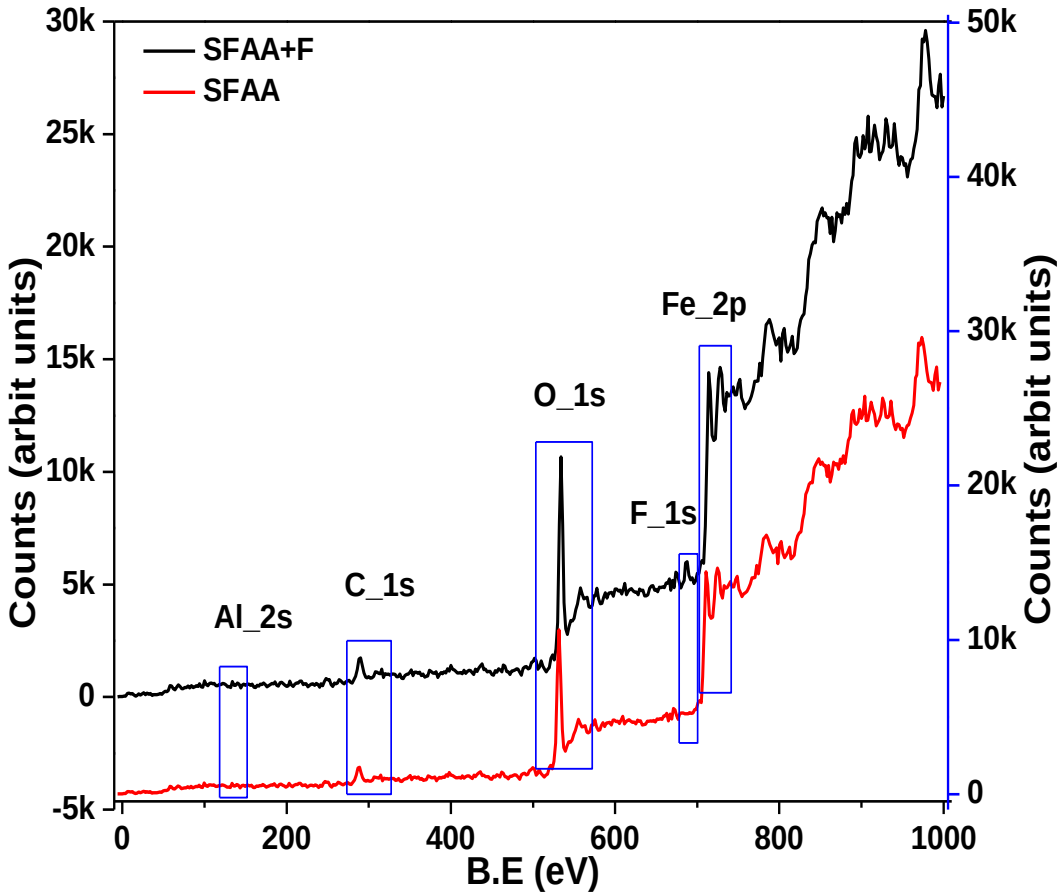

Fig.4.7. XPS spectra of SFAA before and after fluoride adsorption

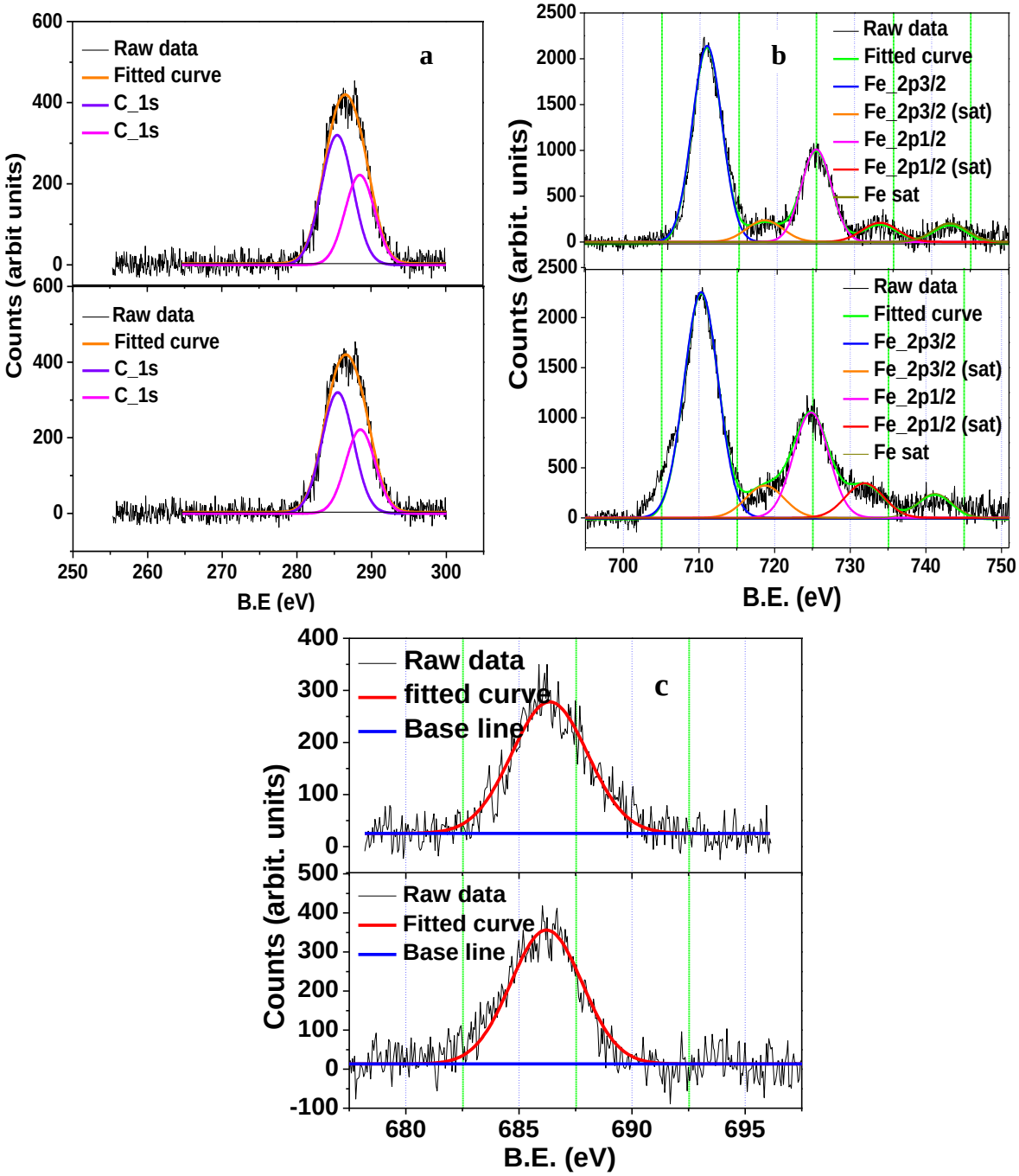

Fig.4.8. XPS spectra of (a) C 1s, (b) Fe 2p, (c) F 1s

4.2 BATCH STUDIES

4.2.1 Effect of contact time

The contact time was varied from 0 to 150 minutes, keeping adsorbent dose of 0.1g/10mL at pH of 6.5. Fig.4.9 shows the variation of fluoride removal for different contact times. The removal of fluoride increased with increase in contact time rapidly up to 40 min. Beyond 40 minutes, it gradually approached a constant value, indicating that equilibrium was attained. Based on these

results, it is deduced that 40 min is the contact time required for effective defluoridation using this sorbent.

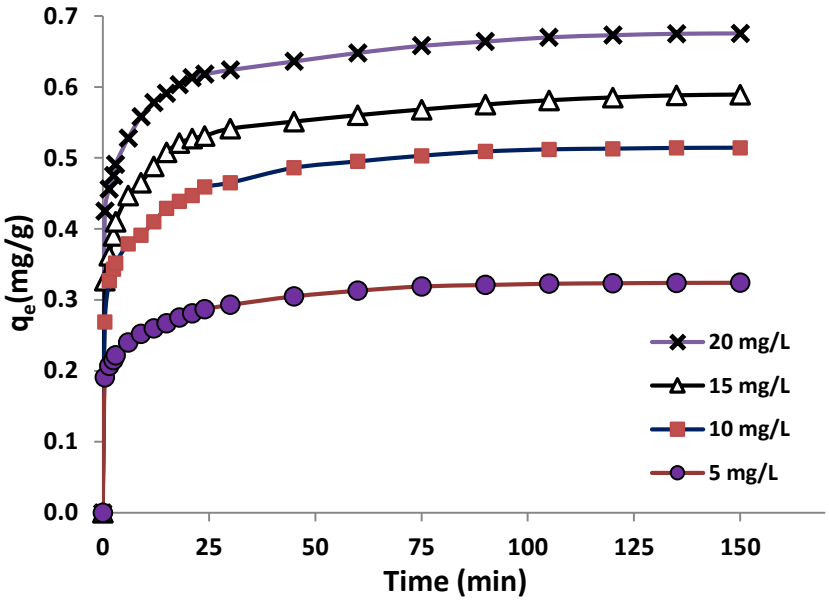

Fig.4.9. Effect of contact time

As can be seen from Fig.4.9, the uptake is fast initially and slows down in subsequent phases and towards the end becomes almost constant. In the initial phase, as the adsorbent is fresh, more sites for adsorption and more functional groups were available, which decrease with progress of adsorption, covering the available sites.

4.2.2 Adsorption Kinetics

I. Chemical reaction based kinetic modeling

i) Pseudo first order Lagergren model

Based on equation 3.7, the plot of $log(q_e - q_t)$ versus t as shown in Fig. 4.10 should give a linear relation, from which K_1 and q_e can be determined from the slope and intercept, respectively (Table 4.2). It can be seen that the Lagergren equation does not fit well for the whole range, particularly the initial times.

ii) Pseudo second order Ho model

Based on equation 3.9 a plot t/q_t versus t has drawn. From the slope and intercept of the straight line obtained from the plot of t/q_t versus t (Fig 4.11), the values of q_e and K_2 are calculated and presented in Table 4.2.

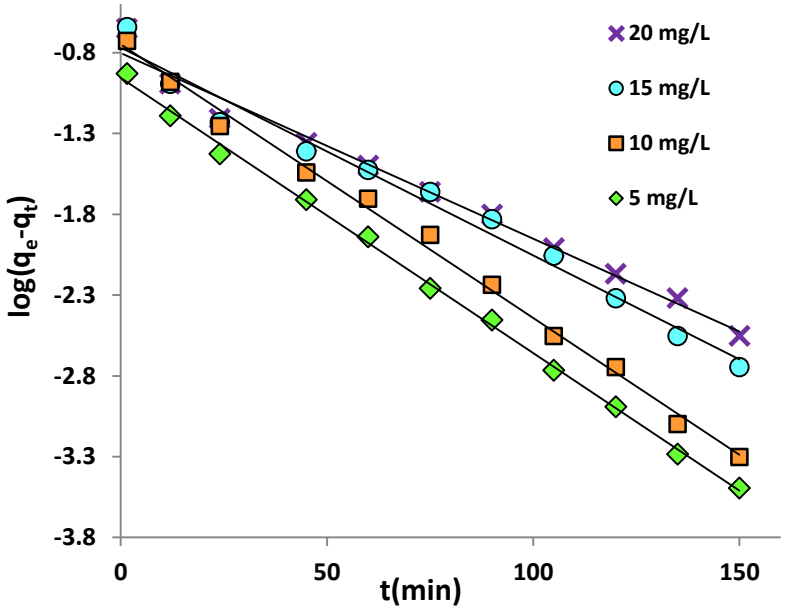

Fig.4.10. Pseudo first order sorption kinetics of fluoride adsorption on SFAA at various concentrations

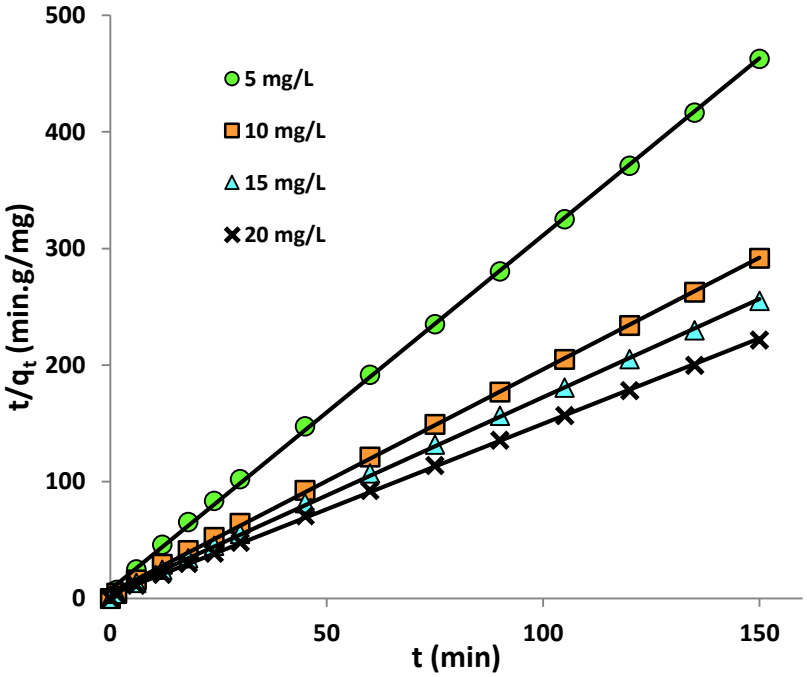

Fig.4.11. Pseudo second order sorption kinetics of fluoride adsorption on SFAA at various concentrations

It can be seen from R^2 values presented in Table 4.2 that Ho's model gives a much better fit of the experimental data than Lagergren equation, for the entire range of concentrations studied. This shows that fluoride adsorption by SFAA follows pseudo second order kinetics and is chemical adsorption. Equilibrium adsorption capacities (q_e) predicted by this model are close to the experimental values, as shown by the % Error.

Table 4.2 Chemical reaction based kinetic model parameters

Experimental		Pseudo first order				Pseudo Second order			
C_O	q_{exp}	q_e	K_1	R_1^2	% Error	q_e	K_2	R_2^2	% Error
5	0.3242	0.3844	0.0394	0.998	15.66	0.3293	1.298	0.999	1.55
10	0.5143	0.4737	0.0389	0.996	-8.57	0.5219	0.514	0.999	1.46
15	0.5880	0.4640	0.0297	0.982	-26.72	0.5933	0.398	0.999	0.89
20	0.6770	0.4483	0.0265	0.984	-51.01	0.6821	0.301	0.999	0.75

C_O - initial concentration (mg/L); q_e-equilibrium uptake (mg/g); K_1- Pseudo first order rate constant (min^{-1}); K_2-Pseudo second order rate constant (g/mg.min)

II. Diffusion based kinetic modeling- Intra particle diffusion model (Pore diffusion)

Fluoride adsorption can involve several mechanisms, such as physico-chemical sorption, ion exchange, precipitation or complexation [281, 282]. The initial rate of intra particle diffusion is obtained by linearization of the curve $q_t = f(t^{0.5})$ (Equation 3.10). The plot of q_t against $t^{0.5}$ may present multi-linearity [283, 284]. The plot of q_t against $t^{0.5}$ indicates that three steps occur in the adsorption processes as shown in Fig.4.12. The first linear portion 0-4 min is external surface adsorption (external mass transfer- film diffusion) which is an instantaneous adsorption stage. This represents binding of fluoride ions by the active sites are distributed on the outer surface of SFAA particles. The second linear portion 4-30 min represents intra particle diffusion (pore diffusion) in the macro, meso and micro pores of adsorbent (SFAA). The third linear portion in the time period of 30-160 min indicates the final equilibrium stage, where the intra particle diffusion starts to slow down due to the extremely low solute concentration in solution. The linear portion of the plot for a wide range of contact time does not pass through the origin and the intercept after 4 min of contact time is significant. This implies that both external mass transfer and intraparticle diffusion contribute to the overall adsorption. The intraparticle diffusion model parameters are given in Table 4.3.

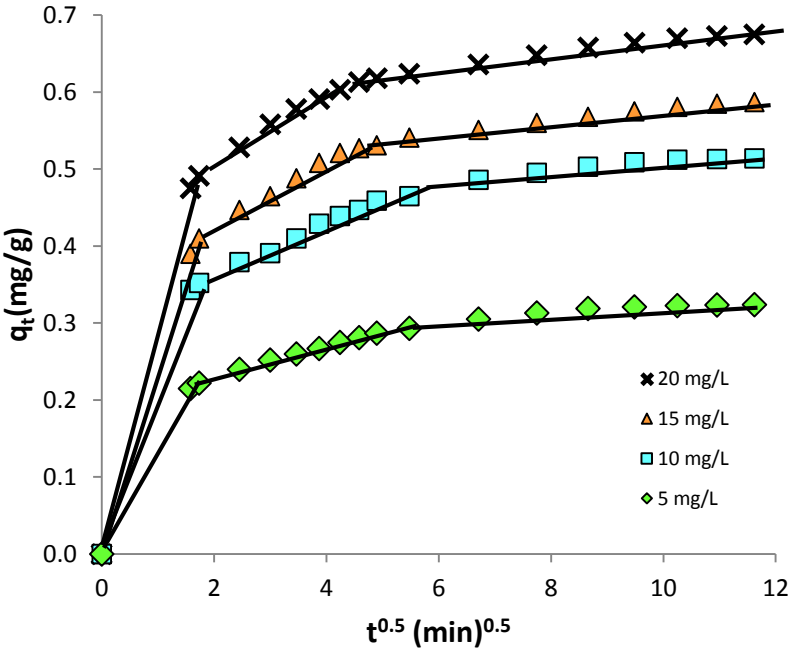

Fig.4.12. Intra particle diffusion model for fluoride adsorption on SFAA

III. External mass transfer model

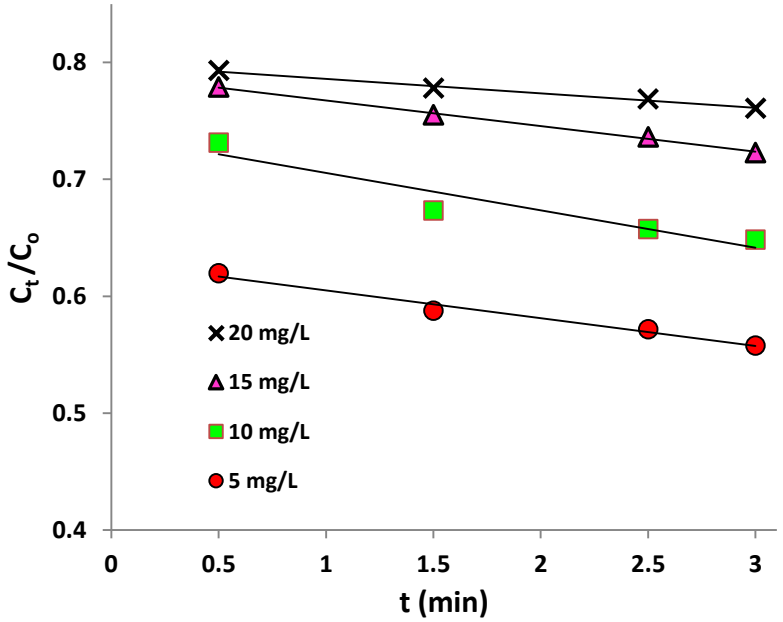

Fig.4.13. External mass transfer model for fluoride adsorption on SFAA

External mass transfer model is tested for the initial time period, where the adsorption is seen to be external mass transfer controlled. By this model, the ratio of concentration of fluoride at any time to the initially present will vary with time linearly,

$$\left[\frac{d(C_t/C_o)}{dt}\right]_{t=0} = -k_s \quad \text{..... 4.6}$$

After rearranging and integrating the above equation we get

$$\frac{C_t}{C_o} = -k_s t \quad \text{..... 4.7}$$

where, C_o, C_t are concentration in the initial and at time 't' (mg/L), k_s is external mass transfer rate constant (min^{-1}). Plots of C_t/C_o Vs t are shown in Fig.4.13 for various initial concentrations and k_s is given by the slope.

IV. Boyd plot

To determine whether the adsorption process occurs via external diffusion or an intraparticle mechanism, the kinetic data are analysed by the model of Boyd [285].

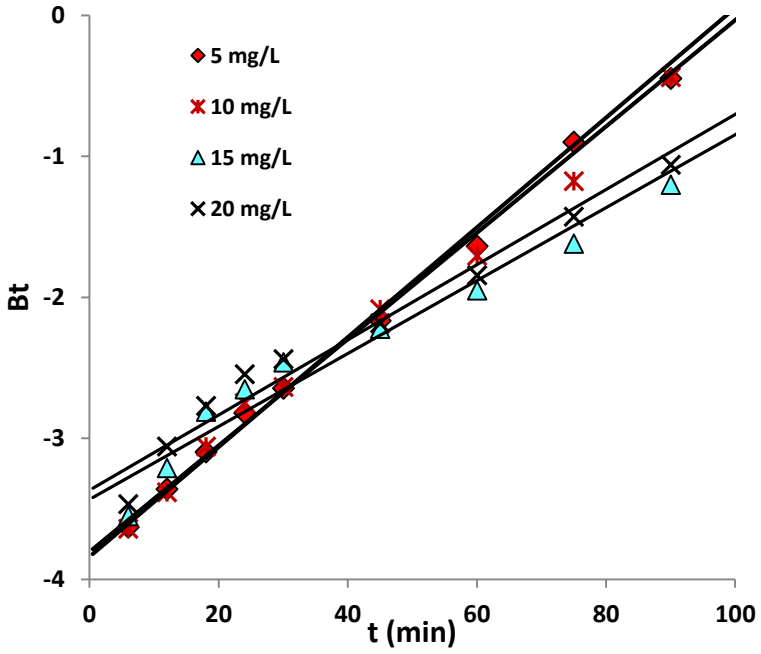

Fig.4.14. Boyd plot for fluoride adsorption on SFAA

The fraction of solute adsorbed at any time t to that can be adsorbed at an infinite time is given by this model as

$$\frac{q_t}{q_\infty} = 1 - \left(\frac{6}{\pi^2}\right) \exp[-Bt] \quad \text{..... 4.8}$$

Or

$$Bt = -0.4977 - ln\left(1 - \frac{q_t}{q_\infty}\right) \quad \text{..... 4.9}$$

where, q_t and q_∞ are fluoride adsorbed (mg/g) at any time 't' and at infinite time. The Boyd plot is obtained by plotting Bt Vs time (Fig.4.14).

Table 4.3 Diffusion based kinetic model parameters

Experimental		Intra particle diffusion			External mass transfer		Boyd plot	
C_O	q_{exp}	K_{id}	q_{id}	R_i^2	k_s	R_{Ex}^2	$D_i X10^{-4}$	R_{Bd}^2
5	0.324	0.009	0.335	0.871	0.0237	0.979	1.300	0.987
10	0.514	0.015	0.541	0.864	0.0319	0.903	1.269	0.988
15	0.588	0.015	0.609	0.814	0.0219	0.996	1.047	0.954
20	0.677	0.016	0.704	0.822	0.0214	0.989	1.015	0.952

C_O – initial concentration (mg/L); q – Equilibrium uptake (mg/g); K_{id} – intra particle diffusion model constant (mg/g.min$^{0.5}$); k_s – External mass transfer constant (min^{-1}); D_i – Diffusion coefficient (cm^2/s)

4.2.3 Effect of adsorbent dose

Effect of adsorbent dose on fluoride adsorption was studied for an initial fluoride concentration of 25 mg/L with a contact time of 60 min and the results are presented in Fig.4.15.

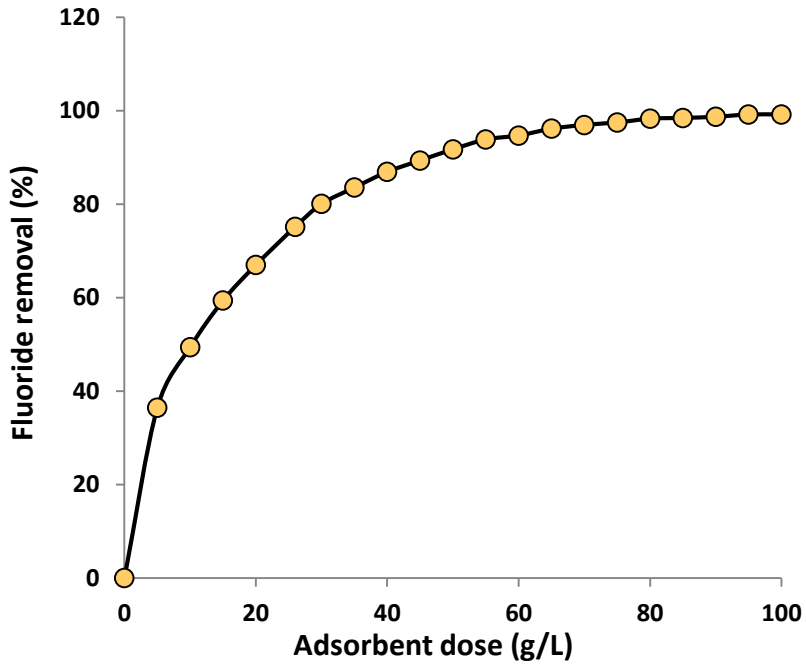

Fig.4.15. Effect of adsorbent dose

Removal of fluoride increased with increase in adsorbent dose and reached asymptotically a value of 99%. It is seen that the rate of removal is high for low doses of 10 g/L and this is the dose used for studying the effect of many other parameters, in the present study. For adsorption the distribution coefficient is given by $K_D = q_e/C_e$, where q_e is mass of fluoride adsorbed per unit mass of adsorbent and C_e is the concentration of fluoride in the solution at equilibrium. This

reflects the binding ability of the surface for an element and is dependent on pH and surface type. The distribution coefficient values for fluoride on SFAA at initial pH of 6.5 were calculated and presented in Fig.4.16. K_D values increased with an increase in adsorbent dose, indicating that the adsorbent has a heterogeneous surface [286]. K_D value is 97.6 L/kg at the dose rate of 10 g/L and this increased to 1226 L/kg at the dose rate of 100 g/L.

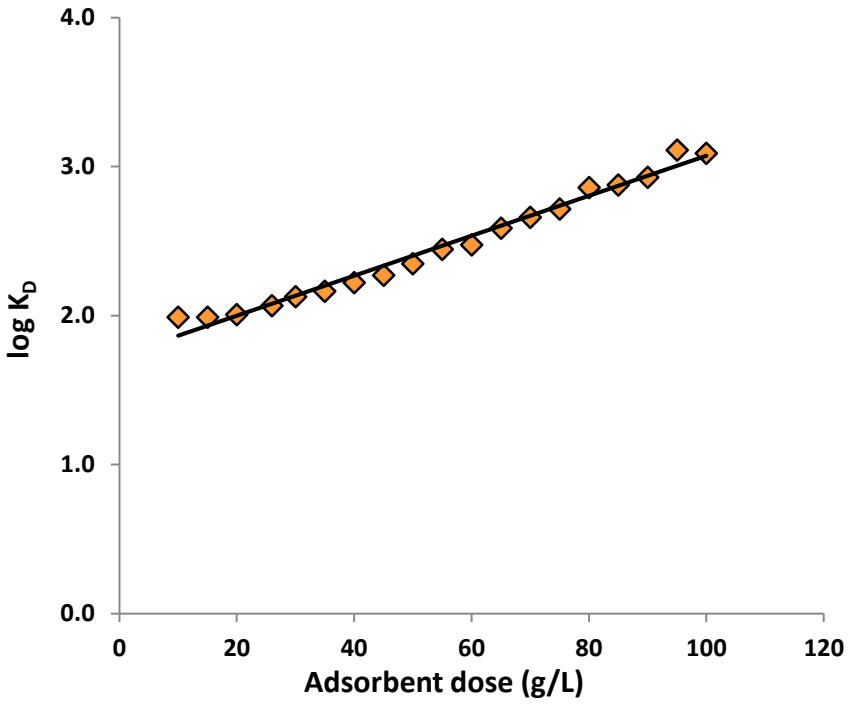

Fig.4.16. Variation of distribution coefficient with adsorbent dose

4.2.4 Effect of initial concentration

Though fluoride concentration prevalent in groundwater is limited to less than 50 mg/L, effect of initial concentration was studied over a wide range, up to 1000 mg/L, so as to assess the suitability of SFAA for industrial waste water treatment. Fluoride solutions of various concentrations were used (25, 50, 200, 250, 375, 450, 725 and 1000 mg/L) to find the adsorbing capacity of SFAA as a function of initial fluoride concentration. Solution of 10mL was taken with 0.1g of adsorbent and kept in a thermostatic shaker for 4 hr at constant temperature. The maximum adsorption capacity of SFAA for fluoride at room temperature (30ºC) is 40.28 mg/g, which was achieved for an initial fluoride concentration of 954 mg/L. This is considerably higher than the capacities reported for activated alumina (12 mg/g) and granular ferric hydroxide

(7.0 mg/g) [287, 288]. Fig.4.17 shows the effect of initial concentration of fluoride solution. It can be seen that the adsorbent is very effective at low concentrations, for the given adsorbent dose and contact time. At an initial concentration of 22 mg/L fluoride, removal of more than 99% is achieved. Thus, this adsorbent is highly suitable for treating groundwater polluted with fluoride, to bring down the fluoride levels to WHO limits. In the range of 200 to 1000 mg/L, removal of 40-50% was achieved with the adsorbent dose used. This establishes that SFAA can be used for industrial waste water treatment by designing a suitable process scheme. Fluoride adsorption capacities of various adsorbents reported in the literature are compared with Table 4.4.

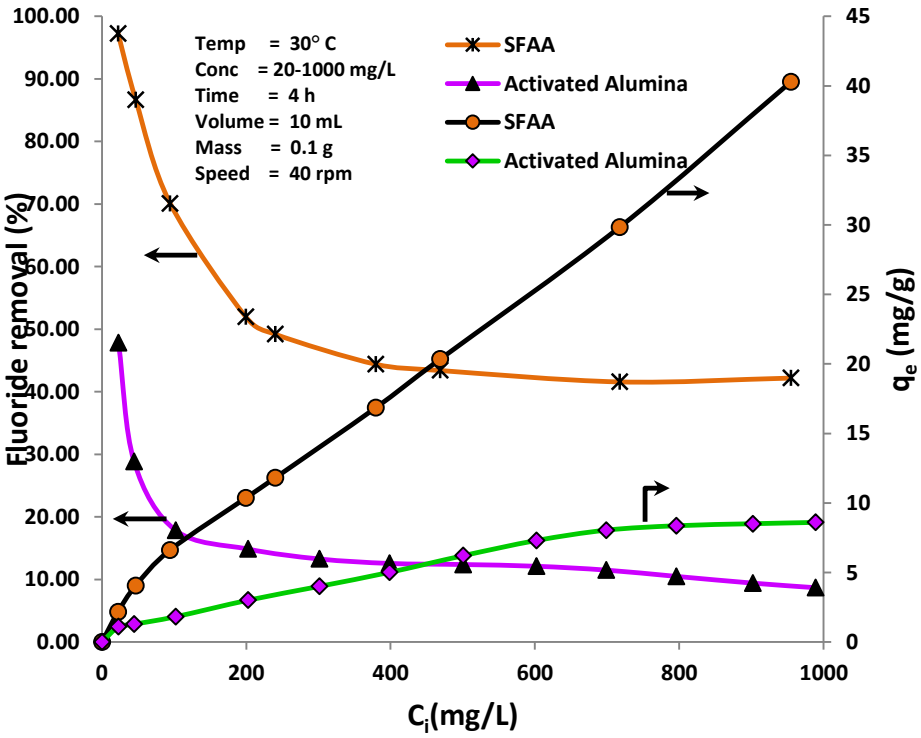

Fig.4.17. Effect of initial fluoride concentration

Table 4.4 Fluoride adsorption capacities of various adsorbents

Adsorbent	Capacity (mg/g)	Experimental conditions			Reference
		Temp (°C)	pH	Conc. (mg/L)	
SFAA	40.28	30	6.5	20-1000	Current study
Activated Alumina	8.60	30	6.5	20-1000	Current study

4.2.5 Effect of temperature

Though practical application of this adsorbent is defluoridation of water at room temperature, effect of temperature gives an insight into the mechanism of adsorption of fluoride. These sorption experiments were carried out at various temperatures, viz., 303, 308, 313, 323 and 333 K. Fig.4.18 shows the plot of uptake of fluoride (q_e) as a function of concentration of fluoride in solution at equilibrium (C_e). When the temperature was increased from 303 K to 308 K, 313 K, 323 K and subsequently to 333 K, the adsorption increased, indicating that the mechanism is chemisorption.

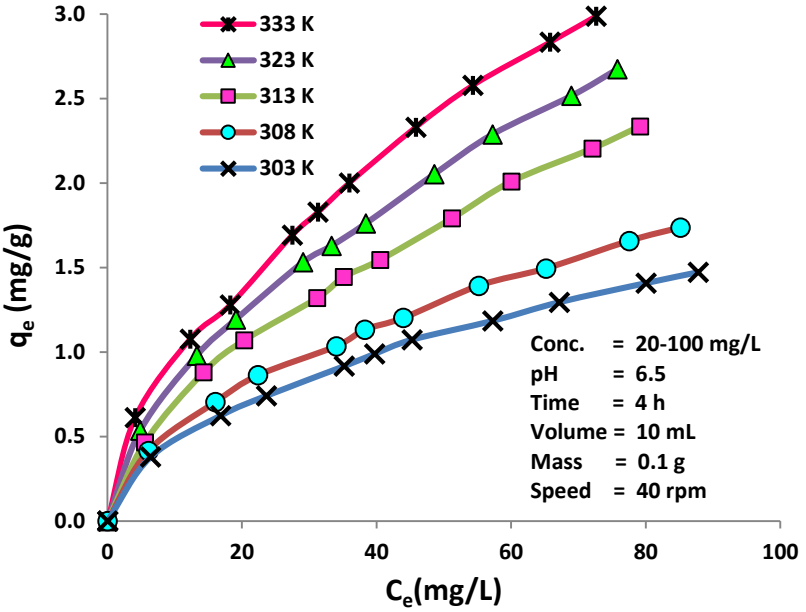

Fig.4.18. Effect of temperature

4.2.6 Adsorption isotherms

Adsorption of fluoride from aqueous solutions was reported to follow, in general, either Freundlich or Langmuir Isotherm [238]. Based on equations 3.4 & 3.5, both these models are used for analysis of adsorption data on SFAA and the results are presented. Fig.4.19 shows the linearized isotherms, which indicate that Freundlich adsorption model is applicable at all the temperatures studied. This confirms the heterogeneous nature of the surface of SFAA, which is already indicated by the effect of adsorbent dose, as explained in section 4.8. Freundlich isotherm constants and n were estimated from Fig.4.19 and presented in Table 4.5. It can be seen that the correlation coefficient, R^2 is very good (>0.995) for all the temperatures.

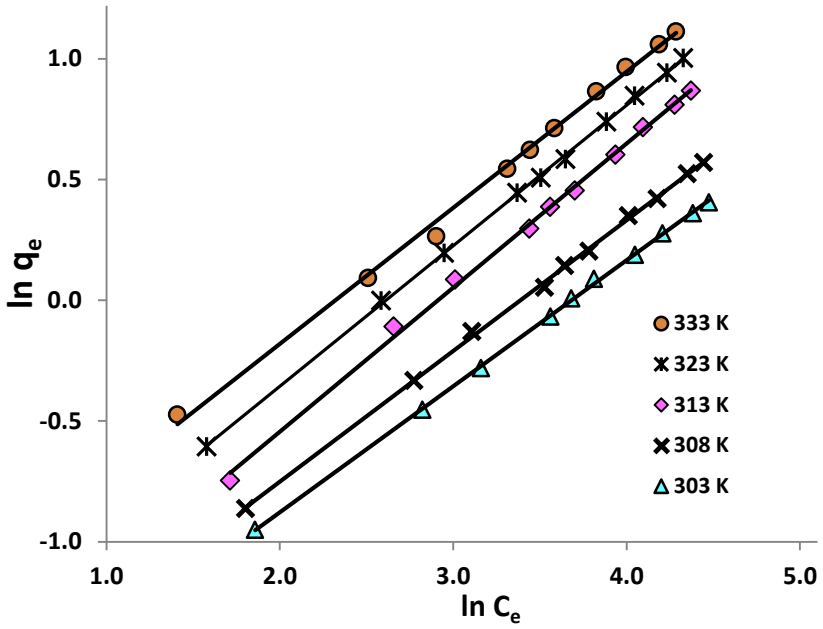

Fig.4.19. Freundlich adsorption isotherm

Freundlich constant, K_F, increases with temperature, indicating the general tendency for increased adsorption. However, n decreased when temperature increased from 303 to 313 K and increased for 323 K, subsequently decreasing for 333 K. Inverse of this constant, 1/n is called the heterogeneity factor and is an indication of the heterogeneity of the surface. Thus there is an increase in the heterogeneity of the surface from 303 to 313 K. Increase in the value of n from 313 to 323 K may be due to a shift in the mechanism in this range. Similar results were observed by Tao Zhang et al in their studies on fluoride adsorption on CeO_2/Al_2O_3 [289].

Table 4.5 Freundlich isotherm model constants and correlation coefficients for adsorption of fluoride onto SFAA adsorbent at different temperatures (From Fig.4.19)

Temp (K)	R^2	n	lnK_F	K_F (mg/g)(L/mg)$^{1/n}$
303	0.995	2.25	-1.955	0.142
308	0.998	1.87	-1.833	0.159
313	0.998	1.67	-1.757	0.172
323	0.998	2.09	-1.500	0.223
333	0.996	1.77	-1.325	0.265

The Langmuir isotherm, on the other hand, assumes uniform adsorption on the surface with a monolayer formation and no transmigration in the plane of the surface.

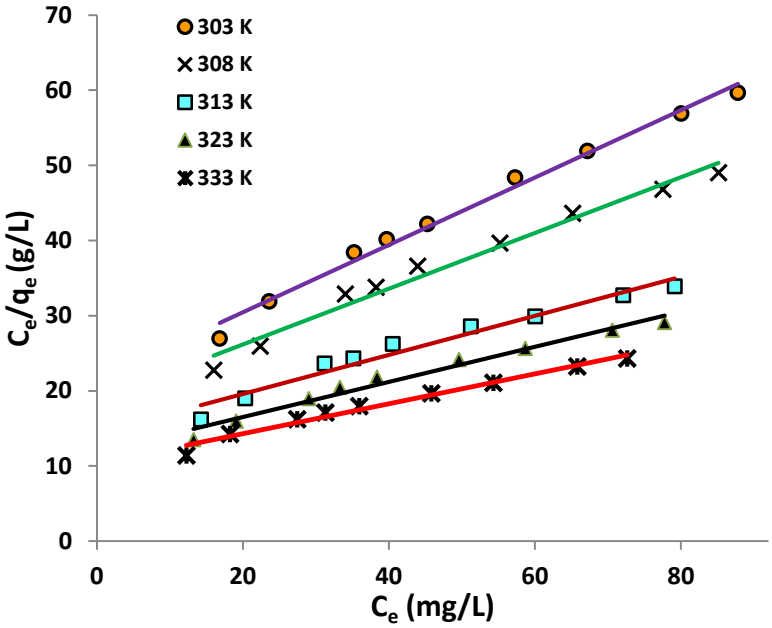

Fig.4.20. Langmuir adsorption isotherm

Fig. 4.20 shows the Langmuir adsorption isotherms. The plots are not linear, except possibly in the initial range of up to 25 mg/L fluoride concentration. Thus, fluoride adsorption on SFAA does not conform to Langmuir isotherm, confirming the heterogeneity of the surface of SFAA.

Table 4.6 Langmuir isotherm model parameters (From Fig.4.20)

Temp (K)	R^2	q_{max} (mg/g)	K_L (L/mg)
303	0.972	1.49	0.025
308	0.980	2.60	0.021
313	0.966	3.85	0.018
323	0.984	2.69	0.025
333	0.978	5.03	0.019

4.2.7 Thermodynamic study

To evaluate the thermodynamic feasibility and to confirm the nature of the adsorption process, three basic thermodynamic parameters, standard enthalpy (ΔH^o), standard entropy (ΔS^o) and standard free energy (ΔG^o) were calculated.

Due to the good conformity of the adsorption data to Freundlich isotherm, K_F is used to calculate the thermodynamic parameters. The thermodynamic equilibrium constant K_d is dimensionless and is obtained by multiplying K_F (in the units of L/g) with water density, 1000 g/L [277, 290].

Van't Hoff plot of $\ln K_d$ with reciprocal of temperature (1/T) is shown in Fig.4.21. The value of ΔH^o, and ΔS^o were obtained from the slope and intercept of the plot. The thermodynamic parameters were determined using the equations 3.11, 3.12 explained in section 3.2.5 [291].

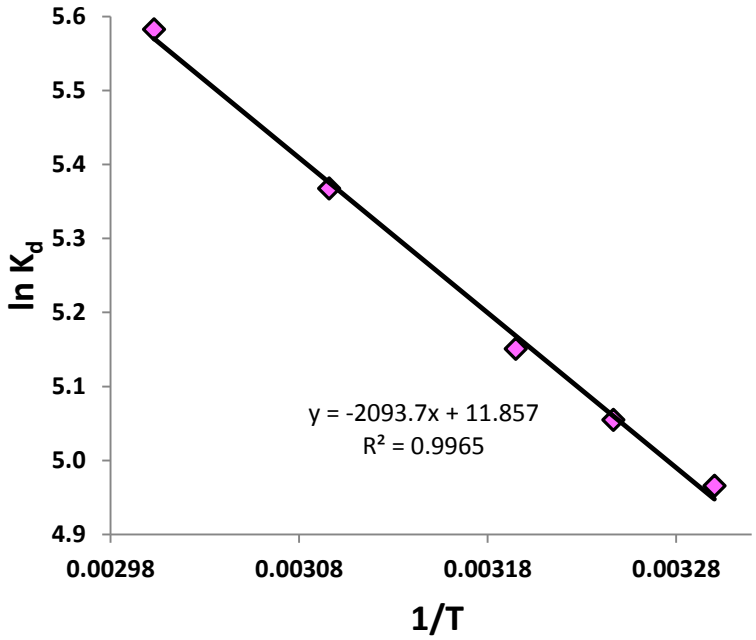

Fig.4.21. Van't Hoff plot

Table 4.7 Van't Hoff plot parameters

Temp (K)	1/T (K^{-1})	C_e (mg/L)	q_e (mg/g)	K_d (No unit)	$\ln K_d$	ΔG^o (kJ/mol)	ΔH^o (kJ/mol)	ΔS^o (kJ/mol.K)
303	0.00330	87.79	1.47	143.42	4.97	-12.51		
308	0.00325	85.14	1.74	156.77	5.05	-12.94		
313	0.00319	79.15	2.34	172.56	5.15	-13.40	17.86	0.10
323	0.00310	75.77	2.67	214.38	5.37	-14.41		
333	0.00300	72.63	2.99	265.80	5.58	-15.46		

From Fig.4.21, ΔH^o and ΔS^o were calculated to be 17.86 kJ/mol and 0.10 kJ/mol.K respectively. The endothermic nature of adsorption is indicated by an increase in K_d with the temperature and the positive value of ΔH^o. The value of ΔH^o indicates that the process is chemisorption. The negative value of ΔG^o confirms the feasibility of adsorption at all the temperatures and indicates that it is a spontaneous process. The value of ΔS^o being positive indicates that both enthalpy and

entropy are responsible for making ΔG^{o} negative, which showed the increasing randomness at the solid – solution interface during adsorption. The adsorption mechanism of defluoridation is mainly by F^{-} and OH^{-} exchange. Desorption of OH^{-} attached to active sites on the surface needs some activation energy to leave the surface, which might explain the endothermic nature of the adsorption process.

4.2.8 Effect of particle size

Fluoride adsorption experiments were conducted using SFAA with different particle sizes, viz., <89, 89-152, 152-210, 210-354 and 354-500 μm.

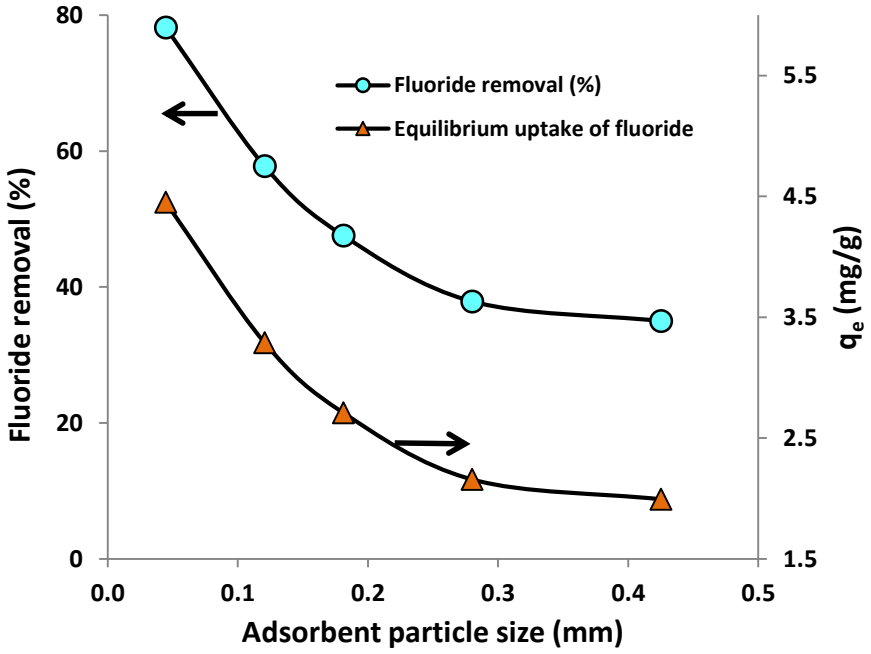

Fig.4.22. Effect of adsorbent particle size

Fig.4.22 shows the extent of fluoride removal as a function of average particle size. Adsorption is a known surface phenomenon. Resistance to mass transfer by film diffusion would be negligible, because the solution is continuously stirred at 40 rpm. As SFAA is not known to be highly porous, pore diffusion is not anticipated. As the external surface area per unit volume increases with decrease in particle size, smaller particles exhibit more external surface area for adsorption. Thus, there is a marked decrease in the adsorption capacity with increasing particle size, as can be seen in Fig.4.22.

4.2.9 Interference of other ions

Presence of anions and cations in groundwater was reported to affect the fluoride adsorption. The effect of anions such as chloride, sulfate, nitrate, bicarbonate and cations such as calcium, magnesium, and potassium, on the adsorption of fluoride by SFAA was examined experimentally and the results are given in Figs.4.23 and 4.24. Hydroxide, carbonate and bicarbonate interfere with fluoride adsorption by SFAA in decreasing order (Fig.4.23). Chloride, sulfate and nitrate did not show significant interference.

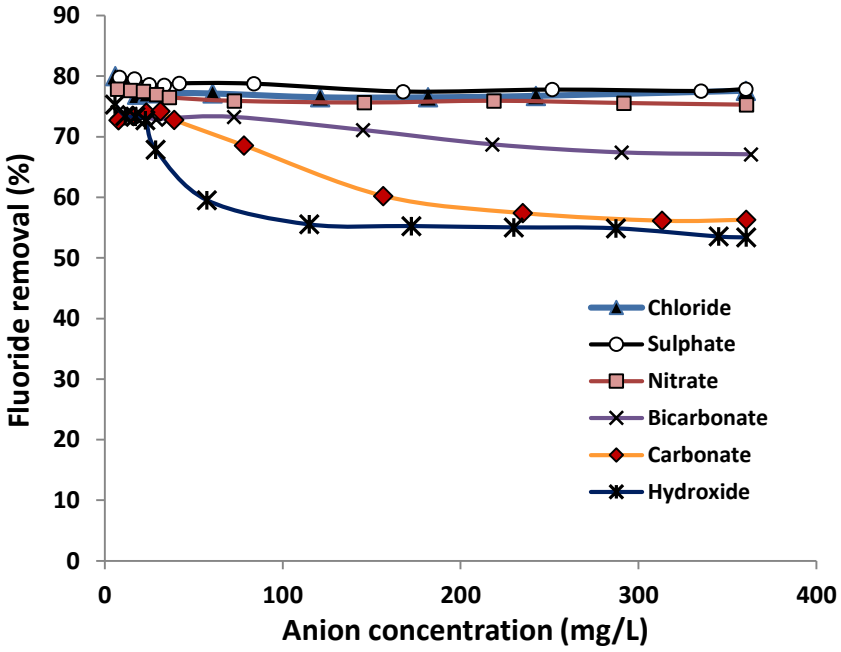

Fig.4.23. Interference of anions

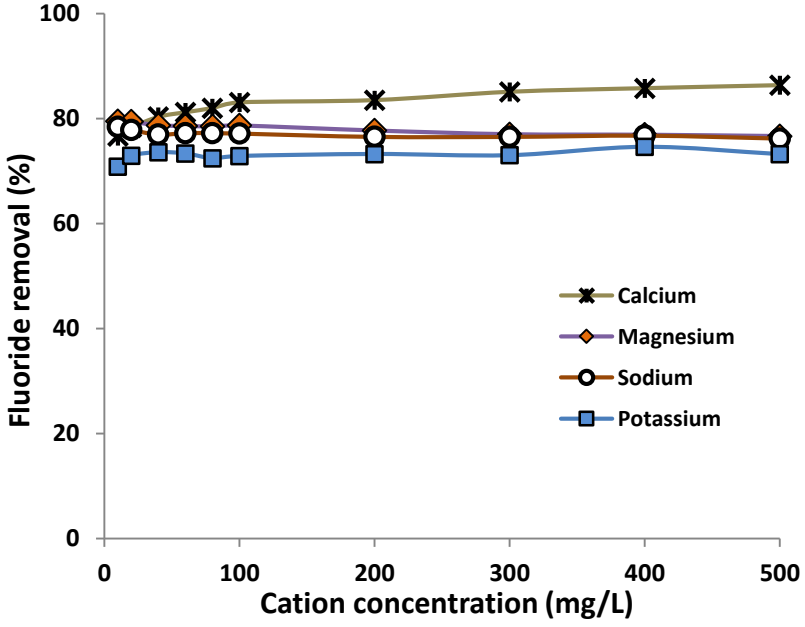

Fig.4.24. Interference of cations

The order of ions reducing fluoride removal efficiency by SFAA is observed to be $OH^- > CO_3^{2-} > HCO_3^- > NO_3^- > SO_4^{2-} > Cl^-$. Hydroxide ion, as already explained in section 4.1.3, is a competitor of fluoride for ion exchange on the surface of the adsorbent [292]. Moreover, increase of OH^- increases pH, which results in decrease in fluoride adsorption. Similarly, increase in carbonates and bicarbonates also increased the pH beyond 9, as seen from the experimental data, and hence there is a reduction in fluoride removal. Eva Kumar et al [203] also reported similar findings that presence of chloride and nitrate ions had negligible effect on fluoride removal by activated alumina, as these ions are outer-spherically sorbing anions.

Similarly interference of cations was studied and reported in Fig.4.24. It is seen that increasing sodium or potassium reduces fluoride adsorption, possibly due to the high solubility of sodium or potassium fluoride. Calcium enhances (77% to 87%) the fluoride adsorption by forming calcium fluoride, which is insoluble in water.

4.2.10 Fluoride removal from groundwater

SFAA was assessed for fluoride removal from groundwater from Avarangattur, Tamilnadu and the results are given in Table 4.8.

Table 4.8 Defluoridation of groundwater

Water parameter	Raw water			Treated water		
	A	**B**	**C**	**A**	**B**	**C**
pH	8.41	6.05	5.89	6.91	7.01	7.01
Temp (K)	303	303	303	303	303	303
Anions						
F^-	**8.2**	**4.4**	**5.2**	**1.12**	**0.55**	**0.42**
Cl^-	119.2	156.5	37.9	75.8	13.9	2.98
NO_3^-	95.9	84.6	11.8	15.7	7.61	0.0
SO_4^{2-}	73.9	49.9	1.82	0.0	0.0	0.0

(Temp = 303 K, Speed = 40 rpm, Time = 4 h, Volume = 10 mL, Mass = 0.1 g)

A =Avarangattur (Tamilnadu), B & C = Hot spring, Chandana village [Godda district, Jharkhand]

It can be seen that SFAA was effective inspite of the presence of other competing ions. SFAA reduced fluoride concentration from 8.2 mg/L to 1.12 mg/L. Similarly Chandana village, Godda district, Jharkhand water containing 5.2 mg/L fluoride reduced to 0.42 mg/L by SFAA. Along with defluoridation other anions also removed from groundwater which is shown in Table 4.8. From Table 4.8 it as shown that sulphate ion completely removed from the groundwater.

4.3 COLUMN STUDIES

The effect of the following operating parameters on column performance was investigated in the ranges mentioned: adsorbent particle size (0.082-0.181 mm), flow rate (0.5-2 mL/min) and fluoride concentration (12-50 mg/L). To describe the fixed bed column behavior and scale it up for industrial applications, various breakthrough models, viz., Thomas, Clark, Bohart-Adam and Yoon-Nelson models were used to fit the experimental data of the column studies. For continuous application on industrial scale, the adsorbent should be amenable for column operation under different process conditions. The effect of various operating parameters on the column performance is tested and presented in the form of breakthrough curves.

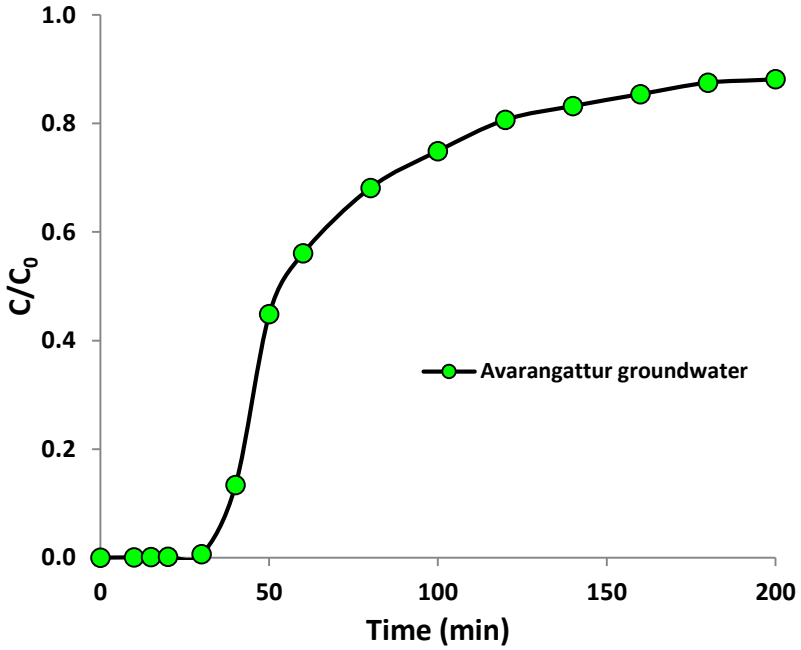

Fig.4.25. Column study on groundwater collected from Avarangattur

The groundwater sample collected from Avarangattur village in Dharmapuri district, Tamilnadu contains the fluoride level 8.2 mg/L, which was passed through the column packed with SFAA

at the flow rate of 2 mL/min and the results are plotted as shown in Fig.4.25. From the plot it is clear that the fluoride adsorption is slower and it takes more time to reach equilibrium.

4.3.1 Performance of different constituents

Removal of fluoride by different adsorbents was studied in the column setup. Sawdust, SFAA and only activated alumina were used for the column packing and the fluoride solution with 20 mg/L concentration pumped by a peristaltic pump at a constant flow rate (2 mL/min) for the required time. Samples were collected for the frequent time interval and analysed. The results are plotted. From Fig.4.26 SFAA shows effective removal of fluoride from water than activated alumina.

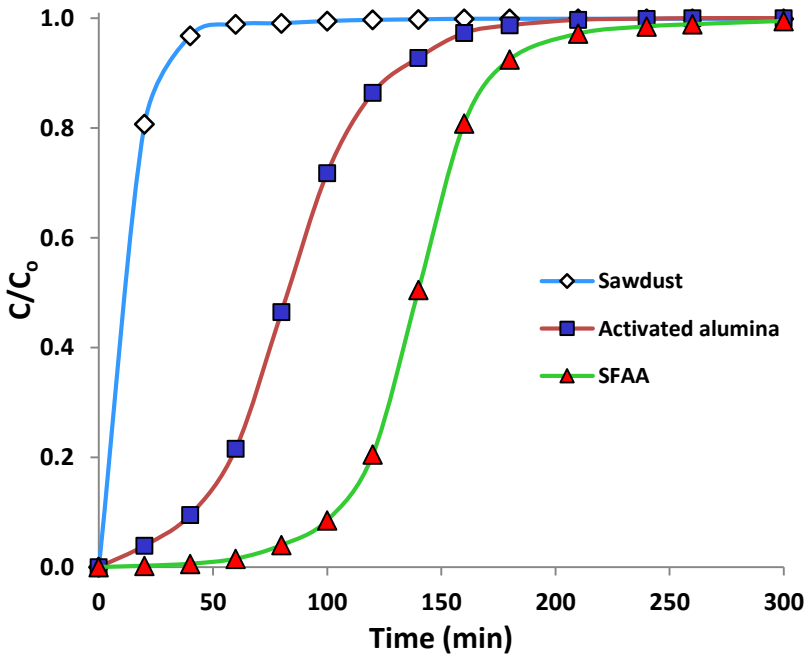

Fig.4.26. Fixed bed adsorption of fluoride by different constituents

4.3.2 Application of models for different constituents

The models are tested for prediction of experimental breakthrough curves for different adsorbents and presented in Fig.4.27 and Table 4.9. The data could be predicted by three models, viz., Thomas model, Yoon-Nelson model and Clark model. But Clark model gave the best fit with R^2 values of 0.999 and low % error for sawdust, activated alumina and SFAA. This is because sawdust, activated alumina and SFAA follows Freundlich adsorption isotherm.

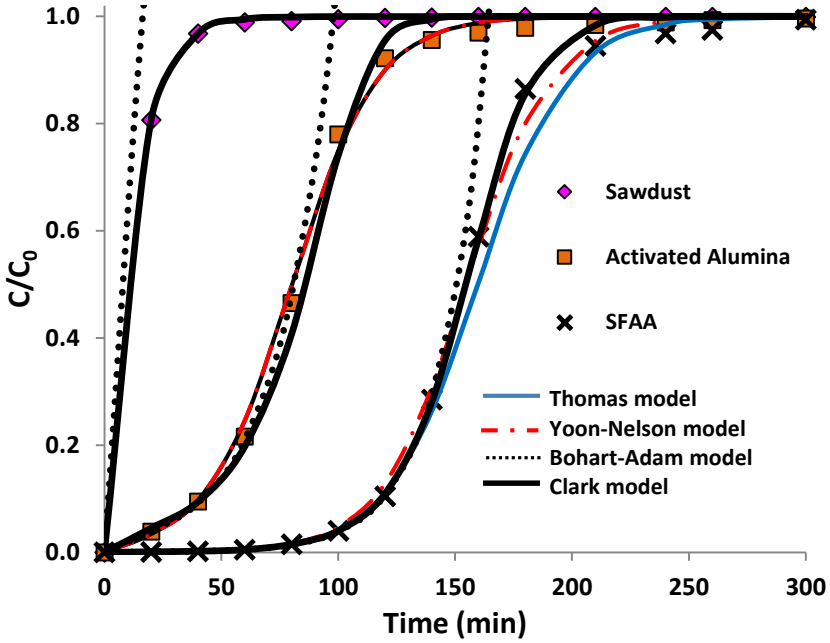

Fig.4.27. Application of models for different constituents

Table 4.9 Model parameters for different constituents

Adsorbent	q_{exp}	Thomas model				Yoon-Nelson model				
		k_{Th}	q_e	% Error	R^2	K_{YN}	τ	q_e	% Error	R^2
Sawdust	0.114	0.0047	0.12	0.88	0.999	0.0989	5.5	0.115	0.88	0.999
A.A	2.06	0.0034	1.56	24.27	0.990	0.0698	73.7	1.54	30.0	0.990
SFAA	3.20	0.0024	2.92	8.75	0.970	0.0544	134.8	2.84	11.25	0.993
		Bohart-Adam model				Clark model				
		k_{BA}	N_0	q_e	% Error	R^2	K_C	N_0	q_e	% Error	R^2
Sawdust		0.0004	22.6	0.09	21.05	0.878	0.0048	28.8	0.115	0.88	0.999
A.A		0.0028	1475.6	1.74	15.53	0.974	0.0063	1732.9	2.042	0.87	0.999
SFAA		0.0023	955.5	3.08	3.75	0.999	0.0052	966.6	3.11	2.81	0.999

k_{Th}, K_{BA}, K_C – Thomas, Bohart-Adam, Clark rate constants (L/mg.min), K_{YN} –Yoon-Nelson rate constant (min^{-1}),

q_e – Equilibrium uptake (mg/g), τ – time required for 50% adsorbate breakthrough (min), *N_0 – Saturation concentration (mg/L).*

4.3.3 Effect of particle size

Particle size of the adsorbent (ϕ) is an important parameter in column operation, as smaller particle sizes offer higher pressure drops, in addition to being prone for attrition. Column studies were conducted for different particle sizes by loading 1 g of SFAA in a column of 0.5cm inner

diameter (d_i) at a constant flow rate of 1 mL/min with C_0 = 50 mg/L. The breakthrough curves obtained for different particle sizes are shown in Fig.4.28. All the breakthrough curves showed the standard S shape, with different breakthrough and exhaustion times. When the particle size was increased from 0.082 mm to 0.181 mm, time for breakthrough decreased considerably from 55 min to 25 min (Fig.4.28) and adsorption capacity decreased from 6.19 mg/g to 3.72 mg/g (Table 4.10). Decrease in particle size enhances the adsorption capacity (q_t) due to higher available interfacial surface area and shorter intraparticle diffusion paths. Similar observations were made by the other researchers with respect to the effect of particle size [280, 293].

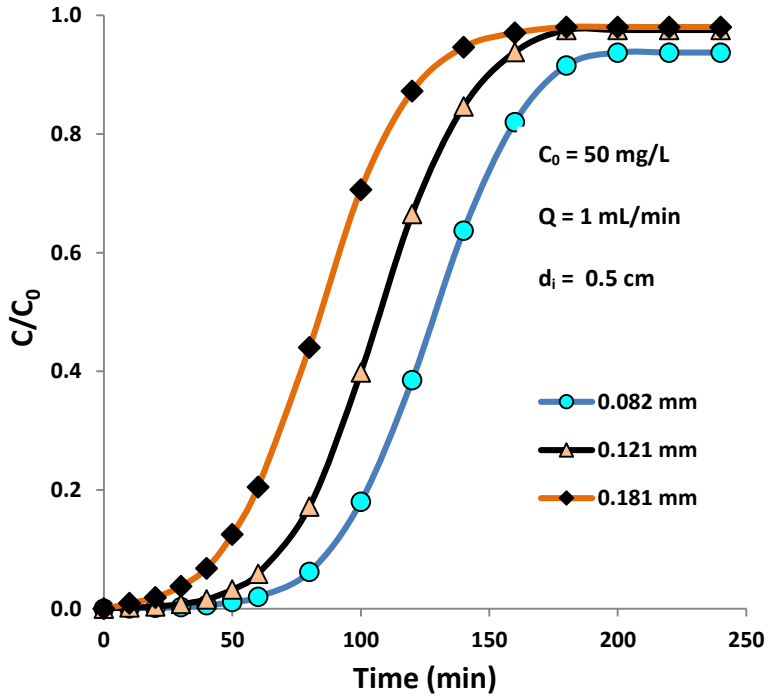

Fig.4.28. Breakthrough curves for different particle sizes

4.3.4 Application of models for different particle sizes

Experimental data for different particle sizes is tested to the four models as shown in Fig. 4.29. All model rate constants and maximum solid phase concentration of solute or equilibrium uptake (q) are calculated and listed in Table 4.10. It can be seen that of the four models tested, Clark's model gives the best fit of experimental data with R^2 value close to 1.0, Thomas (k_{Th}), Yoon-Nelson (K_{YN}), Bohart-Adam (k_{BA}) and Clark (K_C) rate constants increases with increasing particle size (0.089 to 0.182 mm). From experimental data

adsorption capacity (q) decreases from 6.19 to 3.72 with increase in particle size from 0.082 to 0.181 mm. Similarly adsorption capacity (q) obtained from models decreases with increase in particle size. It can be seen that Clark model predicts the experimental data well, with R^2 of 0.999 and % error of 0.02 to 3.03.

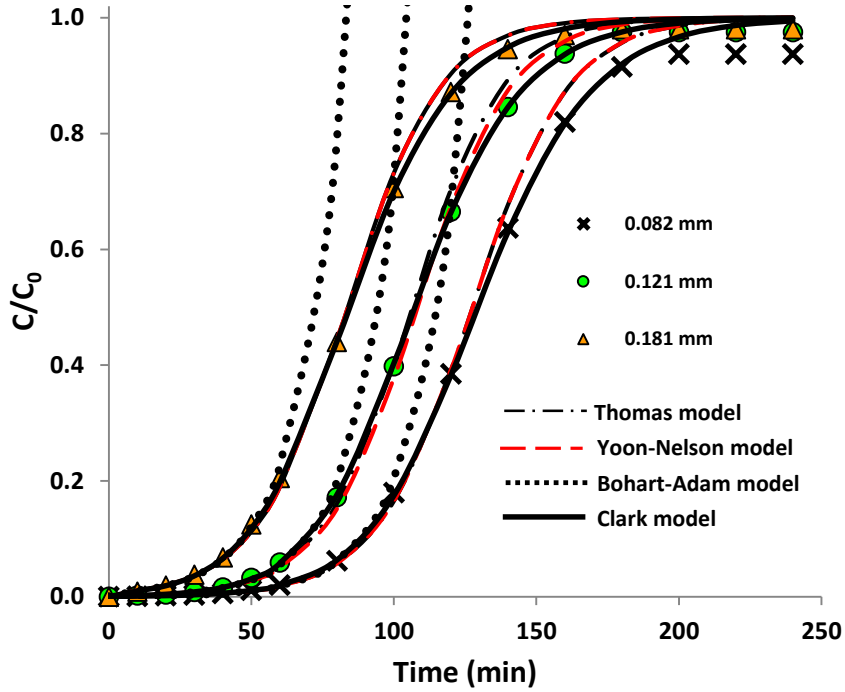

Fig.4.29. Application of models for different particle sizes

Table 4.10 Model parameters for different particle sizes

ϕ	q_{exp}	Thomas model				Yoon-Nelson model				
		k_{Th}	q_e	% Error	R^2	K_{YN}	τ	q_e	% Error	R^2
0.082	6.19	0.00116	6.48	3.41	0.998	0.0590	127.5	6.48	3.41	0.998
0.121	5.37	0.00117	5.72	6.62	0.997	0.0611	108.2	5.79	7.84	0.996
0.181	3.72	0.00126	4.09	9.97	0.996	0.0614	83.7	4.09	9.97	0.996
		Bohart-Adam model				Clark model				
		k_{BA}	N_0	q_e	% Error	R^2	K_C	N_0	q_e	% Error	R^2
0.082		0.00118	9366.1	6.43	2.55	0.997	0.00091	8674.6	6.12	2.36	0.999
0.121		0.00120	5240.6	5.65	5.34	0.996	0.00092	4790.5	5.20	3.03	0.999
0.181		0.00128	3480.5	4.09	10.16	0.995	0.00104	2946.3	3.72	0.02	0.999

ϕ - Particle size (mm), k_{Th} , K_{BA}, K_C –Thomas, Bohart-Adam, Clark rate constants (L/mg.min), K_{YN} –Yoon-Nelson rate constant (min^{-1}), q_e - Equilibrium uptake (mg/g), τ- time required for 50% adsorbate breakthrough (min), N_0- Saturation concentration(mg/L).

4.3.5 Effect of flow rate

Industrial scale operations aim to achieve the maximum flow rate possible maintaining the desired outlet concentration, thus operating at higher throughputs. Effect of flow rate is studied by taking 1 g of adsorbent (SFAA) in a 0.5 cm inner diameter column and passing water containing 20 mg/L fluoride at different flow rates. The breakthrough curves obtained are shown in Fig.4.30. Higher flow rates resulted in earlier breakthrough due to insufficient contact time. Adsorption capacity increased with increase in flow rate up to 1.5 mL/min (Table 4.11). At low flow rate of 2 mL/min, adsorption capacity decreased, due to insufficient contact time. Earlier researchers also reported decrease of adsorption capacity at higher flow rates [259, 294].

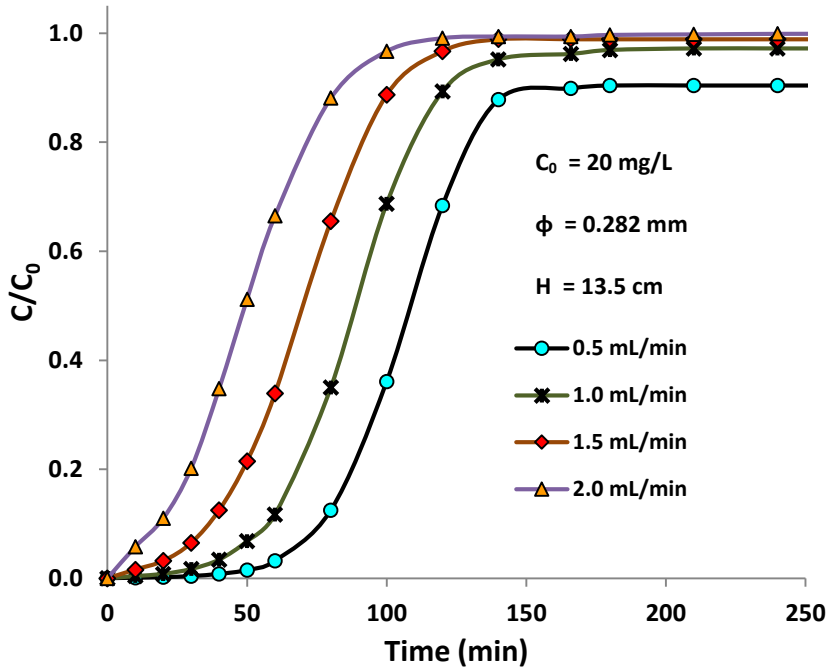

Fig.4.30. Breakthrough curves for different flow rates

4.3.6 Application of models for different flow rates

Breakthrough curves for different flow rates are compared with the models as shown in Fig. 4.31. Three models, Thomas, Yoon-Nelson and Clark are well fit the experimental data with very good R^2 and minimum % Error. Bohart-Adam model not able to predict the performance satisfactorily, but from Table 4.11 it can be predicted that k_{Th} and K_C increases with increase in flow rate, and k_{BA} & K_{YN} decreases with increase in flow rate. Usually adsorption capacity decreases with increase in flow rate due to insufficient contact time. But at low flow rate

(< 2 mL/min) adsorption capacity increases with increase in flow rate because of sufficient contact time and rate of adsorption is faster.

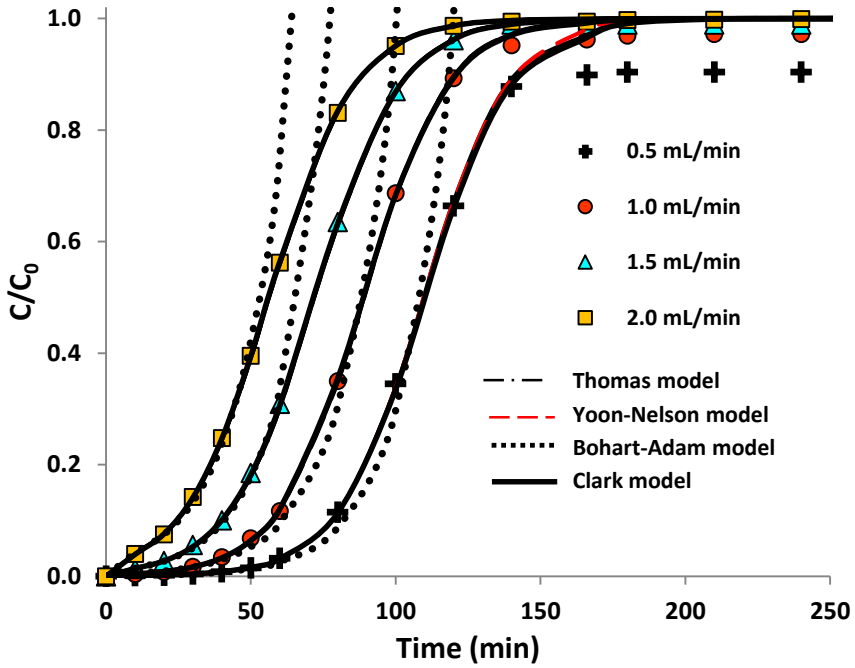

Fig.4.31. Application of models for different flow rates

Table 4.11 Model parameters for different flow rates

Q	q_{exp}	Thomas model				Yoon-Nelson model				
		k_{Th}	q_e	% Error	R^2	K_{YN}	τ	q_e	% Error	R^2
0.5	1.10	0.0036	1.08	2.1	0.999	0.069	109.6	1.08	2.1	0.999
1.0	1.62	0.0037	1.67	3.6	0.999	0.069	88.9	1.67	3.1	0.999
1.5	1.93	0.0035	1.96	1.3	0.999	0.068	72.2	1.96	1.0	0.999
2.0	1.86	0.0037	1.91	2.7	1.000	0.068	56.4	1.91	2.7	1.000
		Bohart-Adam model				**Clark model**				
		k_{BA}	N_0	q_e	% Error	R^2	K_C	N_0	q_e	% Error	R^2
0.5	0.0032	434.7	1.15	4.5	0.990	0.0035	395.8	1.07	2.7	0.999
1.0	0.0031	672.9	1.90	16.7	0.984	0.0036	623.2	1.65	1.9	0.999
1.5	0.0033	850.4	2.09	8.3	0.994	0.0034	782.4	1.92	0.5	0.999
2.0	0.0031	882.5	2.19	17.7	0.996	0.0037	767.8	1.87	0.5	1.000

Q –Flow rate (mL/min), k_{Th} *,* K_{BA}*,* K_C *–Thomas, Yoon-Nelson, Bohart-Adam, Clark rate constants (L/mg.min),* K_{YN} *–Yoon-Nelson rate constant (*min^{-1}*), q–Equilibrium uptake (mg/g),* τ – time required for 50% adsorbate breakthrough (min), N_0 *– Saturation concentration(mg/L).*

4.3.7 Effect of initial concentration

Concentration has a significant effect on the breakthrough due to variation in the driving force. Fluoride concentration in natural waters varies over a wide range based on the source. To study the effect of fluoride concentration, water with fluoride concentration of 12, 30, 50 mg/L was passed through 1.0 cm inner diameter (d_i) column packed with 2 g of SFAA at a constant flow rate 2 mL/min. The breakthrough curves are shown in Fig.4.32. Higher concentration resulted in earlier breakthrough due to earlier saturation of SFAA. As can be seen from Table 4.12 the adsorption capacity (q_t) increases with increase in feed concentration, due to increase in driving force for mass transfer, which enhances the adsorption rate and faster consumption of active sites [295]. Higher influent concentration causes sharper breakthrough curves due to quick adsorbent saturation, which causes decrease in adsorption zone length and exhaustion time [296].

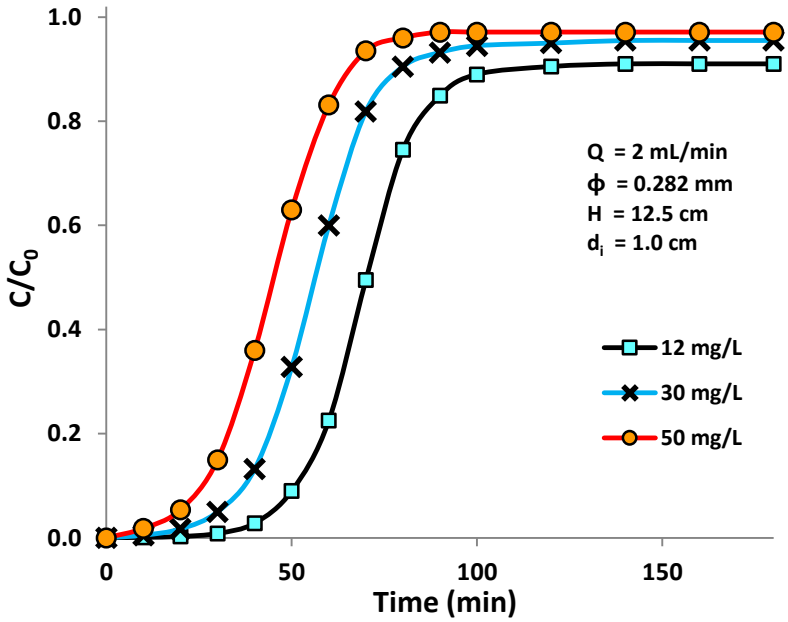

Fig.4.32. Fluoride adsorption at different concentrations

4.3.8 Application of models for different initial concentrations

The experimental data obtained for different feed concentration is also compared with these models to predict the performance of the breakthrough. In this case, the Thomas model predicted the experimental breakthrough curves quite well as shown in Fig.4.33. Thomas rate constant (k_{Th}), Bohart-Adam (k_{BA}) and Clark rate constants (K_C) decreases with increasing the

initial concentration (Table 4.12). It shows that k_{Th}, k_{BA}, K_C is inversely proportional to the initial concentration. Yoon-Nelson rate constant (K_{YN}) is not linear with varying initial concentration. While increasing initial concentration the concentration gradient increases thereby adsorption capacity increases. From Table 4.12 Clark model predicts the experimental data well with R^2 close to 1 and % error of 0.24 to 2.54.

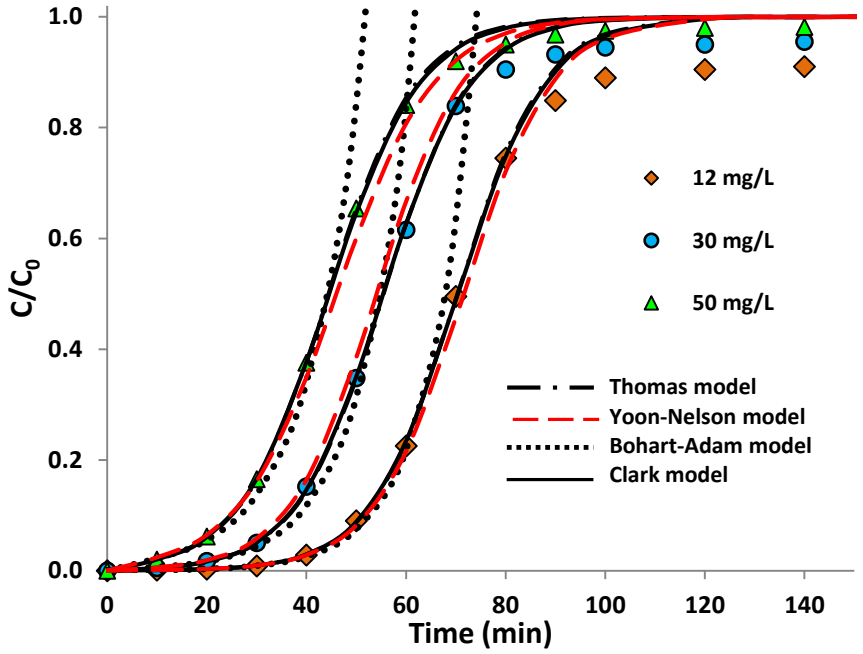

Fig.4.33. Application of models for different initial concentrations

Table 4.12 Model parameters for different initial concentrations

C_0	q_{exp}	Thomas model				Yoon-Nelson model				
		k_{Th}	q_e	% Error	R^2	K_{YN}	τ	q_e	% Error	R^2
12	0.852	0.0098	0.851	0.09	0.999	0.112	71.6	0.866	5.14	0.997
30	1.734	0.0037	1.730	0.23	0.999	0.116	54.1	1.733	0.06	0.998
50	2.237	0.0023	2.242	0.22	0.999	0.103	46.1	2.293	8.58	0.994
C_0		Bohart-Adam model				Clark model				
		k_{BA}	N_0	q_e	% Error	R^2	K_C	N_0	q_e	% Error	R^2
12	0.0091	185.4	0.893	4.8	0.995	0.0094	174.8	0.843	0.24	0.999
30	0.0032	406.6	1.898	9.1	0.989	0.0036	362.1	1.682	2.54	0.999
50	0.0018	524.8	2.67	19.2	0.986	0.0022	444.8	2.259	0.98	0.999

C_0 – Initial concentration (mg/L), k_{Th} ,K_{BA}, K_C –Thomas, Bohart-Adam, Clark rate constants (L/mg.min), K_{YN} –Yoon-Nelson rate constant (min^{-1}), q_e – Equilibrium uptake (mg/g), τ – time required for 50% adsorbate breakthrough (min), N_0 – Saturation concentration(mg/L).

4.4 ANALYSIS OF MASS TRANSFER ZONE

The effect of operating parameters such as initial concentration, flow rate and adsorbent particle size on the mass transfer zone were studied as was done for the case of arsenic adsorption. All the mass transfer zone related parameters are calculated and presented in Table 4.13. The effects are similar to those of adsorption of arsenic. By increasing the initial concentration, fractional capacity, %saturation and rate of movement of MTZ (U_Z) increase, but height of the mass transfer zone (H_{MTZ}) decreases. This is due to high concentration gradient, which speeds up the adsorption process. Similarly increasing flow rate can increases the H_{MTZ} and $U_{Z,}$ while decreasing the % saturation, because of insufficient contact time during adsorption at higher flow rate (Table 4.13). Effect of adsorbent particle size on mass transfer zone was also studied. Small particle size has smaller MTZ compared with larger particle size. Small MTZ leads to high adsorption of solute by the sorbent, hence the % saturation decreases with increase in particle size.

Table 4.13 Mass Transfer Zone (MTZ) related parameters

Conc. (mg/L)	Q (mL/min)	H (cm)	t_B (min)	t_E (min)	t_Z (min)	F	H_{MTZ} (cm)	U_Z (cm/min)	% Sat.
12	2.0	12.3	45	210	165	0.580	14.42	0.087	50.75
30	2.0	12.3	30	120	90	0.650	12.51	0.139	64.41
50	2.0	12.3	20	75	55	0.779	10.76	0.196	80.66
20	0.5	13.5	65	180	115	0.578	11.81	0.103	63.09
20	1.0	13.5	45	140	95	0.653	11.98	0.126	69.20
20	1.5	13.5	27	115	88	0.697	13.45	0.153	69.82
20	2.0	13.5	10	95	85	0.790	14.87	0.175	76.86
50	1.0	3.5	70	250	180	0.644	3.39	0.019	65.53
50	1.0	5.5	55	170	115	0.610	5.05	0.044	64.13
50	1.0	6.0	35	140	105	0.625	6.26	0.060	60.87

Conc.- concentration (mg/L), Q-Volumetric flow rate (mL/min), H- Bed height (cm), t_B- Breakthrough time (min), t_E- Exhaust time (min), $t_Z = t_E - t_B$, F-Fractional capacity, H_{MTZ} - Height of Mass Transfer Zone (cm), U_Z -Rate of movement of mass transfer zone (cm/min), % Sat.- Percentage saturation.

4.5 REGENERATION OF THE ADSORBENT

Column studies were conducted to test the regeneration and reusability of the adsorbent with a packed bed volume of 9.60 mL. The bed was regenerated for two cycles using 0.5 N NaOH and the breakthrough curves are shown in Fig. 4.34. Data on regeneration and reuse of the adsorbent is presented in Table 4.14. For the fresh adsorbent, breakthrough was achieved after 35 min. After the first regeneration, 85 % of fluoride could be recovered from the bed. In the second cycle breakthrough was achieved after 25 min. For this cycle 0.552 mg/g fluoride was picked up by the bed. In the second regeneration, 76% of fluoride could be recovered from the bed. In the third cycle the breakthrough and exhaustion times being 17 and 200 min respectively. In this cycle 0.470 mg/g fluoride was picked up by the bed.

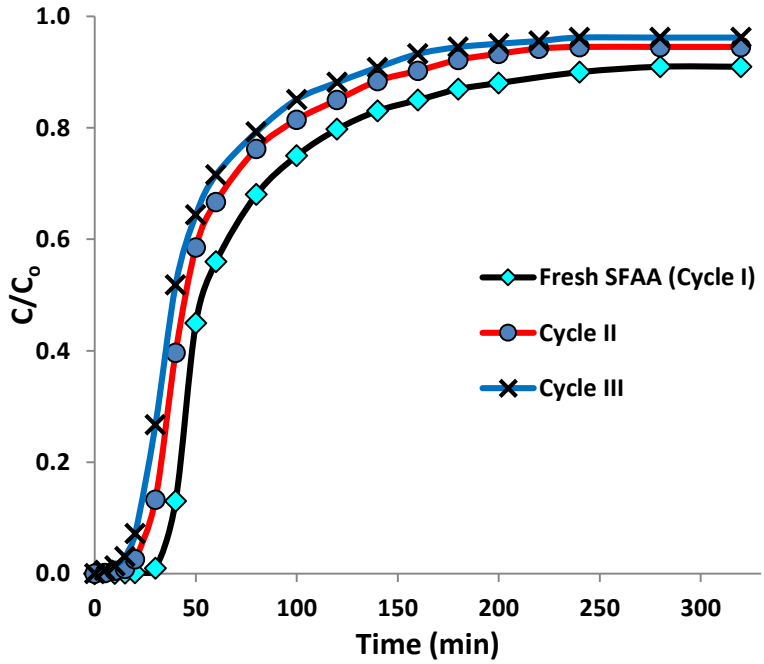

Fig.4.34. Regeneration studies on fluoride loaded SFAA

Table 4.14 Regeneration and reusability of SFAA for fluoride adsorption

Cycle No.	Breakthrough time (min)	Breakthrough uptake (mg/g)	Bed exhaustion time (min)	Regeneration efficiency (%)
1	35	0.710	280	Original
2	25	0.552	240	78
3	17	0.470	200	66

5 ADSORPTION OF ARSENIC AND FLUORIDE TOGETHER FROM GROUNDWATER BY SFAA

Presence of both arsenic and fluoride together above the WHO levels was reported in Pakistan, China, Mexico, Argentina, Bangladesh, Tanzania, USA and India [244, 253, 297-300]. SFAA was tested for removal of these pollutants from water when both are present together.

5.1 CHARACTERIZATION OF ADSORBENT

5.1.1 Scanning Electron Microscopy

The surface morphology before and after As(V) and fluoride adsorption was characterized separately using Philips XL-30 scanning electron microscope at 15 kV. The SEM image shown in Fig.5.1 indicates that in SFAA the pores are in the range of 0.1 to 2 µm in diameter (macro porous). From these SEM images, it can be seen that the granules remained intact after grafting As(V) and fluoride, except for the appearance of some pores on the surface of SFAA. EDX spectra confirms the adsorption of fluoride and As(V) on SFAA by Fig.5.2. From the EDX spectra, only the SFAA contains atomic % of Al and Fe are 35.9 and 37.1%. Arsenic and fluoride adsorbed sample shows the presence of arsenic and fluoride on its surface which confirms the adsorption of both.

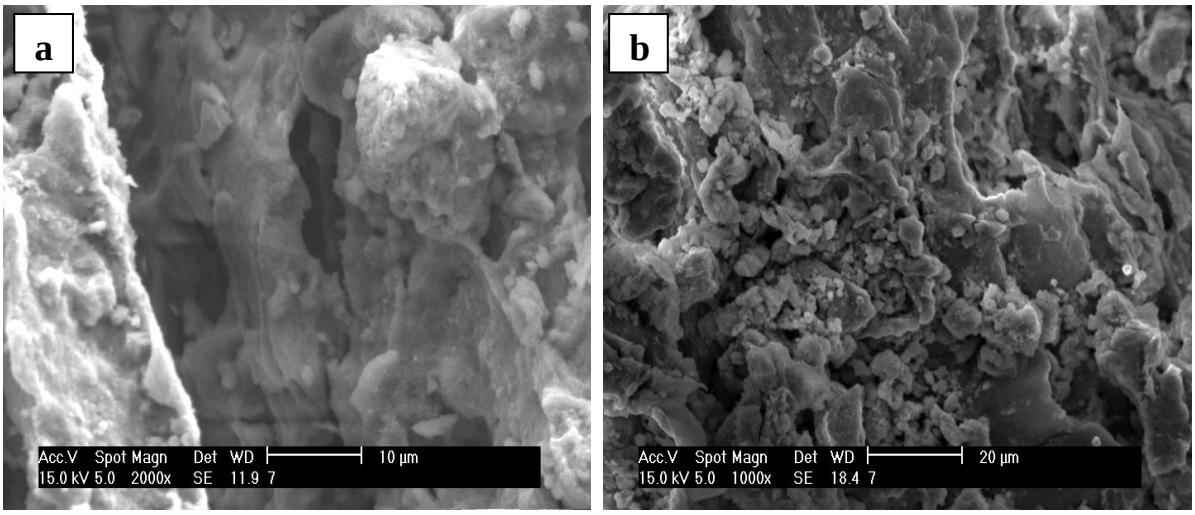

Fig.5.1. SEM image of SFAA (a) before and (b) after adsorption of As(V), F

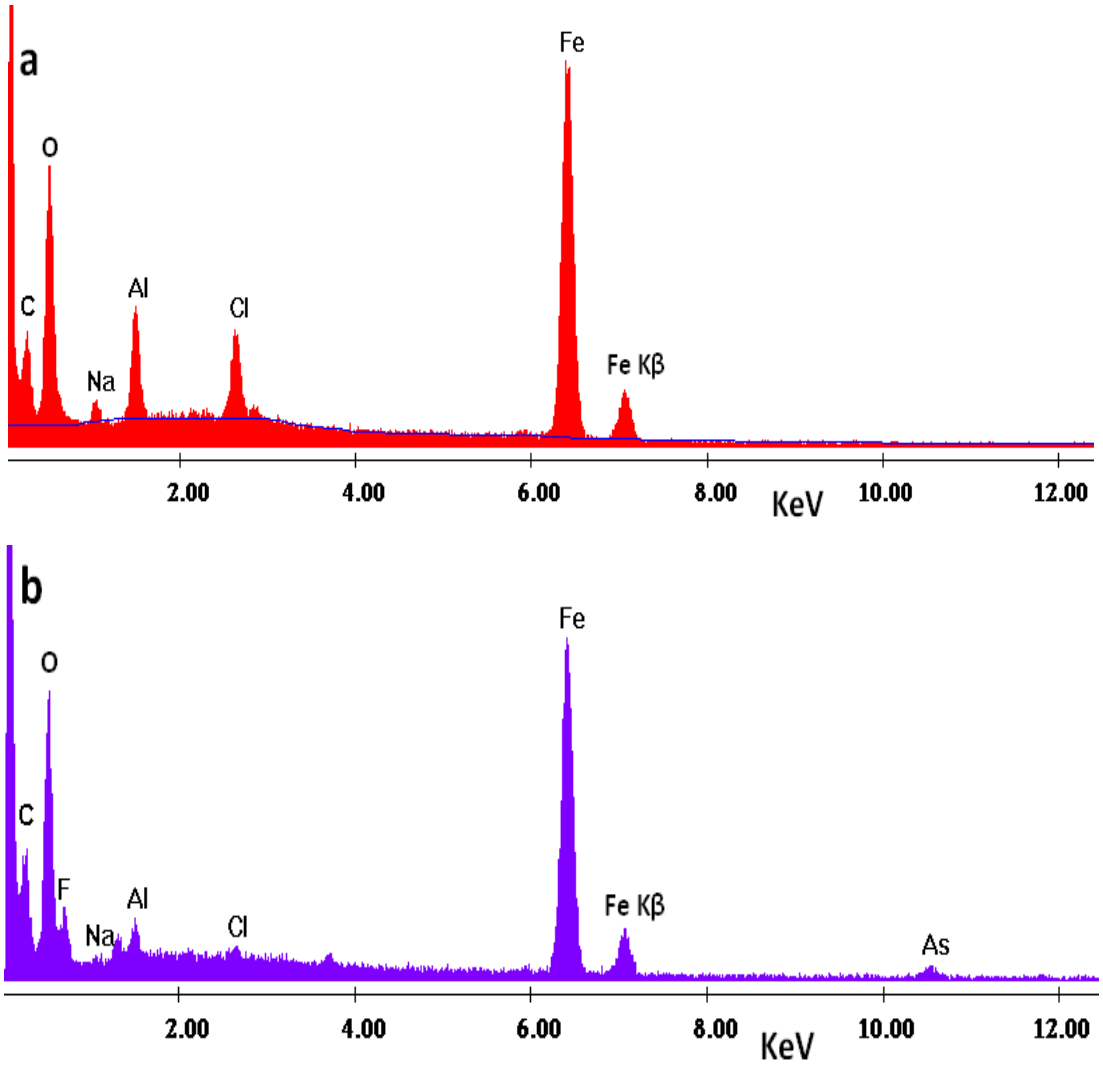

Fig.5.2. EDX spectra of SFAA (a) before and (b) after adsorption of As(V), F

5.1.2 X-ray Photoelectron Spectroscopy

The X-ray Photoelectron Spectroscopy (XPS) patterns of As 3p, O 1s, F 1s, Al 2s and Fe 2p levels were recorded at room temperature. The XPS survey scans of SFAA, arsenic with fluoride loaded specimens were shown in Fig. 5.3. Selected area scans were performed for As 3d, As 3p, C 1s, O 1s and Fe 2p along with the auger lines of arsenic, oxygen and Fe as marked in Fig.5.3. Iron and Aluminium oxide are present on the SFAA surface which was confirmed by the corresponding peaks. Fe $2p_1$, $2p_3$ peaks have been obtained at 710.8, 724.8 eV, similarly Al 2s peak at 117.9 eV. The C1s peak position of 285.0 eV for the adventitious carbon was used to calibrate the recorded spectra. In addition, there is broad peak starting from 265 with a peak centre at 269 eV is characteristic of the auger line of As. This is confirmed by the reduction in

intensity of the auger peak of As in simultaneously loaded arsenic specimen as observed in Fig.5.4(c). This confirms the presence of As in the specimens as it is absent for only SFAA specimen as seen in Fig.5.3.

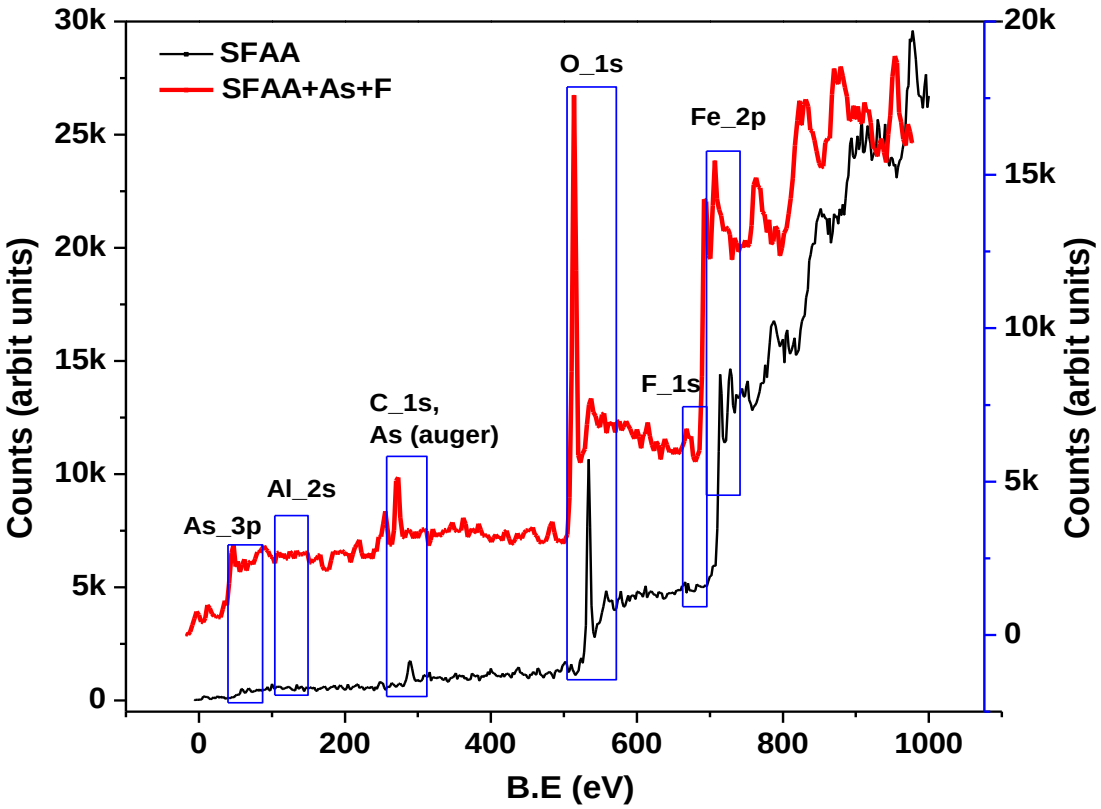

Fig.5.3. XPS spectra of SFAA before and after adsorption of As(V) and F

To confirm the presence of arsenic, the region for As 2p is scanned and patterns were recorded for the arsenic loaded specimens and shown in Fig.5.4(c). The graph can be fitted with Gaussian functions marking $3p_{3/2}$ and $3p_{1/2}$ components of As and the analysis of peak position shows that As in +5 valence state. This again confirms that As is trapped in the matrix and that the oxidation state of As is +5. Finally, Fe 2p patterns were recorded to investigate the oxidation state of Fe under the influence of arsenic or fluoride ions. Fig.5.4(b) shows the Fe 2p patterns of fluoride and arsenic loaded specimens. Fe $2p_{3/2}$, Fe $2p_{1/2}$ and their respective satellites are seen from the graph for both the specimens. In addition, an additional satellite at 736 eV appears for both the specimens. The positions of the peaks and the satellite at 736 eV confirm that Fe is present in +3 valence state and does not undergo any change. It is clear that Fe in a single valence state. The patterns are similar for both the specimens indicating neither fluoride nor arsenic change the

valence state of Fe. Simultaneously selected area was scanned for F 1s and As 2p region for the adsorbed arsenic and fluoride present in the sorbent which were recorded for the arsenic and fluoride loaded specimens. F peak was observed near 685 eV of binding energy and arsenic peak was observed at 146.2 eV.

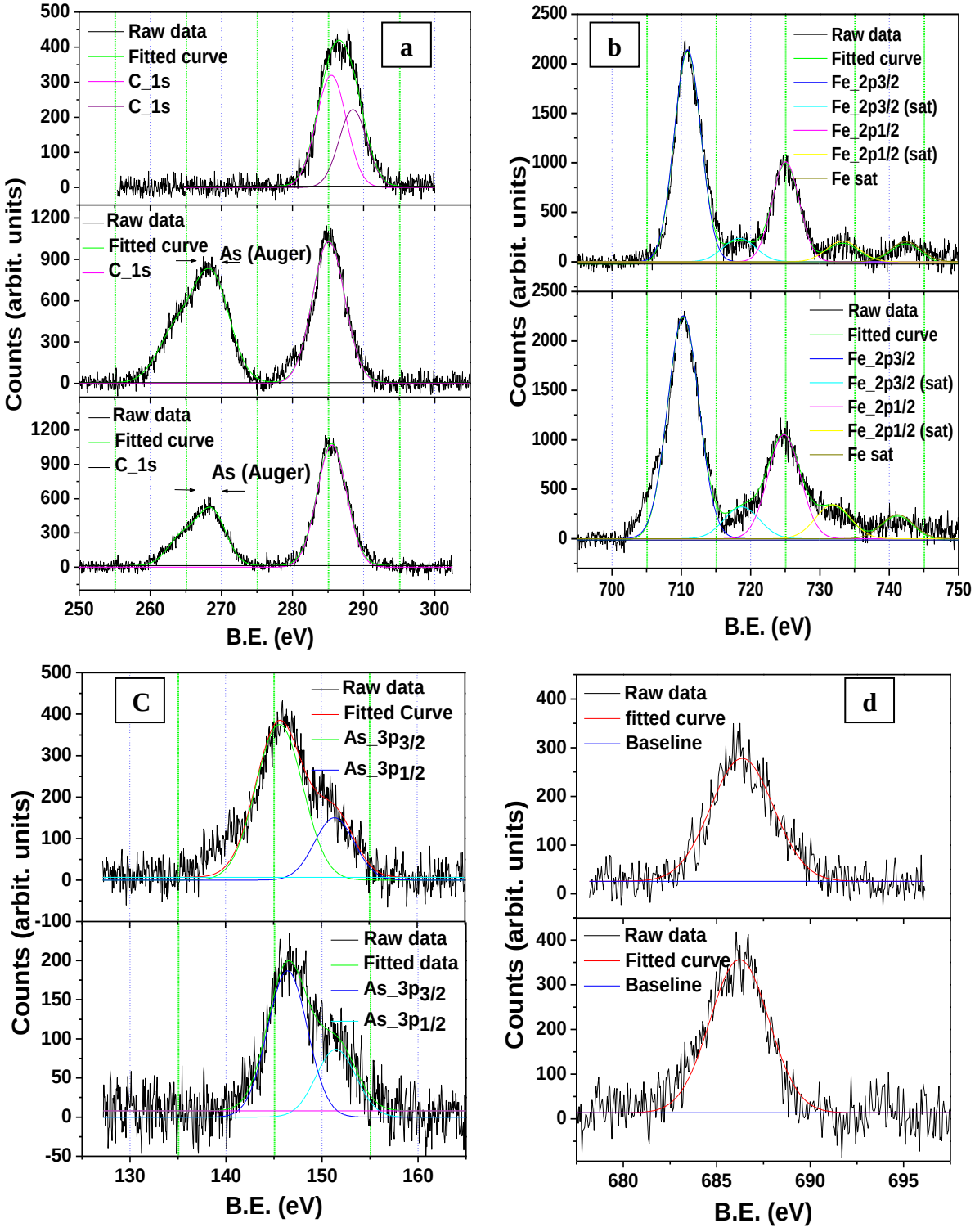

Fig.5.4. XPS spectra of (a) C 1s, As (Auger), (b) Fe 2p, (c) As 3p, (d) F 1s

5.2 BATCH STUDIES

5.2.1 Effect of pH

The effect of pH on removal of arsenic and fluoride by SFAA was studied using 0.10 g of adsorbent in 10mL of 25 mg/L arsenate and fluoride solutions. The pH of the solution was adjusted by adding dilute NaOH or HNO_3 drop wise to obtain pH of 1.0 through 12.0. The percentage removal of As(V) and F from solutions of different pH is shown in Fig. 5.5.

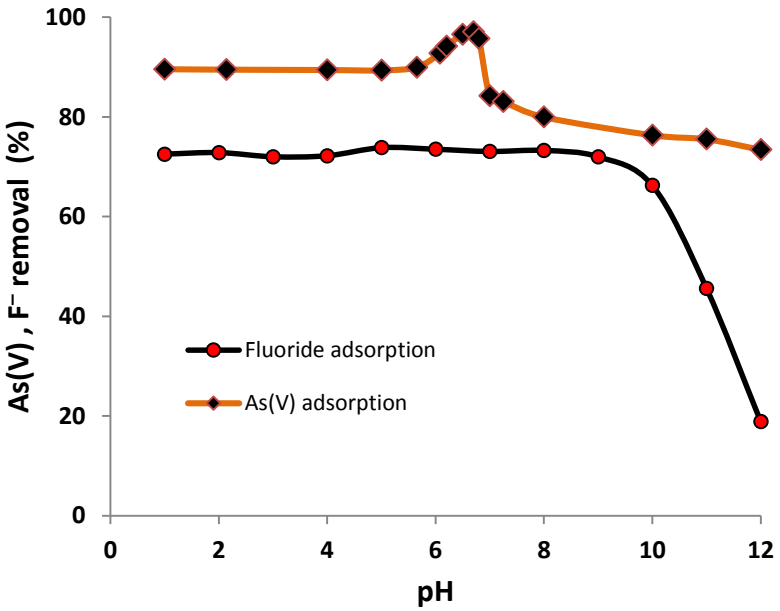

Fig.5.5. Effect of pH (C_{As} = 2 mg/L, C_F = 20 mg/L, time = 4h, Temp = 303K)

5.2.2 Effect of contact time

The effect of contact time for As(V) and F adsorption on SFAA was studied with adsorbent dose of 0.1 g per 10 mL solution. The As(V) and F adsorption capacity of the SFAA with time is shown in Fig. 5.6. As can be seen, within 10 min SFAA reaches equilibrium in As(V) adsorption but for F it takes more time (> 50 min) to reach equilibrium. The adsorption capacity increased from 0.59 to 0.70 mg/g with increasing the contact time. Different kinetic models like pseudo-first order, pseudo-second order and intra-particle diffusion adsorption kinetic models were tested by various researchers to find the mechanisms of the adsorption and rate controlling steps [272, 273]. Based on Pseudo first order Lagergren model linear form given in equation 3.7 the plot of $log(q_e - q_t)$ versus t has drawn as shown in Fig.5.7 should give a linear relation, from which K_1 and q_e can be determined from the slope and intercept, respectively.

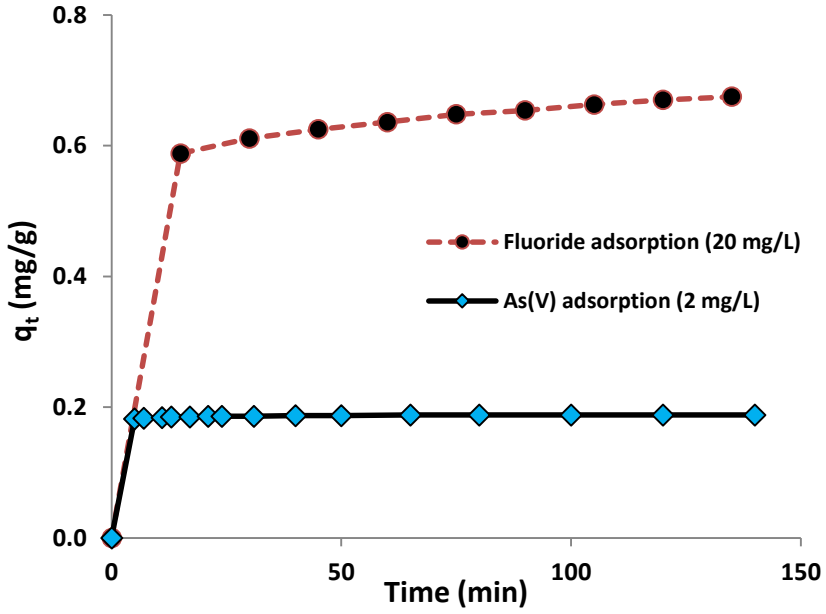

Fig.5.6. Effect of contact time
(C_{As} = 2 mg/L, C_F = 20 mg/L, pH = 6.5, time = 3h, Temp = 303 K)

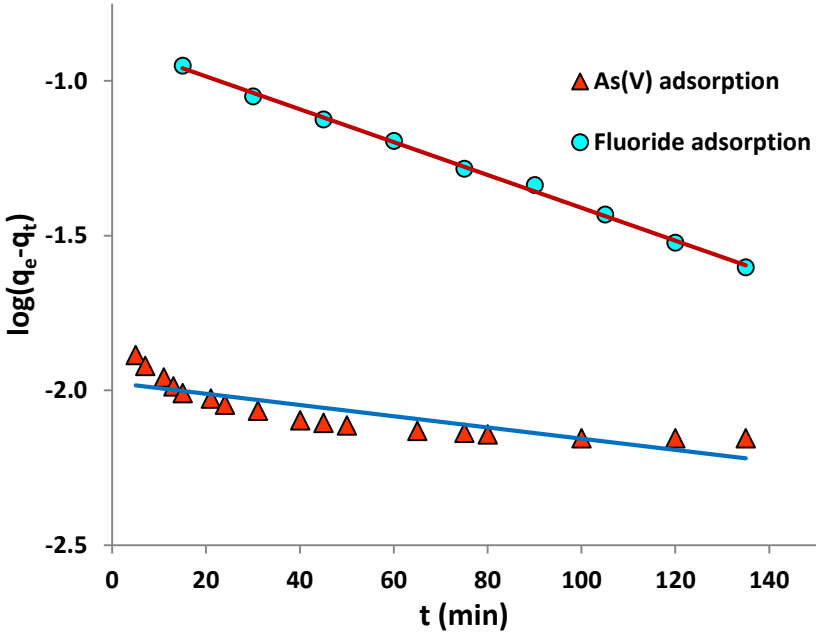

Fig.5.7. Pseudo first order sorption kinetics of As(V) and F on SFAA

Based on equation 3.9 a plot t/q_t versus t has drawn. From the slope and intercept of the straight line obtained from the Fig. 5.8, the values of q_e and K_2 are calculated and presented in Table 5.1. The intra particle diffusion model [275] is applied to describe competitive arsenic and fluoride adsorption by SFAA. This intra particle diffusion occurs in macro, meso and micropores present within the adsorbent SFAA. Based on equation 3.10 the plot of q_t against $t^{0.5}$ gives the adsorption may be due to pore diffusion or film diffusion or combination of both (Fig. 5.9).

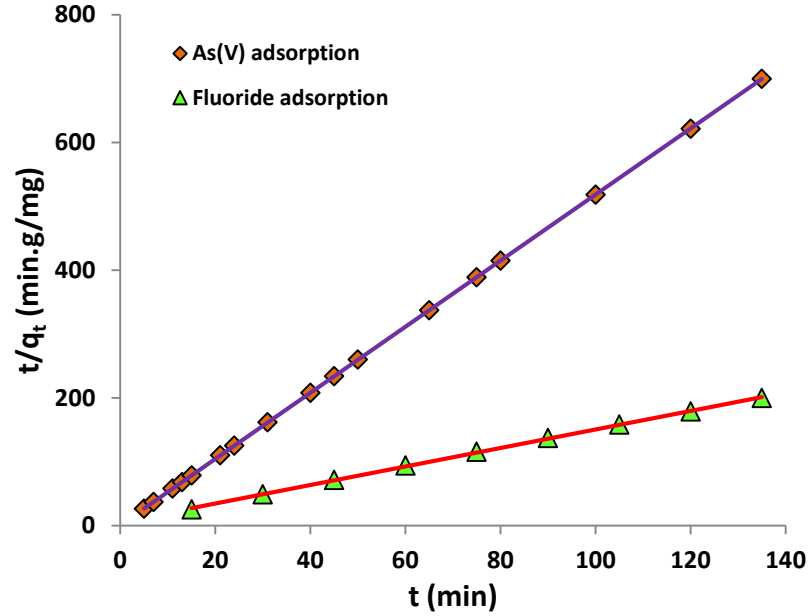

Fig.5.8. Pseudo second order sorption kinetics of As(V) and F on SFAA

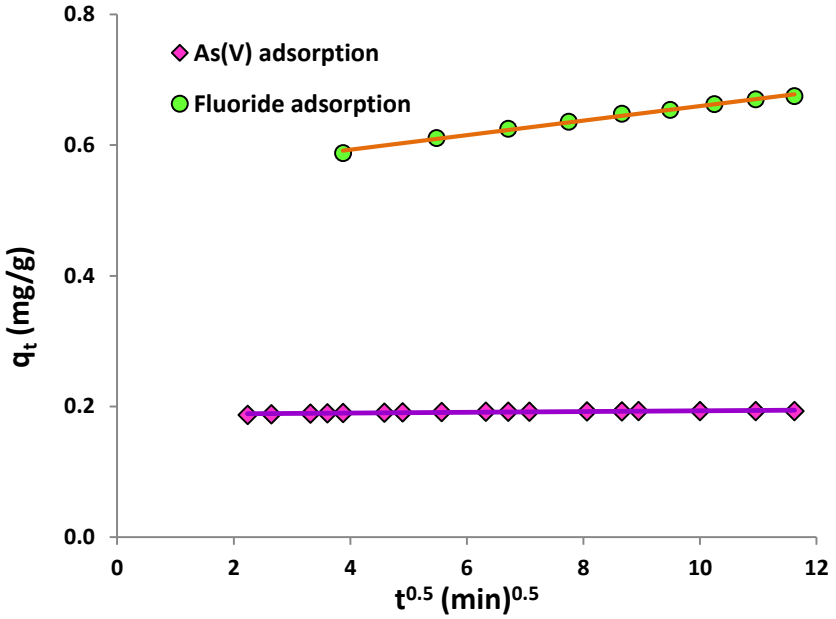

Fig.5.9. Intra particle diffusion model for As(V) and F adsorption on SFAA

Table 5.1 Kinetic model parameters

Experimental		Pseudo first order			Pseudo Second order			Intraparticle diffusion	
C_O	q_{exp}	q_{e1}	K_1	R^2	q_{e2}	K_2	R^2	K_{id}	R^2
2	0.195	0.139	0.004	0. 724	0.193	19.88	1.000	0.0006	0.819
20	0.700	0.415	0.012	0.997	0.690	0.979	0.999	0.0111	0.994

C_O – initial concentration (mg/L); q_e – Equilibrium uptake (mg/g); K_{id} – intra particle diffusion model constant (mg/g.min$^{0.5}$); K_s – External mass transfer constant (min^{-1}); D_i – Diffusion coefficient (cm^2/s)

5.2.3 Effect of initial concentration

Initial concentration of fluoride was varied from 5 to 50 mg/L with constant arsenic concentration of 1.0 mg/L. The solution was added with 0.1 g of SFAA in 15 mL sample vials and was agitated at 40 rpm in a thermostatically controlled orbital shaker. The temperature for the equilibrium was maintained at 303K. Results obtained from the experiment were plotted as shown in Fig.5.10.

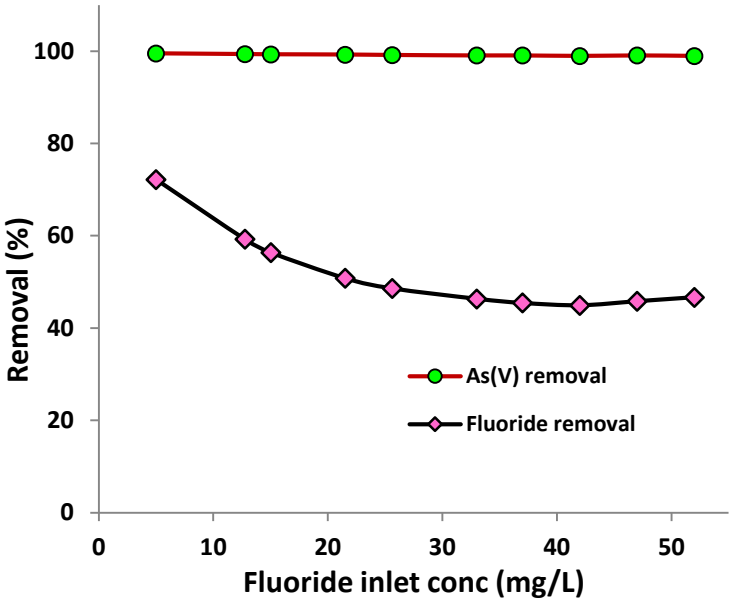

Fig.5.10. Effect of initial concentration on % removal of fluoride (C_{As} = 1 mg/L, C_F = 5-50 mg/L, Contact time = 4h, Temp = 303K)

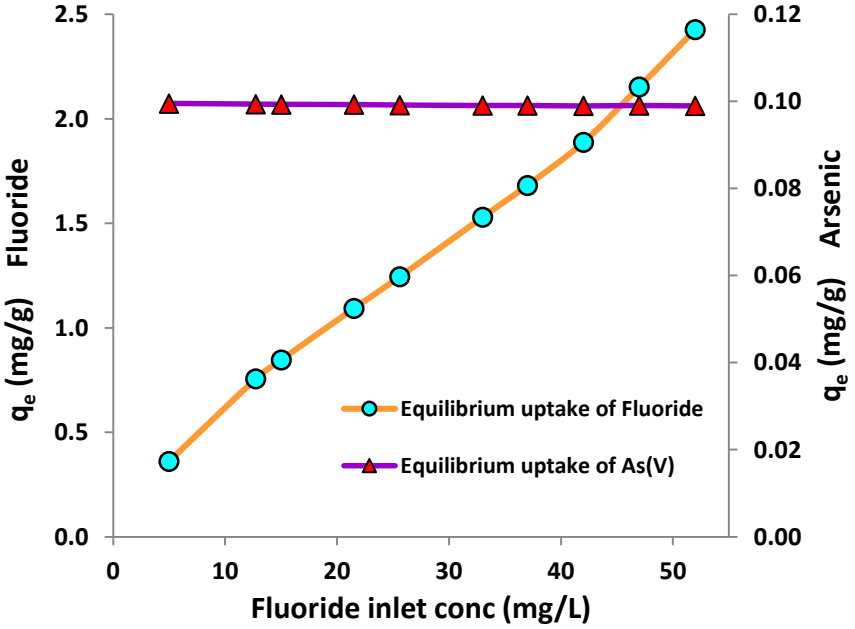

Fig.5.11. Effect of initial concentration on equilibrium uptake of fluoride (C_{As} = 2 mg/L, C_F = 5-50 mg/L, Contact time = 4h, Temp = 303K)

It is seen that adsorption of arsenic was constant, but the fluoride adsorption varies with initial concentration. Equilibrium uptake of arsenic was not affected by the presence of fluoride and hence the arsenic equilibrium uptake and removal percentage remains constant. From the results it is deduced that arsenic was strongly adsorbed by SFAA without interference by the presence of fluoride.

Similarly the initial concentration of arsenic was varied from 0.1 to 2 mg/L, keeping fluoride concentration of 20 mg/L solution. Results from the adsorption experiments were plotted in Fig.5.12 and 5.13. It can be seen that adsorption of arsenic is constant, but the fluoride adsorption decreases with increase in arsenic initial concentration. Equilibrium uptake of fluoride is affected by the presence of arsenic and hence the fluoride uptake and removal percentage decreases with increase in arsenic initial concentration. Thus fluoride adsorption by SFAA is strongly affected by the presence of arsenic. SFAA preferentially adsorbs arsenic. Hence the increase in concentration of arsenic which occupies the active sites of SFAA and makes it to disturb the fluoride adsorption.

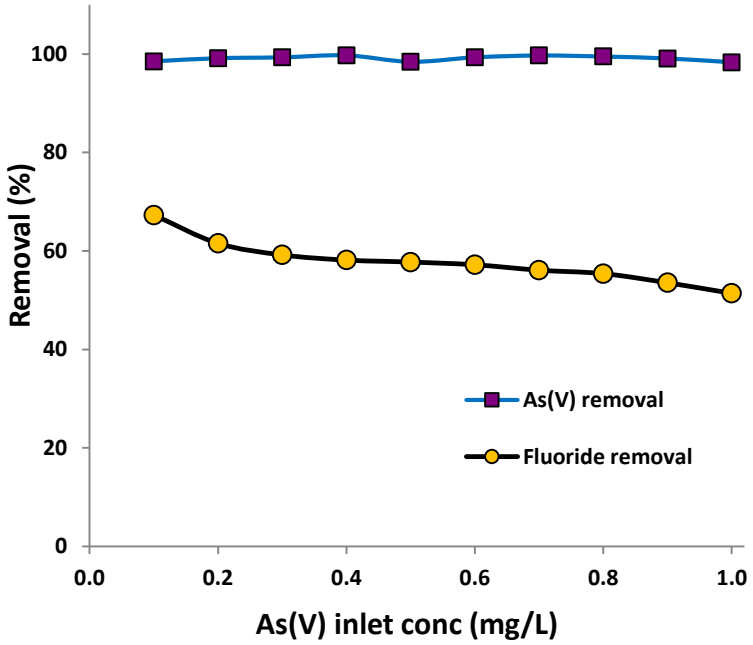

Fig.5.12. Effect of initial concentration on % removal of As(V)
(C_{As}= 0.1-1 mg/L, C_F= 10 mg/L, Contact time = 4h, Temp = 303K)

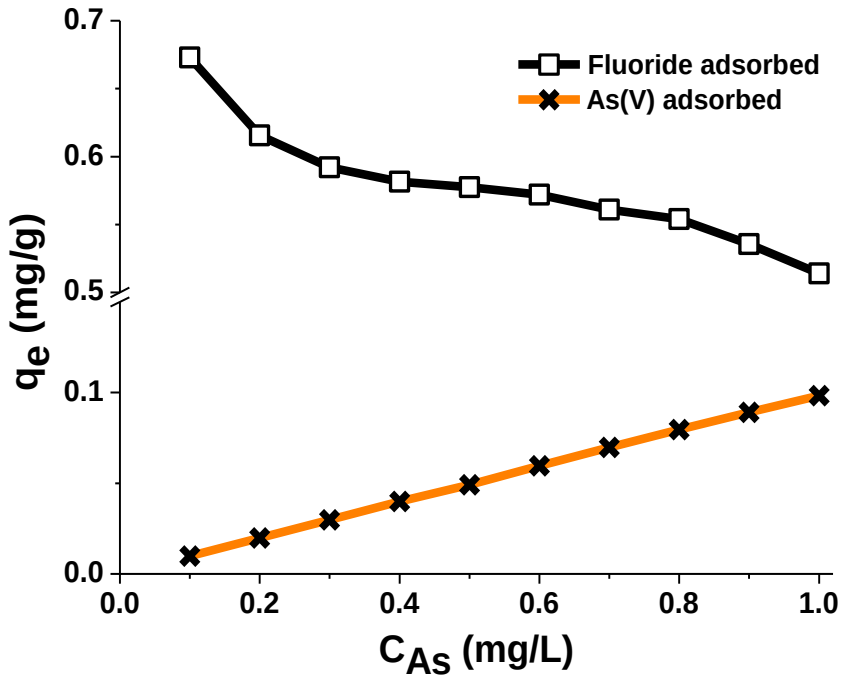

Fig.5.13. Effect of initial concentration on equilibrium uptake of As(V)
(C_{As} = 0.1-2 mg/L, C_F = 20 mg/L, Contact time = 4h, Temp = 303K)

5.2.4 Adsorption isotherms

Inorder to find out the adsorption mechanism Langmuir and Freundlich isotherms were used to model the adsorption. Based on sorption on a heterogeneous surface an isotherm Freundlich is expressed in the equation 3.4. For monolayer adsorption Langmuir isotherm used, which is studied in equation 3.5.

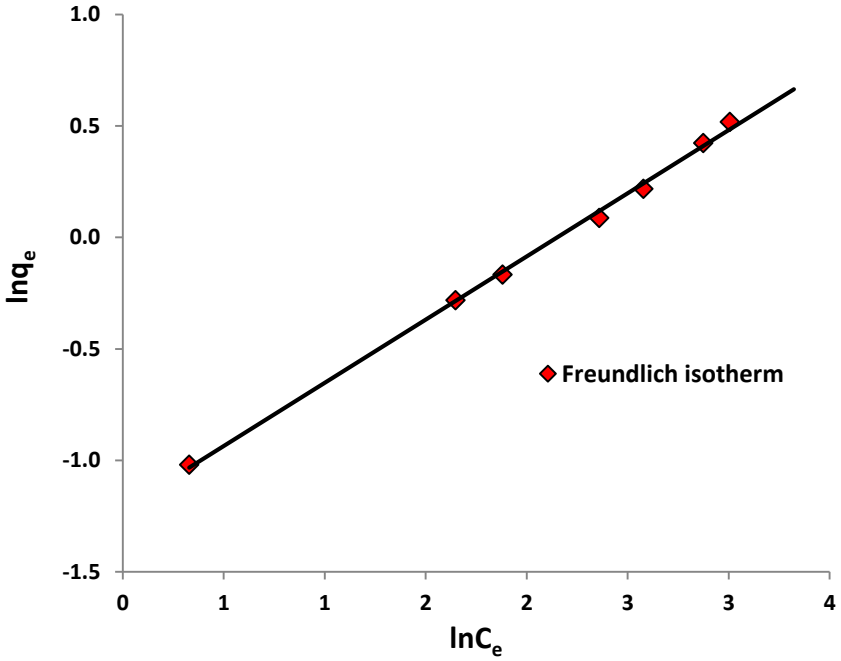

Fig.5.14. Freundlich isotherm for fluoride adsorption

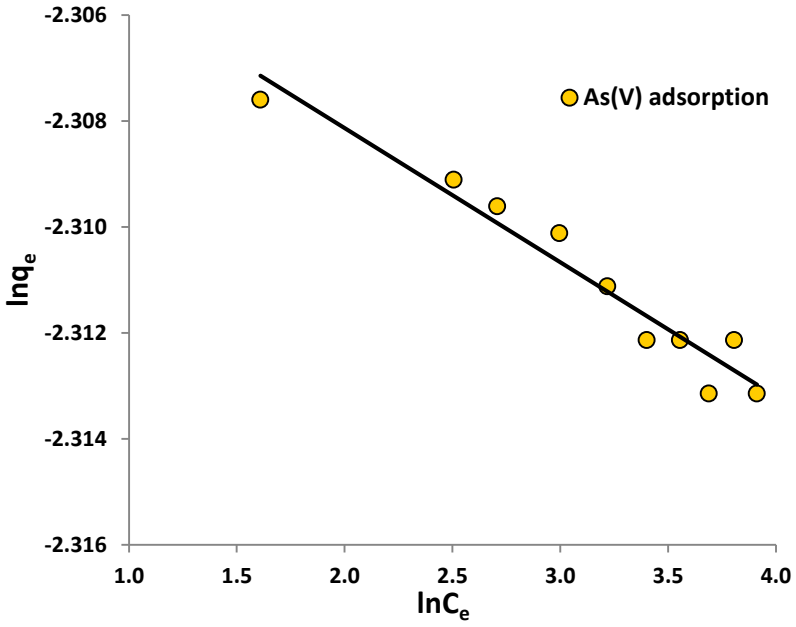

Fig.5.15. Freundlich isotherm for As(V) adsorption

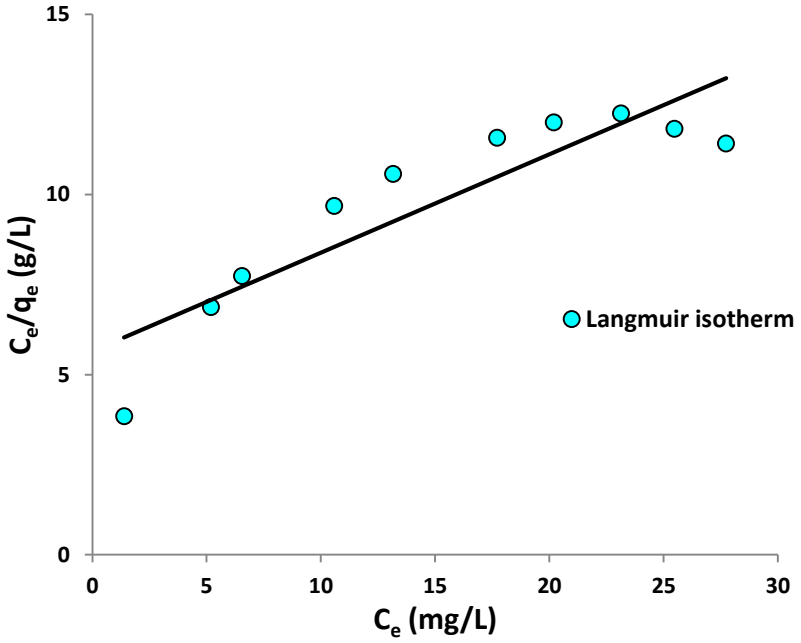

Fig.5.16. Langmuir isotherm for fluoride adsorption

Table 5.2 Langmuir and Freundlich isotherm model parameters (From Fig.5.14 to 5.17)

	Langmuir Isotherm			**Freundlich Isotherm**				q_{exp} (mg/g)
	K_L (L/mg)	q_{max} (mg/g)	R^2	K_F ($mg.g^{-1}(Lmg^{-1})^{1/n}$)	1/n	q_{max} (mg/g)	R^2	
As(V)	-208.6	0.0001	0.899	0.100	-0.002	0.101	0.941	0.100
F	0.0608	3.659	0.802	0.295	0.6065	2.017	0.998	2.427

K_L, K_F – Langmuir, Freundlich constant, q_{max} q_{exp} – Maximum, experimental equilibrium uptake, n – Adsorption intensity, R^2– Regression coefficient

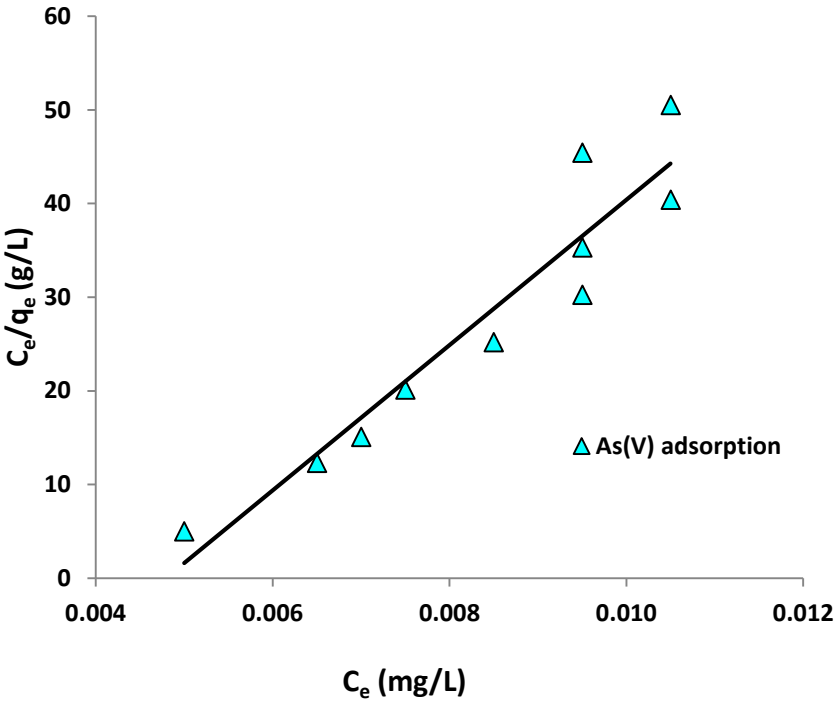

Fig.5.17. Langmuir isotherm for As(V) adsorption

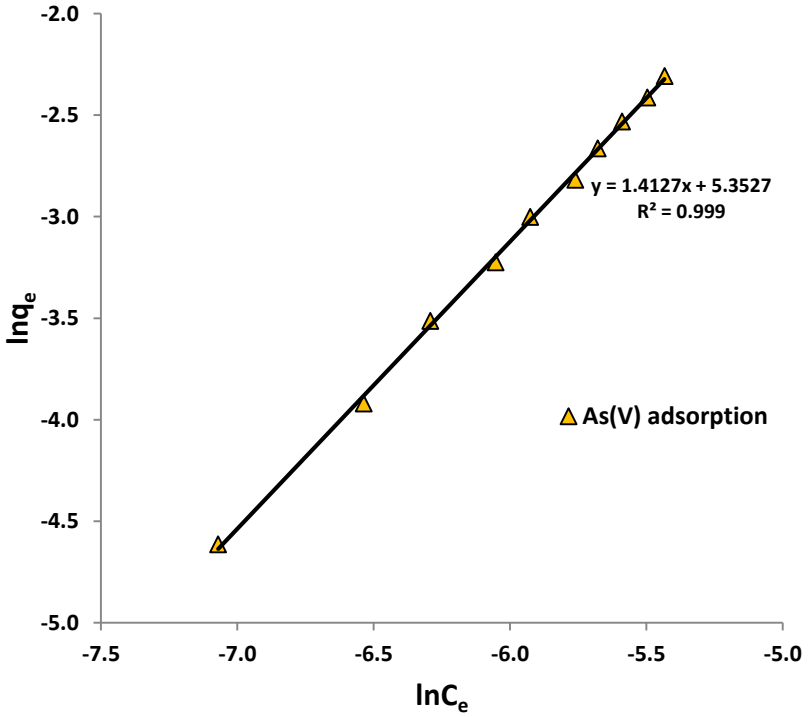

Fig.5.18. Freundlich isotherm for As(V) adsorption

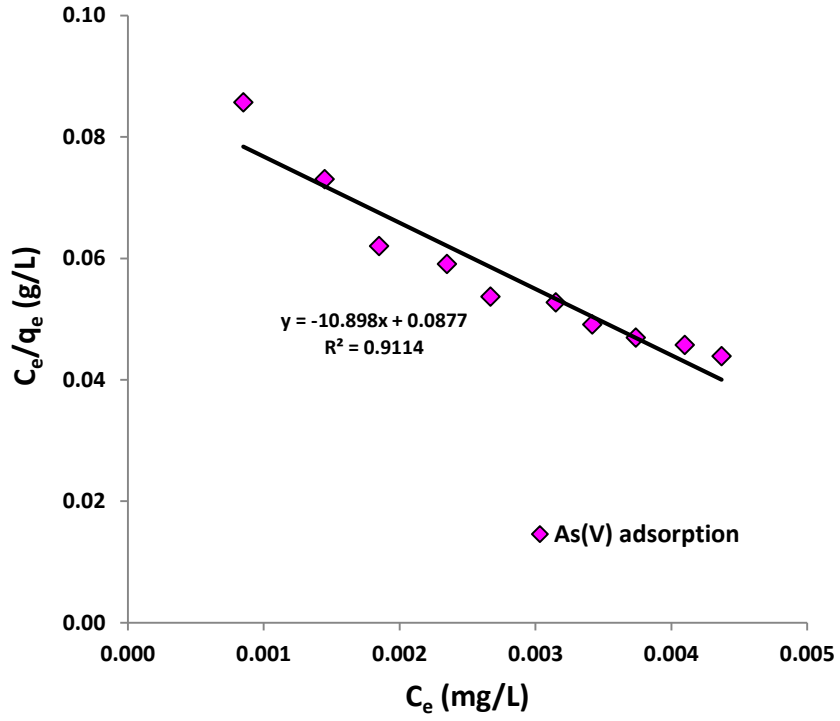

Fig.5.19. Langmuir isotherm for As(V) adsorption

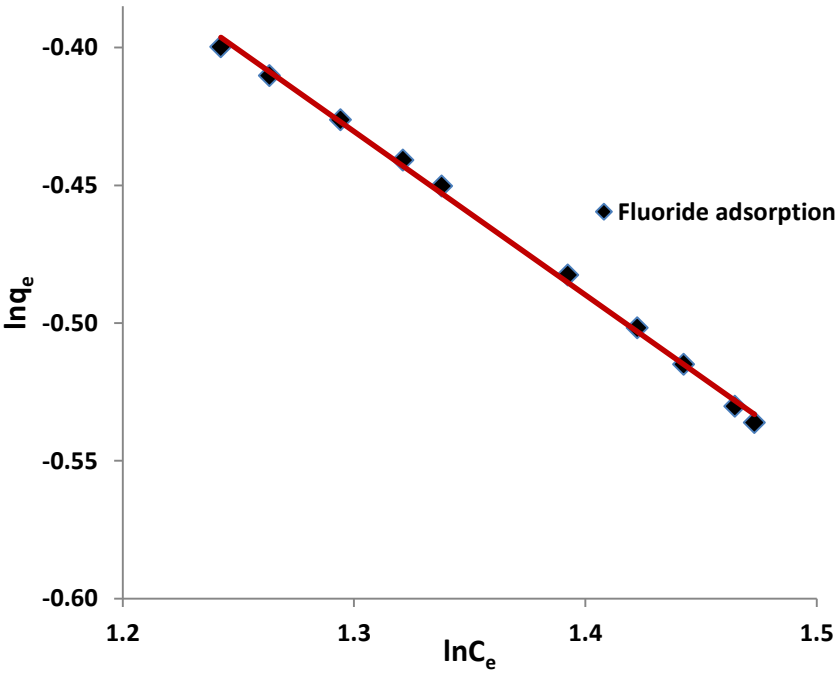

Fig.5.20. Freundlich isotherm for fluoride adsorption

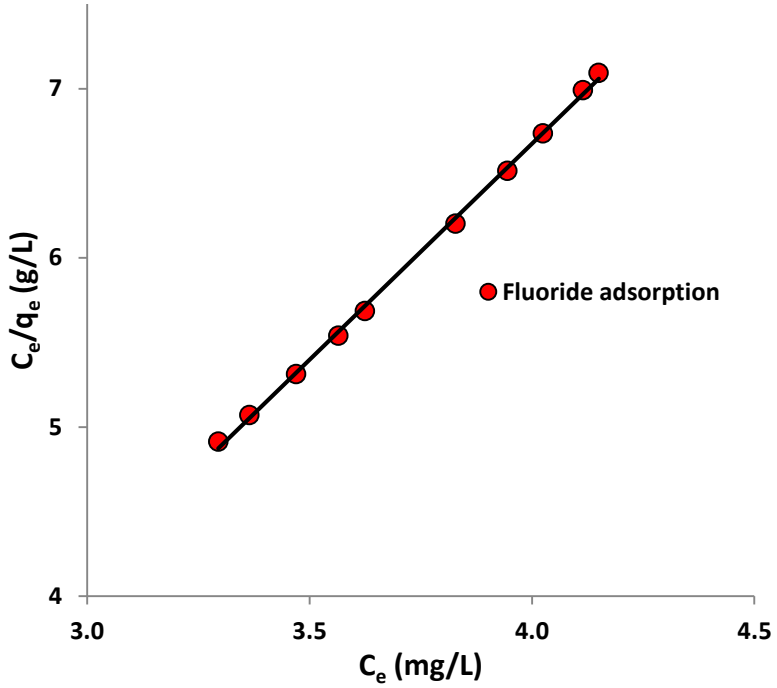

Fig.5.21. Langmuir isotherm for fluoride adsorption

Table 5.3 Langmuir and Freundlich isotherm model parameters (From Fig.5.18 to 5.21)

Adsorbate	Langmuir Isotherm			Freundlich Isotherm				q_{exp} (mg/g)
	K_L (L/mg)	q_{max} (mg/g)	R^2	K_F (mg/g)(L/mg)$^{1/n}$	1/n	q_{max} (mg/g)	R^2	
As(V)	124.265	0.092	0.911	211.178	0.546	0.098	0.999	0.100
F	-0.720	0.392	0.990	1.366	-0.594	0.676	0.999	0.673

K_L, K_F – Langmuir, Freundlich constant, q_{max} q_{exp} – Maximum, experimental equilibrium uptake, n – Adsorption intensity, R^2– Regression coefficient

5.3 COLUMN STUDIES

5.3.1 Colum studies for removal of arsenic and fluoride

Arsenic and fluoride bearing water was passed through the bed of SFAA by the use of peristaltic pump at desired flow rate and treated water was collected in the bottom of the column and periodical analysis was done for both arsenic and fluoride. The treated water meets the criteria for arsenic and fluoride in the drinking water range, given by Bureau of Indian Standard (BIS) and WHO, hence the treated water is potable.

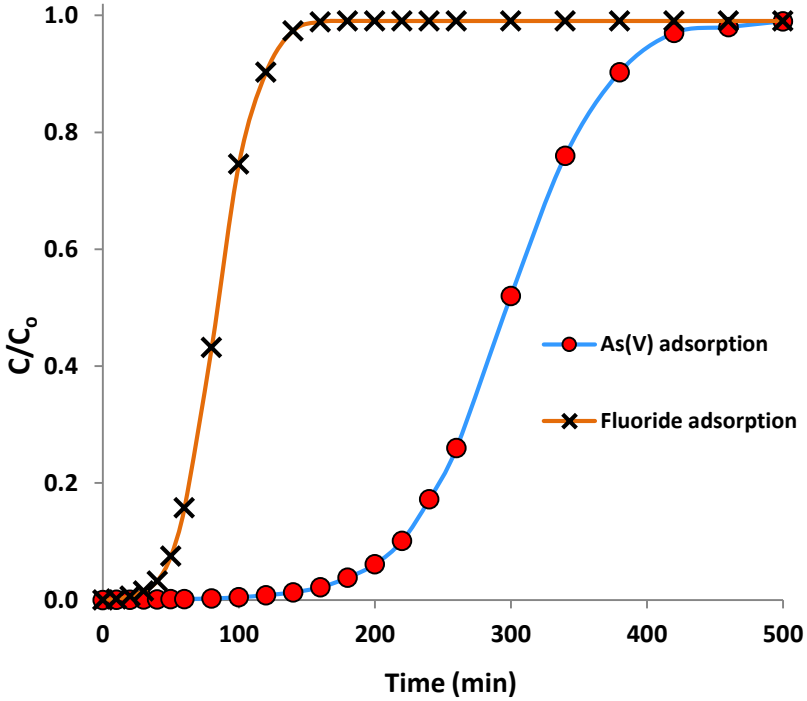

Fig.5.22. Fixed bed adsorption breakthrough of As(V) and fluoride

5.3.2 Application of models for different adsorbates

The experimental data is tested with four different models, Thomas, Yoon-Nelson, Bohart-Adam and Clark model. The models are tested for prediction of experimental breakthrough curves for different adsorbate (arsenic, fluoride) and presented in Fig.5.23 and Table 5.4. The experimental, model rate constants and maximum equilibrium uptake (q_e) are calculated and listed in Table 5.4. Based on adsorption capacity (q) the % error has been calculated and tabulated in Table 5.4. The data could be predicted by three models, viz., Thomas model, Yoon-Nelson model and Clark model. From Table 5.4 Clark model predicts the experimental data well with R^2 close to 1 and % error of 0.7. This because of both arsenic and fluoride adsorption by SFAA follows Freundlich adsorption isotherm.

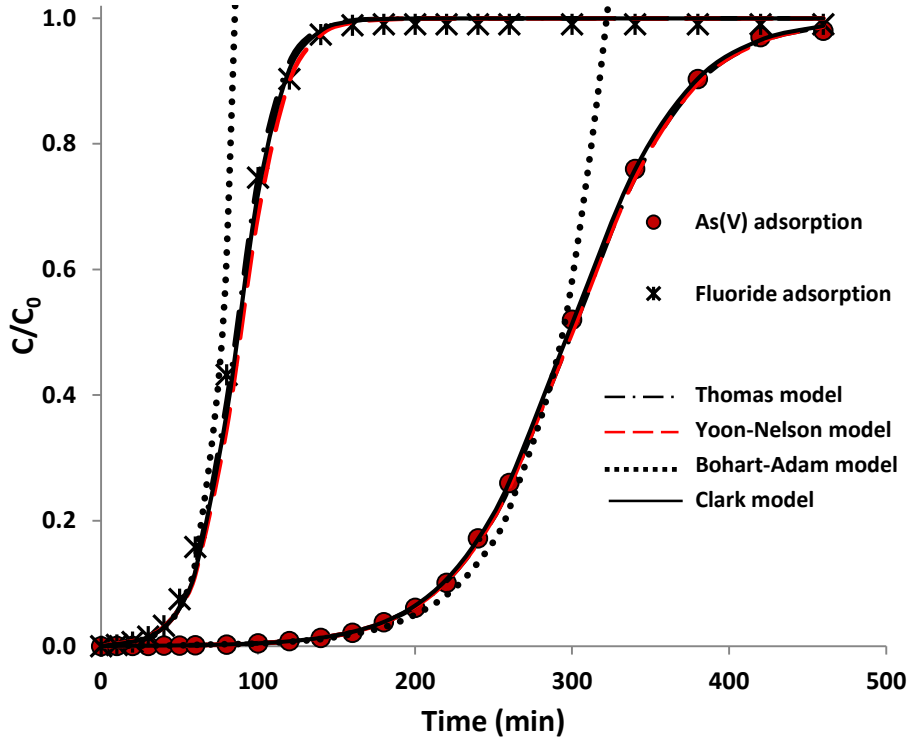

Fig.5.23. Application of models for As(V) and fluoride adsorption

Table 5.4 Model parameters for As(V) and fluoride adsorption

	q_{exp}	Thomas model				Yoon-Nelson model				
		k_{Th}	q_e	% Error	R^2	K_{YN}	τ	q_e	% Error	R^2
As	**0.272**	0.0294	0.276	1.51	0.998	0.0270	300.11	0.300	10.33	0.998
F	**0.924**	0.0072	0.904	2.21	0.991	0.0709	88.92	0.935	1.23	0.991
		Bohart-Adam model				**Clark model**				
	k_{BA}	N_0	q_e	% Error	R^2	K_C	N_0	q_e	% Error	R^2
As	0.0246	65.63	0.322	18.38	0.991	0.0297	55.89	0.274	0.73	0.999
F	0.0073	184.93	0.907	1.81	0.981	0.0070	187.00	0.918	0.70	0.998

k_{Th}, K_{BA}, K_C – Thomas, Bohart-Adam, Clark rate constants (L/mg.min), K_{YN} –Yoon-Nelson rate constant (min^{-1}), q_e – Equilibrium uptake (mg/g), τ – time required for 50% adsorbate breakthrough (min), *N_0 – Saturation concentration (mg/L).*

6 CONCLUSION

A novel adsorbent for removal of arsenic and fluoride from water was developed. Sawdust of *Artocarpus hirsutus*, called "Anjili" locally, showed the highest adsorption capacity for arsenic and fluoride from water and hence it was selected for preparation of the adsorbent. The adsorbent was synthesized by impregnating the sawdust with ferric hydroxide and activated alumina. Various combinations of impregnations ratios were tested and it was being seen that adsorbent of 1.5:1:1 ratio of sawdust, ferric hydroxide, activated alumina resulted in an effective removal of arsenic, fluoride from water. This adsorbent can be used very effectively for arsenic removal of groundwater to meet the drinking water standards laid down by World Health Organization (WHO) and Bureau of Indian Standard (BIS).

Adsorption capacity of SFAA for both arsenic and fluoride is considerably higher than many of the adsorbents reported in literature. Pore size distribution of SFAA concludes that it has an appropriate combination of micro, meso and macro pores in its structure, which is the reason for its effective removal of both pollutants. Because of this pore size distribution, the uptake of arsenic and fluoride by SFAA is higher than that of only activated alumina, which is traditionally used for fluoride removal. However, as activated alumina is less than 30% of this adsorbent, the present adsorbent is economical compared to activated alumina. It may be noted that about 43% by weight, of the adsorbent is 'Anjili tree' sawdust. Thus, SFAA proves to be cost effective in comparison to other adsorbents. Water treated by SFAA was analyzed for Fe and Al and was found to contain less than 0.1 mg/L, which is within the permissible limit for drinking water.

Maximum removal of As(V) and As(III) was observed in the pH range of 6.5-7 and hence water does not need pH adjustment prior to treatment by SFAA. Maximum adsorption capacity of SFAA is 54.32 mg/g for As(III) and 77.60 mg/g for As(V). The removal of As(V) increased from 27.33 to 98.64 percent with increase in the adsorbent dose from 1 to 10 g/L . An adsorbent dose

of 10 g/L and contact time of 5 minutes are found to be the optimum for arsenic removal from water having arsenic concentration upto 2 mg/L. From the batch equilibrium and kinetic studies, it was observed that As(V) adsorption by SFAA follows Freundlich isotherm and pseudo second order kinetics. Both removal percentage and adsorption capacities of the adsorbent decreased with increase in the particle size of the adsorbent. Presence of Phosphate and Sulphate decreases the adsorption of As(V) by SFAA.

Column studies show that the SFAA is effective for the removal of As(V) from ground water. Small particle size of adsorbent gave higher As(V) adsorption and low flow rate result in effective removal of As(V) due to availability of sufficient contact. Arsenic adsorption increases with increase in bed height of SFAA in a fixed bed adsorption. Thomas, Yoon-Nelson, Bohart-Adam and Clark models were tested with the experimental data for arsenic adsorption. Clark model shows a good fit for different adsorbents studied, viz., sawdust, activated alumina and SFAA. Clark model fits well for different particle sizes and flow rates studied. In addition to Clark model, Thomas, Yoon-Nelson models also show a good fit for different concentrations and different bed heights.

SFAA showed good adsorption capacities for fluoride under different conditions. Compared to the fluoride adsorption capacity of 8.6 mg/g for activated alumina, capacity for SFAA is 40.28 mg/g for batch adsorption from initial fluoride concentration of 1000 mg/L. Superiority of SFAA over activated alumina is due to the contribution of the saw dust in improving the macro and micro pores in the adsorbent. Adsorption capacity is unchanged over a wide range of pH, 1 to 9, making it useful for defluoridation of groundwater as well as industrial effluents. Adsorption of fluoride by SFAA follows Freundlich adsorption isotherm and follows pseudo second order kinetic model. Hydroxides, carbonates, bicarbonates, sodium and potassium decrease the adsorption. Groundwater sample collected from Avarangattur was tested with SFAA and effective defluoridation was observed. .

Column studies confirm that the SFAA is effective for the removal of fluoride from water Breakthrough adsorption capacity of SFAA is 1.21 mg/g, which is 4 times higher than that of activated alumina employed in the study. Small particle size, optimum flow rate and high initial concentration result in higher fluoride adsorption. Higher flow rates result in earlier breakthrough due to insufficient contact time. Decrease in particle size enhances the adsorption capacity (q_t) due to higher available interfacial surface area and shorter intraparticle diffusion paths. The adsorption capacity (q_t) increases with increase in feed concentration, due to increase in driving force for mass transfer, which enhances the adsorption rate and faster consumption of active sites. Adsorption fluoride by SFAA also fits well to Clark model for various operating conditions studied. The other adsorbents studied, activated alumina and SFAA also follow Clark model. The interaction of operating parameters such as initial concentration, flow rate and adsorbent particle size with the mass transfer zone were studied and explained for both arsenic and fluoride adsorption.

Adsorption of both arsenic and fluoride from water by SFAA shows that SFAA can remove both pollutants together effectively to meet the BIS and WHO standards.

Scope for future studies

Removal of toxic heavy metals such as lead, chromium and cadmium from groundwater by adsorption using SFAA can be studied. Arsenic containing groundwater samples from different places can be tested with SFAA for finalizing a process flow sheet. Arsenic and fluoride containing groundwater samples from various locations will be tested with SFAA and effectiveness of SFAA compared with other adsorbents. Improvement of column properties of SFAA, by suitable granulation may be investigated, along with desorption of the column with various chemicals. Efficacy of SFAA in industrial waste water treatment may be explored.

References

1. P.H. Gleick, "Water in crisis: a guide to the world's fresh water resources", Oxford University Press, Inc., 1993.
2. R. Enderlein, "Protection and sustainable use of waters: agricultural policy requirements in Europe", *HRVAT VODE*, 4 (1996) 69-76.
3. J. Fawell, M.J. Nieuwenhuijsen, "Contaminants in drinking water Environmental pollution and health", *British Medical Bulletin*, 68 (2003) 199-208.
4. "Indian Standard Drinking water-Speciation", *Bureau of Indian Standards*, (2012) 1-18.
5. "2011 Edition of the Drinking Water Standards and Health Advisories", *United States Enivironmental Protection Agency*, (2011) 1-18.
6. "WHO, Guidelines for drinking-water quality", *World Health Organization*, Geneva, Switzerland (2011).
7. B.K. Mandal, K.T. Suzuki, "Arsenic round the world: a review", *Talanta*, 58 (2002) 201-235.
8. A.H. Welch, K.G. Stollenwerk, "Arsenic in ground water: Geochemistry and occurrence", *Kluwer Academic Publishers*, Boston, (2003) 9-10.
9. P. Ravenscroft, J. McArthur, B. Hoque, "Geochemical and palaeohydrological controls on pollution of groundwater by arsenic", *Arsenic Exposure and Health Effects IV*, (2001) 53-77.
10. K. Fields, A.S.C. Chen, L. Wang, T.J. Sorg, O.H. Columbus, "Arsenic removal from drinking water by iron removal plants", National Risk Management Research Laboratory, Office of Research and Development, *United States Environmental Protection Agency*, 2000.
11. W.J. Liu, Y.G. Zhu, F.A. Smith, S.E. Smith, "Do iron plaque and genotypes affect arsenate uptake and translocation by rice seedlings (Oryza sativa L.) grown in solution culture?", *Journal of Experimental Botany*, 55 (2004) 1707-1713.
12. P.L. Smedley, D.G. Kinniburgh, "Source and behaviour of arsenic in natural waters, United Nations synthesis report on arsenic in drinking water", *World Health Organization*, Geneva, Switzerland (2001) 1-61.
13. P. Smedley, J. Knudsen, D. Maiga, "Arsenic in groundwater from mineralised Proterozoic basement rocks of Burkina Faso", *Applied Geochemistry*, 22 (2007) 1074-1092.

14. UNICEF, “Arsenic mitigation in Bangladesh”, Report by UNICEF, New York, (2008) 1- 4.
15. K. Lizama A, T.D. Fletcher, G. Sun, “Removal processes for arsenic in constructed wetlands”, *Chemosphere*, 84 (2011) 1032-1043.
16. M. Bissen, F.H. Frimmel, “Arsenic–a review. Part II: oxidation of arsenic and its removal in water treatment”, *Acta Hydrochimica Et Hydrobiologica*, 31 (2003) 97-107.
17. A. Holloway, S.E. Taylor, M. Dubikova, S.L. Simpson, Woodroffe, “Natural attenuation of arsenic by ferric hydroxide in a coastal aquifer”, *Securing Gorundwater Quality in Urban and Industrial Environments*, (2007) 1-8.
18. M. Nair, T. Joseph, K. Balachandran, K. Nair, J. Paimpillil, “Arsenic Enrichment in Estuarine Sediments–Impact of Iron and Manganese Mining”, *Fate of Arsenic in the Environment*, (2003) 57-67.
19. “Arsenic mitigation for safe groundwater”, in, Executive Board, WHO, (2006) 1-5.
20. I. Abe, S. Iwasaki, T. Tokimoto, N. Kawasaki, T. Nakamura, S. Tanada, “Adsorption of fluoride ions onto carbonaceous materials”, *Journal of Colloid and Interface Science*, 275 (2004) 35-39.
21. D. Banks, C. Reimann, O. Røyset, H. Skarphagen, O.M. Sæther, “Natural concentrations of major and trace elements in some Norwegian bedrock groundwaters”, *Applied Geochemistry*, 10 (1995) 1-16.
22. W.M. Edmunds, P.L. Smedley, “Fluoride in natural waters”, *Essentials of Medical Geology*, *Springer*, 13 (2013) 311-336.
23. W. Apambire, D. Boyle, F. Michel, “Geochemistry, genesis, and health implications of fluoriferous groundwaters in the upper regions of Ghana”, *Environmental Geology*, 33 (1997) 13-24.
24. “Arsenic”, WHO Regional Office for Europe, *Air Quality Guidelines Seond Edition*, Chapter 6.1, Copenhagen, Denmark (2000) 1-14.
25. N. Reddy, K. Prasad, “Pyroclastic fluoride in ground waters in some parts of Tadpatri Taluk, Anantapur district, Andhra Pradesh”, *Indian Journal of Environmental Health*, 45 (2003) 285-288.
26. WHO, others, “Fluoride in drinking-water: Background document for development of WHO Guidelines for Drinking-water Quality”, (2004) 1-2.

27. S. Ayoob, A.K. Gupta, “Fluoride in drinking water: a review on the status and stress effects”, *Critical Reviews in Environmental Science and Technology*, 36 (2006) 433-487.
28. W.G. IARC, "Arsenic and Arsenic compounds”, in, IARC,Working Group, (2004) 41-93.
29. S. Kapaj, H. Peterson, K. Liber, P. Bhattacharya, “Human Health Effects From Chronic Arsenic Poisoning–A Review”, *Journal of Environmental Science and Health- Part A*, 41 (2006) 2399-2428.
30. A. Aitio, G. Becking, “Arsenic and arsenic compounds”, *Environmental Health Criteria, No. 224 - Second Edition*, World Health Organization Geneva (2001) 6-7.
31. E. Lomaquahu, A. Smith, “Feasibility of new epidemiology studies on arsenic exposures at low levels”, *AWWA Inorganic Contaminants Workshop, San Antonio*, TX, (1998) 23-24.
32. L.M. Del Razo, G.G. García-Vargas, O.L. Valenzuela, E.H. Castellanos, L.C. Sánchez-Peña, J.M. Currier, Z. Drobná, D. Loomis, M. Stỳblo, “Exposure to arsenic in drinking water is associated with increased prevalence of diabetes: a cross-sectional study in the Zimapan and Lagunera regions in Mexico”, *Environmental Health*, 10 (2011) 73-84.
33. Desarrollo, “Relationship between arsenic, heart disease and diabetes discovered”, *Medical X press*, (2014) 1-3.
34. K.A. James, T. Byers, J.E. Hokanson, J.R. Meliker, G.O. Zerbe, J.A. Marshall, “Association between lifetime exposure to inorganic arsenic in drinking water and coronary heart disease in Colorado residents”, *Environmental Health Perspectives*, 123 (2014) 128-134.
35. J.S. Tsuji, V. Perez, M.R. Garry, D.D. Alexander, “Association of low-level arsenic exposure in drinking water with cardiovascular disease: A systematic review and risk assessment”, *Toxicology*, 323 (2014) 78-94.
36. X. Fan, “Adsorption kinetics of fluoride on low cost materials”, *Water Research*, 37 (2003) 4929-4937.
37. A. Tewari, A. Dubey, others, “Defluoridation of drinking water: efficacy and need”, *Journal of Chemical and Pharmaceutical Research*, 1 (2009) 31-37.
38. L. Fewtrell, S. Smith, D. Kay, J. Bartram, “An attempt to estimate the global burden of disease due to fluoride in drinking water*”, Journal of Water and Health*, 4 (2006) 533-542.

39. N. Chinoy, “Effects of fluoride on physiology of animals and human beings”, *Indian Journal of Environmental Toxicology*, 1 (1991) 17-32.
40. M.C. Shih, “An overview of arsenic removal by pressure-drivenmembrane processes”, *Desalination*, 172 (2005) 85-97.
41. A. Saldivar, V. Soto, “Arsenic: An Abundant Natural Poison”, *ProQuest Discovery Guides*, (2009) 1-13.
42. P.E. Frank Bauman, “The Removal of Arsenic from Potable Water, in: Water Conditioning & Purification”, *PureFlow*, (2006) 1-4.
43. T. Strickland, L. Fisher, C. Korleski, “Guidelines for arsenic removal treatment for small public drinking water systems”, *Ohio Environmental Protection Agency Division of Drinking and Ground Waters*, (2010) 1-106.
44. A.A.L.S. Duarte, S.J.A. Cardoso, A.J. Alçada, “Emerging and Innovative techniques for arsenic removal applied to a small water supply system”, *Sustainability*, 1 (2009) 1288-1304.
45. M.F. Ahmed, “An overview of arsenic removal technologies in Bangladesh and India”, *Technologies for Arsenic Removal from Drinking Water* (2001) 251-269.
46. K.A. Fields, A.S.C. Chen, L. Wang, “Arsenic removal from drinking water by coagulation/filtration and lime softening plants”, National Risk Management Research Laboratory, Office of Research and Development, *US Environmental Protection Agency*, (2000) 1-112.
47. A.M. Sancha, “Review of coagulation technology for removal of arsenic: case of Chile”, *Journal of Health, Population and Nutrition*, 24 (2006) 267-272.
48. K.B. Vu, M.D. Kaminski, “Review of arsenic removal technologies for contaminated groundwaters”, in: U.S. Department of Energy Office of Scientific and Technical Information, Argonne National Laboratory, The University of Chicago, Chicago, USA, (2003) 1-43.
49. R. Johnston, H. Heijnen, “Safe water technology for arsenic removal”, *Technologies for Arsenic Removal from Drinking Water*, (2001) 1-22.
50. N.B. Issa, V.N. Rajakovic-Ognjanovic, A.D. Marinkovic, L.V. Rajakovic, “Separation and determination of arsenic species in water by selective exchange and hybrid resins”, *Analytica Chimica Acta*, 706 (2011) 191-198.
51. A.M. Donia, A.A. Atia, D.H. Mabrouk, “Fast kinetic and efficient removal of As(V) from aqueous solution using anion exchange resins”, *Journal of Hazardous Materials*, 191 (2011) 1-7.

52. Z. He, S. Tian, P. Ning, "Adsorption of arsenate and arsenite from aqueous solutions by cerium-loaded cation exchange resin", *Journal of Rare Earths*, 30 (2012) 563-572.
53. W. Wan, T.J. Pepping, T. Banerji, S. Chaudhari, D.E. Giammar, "Effects of water chemistry on arsenic removal from drinking water by electrocoagulation", *Water Research*, 45 (2011) 384-392.
54. M. Kobya, A. Akyol, E. Demirbas, M.S. Oncel, "Removal of arsenic from drinking water by batch and continuous electrocoagulation processes using hybrid Al-Fe plate electrodes", *Environmental Progress & Sustainable Energy*, 33 (2014) 131-140.
55. I. Akin, G. Arslan, A. Tor, Y. Cengeloglu, M. Ersoz, "Removal of arsenate [As(V)] and arsenite [As(III)] from water by SWHR and BW-30 reverse osmosis", *Desalination*, 281 (2011) 88-92.
56. T. Uddin, S.I. Mozumder, A. Figoli, A. Islam, E. Drioli, "Arsenic removal by conventional and membrane technology: an overview", *Indian Journal of Chemical Technology*, 14 (2007) 441-450.
57. S. Xia, B. Dong, Q. Zhang, B. Xu, N. Gao, C. Causseranda, "Study of arsenic removal by nanofiltration and its application in China", *Desalination*, 204 (2007) 374-379.
58. C.T. Yavuz, J.T. Mayo, C. Suchecki, J. Wang, A.Z. Ellsworth, H. D'Couto, E. Quevedo, A. Prakash, L. Gonzalez, C. Nguyen, C. Kelty, V.L. Colvin, "Pollution magnet: nano-magnetite for arsenic removal from drinking water", *Environmental Geochemistry and Health*, 32 (2010) 327-334.
59. M. Islam, P.C. Mishra, R. Patel, "Arsenate removal from aqueous solution by cellulose-carbonated hydroxyapatite nanocomposites", *Journal of Hazardous Materials*, 189 (2011) 755-763.
60. R. Chen, C. Zhi, H. Yang, Y. Bando, Z. Zhang, N. Sugiur, D. Golberg, "Arsenic (V) adsorption on Fe_3O_4 nanoparticle-coated boron nitride nanotubes", *Journal of Colloid and Interface Science*, 359 (2011) 261-268.
61. M.A. Malana, R.B. Qureshi, M.N. Ashiq, "Adsorption studies of arsenic on nano aluminium doped manganese copper ferrite polymer (MA, VA, AA) composite: Kinetics and mechanism", *Chemical Engineering Journal*, 172 (2011) 721-727.
62. I.N. Savina, C.J. English, R.L.D. Whitby, Y. Zheng, A. Leistner, S.V. Mikhalovsky, A.B. Cundy, "High efficiency removal of dissolved As(III) using iron nanoparticle-embedded macroporous polymer composites", *Journal of Hazardous Materials*, 192 (2011) 1002-1008.

63. E. Deliyanni, T.J. Bandosz, "Importance of carbon surface chemistry in development of iron–carbon composite adsorbents for arsenate removal", *Journal of Hazardous Materials*, 186 (2011) 667-674.
64. H. Amiri, N. Jaafarzadeh, M. Ahmadi, S.S. Martínez, "Application of LECA modified with Fenton in arsenite and arsenate removal as an adsorbent", *Desalination*, 272 (2011) 212-217.
65. X. Guan, H. Dong, J. Ma, I.M.C. Lo, "Simultaneous removal of chromium and arsenate from contaminated groundwater by ferrous sulfate: Batch uptake behavior", *Journal of Environmental Sciences*, 23 (2011) 372-380.
66. Z. Wei, S. Zhang, Z. Pan, Y. Liu, "Theoretical studies of arsenite adsorption and its oxidation mechanism on a perfect TiO_2 anatase (101) surface", *Applied Surface Science*, 258 (2011) 1192-1198.
67. R. Chen, Z. Zhang, Y. Yang, Z. Lei, N. Chen, X. Guo, C. Zhao, N. Sugiura, "Use of ferric-impregnated volcanic ash for arsenate (V) adsorption from contaminated water with various mineralization degrees", *Journal of Colloid and Interface Science*, 353 (2011) 542-548.
68. Y. Tian, M. Wu, X. Lin, P. Huang, Y. Huang, "Synthesis of magnetic wheat straw for arsenic adsorption", *Journal of Hazardous Materials*, 193 (2011) 10-16.
69. H. Erdoğan, Ö. Yalçınkaya, A.R. Türker, "Determination of inorganic arsenic species by hydride generation atomic absorption spectrometry in water samples after preconcentration/separation on nano ZrO_2/B_2O_3 by solid phase extraction", *Desalination*, 280 (2011) 391-396.
70. K.V. Snyder, "Removal of arsenic from drinking water by water Hyacinths (Eichhornia crassipes)", *Journal of the U.S. Stockholm Junior Water Prize*, 1 (2006) 41-58.
71. P.R. Baldwin, D.J. Butcher, "Phytoremediation of arsenic by two hyperaccumulators in a hydroponic environment", *Microchemical Journal*, 85 (2007) 297-300.
72. I. Naeem, A. Taskeen, T. Moeen, B. Mateen, "A new biomaterial for removal of arsenic from drinking water", *Journal of Environmental Research And Development* , 2 (2008) 295-302.
73. R. Selvakumar, N. Arul Jothi, V. Jayavignesh, K. Karthikaiselvi, G.I. Antony, P.R. Sharmila, S. Kavitha, K. Swaminathan, "As(V) removal using carbonized yeast cells containing silver nanoparticles", *Water Research*, 45 (2011) 583-592.

74. M. Urik, P. Littera, M. Kolen, others, “Removal of arsenic (V) from aqueous solutions using chemically modified sawdust of spruce (Picea abies): Kinetics and isotherm studies”, *International Journal of Environmental Science & Technology*, 6 (2009) 451-456.

75. Y. Liao, J. Liang, L. Zhou, “Adsorptive removal of As(III) by biogenic schwertmannite from simulated As-contaminated groundwater”, *Chemosphere*, 83 (2011) 295-301.

76. J. Jiang, “Removing arsenic from groundwater for the developing world-a review”, *Water Science & Technology*, 44 (2001) 89-98.

77. P.L. Smedley, H. Nkotagu, K. Pelig-Ba, A.M. MacDonald, R.T. Whittle, E.J. Whitehead, D.G. Kinniburgh, “Fluoride in groundwater from high-fluoride areas of Ghana and Tanzania”, in, *British Geological Survey Commissioned Report* CR/02/316 (2002) 1-74.

78. D. Sutherland, P. Swash, A. Macqueen, L. McWilliam, D. Ross, S. Wood, “A field based evaluation of household arsenic removal technologies for the treatment of drinking water”, *Environmental Technology*, 23 (2002) 1385-1404.

79. R. Hohn, M. Isenbeck-Schroter, D.B. Kent, J.A. Davis, R. Jakobsen, S. Jann, V. Niedan, C. Scholz, S. Stadler, A. Tretner, “Tracer test with As(V) under variable redox conditions controlling arsenic transport in the presence of elevated ferrous iron concentrations”, *Journal of Contaminant Hydrology*, 88 (2006) 36-54.

80. D. Mohan, C.U. Pittman, “Arsenic removal from water/wastewater using adsorbents–A critical review”, *Journal of Hazardous Materials*, 142 (2007) 1-53.

81. M.A. Shannon, P.W. Bohn, M. Elimelech, J.G. Georgiadis, B.J. Mariñas, A.M. Mayes, “Science and technology for water purification in the coming decades”, *Nature*, 452 (2008) 301-310.

82. Q. Jiuhui, “Research progress of novel adsorption processes in water purification: A review”, *Journal of Environmental Sciences*, 20 (2008) 1-13.

83. M. Vaclavikova, G.P. Gallios, S. Hredzak, S. Jakabsky, “Removal of arsenic from water streams: an overview of available techniques”, *Clean Technologies and Environmental Policy*, 10 (2008) 89-95.

84. V. Gupta, P. Carrott, M. Ribeiro Carrott, Suhas, “Low-cost adsorbents: growing approach to wastewater treatment–a review”, *Critical Reviews in Environmental Science and Technology*, 39 (2009) 783-842.

85. S.P. Mishra, M. Das, U.N. Dash, "Review on the adverse effects of water contaminants like arsenic, fluoride and phosphate and their remediation", *Journal of Scientific & Industrial Research*, 69 (2010) 249-253.
86. S. Tresintsi, K. Simeonidis, G. Vourlias, G. Stavropoulos, M. Mitrakas, "Kilogram-scale synthesis of iron oxy-hydroxides with improved arsenic removal capacity: Study of Fe(II) oxidation–precipitation parameters", *Water Research*, 46 (2012) 5255-5267.
87. J. Youngran, F. Maohong, J. Van Leeuwen, J.F. Belczyk, "Effect of competing solutes on arsenic (V) adsorption using iron and aluminum oxides", *Journal of Environmental Sciences*, 19 (2007) 910-919.
88. O. Thirunavukkarasu, T. Viraraghavan, K. Subramanian, "Arsenic removal from drinking water using granular ferric hydroxide", *Water SA*, 29 (2003) 161-170.
89. V.L. Nguyen, W.-H. Chen, T. Young, J. Darby, "Effect of interferences on the breakthrough of arsenic: Rapid small scale column tests", *Water Research*, 45 (2011) 4069- 4080.
90. Z. Ren, G. Zhang, J. Paul Chen, "Adsorptive removal of arsenic from water by an iron–zirconium binary oxide adsorbent", *Journal of Colloid and Interface Science*, 358 (2011) 230-237.
91. M.A. Anderson, J.F. Ferguson, J. Gavis, "Arsenate adsorption on amorphous aluminium hydroxide", *Journal of Colloid and Interface Science*, 54 (1976) 391-399.
92. J.G. Hering, "Chinatown revisited: arsenic and the Los Angeles water supply", *Engineering and Science*, 60 (1997) 34-40.
93. J. Gregor, "Arsenic removal during conventional aluminium-based drinking-water treatment", *Water Research*, 35 (2001) 1659-1664.
94. J.G. Hering, S. Dixit, "Contrasting sorption behavior of arsenic (III) and arsenic (V) in suspensions of iron and aluminum oxyhydroxides", Advances in Arsenic Research, *ACS symposium series*, 915 (2005) 8-24.
95. J.H. Gulledge, J.T. O'Connor, "Removal of arsenic (V) from water by adsorption on aluminum and ferric hydroxides", *Journal-American Water Works Association*, 65 (1973) 548-552.
96. S. Tokunaga, S. Yokoyama, S. Wasay, "Removal of arsenic (III) and arsenic (V) ions from aqueous solutions with lanthanum (III) salt and comparison with aluminum (III), calcium (II), and iron (III) salts", *Water Environment Research*, 71 (1999) 299-306.

97. X. Meng, G.P. Korfiatis, C. Jing, C. Christodoulatos, "Redox transformations of arsenic and iron in water treatment sludge during aging and TCLP extraction", *Environmental Science & Technology*, 35 (2001) 3476-3481.

98. L. Zeng, "Arsenic adsorption from aqueous solutions on an Fe (III)-Si binary oxide adsorbent", *Water Quality Research Journal of Canada*, 39 (2004) 267-275.

99. Y. Masue, R.H. Loeppert, T.A. Kramer, "Arsenate and arsenite adsorption and desorption behavior on coprecipitated aluminum: iron hydroxides", *Environmental Science & Technology*, 41 (2007) 837-842.

100. X. Guo, Y. Du, F. Chen, H.-S. Park, Y. Xie, "Mechanism of removal of arsenic by bead cellulose loaded with iron oxyhydroxide (β-FeOOH): EXAFS study", *Journal of Colloid and Interface Science*, 314 (2007) 427-433.

101. Y. Jia, G. Demopoulos, N. Chen, J. Cutler, D.T. Jiang, "Preparation, characterization and solubilities of adsorbed and co-precipitated iron (III)-arsenate solids", *Electrometallurgy and Environmental Hydrometallurgy*, 2 (2003) 1923-1935.

102. M.C.F. Magalhaes, "Arsenic. An environmental problem limited by solubility", *Pure and Applied Chemistry*, 74 (2002) 1843-1850.

103. C.A.J. Appelo, M.J.J. Van Der Weiden, C. Tournassat, L. Charlet, "Surface complexation of ferrous iron and carbonate on ferrihydrite and the mobilization of arsenic", *Environmental Science & Technology*, 36 (2002) 3096-3103.

104. H.J. Hong, W. Farooq, J.S. Yang, J.W. Yang, "Preparation and evaluation of Fe-Al binary oxide for arsenic removal: comparative study with single metal oxides", *Separation Science and Technology*, 45 (2010) 1975-1981.

105. S.K. Maji, Y.H. Kao, C.W. Liu, "Arsenic removal from real arsenic-bearing groundwater by adsorption on iron-oxide-coated natural rock (IOCNR)", *Desalination*, 280 (2011) 72-79.

106. L. Zeng, "A method for preparing silica-containing iron(III) oxide adsorbents for arsenic removal", *Water Research*, 37 (2003) 4351-4358.

107. Y. Kim, C. Kim, I. Choi, S. Rengaraj, J. Yi, "Arsenic removal using mesoporous alumina prepared via a templating method", *Environmental Science & Technology*, 38 (2004) 924-931.

108. M.A. Abedin, T. Katsumi, T. Inui, "Remediation of natural arsenic contamination in groundwater using zero valent iron", *Annuals of Diaster Prevention Research Institute*, 52 (2009) 365-370.

109. Y. Mamindy-Pajany, C. Hurel, N. Marmier, M. Roméo, “Arsenic adsorption onto hematite and goethite”, *Comptes Rendus Chimie*, 12 (2009) 876-881.
110. M.P. Asta, J. Cama, M. Martínez, J. Giménez, “Arsenic removal by goethite and jarosite in acidic conditions and its environmental implications”, *Journal of Hazardous Materials*, 171 (2009) 965-972.
111. T.V. Nguyen, S. Vigneswaran, H.H. Ngo, J. Kandasamy, “Arsenic removal by iron oxide coated sponge: Experimental performance and mathematical models”, *Journal of Hazardous Materials*, 182 (2010) 723-729.
112. H. Zhu, Y. Jia, X. Wu, H. Wang, “Removal of arsenic from water by supported nano zero-valent iron on activated carbon”, *Journal of Hazardous Materials*, 172 (2009) 1591-1596.
113. A.R. Rahmani, H.R. Ghaffari, M.T. Samadi, “Removal of arsenic (III) from contaminated water by synthetic nano size zerovalent iron”, *World Academy of Science, Engineering and Technology*, 38 (2010) 737-740.
114. C. Luengo, V. Puccia, M. Avena, “Arsenate adsorption and desorption kinetics on a Fe(III)-modified montmorillonite”, *Journal of Hazardous Materials*, 186 (2011) 1713-1719.
115. D.D. Gang, B. Deng, L. Lin, “As(III) removal using an iron-impregnated chitosan sorbent”, *Journal of Hazardous Materials*, 182 (2010) 156-161.
116. S. Shevade, R.G. Ford, “Use of synthetic zeolites for arsenate removal from pollutant water”, *Water Research*, 38 (2004) 3197-3204.
117. T.S. Singh, K. Pant, “Equilibrium, kinetics and thermodynamic studies for adsorption of As (III) on activated alumina”, *Separation and Purification Technology*, 36 (2004) 139-147.
118. D. Setyono, S. Valiyaveettil, “Chemically modified sawdust as renewable adsorbent for arsenic removal from water”, *ACS Sustainable Chemistry & Engineering*, 2 (2014) 2722-2729.
119. P. Nagarnaik, A. Bhole, G. Natarajan, “Arsenic (III) removal by adsorption on sawdust carbon”, *International Journal of Environment and Pollution*, 19 (2003) 177-187.
120. P.J. Swedlund, J.G. Webster, “Adsorption and polymerisation of silicic acid on ferrihydrite, and its effect on arsenic adsorption”, *Water Research*, 33 (1999) 3413-3422.

121. M. Auffan, J. Rose, O. Proux, D. Borschneck, A. Masion, P. Chaurand, J.L. Hazemann, C. Chaneac, J.-P. Jolivet, M.R. Wiesner, A. Van Geen, J.Y. Bottero, "Enhanced adsorption of arsenic onto Maghemites nanoparticles: As(III) as a probe of the surface structure and heterogeneity", *Langmuir*, 24 (2008) 3215-3222.

122. G. Liu, H. Zhang, "The Adsorption of arsenic on magnetic iron-Manganese Oxide in Aqueous Medium", in: *Proceedings of the International Multi Conference of Engineers and Computer*, 2008.

123. M.M. Ghosh, J.R. Yuan, "Adsorption of inorganic arsenic and organoarsenicals on hydrous oxides", *Environmental Progress*, 6 (1987) 150-157.

124. S.S. Tripathy, A.M. Raichur, "Enhanced adsorption capacity of activated alumina by impregnation with alum for removal of As(V) from water", *Chemical Engineering Journal*, 138 (2008) 179-186.

125. X. Guan, J. Ma, H. Dong, L. Jiang, "Removal of arsenic from water: Effect of calcium ions on As(III) removal in the $KMnO_4$–Fe(II) process", *Water Research*, 43 (2009) 5119-5128.

126. B. Dousova, V. Machovic, D. Kolousek, F. Kovanda, V. Dornicak, "Sorption of As(V) species from aqueous systems", *Water, Air, and Soil Pollution*, 149 (2003) 251-267.

127. B.E. Erickson, "Field kits fail to provide accurate measure of arsenic in groundwater", *Environmental Science & Technology*, 37 (2003) 35A-38A.

128. L. Yang, M. Dadwhal, Z. Shahrivari, M. Ostwal, P.K.T. Liu, M. Sahimi, T.T. Tsotsis, "Adsorption of arsenic on layered double hydroxides: Effect of the particle size", *Industrial & Engineering Chemistry Research*, 45 (2006) 4742-4751.

129. K.H. Goh, T.T. Lim, Z. Dong, "Application of layered double hydroxides for removal of oxyanions: a review", *Water Research*, 42 (2008) 1343-1368.

130. A. Violante, M. Pucci, V. Cozzolino, J. Zhu, M. Pigna, "Sorption/desorption of arsenate on/from Mg–Al layered double hydroxides: influence of phosphate", *Journal of Colloid and Interface Science*, 333 (2009) 63-70.

131. Y.H. Huang, Y.J. Shih, F.J. Cheng, "Novel $KMnO_4$-modified iron oxide for effective arsenite removal", *Journal of Hazardous Materials*, 198 (2011) 1-6.

132. D. Nguyen Thanh, M. Singh, P. Ulbrich, N. Strnadova, F. Stepanek, "Perlite incorporating γ-Fe_2O_3 and α-MnO_2 nanomaterials: Preparation and evaluation of a new adsorbent for As(V) removal", *Separation and Purification Technology*, 82 (2011) 93-101.

133. R.M. Dhoble, S. Lunge, A.G. Bhole, S. Rayalu, “Magnetic binary oxide particles (MBOP): A promising adsorbent for removal of As (III) in water”, *Water Research*, 45 (2011) 4769-4781.
134. M.G. Mostafa, Y.H. Chen, J.S. Jean, C.C. Liu, Y.C. Lee, “Kinetics and mechanism of arsenate removal by nanosized iron oxide-coated perlite”, *Journal of Hazardous Materials*, 187 (2011) 89-95.
135. X. Dou, Y. Zhang, B. Zhao, X. Wu, Z. Wu, M. Yang, “Arsenate adsorption on an Fe-Ce bimetal oxide adsorbent: EXAFS study and surface complexation modeling”, *Colloids and Surfaces A: Physicochemical and Engineering Aspects*, 379 (2011) 109-115.
136. S.C. Ying, B.D. Kocar, S. Fendorf, “Oxidation and competitive retention of arsenic between iron- and manganese oxides”, *Geochimica et Cosmochimica Acta*, 96 (2012) 294-303.
137. Y.J. Tu, C.F. You, C.K. Chang, S.L. Wang, T.S. Chan, “Arsenate adsorption from water using a novel fabricated copper ferrite”, *Chemical Engineering Journal*, 198-199 (2012) 440-448.
138. M. Kanematsu, T.M. Young, K. Fukushi, P.G. Green, J.L. Darby, “Arsenic(III, V) adsorption on a goethite-based adsorbent in the presence of major co-existing ions: Modeling competitive adsorption consistent with spectroscopic and molecular evidence”, *Geochimica et Cosmochimica Acta*, 106 (2013) 404-428.
139. F. Li, “Layer-by-layer loading iron onto mesoporous silica surfaces: Synthesis, characterization and application for As(V) removal”, *Microporous and Mesoporous Materials*, 171 (2013) 139-146.
140. M. Kanematsu, T.M. Young, K. Fukushi, P.G. Green, J.L. Darby, “Individual and combined effects of water quality and empty bed contact time on As(V) removal by a fixed-bed iron oxide adsorber: Implication for silicate precoating”, *Water Research*, 46 (2012) 5061-5070.
141. T. Mahmood, S.U. Din, A. Naeem, S. Mustafa, M. Waseem, M. Hamayun, “Adsorption of arsenate from aqueous solution on binary mixed oxide of iron and silicon”, *Chemical Engineering Journal*, 192 (2012) 90-98.
142. S. Aredes, B. Klein, M. Pawlik, “The removal of arsenic from water using natural iron oxide minerals”, *Journal of Cleaner Production*, 60 (2013) 71-76.

143. D. Ghosh, A. Gupta, "Economic justification and eco-friendly approach for regeneration of spent activated alumina for arsenic contaminated groundwater treatment", *Resources, Conservation and Recycling*, 61 (2012) 118-124.

144. A. Maiti, J.K. Basu, S. De, "Experimental and kinetic modeling of As(V) and As(III) adsorption on treated laterite using synthetic and contaminated groundwater: Effects of phosphate, silicate and carbonate ions", *Chemical Engineering Journal*, 191 (2012) 1-12.

145. G. Lopes, L.R.G. Guilherme, E.T.S. Costa, N. Curi, H.G.V. Penha, "Increasing arsenic sorption on red mud by phosphogypsum addition", *Journal of Hazardous Materials*, 262 (2013) 1196-1203.

146. B. Dousova, F. Buzek, J. Rothwell, S. Krejcova, M. Lhotka, "Adsorption behavior of arsenic relating to different natural solids: Soils, stream sediments and peats", *Science of The Total Environment*, 433 (2012) 456-461.

147. N.C. Choi, S.B. Kim, S.O. Kim, J.W. Lee, J.B. Park, "Removal of arsenate and arsenite from aqueous solution by waste cast iron", *Journal of Environmental Sciences*, 24 (2012) 589-595.

148. F. Zha, W. Huang, J. Wang, Y. Chang, J. Ding, J. Ma, "Kinetic and thermodynamic aspects of arsenate adsorption on aluminum oxide modified palygorskite nanocomposites", *Chemical Engineering Journal*, 215-216 (2013) 579-585.

149. C. Han, H. Li, H. Pu, H. Yu, L. Deng, S. Huang, Y. Luo, "Synthesis and characterization of mesoporous alumina and their performances for removing arsenic(V)", *Chemical Engineering Journal*, 217 (2013) 1-9.

150. R.R. Devi, I.M. Umlong, B. Das, K. Borah, A.J. Thakur, P.K. Raul, S. Banerjee, L.Singh, "Removal of iron and arsenic (III) from drinking water using iron oxide-coated sand and limestone", *Applied Water Science*, 4 (2014) 175-182.

151. S. Yao, Z. Liu, Z. Shi, "Arsenic removal from aqueous solutions by adsorption onto iron oxide/activated carbon magnetic composite", *Journal of Environmental Health Science & Engineering*, 12 (2014) 1-8.

152. G.K. Das, C.S. Bonifacio, J. De Rojas, K. Liu, K. van Benthem, I.M. Kennedy, "Ultra-long magnetic nanochains for highly efficient arsenic removal from water", *Journal of Materials Chemistry A*, 2 (2014) 12974-12981.

153. K. Qureshi, S. Almani, Z. Solangi, Z. Bhatti, I. Bhatti, "Modified Hematite iron for removing arsenic (V) from water", *Sindh University Research Journal (Science Series)*, 46 (2014) 83-86.

154. J.W. Farrell, J. Fortner, S. Work, C. Avendano, N.I. Gonzalez-Pech, R. Zárate Araiza, Q.Li, P.J.J. Álvarez, V. Colvin, A. Kan, M. Tomson, "Arsenic removal by nanoscale magnetite in Guanajuato, Mexico", *Environmental Engineering Science*, 31 (2014) 393-402.
155. C. Wang, H. Luo, Z. Zhang, Y. Wu, J. Zhang, S. Chen, "Removal of As(III) and As(V) from aqueous solutions using nanoscale zero valent iron-reduced graphite oxide modified composites", *Journal of Hazardous Materials*, 268 (2014) 124-131.
156. M. Mosaferi, S. Nemati, A. Khataee, S. Nasseri, A.A. Hashemi, "Removal of Arsenic (III, V) from aqueous solution by nanoscale zero-valent iron stabilized with starch and carboxymethyl cellulose", *Journal of Environmental Health Science and Engineering*, 12 (2014) 1-11.
157. T.F. Lin, J.K. Wu, "Adsorption of arsenite and arsenate within activated alumina grains: equilibrium and kinetics", *Water Research*, 35 (2001) 2049-2057.
158. M. Jang, E.W. Shin, J.K. Park, S.I. Choi, "Mechanisms of arsenate adsorption by highly-ordered nano-structured silicate media impregnated with metal oxides", *Environmental Science & Technology*, 37 (2003) 5062-5070.
159. Y.H. Xu, T. Nakajima, A. Ohki, "Adsorption and removal of arsenic (V) from drinking water by aluminum-loaded Shirasu-zeolite", *Journal of Hazardous Materials*, 92 (2002) 275-287.
160. M. Hodi, K. Polyak, J. Hlavay, "Removal of pollutants from drinking water by combined ion exchange and adsorption methods", *Environment International*, 21 (1995) 325-331.
161. X. Guo, F. Chen, "Removal of arsenic by bead cellulose loaded with iron oxyhydroxide from groundwater", *Environmental Science & Technology*, 39 (2005) 6808-6818.
162. J. Pattanayak, K. Mondal, S. Mathew, S.B. Lalvani, "A parametric evaluation of the removal of As (V) and As (III) by carbon-based adsorbents", *Carbon*, 38 (2000) 589-596.
163. L. Pontoni, M. Fabbricino, "Use of chitosan and chitosan-derivatives to remove arsenic from aqueous solutions–a mini review", *Carbohydrate Research*, 356 (2012) 86-92.
164. G. Murugesan, M. Sathishkumar, K. Swaminathan, "Arsenic removal from groundwater by pretreated waste tea fungal biomass", *Bioresource Technology*, 97 (2006) 483-487.

165. K.P. Raven, A. Jain, R.H. Loeppert, "Arsenite and arsenate adsorption on ferrihydrite: kinetics, equilibrium, and adsorption envelopes", *Environmental Science & Technology*, 32 (1998) 344-349.

166. C.T. Kamala, K.H. Chu, N.S. Chary, P.K. Pandey, S.L. Ramesh, A.R.K. Sastry, K.C.Sekhar, "Removal of arsenic(III) from aqueous solutions using fresh and immobilized plant biomass", *Water Research*, 39 (2005) 2815-2826.

167. W. Driehaus, M. Jekel, U. Hildebrandt, "Granular ferric hydroxide–a new adsorbent for the removal of arsenic from natural water", *Aqua*, 47 (1998) 30-35.

168. B.E. Reed, R. Vaughan, L. Jiang, "As (III), As (V), Hg, and Pb removal by Fe-oxide impregnated activated carbon", *Journal of Environmental Engineering*, 126 (2000) 869-873.

169. J. Hlavay, K. Polyák, "Determination of surface properties of iron hydroxide-coated alumina adsorbent prepared for removal of arsenic from drinking water", *Journal of Colloid and Interface Science*, 284 (2005) 71-77.

170. S.A. Wasay, S. Tokunaga, S.-w. Park, "Removal of hazardous anions from aqueous solutions by La(lll)-and Y(lll)-impregnated alumina", *Separation Science and Technology*, 31 (1996) 1501-1514.

171. S. Kamsonlian, S. Suresh, V. Ramanaiah, C.B. Majumder, S. Chand, A. Kumar, "Biosorptive behaviour of mango leaf powder and rice husk for arsenic(III) from aqueous solutions", *International Journal of Environmental Science and Technology*, 9 (2012) 565-578.

172. H. Seki, A. Suzuki, H. Maruyama, "Biosorption of chromium (VI) and arsenic (V) onto methylated yeast biomass", *Journal of Colloid and Interface Science*, 281 (2005) 261-266.

173. A.K. Darban, Y. Kianinia, E. Taheri-Nassaj, "Synthesis of nano-alumina powder from impure kaolin and its application for arsenite removal from aqueous solutions", *Journal of Environmental Health Science and Engineering*, 11 (2013) 1-11.

174. D. Mohan, C.U. Pittman, M. Bricka, F. Smith, B. Yancey, J. Mohammad, P.H. Steele, M.F. Alexandre-Franco, V. Gomez-Serrano, H. Gong, "Sorption of arsenic, cadmium, and lead by chars produced from fast pyrolysis of wood and bark during bio-oil production", *Journal of Colloid and Interface Science*, 310 (2007) 57-73.

175. R. Say, N. Yılmaz, A. Denizli, "Biosorption of cadmium, lead, mercury, and arsenic ions by the fungus Penicillium purpurogenum", *Separation Science and Technology*, 38 (2003) 2039-2053.

176. M. Chiban, G. Carja, G. Lehutu, F. Sinan, “Equilibrium and thermodynamic studies for the removal of As(V) ions from aqueous solution using dried plants as adsorbents”, *Arabian Journal of Chemistry*, (2012) 1-12.
177. H.S. Altundoğan, S. Altundoğan, F. Tümen, M. Bildik, “Arsenic adsorption from aqueous solutions by activated red mud”, *Waste Management*, 22 (2002) 357-363.
178. D. Ranjan, M. Talat, S.H. Hasan, “Biosorption of arsenic from aqueous solution using agricultural residue ‘rice polish’, *Journal of Hazardous Materials*, 166 (2009) 1050-1059.
179. S. Bang, M. Patel, L. Lippincott, X. Meng, “Removal of arsenic from groundwater by granular titanium dioxide adsorbent”, *Chemosphere*, 60 (2005) 389-397.
180. T. Balaji, T. Yokoyama, H. Matsunaga, “Adsorption and removal of As(V) and As(III) using Zr-loaded lysine diacetic acid chelating resin”, *Chemosphere*, 59 (2005) 1169-1174.
181. M. Ibrahim, S.M. Asim Rasheed, P. Prabhakar, “Effects of fluoride contents in ground water: A review”, *International Journal of Pharmaceutical Applications*, 2 (2011) 128-134.
182. W. Wang, R. Li, J.a. Tan, K. Luo, L. Yang, H. Li, Y. Li, “Adsorption and leaching of fluoride in soils of China”, *Fluoride*, 35 (2002) 122-129.
183. M. Agarwal, K. Rai, R. Shrivastav, S. Dass, “Defluoridation of water using amended clays”, *Fluoride*, 34 (2001) 196-197.
184. S. KL, R. Sewak, “Fluoride consumption in endemic villages of India and its remedial measures”, *International Journal of Engineering Science Invention*, 4 (2015) 58-73.
185. P. Mariappan, T. Vasudevan, “Domestic defluoridation techniques and sector approach for fluorosis mitigation”, Available from www. twadboard. gov. in (Accessed on 2011 Jan. 4th), (2002) 1-11.
186. M.J. Larsen, E.I.F. Pearce, S.J. Jensen, “Defluoridation of water at high pH with use of brushite, calcium hydroxide, and bone char”, *Journal of Dental Research*, 72 (1993) 1519-1525.
187. W.X. Gong, J.H. Qu, R.P. Liu, H.C. Lan, “Effect of aluminum fluoride complexation on fluoride removal by coagulation”, *Colloids and Surfaces A: Physicochemical and Engineering Aspects*, 395 (2012) 88-93.
188. K.O. Pamela, “Investigating contact precipitation as a viable water defluoridation technique”, M.Sc Thesis, Egerton University, (2013) 1-62.

189. J.K. Fawell, K. Bailey, J. Chilton, E. Dahi, L. Fewtrell and Y. Magara “Fluoride in drinking-water”, *World Health Organization* (2006) 1-144.

190. M. Madhukar, B.M. Murthy, T.H. Udayashankara, “A review on conventional and alternative methods for defluoridation of water”, *Journal of Water Pollution & Purification Research*, 1 (2014) 1-12.

191. F. Durmaz, H. Kara, Y. Cengeloglu, M. Ersoz, “Fluoride removal by donnan dialysis with anion exchange membranes”, *Desalination*, 177 (2005) 51-57.

192. D. Ghosh, C.R. Medhi, M.K. Purkait, “Treatment of fluoride containing drinking water by electrocoagulation using monopolar and bipolar electrode connections”, *Chemosphere*, 73 (2008) 1393-1400.

193. S. Ghorai, K.K. Pant, “Investigations on the column performance of fluoride adsorption by activated alumina in a fixed-bed”, *Chemical Engineering Journal*, 98 (2004) 165-173.

194. Y. Tang, X. Guan, T. Su, N. Gao, J. Wang, “Fluoride adsorption onto activated alumina: Modeling the effects of pH and some competing ions”, *Colloids and Surfaces A: Physicochemical and Engineering Aspects*, 337 (2009) 33-38.

195. H. Wu, L. Chen, G. Gao, Y. Zhang, T. Wang, S. Guo, “Treatment effect on the adsorption capacity of alumina for removal fluoride”, *Nano Biomedicine and Engineering*, 2 (2010) 231-235.

196. E. Kumar, A. Bhatnagar, U. Kumar, M. Sillanpää, “Defluoridation from aqueous solutions by nano-alumina: Characterization and sorption studies”, *Journal of Hazardous Materials*, 186 (2011) 1042-1049.

197. R. Liu, W. Gong, H. Lan, Y. Gao, H. Liu, J. Qu, “Defluoridation by freshly prepared aluminum hydroxides”, *Chemical Engineering Journal*, 175 (2011) 144-149.

198. S. Jagtap, M.K.N. Yenkie, N. Labhsetwar, S. Rayalu, “Defluoridation of drinking water using chitosan based mesoporous alumina”, *Microporous and Mesoporous Materials*, 142 (2011) 454-463.

199. A. Goswami, M.K. Purkait, “The defluoridation of water by acidic alumina”, *Chemical Engineering Research and Design*, 90 (2012) 2316-2324.

200. Y. Nie, C. Hu, C. Kong, “Enhanced fluoride adsorption using Al (III) modified calcium hydroxyapatite”, *Journal of Hazardous Materials*, 233-234 (2012) 194-199.

201. S. Lunge, D. Thakre, S. Kamble, N. Labhsetwar, S. Rayalu, “Alumina supported carbon composite material with exceptionally high defluoridation property from eggshell waste”, *Journal of Hazardous Materials*, 237-238 (2012) 161-169.

202. M. Mohapatra, K. Rout, P. Singh, S. Anand, S. Layek, H.C. Verma, B.K. Mishra, "Fluoride adsorption studies on mixed-phase nano iron oxides prepared by surfactant mediation-precipitation technique", *Journal of Hazardous Materials*, 186 (2011) 1751-1757.

203. E. Kumar, A. Bhatnagar, M. Ji, W. Jung, S.-H. Lee, S.J. Kim, G. Lee, H. Song, J.Y. Choi, J.S. Yang, "Defluoridation from aqueous solutions by granular ferric hydroxide (GFH)", *Water research*, 43 (2009) 490-498.

204. A.M. Raichur, M.J. Basu, "Adsorption of fluoride onto mixed rare earth oxides", *Separation and Purification Technology*, 24 (2001) 121-127.

205. A.R. Tembhurkar, S. Dongre, "Studies on fluoride removal using adsorption process", *Journal of Environmental Science & Engineering*, 48 (2006) 151-156.

206. M. Kaseva, "Optimization of regenerated bone char for fluoride removal in drinking water: a case study in Tanzania", *Journal of Water and Health*, 4 (2006) 139-147.

207. X. Wu, Y. Zhang, X. Dou, M. Yang, "Fluoride removal performance of a novel Fe–Al–Ce trimetal oxide adsorbent", *Chemosphere*, 69 (2007) 1758-1764.

208. D. Zhao, T. Steinwinder, B. An, M.O. Barnett, T. Kramer, "Developing a new class of ion exchangers for selective removal of arsenic and exploring an engineered approach for treatment and reuse of spent regenerant brine and for enhanced stability of process waste residuals", WERC and AWWA Research Foundation, (2006) 1-82.

209. L. Chen, H.X. Wu, T.J. Wang, Y. Jin, Y. Zhang, X.M. Dou, "Granulation of Fe-Al-Ce nano-adsorbent for fluoride removal from drinking water by spray coating on sand in a fluidized bed", *Powder Technology*, 193 (2009) 59-64.

210. C.S. Sundaram, N. Viswanathan, S. Meenakshi, "Defluoridation chemistry of synthetic hydroxyapatite at nano scale: Equilibrium and kinetic studies", *Journal of Hazardous Materials*, 155 (2008) 206-215.

211. X. Zhao, J. Wang, F. Wu, T. Wang, Y. Cai, Y. Shi, G. Jiang, "Removal of fluoride from aqueous media by Fe_3O_4@$Al(OH)_3$ magnetic nanoparticles", *Journal of Hazardous Materials*, 173 (2010) 102-109.

212. M. Yang, X. Wu, Y. Zhang, X. Dou, "Composite metal oxide adsorbent for fluoride removal", *United States Patent* (US 7786038 B2) (2010) 1-7.

213. S.K. Nath, R.K. Dutta, "Fluoride removal from water using crushed limestone", *Indian Journal of Chemical Technology*, 17 (2010) 120-125.

214. Q. Liu, H. Guo, Y. Shan, "Adsorption of fluoride on synthetic siderite from aqueous solution", *Journal of Fluorine Chemistry*, 131 (2010) 635-641.

215. M. Ansari, M. Kazemipour, M. Dehghani, M. Kazemipour, "The defluoridation of drinking water using multi-walled carbon nanotubes", *Journal of Fluorine Chemistry*, 132 (2011) 516-520.

216. X.H. Wang, R.H. Song, H.C. Yang, Y.J. Shi, G.B. Dang, S. Yang, Y. Zhao, X.F. Sun, S.G. Wang, "Fluoride adsorption on carboxylated aerobic granules containing Ce(III)", *Bioresource Technology*, 127 (2013) 106-111.

217. V. Sivasankar, S. Murugesh, S. Rajkumar, A. Darchen, "Cerium dispersed in carbon (CeDC) and its adsorption behavior: A first example of tailored adsorbent for fluoride removal from drinking water", *Chemical Engineering Journal*, 214 (2013) 45-54.

218. T. Zhang, Q. Li, H. Xiao, Z. Mei, H. Lu, Y. Zhou, "Enhanced fluoride removal from water by non-thermal plasma modified CeO_2/Mg–Fe layered double hydroxides", *Applied Clay Science*, 72 (2013) 117-123.

219. K. Babaeivelni, A.P. Khodadoust, "Adsorption of fluoride onto crystalline titanium dioxide: Effect of pH, ionic strength, and co-existing ions", *Journal of Colloid and Interface Science*, 394 (2013) 419-427.

220. J. Wang, W. Xu, L. Chen, Y. Jia, L. Wang, X.J. Huang, J. Liu, "Excellent fluoride removal performance by CeO_2–ZrO_2 nanocages in water environment", *Chemical Engineering Journal*, 231 (2013) 198-205.

221. G. Karthikeyan, B.V.Apparao, S.Meenakshi, "Defluoridation properties of Activated Alumina", 2nd International Workshop on Fluorosis Prevention and Defluoridation of Water, *The International Society for Fluoride Research* (1997) 78-82.

222. B. Shimelis, F. Zewge, B.S. Chandravanshi, "Removal of excess fluoride from water by aluminum hydroxide", *Bulletin of the Chemical Society of Ethiopia*, 20 (2006) 17-34.

223. S.S. Tripathy, J.L. Bersillon, K. Gopal, "Removal of fluoride from drinking water by adsorption onto alum-impregnated activated alumina", *Separation and Purification Technology*, 50 (2006) 310-317.

224. V. Ganvir, K. Das, "Removal of fluoride from drinking water using aluminum hydroxide coated rice husk ash", *Journal of Hazardous Materials*, 185 (2011) 1287-1294.

225. G. Alagumuthu, V. Veeraputhiran, R. Venkataraman, "Fluoride sorption using Cynodon dactylon based activated carbon", *Hemijska Industrija*, 65 (2011) 23-35.

226. S.P. Kamble, G. Deshpande, P.P. Barve, S. Rayalu, N.K. Labhsetwar, A. Malyshew, B.D.Kulkarni, "Adsorption of fluoride from aqueous solution by alumina of alkoxide nature: Batch and continuous operation", *Desalination*, 264 (2010) 15-23.

227. X. Yu, S. Tong, M. Ge, J. Zuo, "Removal of fluoride from drinking water by cellulose@hydroxyapatite nanocomposites", *Carbohydrate Polymers*, 92 (2013) 269-275.

228. R. Huang, B. Yang, Q. Liu, K. Ding, "Removal of fluoride ions from aqueous solutions using protonated cross-linked chitosan particles", *Journal of Fluorine Chemistry*, 141 (2012) 29-34.

229. A. Bansiwal, P. Pillewan, R.B. Biniwale, S.S. Rayalu, "Copper oxide incorporated mesoporous alumina for defluoridation of drinking water", *Microporous and Mesoporous Materials*, 129 (2010) 54-61.

230. M.G. Sujana, G. Soma, N. Vasumathi, S. Anand, "Studies on fluoride adsorption capacities of amorphous Fe/Al mixed hydroxides from aqueous solutions", *Journal of Fluorine Chemistry*, 130 (2009) 749-754.

231. S.V. Ramanaiah, S. Venkata Mohan, P.N. Sarma, "Adsorptive removal of fluoride from aqueous phase using waste fungus (Pleurotus ostreatus 1804) biosorbent: Kinetics evaluation", *Ecological Engineering*, 31 (2007) 47-56.

232. S.X. Teng, S.G. Wang, W.X. Gong, X.W. Liu, B.Y. Gao, "Removal of fluoride by hydrous manganese oxide-coated alumina: Performance and mechanism", *Journal of Hazardous Materials*, 168 (2009) 1004-1011.

233. B.K. Puri, S. Balani, "Trace determination of fluoride using lanthanum hydroxide supported on alumina", *Journal of Environmental Science & Health Part A*, 35 (2000) 109-121.

234. A.V. Jamode, V.S. Sapkal, V.S. Jamode, "Defluoridation of water using inexpensive adsorbents", *Journal of the Indian Institute of Science*, 84 (2013) 163-171.

235. S.M. Maliyekkal, A.K. Sharma, L. Philip, "Manganese-oxide-coated alumina: A promising sorbent for defluoridation of water", *Water Research*, 40 (2006) 3497-3506.

236. N. Lakshmaiah, P.K. Paranjape, P.M. Mohan, "Biodefluoridation of fluoride containing water by a fungal biosorbent", *2nd International Workshop on Fluorosis Prevention and Defluoridation of Water* (1997) 123-126.

237. A.K. Yadav, R. Abbassi, A. Gupta, M. Dadashzadeh, “Removal of fluoride from aqueous solution and groundwater by wheat straw, sawdust and activated bagasse carbon of sugarcane”, *Ecological Engineering*, 52 (2013) 211-218.

238. M.G. Sujana, A. Mishra, B.C. Acharya, “Hydrous ferric oxide doped alginate beads for fluoride removal: Adsorption kinetics and equilibrium studies”, *Applied Surface Science*, 270 (2013) 767-776.

239. Y. Shan, H. Guo, “Fluoride adsorption on modified natural siderite: Optimization and performance”, *Chemical Engineering Journal*, 223 (2013) 183-191.

240. H. Paudyal, B. Pangeni, K. Inoue, H. Kawakita, K. Ohto, K.N. Ghimire, H. Harada, S.Alam, “Adsorptive removal of trace concentration of fluoride ion from water by using dried orange juice residue”, *Chemical Engineering Journal*, 223 (2013) 844-853.

241. P. Koilraj, S. Kannan, “Aqueous fluoride removal using ZnCr layered double hydroxides and their polymeric composites: Batch and column studies”, *Chemical Engineering Journal*, 234 (2013) 406-415.

242. Y. Li, Q. Du, J. Wang, T. Liu, J. Sun, Y. Wang, Z. Wang, Y. Xia, L. Xia, “Defluoridation from aqueous solution by manganese oxide coated graphene oxide”, *Journal of Fluorine Chemistry*, 148 (2013) 67-73.

243. M.P. Miramontes, R.G.B. Margulis, A.P. Hernandez, “Removal of Arsenic and Fluoride from drinking water with cake alum and a polymeric anionic flocculent”, *Fluoride*, 36 (2003) 122-128.

244. A. Farooqi, H. Masuda, M. Kusakabe, M. Naseem, N. Firdous, “Distribution of highly arsenic and fluoride contaminated groundwater from east Punjab, Pakistan, and the controlling role of anthropogenic pollutants in the natural hydrological cycle”, *Geochemical Journal*, 41 (2007) 213-234.

245. R. Devi, E. Alemayehu, V. Singh, A. Kumar, E. Mengistie, “Removal of fluoride, arsenic and coliform bacteria by modified homemade filter media from drinking water”, *Bioresource Technology*, 99 (2008) 2269-2274.

246. A.P. Padilla, H. Saitua, “Performance of simultaneous arsenic, fluoride and alkalinity (bicarbonate) rejection by pilot-scale nanofiltration”, *Desalination*, 257 (2010) 16-21.

247. Y. Tang, J. Wang, N. Gao, “Characteristics and model studies for fluoride and arsenic adsorption on goethite”, *Journal of Environmental Sciences*, 22 (2010) 1689-1694.

248. T. Mlilo, L. Brunson, D. Sabatini, “Arsenic and fluoride removal using simple materials”, *Journal of Environmental Engineering*, 136 (2009) 391-398.

249. Y. Tian, M. Wu, R. Liu, D. Wang, X. Lin, W. Liu, L. Ma, Y. Li, Y. Huang, "Modified native cellulose fibers–A novel efficient adsorbent for both fluoride and arsenic", *Journal of Hazardous Materials*, 185 (2011) 93-100.

250. W. Li, C.Y. Cao, L.Y. Wu, M.F. Ge, W.G. Song, "Superb fluoride and arsenic removal performance of highly ordered mesoporous aluminas", *Journal of Hazardous Materials*, 198 (2011) 143-150.

251. H. Guo, Y. Zhang, L. Xing, Y. Jia, "Spatial variation in arsenic and fluoride concentrations of shallow groundwater from the town of Shahai in the Hetao basin, Inner Mongolia", *Applied Geochemistry*, 27 (2012) 2187-2196.

252. S.H. Kim, K. Kim, K.S. Ko, Y. Kim, K.S. Lee, "Co-contamination of arsenic and fluoride in the groundwater of unconsolidated aquifers under reducing environments", *Chemosphere*, 87 (2012) 851-856.

253. K.D. Brahman, T.G. Kazi, H.I. Afridi, S. Naseem, S.S. Arain, N. Ullah, "Evaluation of high levels of fluoride, arsenic species and other physicochemical parameters in underground water of two sub districts of Tharparkar, Pakistan: A multivariate study", *Water Research*, 47 (2013) 1005-1020.

254. M.T. Alarcón-Herrera, J. Bundschuh, B. Nath, H.B. Nicolli, M. Gutierrez, V.M. Reyes-Gomez, D. Nuñez, I.R. Martín-Dominguez, O. Sracek, "Co-occurrence of arsenic and fluoride in groundwater of semi-arid regions in Latin America: Genesis, mobility and remediation", *Journal of Hazardous Materials*, 262 (2013) 960-969.

255. J. Qiao, Z. Cui, Y. Sun, Q. Hu, X. Guan, "Simultaneous removal of arsenate and fluoride from water by Al-Fe (hydr) oxides", *Frontiers of Environmental Science & Engineering*, 8 (2014) 169-179.

256. M.A.S. D. Barros, P. A.Arroyo, E. A.Silva, "General aspects of aqueous sorption process in fixed beds", Mass Transfer - Advances in Sustainable Energy and Environment Oriented Numerical Modeling, Chapter 14 (2013) 361-386.

257. G. Naja, B. Volesky, "Behavior of the mass transfer zone in a biosorption column", *Environmental Science & Technology*, 40 (2006) 3996-4003.

258. N. Vukojevic Medvidovic, J. Peric, M. Trgo, I. Nuic, M. Ugrina, "Design of fixed bed column for lead removal on natural zeolite based on batch studies", *Chemical and Biochemical Engineering Quarterly*, 27 (2013) 21-28.

259. H. Nouri, O. Abdelmottaleb "Modeling of the dynamics adsorption of phenol from an aqueous solution on activated carbon produced from olive stones", *Journal of Chemical Engineering & Process Technology*, 4 (2013) 1-7.

260. H.C. Thomas, “Heterogeneous ion exchange in a flowing system”, *Journal of the American Chemical Society*, 66 (1944) 1664-1666.

261. Z. Aksu, F. Gonen, “Biosorption of phenol by immobilized activated sludge in a continuous packed bed: prediction of breakthrough curves”, *Process Biochemistry*, 39 (2004) 599-613.

262. Y.H. Yoon, J.H. Nelson, “Application of gas adsorption kinetics I. A theoretical model for respirator cartridge service life”, *The American Industrial Hygiene Association Journal*, 45 (1984) 509-516.

263. G.S. Bohart, E.Q. Adams, “Some aspects of the behaviour of charcoal with respect to chlorine”, *Journal of the American Chemical Society*, 42 (1920) 523-544.

264. R.M. Clark, “Evaluating the cost and performance of field-scale granular activated carbon systems”, *Environmental Science & Technology*, 21 (1987) 573-580.

265. J.F. Moulder, J. Chastain, R.C. King, “Handbook of X-ray photoelectron spectroscopy: A reference book of standard spectra for identification and interpretation of XPS data”, Perkin-Elmer Eden Prairie, MN, 1992.

266. I. Tuzun, G. Bayramoglu, E. Yalcin, G. Basaran, G. Celik, M.Y. Arica, “Equilibrium and kinetic studies on biosorption of Hg(II), Cd(II) and Pb(II) ions onto microalgae Chlamydomonas reinhardtii”, *Journal of Environmental Management*, 77 (2005) 85-92.

267. V. Kumar, N. Talreja, D. Deva, N. Sankararamakrishnan, A. Sharma, N. Verma, “Development of bi-metal doped micro-and nano multi-functional polymeric adsorbents for the removal of fluoride and arsenic (V) from wastewater”, *Desalination*, 282 (2011) 27-38.

268. X. Yu, S. Tong, M. Ge, L. Wu, J. Zuo, C. Cao, W. Song, “Synthesis and characterization of multi-amino-functionalized cellulose for arsenic adsorption”, *Carbohydrate Polymers*, 92 (2013) 380-387.

269. T.S. Anirudhan, J. Nima, S. Sandeep, V.R.N. Ratheesh, “Development of an amino functionalized glycidylmethacrylate-grafted-titanium dioxide densified cellulose for the adsorptive removal of arsenic (V) from aqueous solutions”, *Chemical Engineering Journal*, 209 (2012) 362-371.

270. G. Alagumuthu, M. Rajan, “Equilibrium and kinetics of adsorption of fluoride onto zirconium impregnated cashew nut shell carbon”, *Chemical Engineering Journal*, 158 (2010) 451-457.

271. J.D. Allison, T.L. Allison, “Partition coefficients for metals in surface water, soil, and waste”, Rep. EPA/600/R-05, 74 (2005).
272. S. Lagergren, “About the theory of so-called adsorption of soluble substances”, *Kungliga Svenska Vetenskapsakademiens Handlingar*, 24 (1898) 1-39.
273. Y.S. Ho, G. McKay, “The kinetics of sorption of divalent metal ions onto sphagnum moss peat”, *Water Research*, 34 (2000) 735-742.
274. D. Kumar, J.P. Gaur, “Chemical reaction- and particle diffusion-based kinetic modeling of metal biosorption by a Phormidium sp.-dominated cyanobacterial mat”, *Bioresource Technology*, 102 (2011) 633-640.
275. W. Weber, J. Morris, “Kinetics of adsorption on carbon from solution”, *Journal of the Sanitary Engineering Division, American Society of Civil Engineering*, 89 (1963) 31-60.
276. K. Mohanty, D. Das, M. Biswas, “Adsorption of phenol from aqueous solutions using activated carbons prepared from Tectona grandis sawdust by $ZnCl_2$ activation”, *Chemical Engineering Journal*, 115 (2005) 121-131.
277. S. Milonjic, “A consideration of the correct calculation of thermodynamic parameters of adsorption”, *Journal of the Serbian Chemical Society*, 72 (2007) 1363-1367.
278. N.S. Mondal, “Arsenic removal by electrocoagulation and co-precipitation: A comparative study and critical evaluation”, M.E Thesis Synopsis (2014) 1-19.
279. S. Tamilselvi, M. Asaithambi, “Column mode adsorption studies of acid dye using a novel adsorbent”, *Rasayan Journal of Chemistry*, 8 (2015) 84-91.
280. E.N. El Qada, E.A. Abdelghany, Y.H. Magdy, “Utilization of activated carbon for the removal of basic dyes in fixed-bed microcolumn”, *International Journal of Energy and Environment* 4 (2013) 815-824.
281. W.J. Weber Jr, F.A. Digiano, “Process dynamics in environmental systems”, John Wiley & Sons, Inc., New York (1996) 943 pages.
282. G. McKay, V.J. Poots, “Kinetics and diffusion processes in colour removal from effluent using wood as an adsorbent”, *Journal of Chemical Technology and Biotechnology*, 30 (1980) 279-292.
283. S. Allen, G. McKay, K. Khader, “Intraparticle diffusion of a basic dye during adsorption onto sphagnum peat”, *Environmental Pollution*, 56 (1989) 39-50.
284. K. Panday, G. Prasad, V. Singh, “Copper (II) removal from aqueous solutions by fly ash”, *Water Research*, 19 (1985) 869-873.

285. G.E. Boyd, A.W. Adamson, L.S. Myers Jr, "The exchange adsorption of ions from aqueous solutions by organic zeolites. II. Kinetics", *Journal of the American Chemical Society*, 69 (1947) 2836-2848.

286. M.G. Sujana, H.K. Pradhan, S. Anand, "Studies on sorption of some geomaterials for fluoride removal from aqueous solutions", *Journal of Hazardous Materials*, 161 (2009) 120-125.

287. R. Leyva-Ramos, N.A. Medellin-Castillo, A. Jacobo-Azuara, J. Mendoza-Barron, L.E.Landin-Rodriguez, J.M. Martinez-Rosales, A. Aragon-Pina, "Fluoride removal from water solution by adsorption on activated alumina prepared from pseudo-boehmite", *Journal of Environmental Engineering Management*, 18 (2008) 301-309.

288. E. Kumar, A. Bhatnagar, M. Ji, W. Jung, S.H. Lee, S.J. Kim, G. Lee, H. Song, J.Y. Choi, J.S. Yang, B.H. Jeon, "Defluoridation from aqueous solutions by granular ferric hydroxide (GFH)", *Water Research*, 43 (2009) 490-498.

289. T. Zhang, Q. Li, Y. Liu, Y. Duan, W. Zhang, "Equilibrium and kinetics studies of fluoride ions adsorption on CeO_2/Al_2O_3 composites pretreated with non-thermal plasma", *Chemical Engineering Journal*, 168 (2011) 665-671.

290. E. Kumar, A. Bhatnagar, U. Kumar, M. Sillanpaa, "Defluoridation from aqueous solutions by nano-alumina: characterization and sorption studies", *Journal of Hazardous Materials*, 186 (2011) 1042-1049.

291. A. Daifullah, S. Yakout, S. Elreefy, "Adsorption of fluoride in aqueous solutions using $KMnO_4$-modified activated carbon derived from steam pyrolysis of rice straw", *Journal of Hazardous Materials*, 147 (2007) 633-643.

292. H. Wu, L. Chen, G. Gao, Y. Zhang, T. Wang, S. Guo, "Treatment effect on the adsorption capacity of alumina for removal fluoride", *Nano Biomedicine and Engineering*, 2 (2010) 239-245.

293. S. Ouvrard, M.O. Simonnot, P. De Donato, M. Sardin, "Diffusion-controlled adsorption of arsenate on a natural manganese oxide", *Industrial & Engineering Chemistry Research*, 41 (2002) 6194-6199.

294. K.S. Bharathi, S.P.T. Ramesh, "Fixed-bed column studies on biosorption of crystal violet from aqueous solution by Citrullus lanatus rind and Cyperus rotundus", *Applied Water Science*, 3 (2013) 673-687.

295. N.K.Mondal, B.Bhaumik, P.Roy, B.Das, J.K.Datta, "Investigaton of fixed bed column performance of fluoride adsorption by sugarcane charcoal", *Journal of Environmental Biology*, 34 (2013) 1059-1064.

296. S. Chen, Q. Yue, B. Gao, Q. Li, X. Xu, K. Fu, “Adsorption of hexavalent chromium from aqueous solution by modified corn stalk: a fixed-bed column study”, *Bioresource Technology*, 113 (2012) 114-120.

297. S. Chouhan, S.J.S. Flora, “Arsenic and fluoride: Two major ground water pollutants”, *Indian Journal of Experimental Biology*, 48 (2010) 666-678.

298. R. Indu, S. Krishnan, T. Shah, “Impacts of groundwater contamination with fluoride and arsenic affliction severity, medical cost and wage loss in some villages of India”, *International Journal of Rural Management*, 3 (2007) 69-93.

299. A. Singh, S. Bhagowati, T. Das, D. Yubbe, B. Rahman, M. Nath, P. Obing, W. Singh, C.Renthlei, L. Pachuau, “Assessment of arsenic, fluoride, iron, nitrate and heavy metals in drinking water of northeastern India”, *Envis Bulletin Himalayan Ecology*, 16 (2008) 6-12.

300. L.A. Senior, R.A. Sloto, “Arsenic, boron, and fluoride concentrations in ground water in and near diabase intrusions, Newark Basin, Southeastern Pennsylvania", United State Geological Survey Scientific Investigations Report (2006) 1-117.